



# UNIVERSITÀ DEGLI STUDI DI MILANO

DOCTORAL PROGRAM IN TRANSLATIONAL MEDICINE  
XXXIV CYCLE

## Gadolinium-based and iodinated contrast agents in breast imaging: challenges and new trends

PhD Thesis of

**Andrea COZZI**

Matr. n. R12213 – MED/36

Advisor: Prof. **Francesco SARDANELLI**

PhD Coordinator: Prof. **Chiarella SFORZA**

Academic Year 2020 – 2021



*Omnis homines qui sese student praestare ceteris animalibus summa ope niti decet ne vitam silentio transeant veluti pecora, quae natura prona atque ventri oboedientia finxit. Sed nostra omnis vis in animo et corpore sita est; animi imperio, corporis servitio magis utimur; alterum nobis cum dis, alterum cum beluis commune est. Quo mihi rectius videtur ingeni quam virium opibus gloriam quaerere et, quoniam vita ipsa qua fruimur brevis est, memoriam nostri quam maxime longam efficere.*

Gaius Sallustius Crispus

*Where is the knowledge we have lost in information?*

Thomas Stearns Eliot

*Mostrati dunque più umano, che critico; e si accrescerai le proprie Dilettazioni.*

Domenico Scarlatti

Al termine dei miei studi nel corso di dottorato di ricerca in Medicina Traslazionale, a fianco del Professor Francesco Sardanelli—già relatore della mia tesi di laurea in Medicina e Chirurgia il 20 Marzo 2018, poi mio *doctoral advisor* durante gli scorsi intensissimi trentanove mesi (1 Ottobre 2018 – 31 Dicembre 2021) ed infine nuovamente relatore della presente tesi dottorale—intendo esprimere un ringraziamento particolarmente sentito a cinque mentori, colleghi, amici, che hanno accompagnato il mio percorso.

Non posso che nominarli nell'esatto ordine cronologico in cui ho avuto la fortuna ed il grande privilegio di far loro conoscenza: Francesco Secchi, Marco Ali, Marina Codari, Rubina Manuela Trimboli, Simone Schiaffino.

Ciascuno di essi—in diversi modi, tempi, forme—ha apportato un peculiare ed inestimabile contributo alla mia crescita scientifica, professionale, personale. Sono e sempre sarò profondamente onorato di aver potuto beneficiare del loro paziente ascolto, dei loro saggi consigli, del loro tempestivo incoraggiamento: in una espressione, della loro immensa caratura umana.

Grazie,

*Andrea*





# Index

<b>INDEX</b>	<b>I</b>
<b>GENERAL FRAMEWORK AND NARRATIVE OUTLINE OF THE THESIS</b>	<b>III</b>
<b>SECTION I — GADOLINIUM-BASED CONTRAST AGENTS</b>	<b>1</b>
0. Breast imaging across three decades: contrast-enhanced magnetic resonance imaging and the concept of contrast-enhanced breast imaging	2
1. Gadolinium-based contrast agents for breast MRI: uncertainties about brain gadolinium retention and clinical applications	6
2. Gadolinium retention and breast MRI screening: more harm than good?	26
3. Accuracy and inter-reader agreement of breast MRI for cancer staging using 0.08 mmol/kg of gadobutrol	32
<b>SECTION II — IODINATED CONTRAST AGENTS</b>	<b>52</b>
4. The emerging role of contrast-enhanced mammography	53
5. Technique, protocols and adverse reactions of contrast-enhanced mammography: a systematic review	59
6. Contrast-enhanced mammography: a systematic review and meta-analysis of diagnostic performance	84
7. Radiation dose of contrast-enhanced mammography: a two-centre prospective comparison	130
8. Contrast-enhanced mammography can reduce the biopsy rate in the assessment of screening recalls: a two-centre study	154
<b>REFERENCES</b>	<b>183</b>



## General framework and narrative outline of the thesis

Purely morphological imaging modalities—i.e. digital mammography and breast ultrasound—still represent the true backbone of breast imaging. They indisputably account for the vast majority of all breast screening and diagnostic examinations performed worldwide and are used to guide an even larger majority of all breast biopsies.

However—as demonstrated in several other radiological subspecialties with the introduction of contrast-enhanced computed tomography, of contrast-enhanced magnetic resonance, of nuclear medicine, and of molecular imaging—the analysis of the tissue uptake of contrast agents or radiotracers grants tissue characterization and functional information that allow for a considerable and often fundamental diagnostic gain. This holds especially true when functional information are coupled with morphological information, i.e., in morphofunctional imaging techniques.

The advent of “contrast-enhanced breast imaging” is *de facto* traceable to 1986, when an article about the use of paramagnetic gadolinium-based contrast agents in breast magnetic resonance—published by the group of Sylvia Heywang-Köbrunner [1]—inaugurated the era of contrast-enhanced breast magnetic resonance imaging. In the following 20 years, contrast-enhanced breast magnetic resonance imaging enjoyed a true hegemony as the chief morphofunctional breast imaging modality, save for sporadic and experimental applications of molecular breast imaging.

Only in the second half of the 2000s—after three preliminary studies published almost simultaneously in 2003 by the groups of John Lewin [2], Roberta Jong [3], and Felix Diekmann [4]—a new morphofunctional breast imaging modality began to emerge in the research and clinical scenarios of breast care: contrast-enhanced mammography, a dual-energy X-ray-based technique involving the administration of iodinated contrast agents.

Aspects concerning the diagnostic performance and the clinical relevance of these two modalities will be mentioned or thoroughly discussed in several chapters of this thesis. However, it is

paramount to immediately mention that, as for every medical procedure, the administration of contrast agents is not risk-free. Therefore, any kind of contrast-enhanced imaging implies a factual summation of the risks that stem from the administration of contrast agents to the intrinsic risks of the “baseline” morphological imaging modality. Of course, when the development process of any (unenhanced or contrast-enhanced) imaging technique reaches the stage of human application, the risk-benefit balance is usually already outlined as favorable. Indeed, the appropriate justification of risk exposure in this balance is frequently reinforced by evidence coming from subsequent preliminary human studies and case series up to full-fledged prospective trials.

This has been the case for contrast-enhanced breast magnetic resonance and—albeit at a slower pace—also for contrast-enhanced mammography. However, several factors—e.g. the appearance of unexpected adverse effects of contrast agent administration, country-specific differences in the availability and cost-effectiveness of these techniques, and patients’ preferences—may profoundly influence the risk-benefit balance of a contrast-enhanced imaging technique and, eventually, its application. For example, a theoretically risk-free imaging technique whose workflow would however result in considerable patient discomfort would see its risk-benefit balance severely hampered by this aspect, at least until measures to reduce this issue were effectively devised and applied. If this imbalance in the risk-benefit profile persists and a new technique with a more favorable balance emerges, a progressive substitution of roles can sooner or later happen.

These are the factors that determine *challenges* and *trends* in any multi-option scenario. Contrast-enhanced imaging of any organ and system of the human body, breasts included, is no exception to this rule: while the administration of gadolinium-based contrast agents was long thought to be practically risk-free, at least two major international alarms about unforeseen late adverse effects of these contrast agents emerged in 2006 [5] and in 2014 [6], as will be discussed in Chapter 1.

The start of a very long internship for the development of my MD thesis and my first contacts with the research group led by Professor Francesco Sardanelli—Full Professor of Radiology in the

Department of Biomedical Sciences for Health of the University of Milano and Director of the Radiology Unit of IRCCS Policlinico San Donato—date back exactly to October 2014. When I ultimately graduated in late March 2018 and applied for a direct transition to the PhD program in Translational Medicine, the general outcry engendered by the last of the aforementioned major scares about late effects gadolinium-based contrast agents was already waning, due to the substantial absence of findings pointing to detrimental clinical effects of gadolinium retention in the brain. However, preventive measures—e.g., bans or adverse recommendations about the use of some gadolinium-based contrast agents—had been already devised and enforced with surprising efficiency in the previous three years by regulatory authorities, such as the European Medicines Agency and the United States Food and Drug Administration, and were never lifted nor modified. These appeals to caution and these official embargoes had indeed immediately stimulated, also in breast imaging, a profound revision of the safety profile of gadolinium-based contrast agents. Moreover, they had fostered an unprecedented research focus on dose-reduction strategies, and, far more subtly, they had been encouraging an ever stronger urgency towards the development or the definitive clinical translation of alternative contrast-enhanced imaging modalities. Paradoxically, contrast-enhanced mammography—which involves the administration of iodinated contrast agents, long considered far less safe than gadolinium-based contrast agents due to their higher rate of acute adverse reactions—greatly benefited from this reversal of fortune and received a considerable boost in its hitherto languishing competition with contrast-enhanced breast magnetic resonance imaging. When I started my PhD program in the last days of September 2018, the investigation of these “*challenges and new trends* in contrast-enhanced breast imaging” was immediately agreed upon as my main line of research. Section I of this thesis will therefore present all output focused on the evaluation of the risk-benefit balance of the administration of gadolinium-based contrast agents for contrast-enhanced breast magnetic resonance imaging, chiefly developed and executed in the first year of my PhD program, in the form of two reviews and a dose-reduction study. While in the same

year I also took part in another similar study [7] (centered on cardiovascular contrast-enhanced magnetic resonance imaging and therefore not reported in this thesis), in the following two years—alongside a protracted attention to unforeseeable but highly relevant COVID-19-related topics—my main focus shifted to research related to contrast-enhanced mammography. All results of my endeavors in this direction will be presented in Section II, incorporating the two largest available systematic reviews on technical and diagnostic performance aspects of this technique and two very recent studies on crucial issues that still need to be addressed or explored to allow for further establishment of contrast-enhanced mammography as a widely-applied and recognized cornerstone of breast imaging.





# **Section I**



## **Gadolinium-based contrast agents**

**0. Breast imaging across three decades: contrast-enhanced magnetic resonance imaging and the concept of contrast-enhanced breast imaging**

## 0.1. Introduction

In the last 25 years, breast imaging has undergone a profound transformation, driven by four main trends.

First, large-scale implementation of screening mammography for breast cancer reached huge volumes in the early 2000s [8], both in Europe [9] and in the United States [8]. As already postulated in the 1960s, breast cancer screening—combined with improved treatments—is effectively able to reduce breast cancer mortality [8, 10].

Second, needle biopsy progressively replaced surgical breast biopsy, which had shown various technical and clinical shortcomings [11]. While fine-needle aspiration was initially widely employed, needle caliper steadily increased, as in core-needle biopsy and ultimately vacuum-assisted biopsy [12]. This currently allows to collect larger specimens that provide the pathologist more ease to elaborate a diagnosis [13].

Third, established breast imaging modalities went through relevant technical improvements. Breast ultrasound—already known to be fast, readily available and cost-effective—has been enriched by multiparametric approaches (Doppler techniques and elastography) and supplemented by contrast-enhanced ultrasound [14, 15]. Automated breast ultrasound was also developed to address the poor reproducibility of conventional hand-held breast ultrasound [14]. However, the real clinical impact of all these technical innovations remains limited and only partially demonstrated. In x-ray based imaging, screen-film mammography—while still widely used globally—has been replaced in high-income countries by digital mammography [16], which offers radiation exposure reduction, easier integration with modern radiology information systems, higher workflow efficiency, and lower running costs, also boosting detection rates in young women and in women with dense breasts [16, 17]. The yet ongoing implementation of digital breast tomosynthesis (DBT) represented a further turning point. DBT is the true digital evolution of mammography and is able to significantly improve cancer detection rates in various age groups, regardless of breast density [18, 19]. At least

in some studies, DBT use also led to a reduction in recall rates, in particular when recall rates are relatively high [20]. However, the evidence of a significant reduction in interval cancer rates—which would robustly substantiate the use of DBT for breast cancer screening in the general population—has yet to be demonstrated [18, 21].

Fourth, contrast-enhanced breast magnetic resonance imaging (CE-MRI) has seen extensive introduction in clinical practice [22] and is routinely performed for all indications, save for breast implant integrity assessment, where unenhanced MRI scans remain sufficient [22–24]. While mammography and ultrasound only generated a morphological evaluation, CE-MRI offered a comprehensive assessment of morphologic and functional properties of breast tissues [22], with an unprecedented insight on in-vivo pathophysiological conditions tightly linked to carcinogenesis. Tumoral neo-angiogenesis invariably occurs when breast cancer grows larger than 2 mm, but is incapable of producing architecturally sound vessels [25]. Permeable ones are created instead, allowing for the extravasation of gadolinium-based contrast agents (GBCAs) and for their accumulation in the cancer stroma [26]. This results into modifications of local T1 properties easily recognizable on T1-weighted sequences [22], allowing to assess the wash-in and wash-out curve and its correlations with different tissue properties [26]. Contrast enhancement explains the steep increase in sensitivity of CE-MRI compared to ultrasound and mammography. CE-MRI sensitivity often approaches 95%–100%, as demonstrated by large-scale multicenter trials employing CE-MRI to screen high-risk women [27].

Analysis of five registries from the Breast Cancer Surveillance Consortium in the United States [28], across a five-year study period (2005–2009), showed that the diagnostic work-up of a non-MRI finding or of an otherwise unresolved clinical finding (40.3%) was the most common indication, followed by screening women at increased risk for breast cancer (31.7%), cancer staging before treatment (16.2%) and other mixed indications (11.8%).

Given the importance of breast MRI, detailed knowledge of GBCAs properties and of their administration effects is paramount to reach an appropriately tailored risk-benefit balance. While this balance is easily attained in symptomatic women—even more easily when MRI is performed for cancer staging—in other settings such as breast MRI screening this assessment should consider the fact that screened women are typically asymptomatic (i.e. over 95% healthy), are required to undergo an MRI examination yearly, and, if at high-risk, should begin screening at about 25–30 years of age.

## **0.2. Section outline**

In Chapter 1, we will introduce and discuss GBCAs physicochemical properties, the incidence of acute adverse reactions compared with the incidence observed after iodinated contrast agents (ICAs) administration, as well as the late effects of these agents, including nephrogenic systemic fibrosis (NSF) and tissue (primarily brain) gadolinium retention. The orientation of the breast imaging community towards the latter issues, in particular the risk of gadolinium retention, has up to now mirrored the aforementioned need to achieve a sound risk-benefit balance. Therefore, research about dose reduction strategies has been the chief focus when dealing with problem-solving or staging/preoperative breast MRI: we will present a study devoted to this topic in Chapter 3. Conversely, MRI screening still represents a partially uncharted territory, even for high-risk women, who were the first population to benefit from this approach: in Chapter 2 we therefore summarize the evidence pointing towards a positive risk-benefit balance in favor of continuing and extending CE-MRI screening of high-risk women.

# **1. Gadolinium-based contrast agents for breast MRI: uncertainties about brain gadolinium retention and clinical applications**

*Based on:*

Sardanelli F, Schiaffino S, Cozzi A, Carbonaro LA (2020) *Gadolinium-Based Contrast Agents for Breast MRI and Uncertainties About Brain Gadolinium Retention*. In: Sardanelli F, Podo F (eds) **Breast MRI for High-risk Screening**. Springer International Publishing, Cham, pp 63–82

## 1.1. Physicochemical properties of GBCAs used in breast MRI

According to breast cancer genesis theories, a subgroup of breast tumor cells showing an angiogenic phenotype determines two phenomena: tumor growth and the formation of new vessels from neighboring vascular structures, through the production of pro-neoangiogenic factors, such as the vascular endothelial growth factor [22, 25, 26, 29]. These new vessels show wider wall fenestrations which allow a permeability increase up to eight times that of normal breast glandular tissue. Furthermore, tumor interstitial space is 3–5 times larger than that of normal breast glandular tissue. After intravenous injection, MRI contrast agents permeate outside the new vessels and accumulate much more within the cancer tissue than in the normal glandular tissue. The presence of GBCAs can be indirectly observed as a reduction of water relaxation times, particularly on T1-weighted images, where an increased signal intensity in tissues with a higher GBCA concentration (or in which a GBCA with higher relaxivity is present) can be appreciated [29].

In clinical breast MRI, two-compartment (vascular/interstitial) paramagnetic GBCAs are used, typically at a standard dose of 0.1 mmol/kg of body weight, injected at a flow rate of 2–3 mL/s, and followed by saline flushing (20–30 mL) at the same flow rate [23]. These contrast agents are defined as “extracellular”, since they do not accumulate in organs nor they penetrate cell membranes, presenting a linear relationship between dose and tissue concentration. GBCAs are created by chelation of a gadolinium atom (a rare earth metal) with an organic ligand which suppresses the high toxicity of the  $Gd^{3+}$  ion by preventing its release and subsequent cell absorption.

Paramagnetic GBCAs can be subdivided:

1. according to the chemical structure of the chelating moiety into macrocyclic GBCAs (in which the  $Gd^{3+}$  ion is caged in the pre-organized cavity of the ligand) or so-called linear GBCAs (in which  $Gd^{3+}$  is coordinated with an open chain ligand structure);
2. according to the electric charge of the GBCA, either ionic or nonionic.

Macrocyclic GBCAs are generally considered more stable than linear GBCAs, while ionic linear GBCAs are more stable than nonionic linear GBCAs. The characteristics of GBCAs employed in breast MRI are summarized in Table 1.1.

Considering the intrinsic  $Gd^{3+}$  ion toxicity, the ligand must be highly selective for this ion and tightly bound to it in order to prevent its release into blood circulation and its possible binding to different cations (transmetallation). The stability of gadolinium chelates represents a very complex issue [30–32] and can be defined in several ways:

- i) the thermodynamic stability constant, which indicates the affinity of the unprotonated chelator for the metal ion; this parameter (which is determined at non-physiological pH 14) is determined by the in vitro energy required for the metalloligand to release the ion; of note, when thermodynamic stability is weak, the chelator more readily releases  $Gd^{3+}$  ions;
- ii) the thermodynamic conditional stability constant, which is a measure of the stability of the complex at physiological pH (note that its value at pH 7.4 is always substantially lower than the thermodynamic stability constant);
- iii) the selectivity constant which describes the transmetallation from a thermodynamic point of view (i.e. at equilibrium) and corresponds to the difference between the thermodynamic stability constants of the gadolinium chelate and other metalloligands (e.g. endogenous cations such as  $Fe^{3+}$ ,  $Ca^{2+}$ ,  $Mg^{2+}$ ,  $Zn^{2+}$ , and  $Cu^{2+}$  ions);
- iv) the kinetic rate of the metalloligands in vivo, estimated from their half-life dissociation.

The concept of kinetic and thermodynamic stability should be considered very carefully since it remains a somewhat controversial topic, especially in predicting the amount of  $Gd^{3+}$  ion which may result from dechelation in physiological or pathological situations [32]. Other important GBCAs characteristics are the elimination pathway (primarily renal, with the only exception of gadobenate dimeglumine which is partially eliminated [3–5% of the injected dose] by the hepatobiliary



pathway) and osmolality [30]. Importantly, the limited amount of GBCA administered for clinical use is insufficient to affect the overall plasma osmolality.

There is a positive correlation between GBCA relaxivity and the increase in signal intensity in those tissues in which GBCAs preferentially accumulate. Most GBCAs used for breast MRI (gadopentetate dimeglumine, gadoterate meglumine, gadoteridol, gadodiamide, gadobutrol, gadoversetamide) show variable  $r_1$ -relaxivities at 1.5 T, ranging from 3.6 to 5.3 l/mmol s<sup>-1</sup>. Instead, due to its weak and transient interaction with serum albumin, gadobenate dimeglumine has higher  $r_1$ -relaxivity (6.7–7.9 l/mmol s<sup>-1</sup> at 1.5 T) [33–36].

Because of this higher  $r_1$ -relaxivity, gadobenate dimeglumine demonstrates significantly better diagnostic performance for detection and characterization of breast lesions when compared to GBCAs with standard  $r_1$ -relaxivity [37–42]. Although an intra-individual study showed non-inferior diagnostic performance for gadobutrol compared to gadobenate dimeglumine for preoperative breast MRI [43], that study was criticized for its methodology and adopted assessment criteria [44, 45]. A more recent study comparing a three-quarter dose (0.075 mmol/kg) of gadobenate dimeglumine to a two-fold higher dose (0.15 mmol/kg) of gadoterate meglumine at 3 T, revealed significantly better breast lesion detection and characterization with the lower dose of gadobenate dimeglumine [46]. This was attributed to the fact that gadobenate dimeglumine has the highest available  $r_1$ -relaxivity while gadoterate meglumine the lowest.

Most GBCAs are formulated at a concentration of 0.5M. The only exception among GBCAs available for breast MRI is gadobutrol which is formulated at a two-fold higher concentration (1.0 M). This means that an equivalent volume of the gadobutrol formulation contains twice the number of GBCA molecules and that therefore the volume of gadobutrol necessary to achieve an approved dose is half that of the other available GBCAs. While this characteristic may be of interest for certain first-pass perfusion studies, for dynamic studies with a time resolution usually not less than 60 s, this higher concentration is diluted in the blood volume without any effect on signal increase.

The enhancement is therefore mainly determined by the GBCA r1-relaxivity, assuming otherwise identical imaging conditions. Recent studies [47, 48] have shown that the diagnostic performance of the higher concentration gadobutrol is similar to that of gadoterate meglumine, despite slightly higher relative enhancement with gadobutrol. The difference in relative enhancement can again be attributed to the fact that gadoterate meglumine has the lowest r1-relaxivity, while r1-relaxivity of gadobutrol is among the highest between available standard relaxivity GBCAs.

## **1.2. Acute adverse reactions to GBCAs**

Considering acute adverse reactions, contraindications to GBCAs administration in breast MRI are similar to those of other clinical applications. However, some particular issues should be taken into account.

Acute adverse reactions are categorized as allergic-like (also called anaphylactoid or idiosyncratic) or physiologic (non-allergic-like) and are classified by the American College of Radiology (ACR) [49] and European Society of Urogenital Radiology (ESUR) [50] according to severity (Table 1.2): mild (typically self-limiting, non-progressive, and not requiring treatment), moderate (commonly requiring treatment) or severe (life threatening, requiring immediate medical attention and treatment).

Most adverse reactions are mild physiologic reactions. Allergic-like reactions are uncommon and vary in frequency from 0.004% to 0.7% [51], with a mortality rate close to zero [52]. Overall, the incidence of acute adverse events falls between 0.1% and 0.45% [53, 54].

The ACR Manual on Contrast Media [49] states that the adverse event rate for GBCAs administered at clinical doses (0.1–0.2 mmol/kg for most GBCAs) ranges from 0.07% to 2.4%, while ESUR Guidelines on Contrast Agents [50] state that there is no difference in the incidence of acute adverse reactions among available extracellular GBCAs, also specifying that the incidence of adverse reactions is much lower for GBCAs compared to ICAs used in x-ray and computed

tomography procedures. Studies to compare adverse event rates after GBCAs and ICAs have corroborated this statement, showing that the relative risk for an acute adverse reaction is more than 5 times higher for low-osmolar ICAs than for GBCAs, while the relative risk for an acute adverse reaction requiring treatment is almost 3 times higher for ICAs [55] (Table 1.3).

No studies have assessed the relative risk for adverse reactions in a specific breast MRI setting yet. However, it has been shown that the incidence of adverse reactions may be higher for female than for male patients (odds ratio 1.687) and that there might be a correlation between the incidence of adverse reactions and the number of previous exposures to GBCAs [53].

When women with previous acute reactions to a GBCA or with a history of asthma or allergy to drugs or ICAs are referred to undergo breast MRI, it is appropriate to adopt one of the two elective prophylactic protocols suggested by the ACR [49]:

- prednisone 50 mg per os at 13 hours, 7 hours, and 1 hour before contrast administration, AND diphenhydramine 50 mg per os, intramuscularly, or intravenously, 1 hour before contrast administration [56];

or

- methylprednisolone 32 mg per os 12 hours and 2 hours before contrast administration; diphenhydramine 50 mg as in protocol 1 can be also added .

In addition, for patients with a previous acute reaction to GBCAs, the specific GBCA should be changed, ideally to one of a different class [57]. Above all, as with all MRI procedures, it is necessary that imaging departments are adequately prepared to deal with adverse reactions if and whenever they occur [49].

Above all, in any setting of breast MRI application—from screening to neoadjuvant chemotherapy monitoring—a tailored approach is necessary to ensure adequate women’s information.

For example, when MRI is used to annually screen high-risk women the risk-benefit balance could be particularly fragile and an open discussion of advantages and disadvantages of the MRI examination is needed, especially considering the alternative options to GBCA injection, such as: non-contrast imaging strategies combining mammography, digital breast tomosynthesis, ultrasonography (manual or automated), unenhanced MRI sequences (in particular DWI) [58, 59]; breast cancer chemoprevention [60, 61]; prophylactic mastectomy and/or oophorectomy [62]. In these high-risk women, the choice among all options—including annual performance of CE-MRI—frequently requires psycho-oncologic counselling.

### **1.3. Late effects of GBCAs: nephrogenic systemic fibrosis (NSF)—the perfect storm**

The assumption that GBCAs have a uniquely safe profile changed in 2006, when an association between gadodiamide and NSF was firstly described by Thomas Grobner [5]. The risk-benefit balance for this and other GBCAs became matter of a hot debate. NSF is not an imaging finding, but a very late and sometimes fatal adverse reaction to GBCA exposure that occurs in some patients already suffering from acute renal failure or severe chronic renal failure (estimated glomerular filtration rate [eGFR] lower than  $15 \text{ mL}/\text{min} \times 1.73 \text{ m}^2$ ) [49].

NSF is a scleroderma-like illness that typically presents from few weeks to years after exposure to one of the least stable GBCAs [63]. The most commonly held theory on the pathophysiology of NSF is that  $\text{Gd}^{3+}$  ions dissociate from their chelating ligands in the interstitial space forming insoluble salts (e.g. phosphates and carbonates) which are taken up by fibroblasts, ultimately causing fibrotic reactions that result in the symptoms exhibited by sufferers [64]. In patients with normal or moderate renal function GBCAs are excreted sufficiently rapidly before overt dechelation occurs. However, in patients with severely decreased renal elimination the ensuing prolonged GBCA retention favors greater opportunity for dechelation and subsequent fibrosis.

Initial symptoms are primarily skin lesions associated with swelling and pain, particularly in the upper and lower extremities from the ankles to below the knees, usually in a symmetrical manner. Subsequent sclerosis involving joints and major organs typically leads to reduced movement, with resultant significant disability and increased mortality. Unfortunately, there is still no specific treatment for this disease.

In 2007–2008, many international and national scientific societies, together with important health authorities, like the Food and Drug Administration (FDA) and the European Medicines Agency (EMA), established specific safety policies for GBCA use. Until recently, GBCAs were classified into three groups in terms of risk for NSF: high-risk (gadodiamide, gadopentetate dimeglumine, and gadoversetamide), intermediate risk (gadobenate dimeglumine), and low-risk (gadobutrol, gadoterate meglumine, and gadoteridol) [63, 65, 66]. However, concerns about potential long-term harm from gadolinium retention in the brain (see sub-chapter 1.4) prompted the EMA to suspend high-risk agents for all clinical applications and to restrict the intermediate risk agent gadobenate dimeglumine to liver imaging only. Although low-risk agents are still available for use in breast MRI, they are recommended to be used with caution in patients with eGFR lower than 30 mL/min $\times$ 1.73 m<sup>2</sup>. While serum creatinine testing (eGFR) is not mandatory for low-risk agents, it is recommended that at least questionnaire-based renal function screening is performed before their injection [49]. In the United States, the ACR [49] classified GBCAs available for breast MRI as belonging to group I GBCAs associated with the greatest number of NSF cases: gadodiamide, gadopentetate dimeglumine, and gadoversetamide) or group II GBCAs associated with few, if any, indisputable cases of NSF: gadobenate dimeglumine, gadobutrol, gadoteridol, gadoterate meglumine). Based on the lack of clinical evidence of harm associated with brain gadolinium retention, no GBCAs have been suspended from the market in the United States and all are still available for breast MRI. While underpinned by the same evidence, EMA recommendations are very different from the FDA and the ACR approaches.

Contraindication of the high-risk GBCAs in patients with severe chronic kidney disease, in both United States and Europe, reflects the fact that approximately 85% of unquestionable NSF cases were associated with gadodiamide, while the remaining others were associated primarily with gadopentetate dimeglumine and gadoversetamide [49]. Although a recent report notes that three indisputable cases of NSF occurred after administration of the macrocyclic GBCA gadobutrol [67, 68], all others occurred after administration of a simple linear GBCA. The contraindication of these three high-risk GBCAs, together with routine screening of kidney function and GBCA dose curtailing to no more than the approved one (0.1 mmol/kg of body weight), appears to have eliminated NSF as a current disease entity.

Notably, since 2007-2008, in many institutions worldwide serum creatinine testing (eGFR) became a routine practice and GBCAs use at a dosage higher than 0.1 mmol/kg was limited to few cases. A strong decrease of the number of NSF cases was observed after 2009, with rare isolated exceptions [69], and we currently consider NSF a disease of the past, as confirmed by a very recent systematic review reporting a total of 639 NSF cases, only seven of them after GBCA exposure after 2008 [70]. In this review [70], out of 525 patients with documented exposure to GBCAs, 307 had been administered with gadodiamide (58.5%), 49 with gadopentetate dimeglumine (9.3%), 6 with gadoversetamide (1.1%), gadobutrol (0.2%), gadobenate dimeglumine (0.2%), multiple GBCAs (7.8%), or unknown GBCAs (22.9%).

The emergence of NSF was a consequence of a “perfect storm” [71], arising from multiple factors such as: 1) a long-held belief that GBCAs were inherently safe even in patients with renal dysfunction; 2) off-label use of high (often triple or quadruple) doses of GBCAs particularly for MR angiography; and 3) late understanding of the link between GBCA administration and NSF, which mainly reflected the variable interval between injection(s) and disease onset. One important lesson from NSF is that the “available evidence” up until 2006 was in favor of a high safety of GBCAs also in patients with renal failure.

Discrepancies in NSF incidence between different countries were highlighted in 2014 by Thomsen [72]. Out of about 1,600 cases reported to the FDA, 93% came from the United States, 3% from various countries around the world and the remaining 4% came from Denmark, the only country in which a dedicate national investigation has been initiated. Thomsen estimates that, applying the Denmark incidence (20 per 1 million inhabitants) to Europe and North America, NSF patients, all disease degrees included, should be around ten thousand. Thus, even though no further cases of NSF have been reported after 2009, what we have seen is “the tip of the iceberg”. Thomsen’s conclusion has to be considered when discussing safety of GBCAs: NSF is still relevant [72].

Manifold consequences emerged in current practice. Among various positive effects on radiologists’ clinical practice, we have seen the following:

1. rethinking of the value of unenhanced MRI, and better exploitation of technical tools to allow for accurate diagnosis without GBCA injection;
2. screening patients for renal failure when GBCA injection is indicated;
3. halt (or limit) GBCAs administration in high-risk patients (those with an eGFR lower than  $30 \text{ mL/min} \times 1.73 \text{ m}^2$ );
4. stopping (or curtailing) the use of GBCA doses higher than  $0.1 \text{ mmol/kg}$ ;
5. administration of GBCA doses calculated as  $\text{mmol/kg}$  of body weight, ending the administration of fixed GBCA volumes such as 15 or 20 mL;
6. accurate description of GBCA type and dose for each patient in the technical section of the structured radiological report.

Although NSF risk seems to increase along with the number of doses for each examination and many reported cases occurred after multiple injections, records of the used GBCA and of the administered dose have often not been made available, making the knowledge about possible cumulative effects after multiple injections very limited [66].

To summarize, the application of screening policies for renal function and the use of a standard dose of 0.1 mmol/kg of GBCAs lowered the risk of NSF close to zero, even for those linear GBCAs related to the disease, whenever these guidelines were applied [73]. Depending on local regulations, questionnaires or mandatory serum creatinine and eGFR tests are required as screening for renal function before administering GBCAs. GBCA administration is contraindicated in patients with an eGFR below  $30 \text{ mL}/\text{min} \times 1.73 \text{ m}^2$  [49].

#### **1.4. Late effects of GBCAs: brain gadolinium retention**

Despite the absence of new NSF cases since 2010, concern over the risk of NSF was still rife when a first article by the group of Tomonori Kanda [6] appeared reporting T1-signal increases in the dentate nucleus and globus pallidus on unenhanced T1-weighted images after cumulative administration of gadopentetate dimeglumine or gadodiamide (i.e. two simple linear GBCAs) to patients with normal renal function [6]. Numerous reports based on studies performed in human subjects and animal models subsequently appeared, confirming that the appearance of T1-signal increases after cumulative administration of gadopentetate dimeglumine and gadodiamide, but not after the administration of macrocyclic GBCAs. The authors of these studies compared only one linear GBCA and one macrocyclic GBCA but titles and conclusions of the articles mentioned “class-based” differences [74]. With concern about NSF still fresh in mind, the assumption was that linear GBCAs release  $\text{Gd}^{3+}$  ions in a manner similar to that seen in NSF and that this  $\text{Gd}^{3+}$  is then retained in brain and body tissues indefinitely, likely bound to cellular proteins and macromolecules, leading to high  $r_1$ -relaxivity and thus visible T1-hyperintensity. Conversely, it was assumed that  $\text{Gd}^{3+}$  is not released from the more stable macrocyclic GBCAs, hence the lack of evident T1-signal increases.

Although it had been known for many years that gadolinium is retained in body tissues (primarily the bone [75]) after GBCA administration, the demonstration of T1-signal changes in the brain had



a profound, discordant and divisive effect, not only within the radiology community but also amongst patients and regulatory authorities. While no clinical manifestations or adverse clinical outcomes related to brain gadolinium retention have been observed following repeated administration of any GBCA, fear and concern revolve around potential long-term repercussions of gadolinium retention on human health.

Regulatory authorities have responded in very different ways to the gadolinium retention phenomenon. The EMA, concluding a GBCAs review according to data from the Pharmacovigilance Risk Assessment Committee, confirmed recommendations to suspend marketing authorizations of the simple linear GBCAs (gadopentetate dimeglumine, gadodiamide, and gadoversetamide) and to restrict the use of the substituted linear GBCA gadobenate dimeglumine just to liver imaging [76]. Then, as now, there was no evidence that gadolinium retention in the brain causes any harm to patients. Nevertheless, the rationale for this decision was “to prevent any risks that could potentially be associated with gadolinium brain deposition” [76].

Elsewhere, a very different approach has been adopted. Both the ACR and FDA [77] have independently issued statements affirming their positions, and no GBCA has been suspended from clinical use in the United States. The underlying message of both statements is: the radiologist is responsible for the decision to inject a GBCA and this decision should be based on a careful individualized assessment of the risk-benefit ratio, which takes into account not only the risk of acute reactions and potential late effects, but also the possibility of a missed diagnosis if the appropriate contrast-enhanced examination is not performed.

The clinical relevance of gadolinium brain deposition remains unknown. What is now clear, however, is that T1-signal changes can and do occur after administration of all GBCAs, both linear and macrocyclic. Although T1-signal increases are most frequently seen after administration of simple linear GBCAs, changes after administration of macrocyclic GBCAs are increasingly being reported [77]. Moreover, it is well-established that measurable amounts of gadolinium are retained

in brain and body tissues even after the administration of very small doses of both linear and macrocyclic GBCAs [78].

As stated by the Safety Committee of the International Society for Magnetic Resonance in Medicine [77] some commercially available macrocyclic agents might deposit less gadolinium than some linear agents; however, evidence shows that gadolinium deposition in the brain can also occur after the administration of macrocyclic agents [77]. The mistaken—albeit widespread—belief which holds that gadolinium retention is exclusively associated with linear GBCAs, has been dispelled: while less sensitive studies that rely upon visually observable changes in T1-weighted MRI signal do not suggest macrocyclic agents deposit gadolinium within brain tissues, more quantitative mass spectrometry data from multiple sources have confirmed that they do, albeit at lower levels. Further, other studies using mass spectrometry have revealed that gadolinium deposition rates for linear and macrocyclic agents vary within a given class, and that different chemical forms of gadolinium (i.e. different gadolinium complexes) appear to be depositing within tissues, some of which would be undetectable using MRI. Therefore, although MRI signal changes led to the observation that gadolinium was being deposited in the brain, they are less reliable for determining the quantity of gadolinium deposition in general. This is particularly true for gadolinium species that are not detectable with MRI and for lower concentrations of retained gadolinium [77].

It is therefore clear that T1-signal changes suggestive of gadolinium retention are common to all GBCAs, even though visible effects on T1-signal are predominantly seen after cumulative administration of linear GBCAs. The key questions, which remain to be answered, relate to the form in which gadolinium is retained and to whether gadolinium retention entails any clinical risk. Regarding the form in which gadolinium is retained, it is possible that macrocyclic GBCAs are retained intact in tissues, reflecting their greater stability. However, even here, there are differences between macrocyclic GBCAs in terms of retained amounts and their elimination speeds [79]. In the case of linear GBCAs there appear to be large differences between simple linear GBCAs and the

substituted linear GBCA gadobenate dimeglumine [80]. Whether the T1-signal increases seen with linear GBCAs reflect gadolinium release, and its subsequent binding to macromolecules and cellular proteins, remains to be seen. This may be the case for simple linear GBCAs mirroring a mechanism analogous to that seen in NSF. However, no NSF cases have been associated yet with the substituted GBCA gadobenate dimeglumine; again, there may be differences between individual GBCAs within each class, with some retained as intact GBCA and others (principally the simple linear GBCAs) as a mix of intact GBCA and dechelated gadolinium bound to macromolecules.

As to whether retained gadolinium poses a long-term risk to human health, no clinical consequences and no neurological symptoms have hitherto been associated with this phenomenon. Although only a few years passed since the first report of T1-hyperintensities in the brain following GBCA administration [6], more than 30 years have passed since the first GBCA, gadopentetate dimeglumine, was approved for use in humans, and still no long-term effects have been reported, apart from NSF which was effectively dealt with by the contraindication of the simple linear GBCAs.

Studies that assessed potential long-term harm following GBCA administration have frequently focused on patients with multiple sclerosis since these patients typically undergo regular follow-up with CE-MRI examinations and thus receive relatively large volumes of GBCA over a period of many years. Although one retrospective study attempted, somewhat tenuously, to correlate increased signal intensity in the dentate nucleus and globus pallidus with loss of verbal fluency in long-term multiple sclerosis patients [81], other studies revealed no evidence of harm associated with gadolinium exposure [82, 83]. Indeed, since multiple sclerosis is associated with wide-ranging and worsening neurological symptomatology, it is extremely difficult to differentiate potential effects of cumulative GBCA administration from normal disease progression.

Another important study in patients older than 66 years who underwent an initial non-brain/spinal MRI found no effect of GBCA on the incidence of parkinsonism [84]. Specifically, the incidence of

parkinsonism was 1.16% amongst patients never exposed to GBCAs and 1.17% amongst patients exposed to GBCAs. Adjusted analyses showed no significantly increased risk of parkinsonism among patients with cumulative gadolinium exposure to GBCAs compared with those who underwent unenhanced MRI (hazard ratio 1.04, 95% confidence interval, 0.98–1.09). This is a particularly important finding given the physiological roles of the dentate nucleus in the extrapyramidal system, including planning, initiation and control of voluntary movements [77]. Finally, in patients affected by Crohn disease, who also regularly undergo CE-MRI and show gadolinium-related dentate nucleus hyperintensity on T1-weighted images, no resting-state functional connectivity changes were found [85].

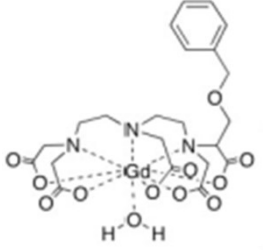
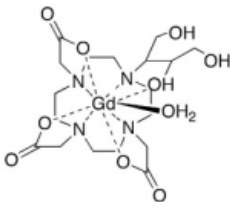
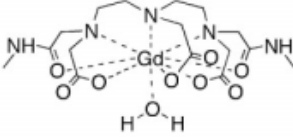
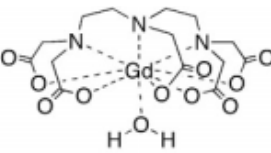
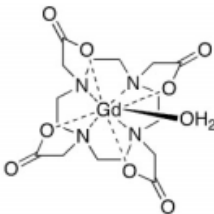
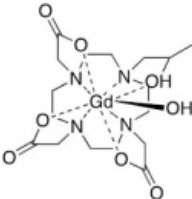
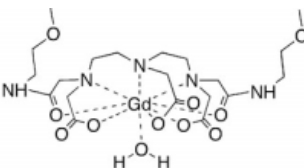
Continuous re-evaluation of available evidence on GBCAs late effects is needed, in particular of brain gadolinium retention. This field requires high-quality multicenter studies on T1-shortening of human tissues as a late effect after GBCA injection, as highlighted by the United States National Institute of Health [86]. However, it is paramount to plan studies with higher methodological quality than those we have had so far, possibly prospective in design and with minimized confounding factors, aiming to reduce the uncertainties we still have in this topic.

The research roadmap outlined by the 2018 NIH/ACR/RSNA Workshop [87] defined the following major priorities: to determine (a) if gadolinium retention adversely affects the function of human tissues; (b) if retention is causally associated with short- or long-term clinical manifestations of disease; and (c) if vulnerable populations, such as children, are at greater risk for experiencing clinical disease. We agree on these priorities and also on the fact that *women undergoing breast cancer screening or men undergoing prostate cancer screening without known central nervous system abnormality* are ideal normal populations to be compared with a healthy unexposed population using standardized neurologic assessments. Another interesting possible line of research might be GBCA dose reduction: here the natural candidates are high-relaxivity GBCAs such as gadobenate dimeglumine but this research could also be performed with gadobutrol, gadoterate

meglumine, or gadoteridol, as will be shown in Chapter 3. Even the old simple adjustment of the contrast dose for the patient's body weight may be changed into adjustments for body composition, considering that different proportions of fat and muscle imply different biodistribution volumes for extracellular contrast agents [88], a perspective that could reduce GBCA doses in post-menopausal women.

In conclusion, although research into potential long-term effects of GBCA administration is necessary and ongoing, initial findings have not revealed any detrimental effects. For breast MRI, these concerns are of lesser importance when the examination is to be performed one time only or at most 2 or 3 times during a lifetime (as in most settings, including cancer staging), but are of paramount relevance in the special case of breast CE-MRI usage as a screening procedure.

**Table 1.1** Gadolinium-based contrasts agents commonly used for breast CE-MRI

Generic name	Gadobenate dimeglumine	Gadobutrol	Gadodiamide	Gadopentetate dimeglumine	Gadoterate meglumine	Gadoteridol	Gadoversetamide
Brand name	MultiHance®	Gadovist®	Omniscan®	Magnevist®	Dotarem®	ProHance®	OptiMARK®
Chemical name	Gd-BOPTA	Gd-BT-DO3A	Gd-DTPA-BMA	Gd-DTPA	Gd-DOTA	Gd-HP-DO3A	Gd-DTPA-BMEA
Structural formula							
Manufacturer	Bracco, Italy	Bayer Healthcare, Germany	General Electric Healthcare, USA	Bayer Healthcare, Germany	Guerbet, France	Bracco, Italy	Mallinckrodt, USA
Molarity (mol/l)	0.5	1.0	0.5	0.5	0.5	0.5	0.5
Molecular structure	Linear	Cyclic	Linear	Linear	Cyclic	Cyclic	Linear
Charge	Ionic	Nonionic	Nonionic	Ionic	Ionic	Nonionic	Nonionic
Osmolality (mOsm/kg H <sub>2</sub> O at 37°C)	1970	1603	650	1960	1350	630	1110
r1-relaxivity at 1.5 T (l/mmol s <sup>-1</sup> )	6.3, 6.7, or 7.9	4.7, 5.2, or 5.3	4.3 or 4.6	3.9, 4.1, or 4.3	3.6 or 4.2	4.1 or 4.4	4.7 or 5.2
Thermodynamic stability constant (log K <sub>therm</sub> )	22.6	21.8	16.8	22.1	25.4	22.8	16.6
Conditional stability constant at pH 7.4	18.4	14.7	14.9	17.7	18.8	17.1	15.0
Elimination half-life (minutes, mean ± SD)	72 ± 5	NA	77.8 ± 16	94 ± 11	91 ± 14	94.2 ± 4.8	103.6 ± 19.5
Elimination pathway	Renal 97%, biliary 3% <sup>1</sup>	Renal	Renal	Renal	Renal	Renal	Renal

Sources: references [29–37]. NA, not available. Gadoversetamide is no longer available for clinical use. It is included in this Table for the sake of completeness.

Take into account that r1-relaxivity values can change according to the method of measure: they depend on serum albumin concentration in plasma used for in vitro measures [34].

<sup>1</sup> In patients with renal impairment, the amount excreted into the bile increases to 7% to 8%.

**Table 1.2** Categories of acute adverse reactions to contrast agents

<b>Grade</b>	<b>Subtype</b>	<b>Signs/symptoms</b>
Mild (self limiting)	Allergic like	Limited urticaria/pruritis; limited cutaneous edema; limited <i>itchy/scratchy</i> throat; nasal congestion, sneezing/conjunctivitis/rhinorrhea
	Physiologic	Limited nausea/vomiting; transient flushing/warmth/chills; headache/dizziness/anxiety/altered taste; mild hypertension; vasovagal reaction that resolves spontaneously
Moderate (requiring treatment)	Allergic like	Diffuse urticaria/pruritis; diffuse erythema with stable vital signs; facial edema
	Physiologic	Protracted nausea/vomiting; hypertensive urgency; isolated chest pain; vasovagal reaction requiring (and responsive to) treatment
Severe (life-threatening)	Allergic like	Diffuse edema, or facial edema with dyspnea; diffuse erythema with hypotension; laryngeal edema with stridor and/or hypoxia; wheezing/bronchospasm, significant hypoxia; anaphylactic shock (hypotension and tachycardia)
	Physiologic	Vasovagal reaction resistant to treatment; arrhythmia; convulsions, seizures; hypertensive emergency

Modified from [49]

**Table 1.3** Acute adverse reactions (AARs): comparison between gadolinium-based contrast agents (GBCAs) and low-osmolar iodinated contrast agents (LOICAs)

	<b>GBCAs</b>	<b>LOICAs</b>	<b><i>p</i> value<sup>1</sup></b>
Number of doses	158439	298491	
Total AARs	45	458	
Incidence	0.028% (0.021–0.038%)	0.153% (0.140–0.168%)	< 0.001
Relative risk	1.00	5.40	
AARs requiring treatment	15	79	
Incidence	0.009% (0.005–0.016%)	0.026% (0.021–0.033%)	< 0.001
Relative risk	1.00	2.80	
AARs requiring transfer to emergency department	6	10	
Incidence	0.004% (0.001–0.008%)	0.003% (0.002–0.006%)	0.812
Relative risk	1	0.88	
Deaths	0 (0.000–0.002%)	1 (0.000–0.019%)	

Calculations on data from Hunt et al [55]; in parentheses, 95% confidence intervals calculated according to the binomial distribution. Here we opted for calculating the relative risk instead of the odds ratio because, even though data come from a retrospective analysis, the authors did not enroll cases of acute reactions verifying how many of them were exposed; they instead analyzed two concurrent prospective series of patients exposed to GBCAs or LOICAs, evaluating how many of them had adverse reactions. However, in this case, due to the very small number of events compared to the number of exposures, the relative risk and the odds ratio gave equivalent results.

<sup>1</sup>  $\chi^2$  test





## **2. Gadolinium retention and breast MRI screening: more harm than good?**

*Based on:*

Sardanelli F, Cozzi A, Trimboli RM, Schiaffino S (2020) *Gadolinium Retention and Breast MRI Screening: More Harm Than Good?* **Am J Roentgenol** 214:324–327. doi:10.2214/AJR.19.21988

## 2.1. Breast CE-MRI before and after *BRCA* genes discovery

As already hinted in the previous chapter, several advantages favored breast applications of contrast-enhanced (CE)-MRI: high sensitivity, absence of ionizing radiation exposure, no need of breast compression, lack of known relevant adverse effects of GBCAs. In particular, when GBCAs were compared to ICAs, the frequencies of all immediate adverse effects (especially hives and nausea) were reported to be 0.04% versus 0.13%, of those requiring treatment 0.01% versus 0.03% [55]. From 2004 to 2009, in the United States, the incidence of GBCA-associated deaths was reported to be 0.2–2.7 per million doses [73]. Non-negligible disadvantages of breast MRI were: need to enter a closed magnet, relatively long examination time, high cost, and—last but not least—the “mantra” about *low specificity of breast MRI* [89]. This attribution of low specificity to breast MRI was due to several factors, mainly to the lack of standardized interpretation criteria such as the MRI Breast Imaging Reporting and Data System, only introduced in 2003 [24], and to the fact that studies reporting low specificity of breast MRI for small series of lesions sent to surgery received more attention than very large studies reporting high specificity [89].

In mid-1990s, while the debate on breast MRI indications was ongoing, the discovery of *BRCA1* and *BRCA2* mutations and the increased general knowledge of breast cancer risk stratification encouraged studies on MRI screening of high-risk women. Results were strongly in favor of the new modality, with a huge advantage in terms of sensitivity versus mammography and/or ultrasonography along with a high specificity, a good answer to the aforementioned “mantra”. In 2007, the American Cancer Society issued the first guideline [90] recommending breast CE-MRI *as an adjunct to mammography* for women with  $\geq 20$ –25% lifetime risk (LTR), including those with a strong family history of breast/ovarian cancer or previous thoracic irradiation. Other guidelines on this topic followed in many countries, in some cases adopting a higher LTR threshold for breast MRI screening, as was for the National Institute for Clinical Excellence (United Kingdom) that suggests breast MRI screening in the presence of LTR  $\geq 30\%$  [91]. Conversely, keeping the LTR

cutoff  $\geq 20\%$ , breast MRI screening should be considered also for women with pathogenic variants detected in moderate-risk genes or with newly discovered suspected genes [92].

Therefore, while further indications to breast MRI were discussed (and still are, as in the case of preoperative setting), the medical community accepted breast MRI screening of high-risk women in the absence of outcome data, considering the huge sensitivity gap in high-risk population as a self-sustaining evidence. Studies showed that no additional diagnostic power is given by mammography and/or ultrasound to screening MRI [93–99] supporting the *MRI alone* approach, avoiding mammography, especially for *BRCA* and *TP53* mutation carriers who have a higher radiosensitivity/radiosusceptibility [100]. Even though this advice has translated into a guideline [23] only for *BRCA* mutation carriers below 35 years of age and for *TP53* mutation carriers without age limitations, this is a general issue to be taken into consideration.

## **2.2. Risk-benefit balance for breast MRI screening**

What is the balance between CE-MRI breast screening benefit (its high sensitivity) and the possible risks associated to yearly repeated GBCA injections? A specific patient-tailored approach should take into account breast cancer risk as estimated using a variety of tools and models, also considering breast density. An LTR  $\geq 20\%$  is commonly accepted as a threshold for CE-MRI breast screening, even though, as mentioned above, some countries such as the United Kingdom adopted the LTR  $\geq 30\%$  threshold [91]. However, *BRCA/TP53* mutation carriers and women who underwent thoracic irradiation have a 40–50% or greater LTR, representing a *very* high-risk group. For *BRCA* mutation carriers, especially *BRCA1* mutation carriers, not only yearly breast CE-MRI but also prophylactic mastectomy is justified, even more when contralateral to a first breast cancer diagnosis. Indirect evidence for a positive impact of MRI (combined with modern therapies) on patient outcome has been reported [101, 102]. We are in favor of extending a breast MRI screening strategy to women with  $\geq 20\%$  LTR (even if *BRCA/TP53* wild-type), in agreement with the results

from a recent randomized controlled trial [103, 104]. Of course, considering both the available evidence and the setting of repeated injections, preference has always to be given to macrocyclic versus linear GBCAs and, among them, possible differences in diagnostic power and washout rate have to be taken into account.

Below the 20% LTR threshold, we enter a largely unexplored territory, where the sensitivity gap may be not enough. For women at intermediate or average risk (10–19% LTR), including patients with previous history of sporadic breast cancer, risk-benefit balance estimation is uncertain. On one side, abbreviated CE-MRI protocols have been demonstrated to reduce test duration and costs without impairing the high sensitivity [105]. On the other side, as we know from the rules of evidence-based medicine, a large-scale application of a screening practice requires a demonstration in terms of patients' outcome. An increased sensitivity is not enough (how much overdiagnosis?), especially in presence of the aforementioned uncertainties.

A very recent study by Wernli et al. [106] reported on over 13,000 women each with a previous history of breast cancer who underwent about 34,000 mammograms and 2,500 MRIs. Breast MRI was associated with significantly higher cancer detection rate (odds ratio [OR] 1.7) and biopsy rate (OR 2.2) than mammography alone. However, no significant differences were found for sensitivity or interval cancer rate. Further studies are necessary to address uncertainty about extending breast MRI screening to women of average risk. As previously stated, for high-risk women, the use of macrocyclic GBCAs is preferred.

### **2.3. Perspectives**

Various new approaches need to be investigated, potentially driving plot twists in this story. Only two major examples: 1) GBCA dose reduction, also obtained using artificial intelligence to generate virtual full-dose images from (very) low-dose images, as already reported for brain applications [107]; 2) use of unenhanced breast MRI for cancer detection, mainly based on diffusion-weighted

sequences [108, 109]. While waiting for clinical application of these techniques, a word of caution should be said on the introduction of breast MRI screening for non-high-risk women: regarding possible late effects of dozens of GBCA injections, we should remember that *the absence of evidence is not the evidence of absence* but also that *evidence of presence is not evidence of harm*. When offering breast MRI screening, we inform women about the risk-benefit balance; for non-high-risk women, we must also strive to communicate a higher grade of uncertainty, as a transparent approach fostering patient empowerment.



### **3. Accuracy and inter-reader agreement of breast MRI for cancer staging using 0.08 mmol/kg of gadobutrol**

*Published as:*

Cozzi A, Buragina G, Spinelli D et al (2021) *Accuracy and inter-reader agreement of breast MRI for cancer staging using 0.08 mmol/kg of gadobutrol*. **Clin Imaging** 72:154–161.

doi:10.1016/j.clinimag.2020.11.014



### 3.1. Abstract

**Background:** Evidence on gadolinium brain accumulation after CE-MRI prompted research in dose reduction. This study aimed to estimate accuracy and inter-reader reproducibility of tumor size measurement of breast MRI using 0.08 mmol/kg of gadobutrol.

**Methods:** We retrospectively analyzed all women who underwent 1.5 T breast MRI for cancer staging at our department with 0.08 mmol/kg of gadobutrol. Two readers (R1 and R2, 12 and 3 years experience) measured the largest lesion diameter. Accuracy was estimated both as correlation with pathology and rate of absolute (>5 mm) overestimation and underestimation, inter-reader reproducibility using the Bland–Altman method. Data are given as median and interquartile range.

**Results:** Thirty-six patients were analyzed (median age 56 years, 49–66) for a total of 38 lesions, 24 (63%) mass enhancement, 14 (37%) non-mass enhancement. Histopathological median size (mm) of all lesions was 15 (9–25): 13 (9–19) for mass lesions, 19 (11–39) for non-mass lesions. On MRI, R1 measured (mm) 14 (10–22) for all lesions, 13 (10–19) for mass lesions, 19 (11–49) for non-mass lesions. MRI-pathology correlation was very high for all lesion categories ( $\rho \geq 0.766$ ). On MRI, R1 overestimated lesion size in 6 cases (16%), and underestimated in 3 (8%); R2, overestimated 7 cases (18%) and underestimated 3 cases (8%). At inter-reader reproducibility analysis (mm): bias 0.9, coefficient of reproducibility 13 for all lesions; -0.1 and 6 for mass lesions; 2.5 and 20 for non-mass lesions.

**Conclusions:** Breast MRI may be performed using 0.08 mmol/kg of gadobutrol with high accuracy and acceptable inter-reader agreement.

### **3.2. Introduction**

In the scenario—outlined in the previous chapters—of an increased focus on research about GBCA dose-reduction strategies in breast MRI, two recent studies reported on the use of a reduced GBCA dose in breast MRI: the first one compared gadobenate dimeglumine at 0.075 mmol/kg and gadoterate meglumine at 0.15 mmol/kg using a 3 T unit, showing the non-inferiority of the former over the latter for breast lesion detection [46]. The latter study showed that tumor size measurements on 3 T breast MRI with 0.05 mmol/kg of gadobutrol correlate well with pathology measurements ( $\rho = 0.630$ ) [110].

If a reduced dose of GBCAs is to be used for preoperative breast MRI also at 1.5 T, it is paramount to first verify that GBCA dose reduction does not hinder both lesion size accuracy and reproducibility. In fact, a reduced dose could result not only in a reduced signal intensity but also in a smaller extent of the enhancement area.

Therefore, the aims of this study were: 1) to estimate the accuracy of tumor size measurement of breast MRI performed at 1.5 T using 0.08 mmol/kg of gadobutrol; and 2) to estimate the inter-reader reproducibility of this measurement between an expert radiologist and a radiology resident.

### **3.3. Methods**

#### *Study design and population*

This retrospective monocentric study was approved by the competent Ethics Committee (protocol code SenoRetro; approved on November 9<sup>th</sup>, 2017 and amended on July 18<sup>th</sup>, 2019). We evaluated all patients who underwent an MRI examination of the breast for cancer staging at the Radiology Department of IRCCS Policlinico San Donato (San Donato Milanese, Italy) between September 1<sup>st</sup>, 2017 and December 31<sup>st</sup>, 2018.

All MRI examinations were performed according to the EUSOMA recommendations [23], in particular to: patients with a newly diagnosed invasive lobular cancer, patients at high-risk for breast cancer, and patients with discrepancy in size  $>1$  cm between digital mammography and breast ultrasound, with expected impact on treatment decision. Patients were excluded from analysis if: the final pathology report was not available or incomplete; they received neoadjuvant therapy before the MRI examination; spatial correlation between MRI and pathology was unclear. In all analyzed patients, malignancy was confirmed by core-needle or vacuum-assisted biopsy and all underwent breast surgery.

### *MRI technique*

All breast MRI examinations were performed using a 1.5 T unit (Magnetom Symphony, Siemens Healthineers, Erlangen, Germany) in prone position using a bilateral 4-channels breast coil. The imaging protocol included unenhanced and enhanced sequences. Before contrast administration, T1-weighted gradient-echo, T2 fat-saturated short-tau inversion recovery, and diffusion-weighted axial sequences were acquired. Five gradient-echo three-dimensional fast low angle shot axial sequences (without using fat saturation technique) were obtained for the dynamic study, one before and four after injection. All patients were administered 0.08 mmol/kg of gadobutrol at a flow rate of 2 mL/s, followed by 20 mL of saline solution at the same injection rate using an automatic injector (Spectris Solaris, Medrad, Pavia, Italy). This reduced dose was adopted as standard practice in consideration of EMA [76] and FDA guidelines [111].

Technical parameters of the T1 dynamic sequences were: repetition time 11 ms, echo time 4.89 ms, flip angle  $45^\circ$ ; echo train length 1, number of excitations 1, slice thickness 1.3 mm; matrix  $512 \times 512$ ; field of view of  $38 \times 41$  cm, and duration 120 s. The acquisition time of the dynamic study was about 8 minutes. Unenhanced T1-weighted images were subtracted from contrast-enhanced images and four subtraction sets were automatically produced on a pixel-by-pixel basis.

### *Image analysis*

All measurements were made on axial subtracted images, selecting the slice with greater evidence of tumor contrast enhancement, as the evaluation of enhancing lesions in non-fat-saturated images could have affected the correct visibility of lesions' margins. Two independent readers with 12 years (a board-certified radiologist with fellowship-level training in breast imaging, R1) and 3 years (a radiology resident in his last year of training, R2) of experience in breast MRI measured the largest lesion diameter using a reporting workstation. For multifocal or multicentric tumors, the largest lesion was considered, while bilateral tumors were considered separately. Both readers were aware of patient clinical history, tumor localization (side and quadrant) and pathological features. Size measurements were performed by R1 at the time of the original reporting, and by R2 (blinded to R1 original measurements) only for this study purpose.

### *Final pathology*

Pathological data were obtained from reports of surgical specimens, where the largest diameter was reported. Microscopic analysis was performed on regular format sections. As for breast MRI, lesion size was reported as the widest diameter for both single and multifocal/multicentric tumors. Tumors were categorized into pathological groups, by histology, and by four molecular subtypes: luminal A (ER and/or PR positive, Ki-67  $\leq$  20%, HER2 negative), luminal B (ER and/or PR positive, Ki-67  $>$  20% or HER2 positive), HER2 positive (ER negative, PR negative, HER2 positive), and triple negative (ER negative, PR negative, HER2 negative).

### *Statistical analysis*

Accuracy of tumor size was estimated using a two-level analysis: first, bivariate correlation between MRI and pathology was calculated using the Spearman correlation coefficient and the Wilcoxon test for paired data; correlation strength was categorized as proposed by Evans [112]. Subgroup analysis was performed for mass and non-mass lesions. Second, differences in tumor size between

MRI and pathology were considered. When the absolute difference was between -5 mm and 5 mm the MRI measurement was considered correct; when the absolute difference was over 5 mm, the MRI measurement was considered overestimated; when the absolute difference was smaller than 5 mm, the MRI measurement was considered underestimated. The choice of the 5 mm cut-off was determined by its adoption by previous studies and considering its clinical relevance [113, 114]. Inter-reader reproducibility was estimated using the Bland–Altman method [115]. We calculated differences in tumor size between the two compared datasets, the mean of this distribution representing the bias, the standard deviation representing the coefficient of repeatability (CoR). This analysis was performed both for mass and non-mass tumors.

Continuous variables were reported as median and interquartile range (IQR), while categorical variables as counts and percentages. All analyses were performed with SPSS (version 26.0, IBM),  $p$  values  $< 0.05$  being considered statistically significant.

### **3.4. Results**

#### *Study population*

From September 1<sup>st</sup>, 2017 to December 31<sup>st</sup>, 2018, 44 women underwent a breast MRI examination for cancer staging. A total of 8 women were excluded from our analysis because of the following reasons: five had an incomplete or altogether unavailable final pathology report; two had already received neoadjuvant therapy; one patient had an unclear spatial correlation between MRI and pathology. Thus, statistical analysis was ultimately performed on 36 women, two of them with a bilateral tumor, for a total of 38 tumors. Age ranged from 41 to 76 years, with a median of 56 years (IQR 49–66 years).

At breast MRI, 24 lesions (63%) were described as mass enhancement, 14 (37%) as non-mass. Two out of 36 patients (6%) had a bilateral tumor, while two other patients (6%) had a multifocal and

multicentric cancer, respectively. Notably, one bilateral lesion was found at MRI and in the other one MRI confirmed mammographic and ultrasonographic findings. Table 3.1 summarizes main tumor characteristics.

#### *Lesion size distribution and measurement accuracy*

Median lesion size at final pathology of all lesions was 15 mm (IQR 9–25 mm): 13 mm (IQR 9–19 mm) for mass lesions, and 19 mm (IQR 11–39 mm) for non-mass lesions. At MRI, the median size obtained by R1 was 14 mm (IQR 10–22 mm) for all lesions, 13 mm (IQR 10–19 mm) for mass lesions, and 19 mm (IQR 11–49 mm) for non-mass lesions. On MRI, R2 obtained a 20 mm median size (IQR 10–21 mm) for all lesions, a 21 mm median size (IQR 10–22 mm) for mass lesions, and a 21 mm median size (IQR 10–23 mm) for non-mass lesions. Comparison between final pathology and MRI was not statistically significant in all cases ( $p \geq 0.549$  for R1;  $p \geq 0.890$  for R2).

Bivariate size correlation between final pathology and MRI obtained by R1 was very strong ( $\rho = 0.877$ ) for all lesions and for non-mass lesions ( $\rho = 0.942$ ), strong for mass lesions ( $\rho = 0.766$ ); it was very strong for R2 in all cases ( $\rho = 0.915$  for all lesions;  $\rho = 0.831$  for mass lesions;  $\rho = 0.958$  for non-mass lesions). All correlation coefficients were statistically significant ( $p < 0.001$ ).

Compared to final pathology, R1 overestimated tumor size in 6 cases (16%) and underestimated tumor size in 3 cases (8%). R2 overestimated tumor size in 7 cases (18%) and underestimated tumor size in 3 cases (8%). Therefore, tumor size on MRI was overestimated or underestimated of more than 5 mm by both R1 in 9 cases (24%) and R2 in 10 cases (26%). Fig. 3.1, Fig. 3.2, Fig. 3.3, and Fig. 3.4 depict four cases of different inter-reader and reader-pathology agreement in tumor size measurement.

#### *Inter-reader reproducibility*

Comparing R1 and R2 measurements on all lesions, we obtained an overall mean diameter of 20.4 mm, a bias of 0.9 mm, and a CoR of 13 mm, respectively; Fig. 3.5 shows the Bland–Altman plot.

When considering mass lesions, we obtained an overall mean diameter of 14.3 mm, a bias of -0.1 mm, and a CoR of 6 mm (Fig. 3.6). When considering non-mass lesions, we obtained an overall mean diameter of 31.5 mm, a bias of 2.5 mm, and a CoR of 20 mm (Fig. 3.7).

### **3.5. Discussion**

In this study we aimed to estimate the accuracy in tumor size measurement of gadobutrol-enhanced breast MRI performed with a 20% reduced gadobutrol dose (0.08 mmol/kg), using histopathology as reference standard. Moreover, we estimated inter-reader reproducibility between an expert breast radiologist and a final-year resident.

Accuracy of breast MRI was first evaluated as the correlation coefficient between pathology size and MRI size, resulting in a strong or very strong correlation ( $\rho = 0.766\text{--}0.958$ ) for all lesions, mass lesions, and also non-mass lesions, in accordance with findings from studies with a standard (0.1 mmol/kg) or higher dose of GBCA. Onesti et al. [113] found a correlation coefficient of 0.650 in 91 tumors, while Yoo et al. [114] and Mann et al. [116] found a correlation coefficient of 0.875 in 307 patients and of 0.862 in 49 lesions from high-risk patients, respectively. In addition, as in our study, a good accuracy of MRI measurements was specifically observed in tumors appearing as non-mass lesions [117], despite the frequently reported low concordance between MRI and pathology for this category of tumors [118].

The second statistical method used to estimate measurement accuracy was to consider a threshold defining overestimation or underestimation of tumor size. As reported, we used an absolute cut-off value of 5 mm. Using this cut-off, both our readers obtained comparable or better results (ranging 8–18% of all cases) than those reported in previous studies with a 5 mm cut-off and a standard or higher GBCA dose. Indeed, in these studies, overestimation occurred in 11–56% of cases, while underestimation in 7–27% [113, 114, 117, 119, 120]. Our data therefore indicate that a reduced

gadobutrol dose is not associated with a loss of accuracy in tumor measurements, good accuracy being obtained by both readers without significant impact from different breast MRI experience.

Agreement in tumor size estimation between R1 and R2 was relatively good. The bias, as the mean difference between measurements, was 0.9 mm for all measurements, being as low as 0.1 mm for mass lesions. As expected [118], a higher bias (2.5 mm) was observed for non-mass lesions.

Intrinsic measurement variability of non-mass lesions—whose larger dimensions make them prone to fluctuations in size estimation (Fig. 3.7)—may moreover explain the apparently suboptimal CoR (representing largest size differences), which was 13 mm for all lesions, i.e. the mean between 6 mm (mass lesions) and 20 mm (non-mass lesions). This variability may appear not negligible if compared to mean tumor size, especially in case of conservative surgery, but we should not forget that: surgeons usually apply wide resection margins of at least 10 mm; conservative therapy is usually followed by radiotherapy; and that patients with tumors > 2 cm can benefit from neoadjuvant therapy [121]. Thus, differences in tumor size between readers as observed in our study may not substantially impact patient management.

As already mentioned, there are only two studies evaluating the performance of breast MRI with a reduced GBCA dose, both having been performed on 3 T MRI units. The first study was centered on diagnostic performance [46], comparing 0.075 mmol/kg of gadobenate dimeglumine and 0.15 mmol/kg of gadoterate meglumine. While sensitivity in tumor detection with gadobenate (85%–89%) was comparable to that of gadoterate (85%–91%), gadobenate demonstrated higher specificity (96%–99% versus 93%–97%) and accuracy (96%–98% versus 94%–96%) compared with gadoterate. The second study found that breast MRI performed with half-dose gadobutrol had an overall good contrast enhancement conspicuity, good correlation with pathological size ( $\rho = 0.63$ ) and a high tumor detection rate (49/49 cancer detected) [110]. The main hypothesis driving our work, i.e. that a reduced gadobutrol dose would not ultimately hamper overall diagnostic performance and exam quality of breast MRI (nor lesion measurement when breast MRI is



performed for cancer staging) was corroborated by these studies suggesting that a reduced dose of GBCAs with higher relaxivity may be used to obtain an accurate exam on 3 T magnets. We showed that this is probably also true for 1.5 T MRI, considering that GBCA relaxivities are greater at 1.5 T than at 3 T [122]. However, if we consider specifically size correlations, our values are higher than those reported in the second study [110] and therefore a 0.08 mmol/kg dose of gadobutrol may be better than a 0.05 mmol/kg dose in terms of tumor size measurement.

Limitations of this study—apart from its retrospective nature and its small sample size—include the lack of intraindividual comparison with breast MRI performed with a full gadobutrol dose, the limited number of compared readers, and the lack of lesion-by-lesion analysis for multifocal and multicentric tumors. The intraindividual comparison issue is however mitigated by the fact that our results in lesion measurement accuracy with a reduced GBCA dose are in accordance with those from studies employing a full dose [113, 114, 116–120]. While the generalizability of our study might be limited by the inclusion of only two readers instead of a full-fledged multireader panel, the relatively good agreement between readers with very different experience levels points to a rather preserved image quality. Since routine pathology reports did not specify lesion location in multifocal and multicentric tumors, we could not perform a lesion-by-lesion analysis, considering only the index lesion with the largest diameter. However, our study reported only one patient with a multifocal cancer and one patient with a multicentric cancer: in both cases, both readers were able to detect and measure all additional lesions (one lesion in the multifocal case and multiple lesions in the other). The limited number of additional lesions prevented any properly powered statistical analysis. We should also note that 71% of lesions measured, and therefore detected, were T1 tumors, half of these being T1a and T1b (Table 3.1). Indeed, also these observations indirectly confirm the diagnostic potential of breast MRI performed with a reduced gadobutrol dose.

In conclusion, this study showed that breast MRI could be performed using a dose of 0.08 mmol/kg of gadobutrol with high accuracy and acceptable inter-reader agreement in tumor size measurement. Larger prospective studies are needed to further prove this dose-reduction approach.

**Table 3.1** Distributions of the main tumor features in the study population

<b>Modality</b>	<b>Feature</b>	<b>n</b>	<b>%</b>	
<b>MRI</b>	Side	Right	17	45%
		Left	17	45%
		Bilateral	2	10%
	Focality	Single focus	36	95%
		Multifocal/multicentric	2	5%
	Appearance	Mass enhancement	24	63%
		Non-mass enhancement	14	37%
	<b>Histopathology</b>	Histological type	IDC	26
ILC			8	21%
DCIS			4	11%
Molecular type		Luminal A	23	61%
		Luminal B	7	18%
		HER2 positive	3	8%
		Triple negative	1	2%
		Unavailable	4	11%
T		Tis	4	11%
		T1a	1	3%
		T1b	13	34%
		T1c	13	34%
		T2	5	13%
		T3	2	5%
		T4	0	0%
	N	N0	31	82%
N1		6	16%	
N2		1	2%	
M	M0	38	100%	
	M1	0	0%	

MRI: magnetic resonance imaging; IDC: invasive ductal carcinoma; ILC: invasive lobular carcinoma; DCIS: ductal carcinoma in situ.

**Fig. 3.1** High agreement in tumor size measurement both between readers and between readers and pathology. The size of this infiltrating lobular carcinoma, presenting as a mass enhancement lesion in the right breast of a 50-year-old woman, was measured 17 mm by both readers. A good agreement was also observed between both readers and pathology measurements (18 mm).

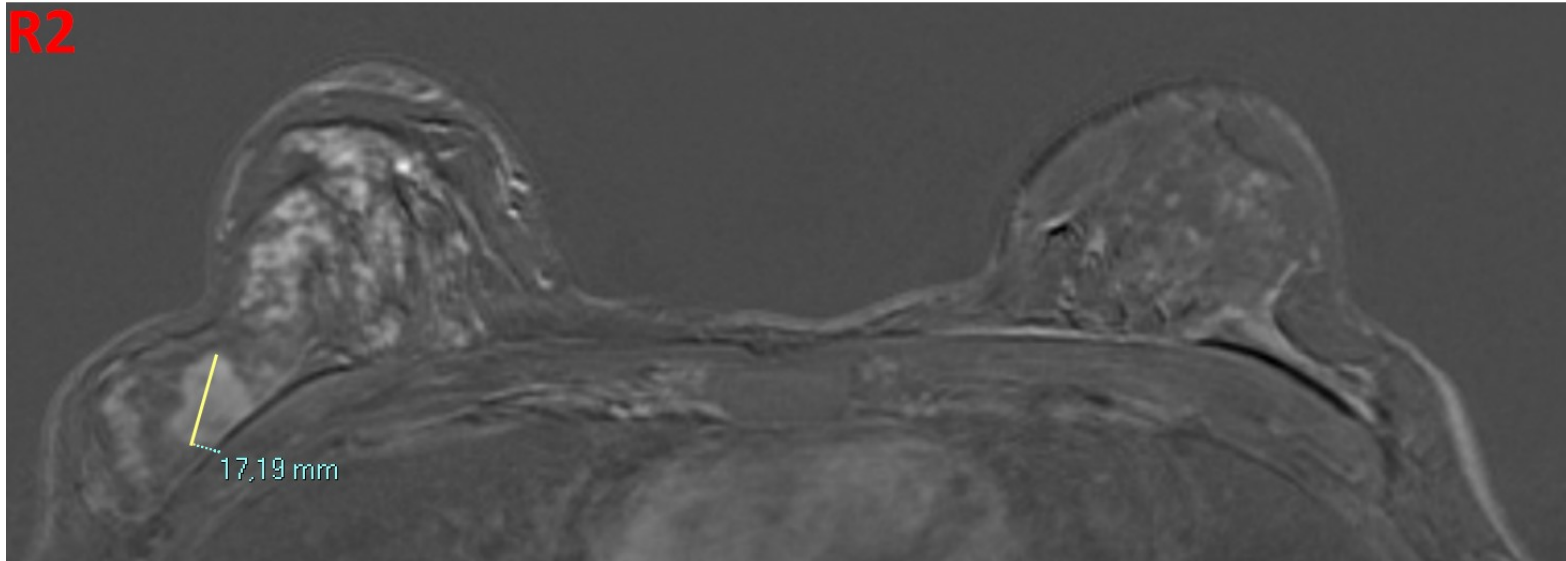
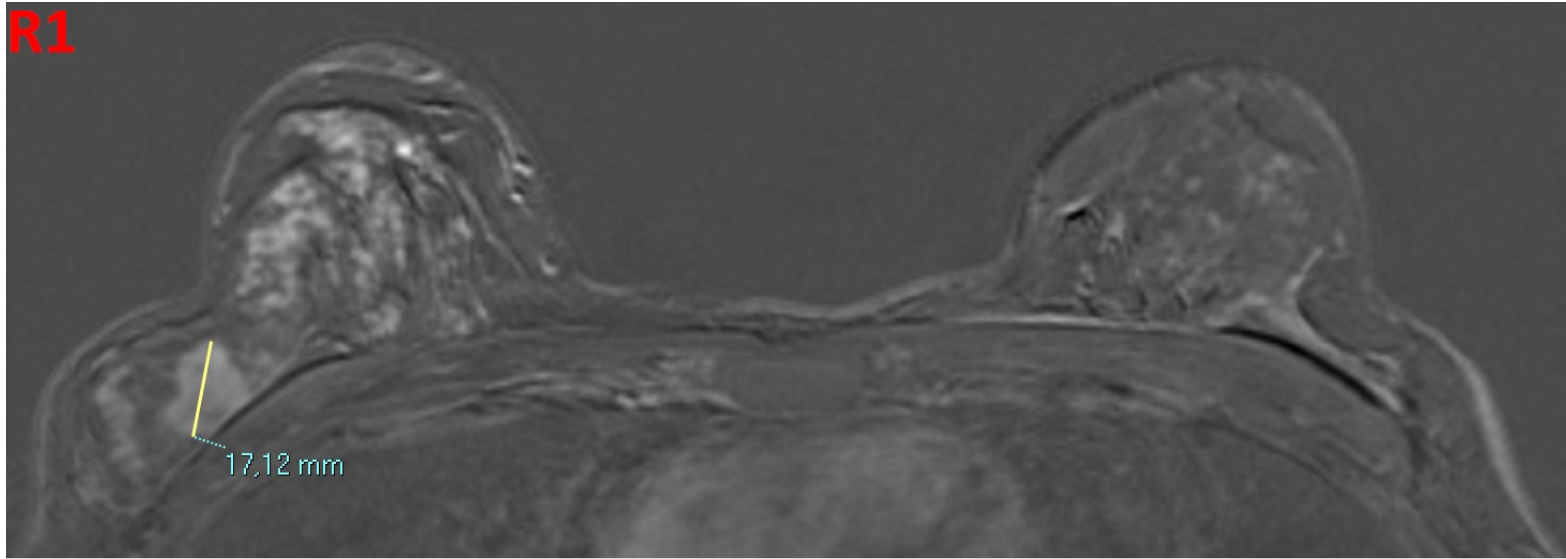


**Fig. 3.2** High agreement in tumor size measurement between readers, with low agreement between readers and pathology. The size of this infiltrating ductal carcinoma, presenting as a mass enhancement lesion with peripheral enhancement and central necrosis in the left breast of a breast of a 72-year-old woman, was measured 30 mm by both readers, but was then found to have only a 15 mm size at pathology

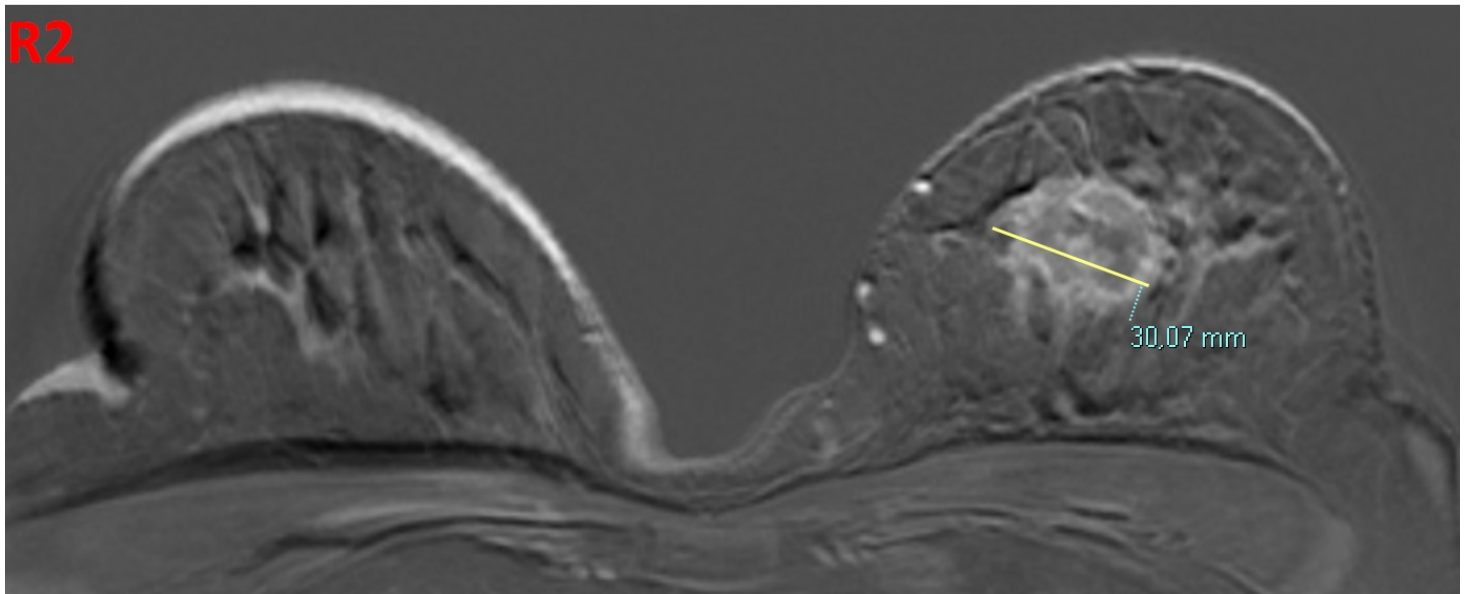
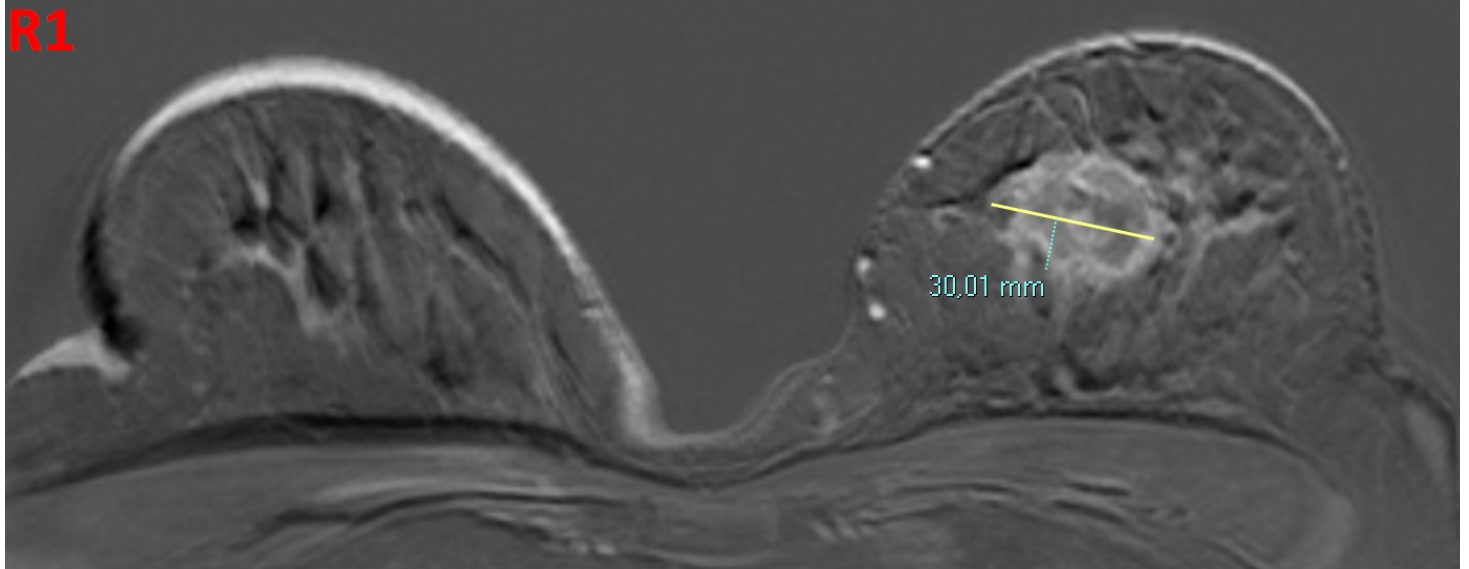


**Fig. 3.3** Low agreement in tumor size measurement between readers, due to tumor size underestimation by Reader 2. The size of this high-grade ductal carcinoma in situ, presenting as a non-mass lesion in the right breast of a 49-year-old woman, was measured 50 mm by Reader 1 and 40 mm by Reader 2. At pathology, cancer size was 50 mm

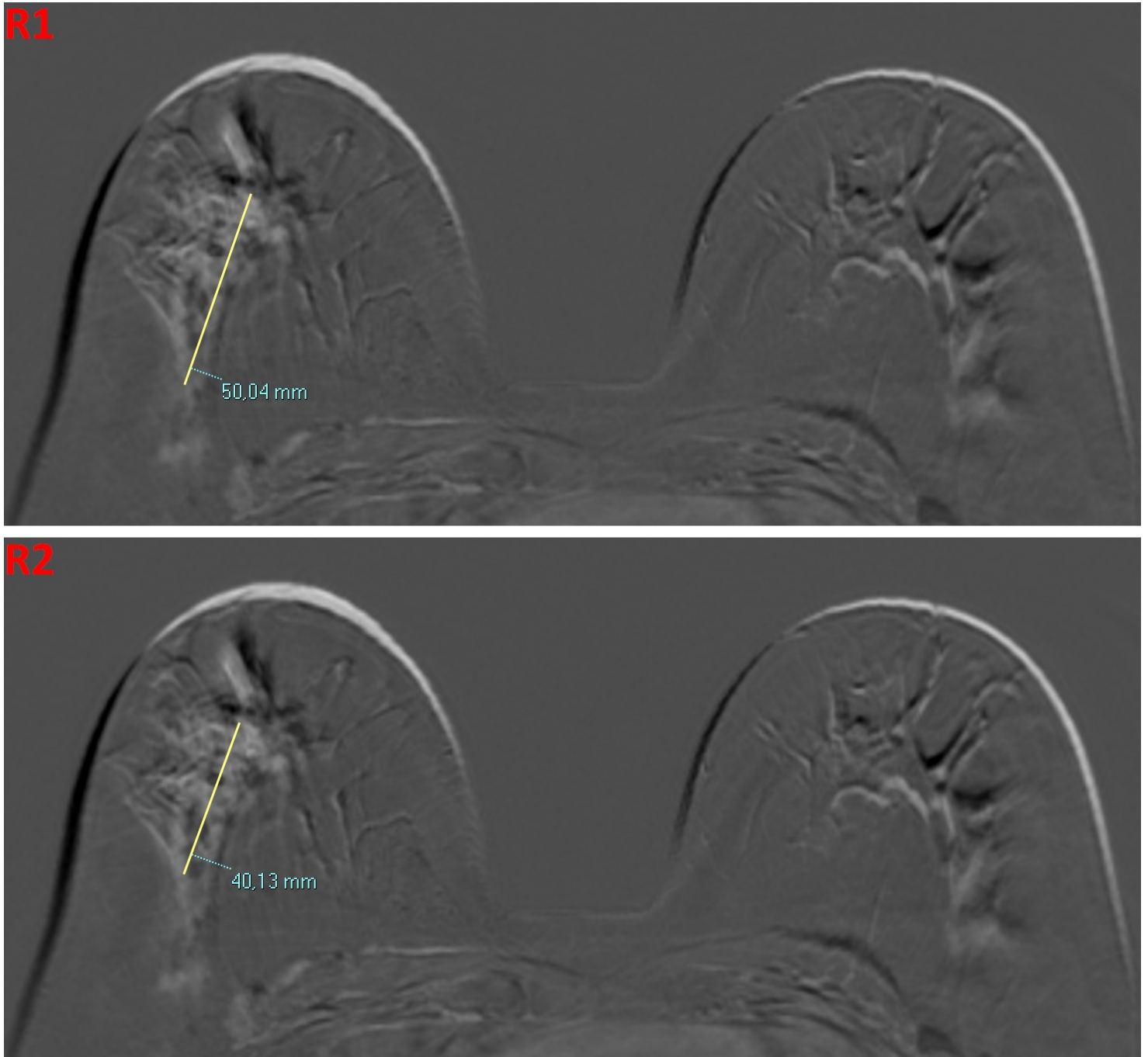


**Fig. 3.4** Low-to-average agreement in tumor size measurement between readers, with tumor size overestimation by both readers. The size of this high-grade ductal carcinoma in situ, presenting as a non-mass lesion in the right breast of a 68-year-old woman, was measured 31 mm by Reader 1 and 35 mm by Reader 2. At pathology, cancer size was 25 mm

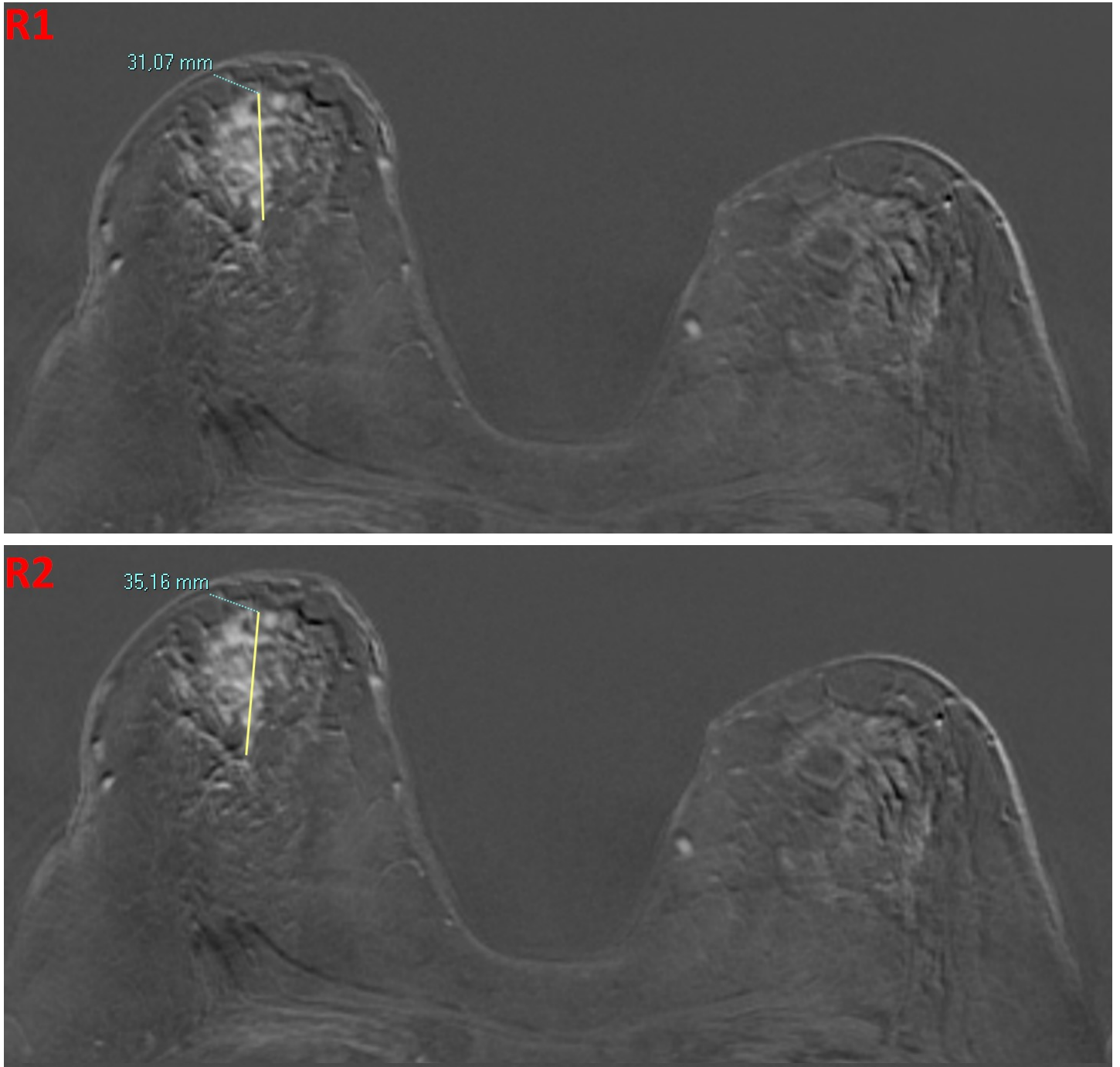


**Fig. 3.5** Bland–Altman plot for overall inter-reader measurement reproducibility.

Central line: bias (mean difference between measurements). Upper and lower lines: limits of agreement

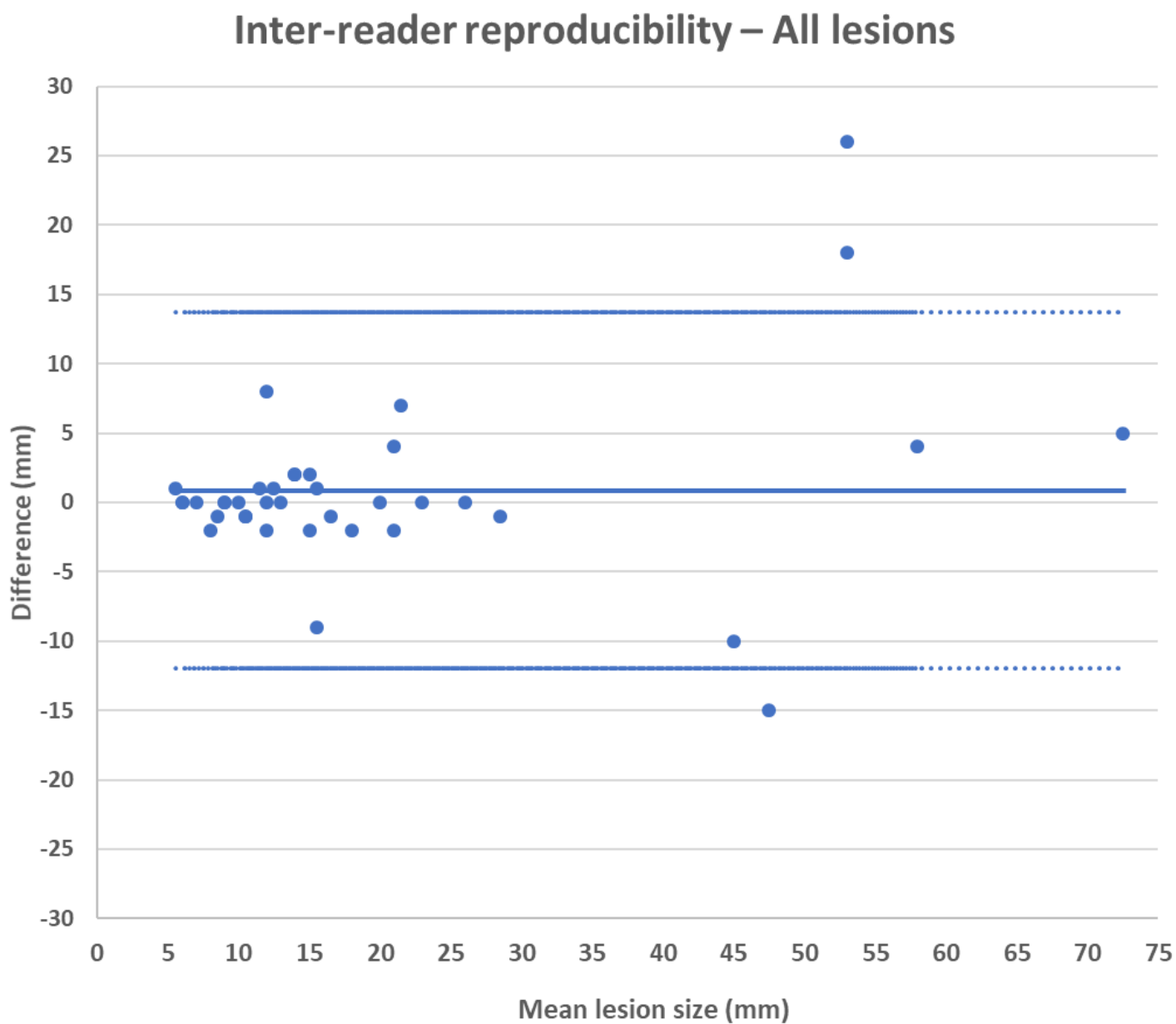




**Fig. 3.6** Bland–Altman plot for inter-reader measurement reproducibility on mass lesions.

Central line: bias (mean difference between measurements). Upper and lower lines: limits of agreement

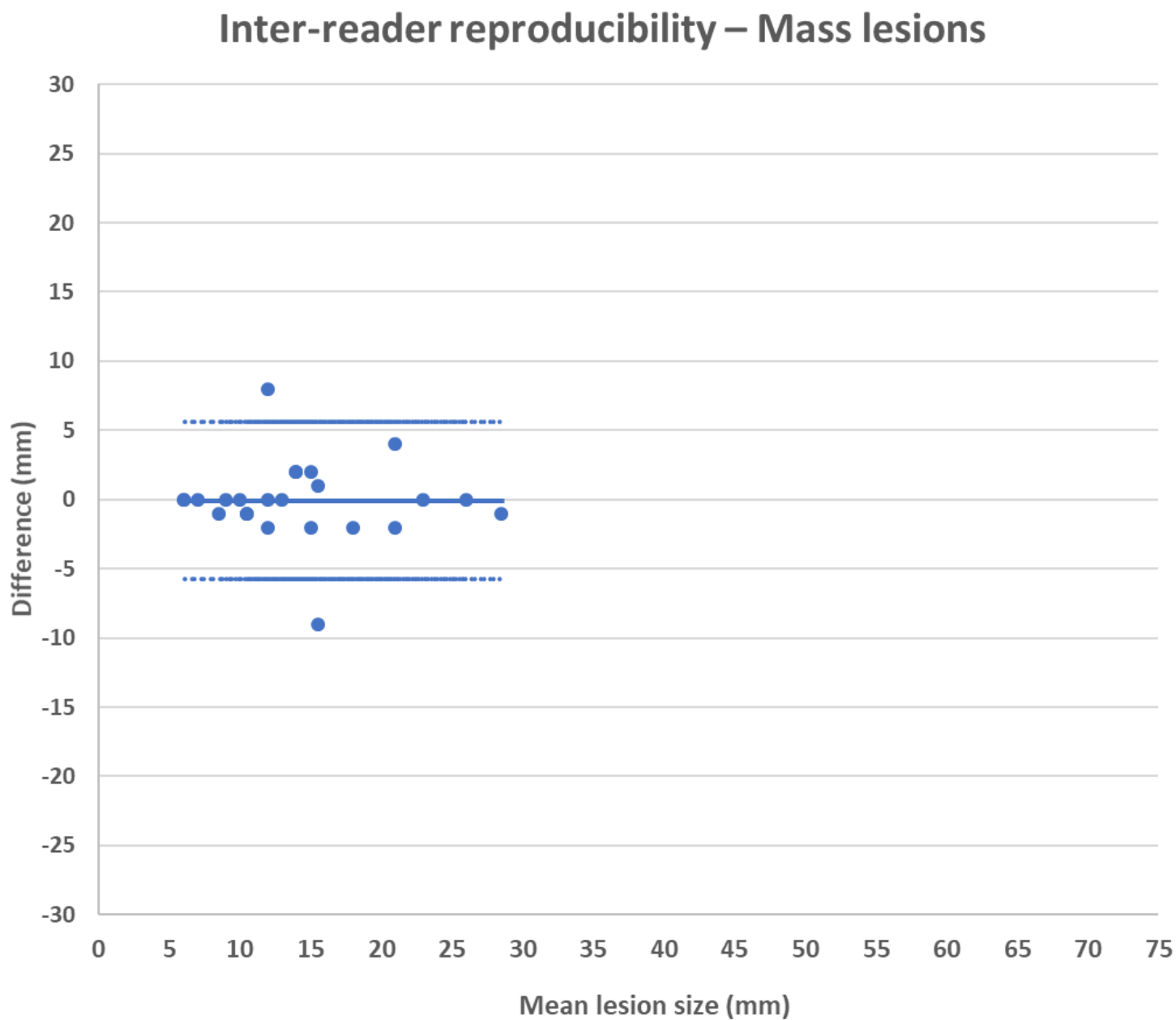
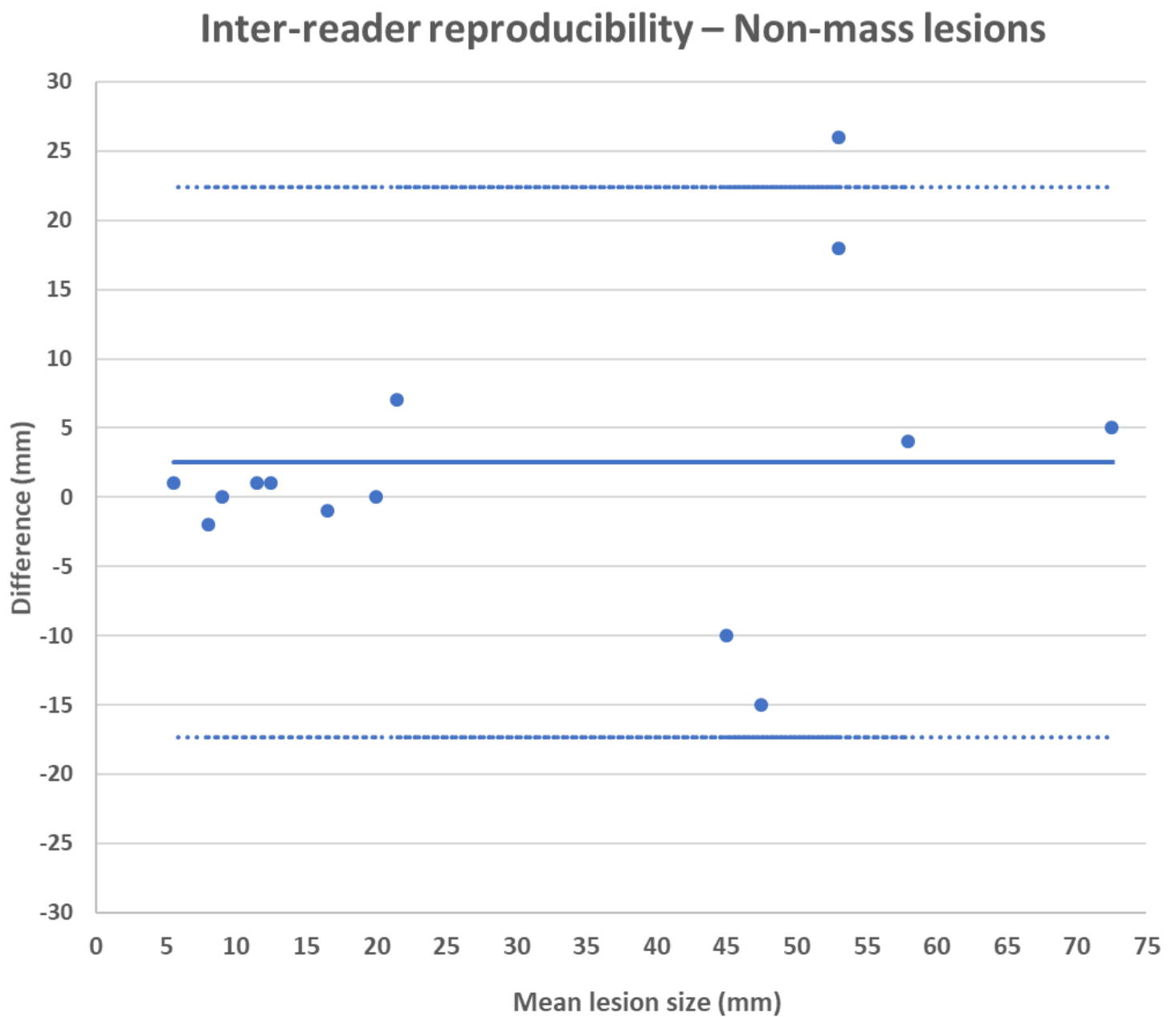


**Fig. 3.7** Bland–Altman plot for inter-reader measurement reproducibility on non-mass lesions.

Central line: bias (mean difference between measurements). Upper and lower lines: limits of agreement





# **Section II**



## **Iodinated contrast agents**

## 4. The emerging role of contrast-enhanced mammography

*Based on:*

Cozzi A, Schiaffino S, Sardanelli F (2019) *The emerging role of contrast-enhanced mammography*.

**Quant Imaging Med Surg** 9:2012–2018. doi:10.21037/qims.2019.11.09

## 4.1. Introduction

The combined morphofunctional approach underpins the rationale of CEM [123], which was developed by translating into an x-ray modality the same physio-pathological principles that allowed for the development of CE-MRI. CEM exploits the preferential uptake of ICAs by breast tumors, observed both in computed tomography and in subtraction angiography [3]. At first, the visualization of contrast uptake in the breast against fibroglandular tissue and fat was attempted with a temporal subtraction technique [3]. However, since technical drawbacks made this procedure highly impractical, a digital recombination of low- and high-energy images acquired after intravenous injection of ICA was swiftly adopted [2]. This recombination is generated by vendor-specific algorithms that gave rise to different denominations of the same technique: contrast-enhanced digital mammography (CEDM), contrast-enhanced spectral mammography (CESM), contrast-enhanced dual-energy mammography (CEDEM).

Notwithstanding the still persisting lack of technical and procedural standardization [124], across the last 19 years CEM has been experimentally introduced in various breast imaging settings, such as the diagnostic work-up of symptomatic women and screening recalls, problem-solving of specific mammographic findings, pre-operative local staging, post-operative surveillance, neoadjuvant therapy monitoring, and screening of women at increased risk or with dense breasts [123, 125]. Due to the morphofunctional nature of its images, in all these applications CEM consistently improved diagnostic performance when compared to digital mammography, ultrasound, and DBT, also frequently matching CE-MRI overall performance [125].

Another relevant advantage of CEM was also observed considering patient experience and preferences: two surveys pitching CEM against CE-MRI in high-risk women screening [126] and in the problem-solving setting [127] found that shorter examination time and globally less taxing procedure made CEM to be much better tolerated by patients.

We are witnessing how CEM is challenging the hitherto uncontested CE-MRI dominance in crucial aspects of breast imaging [22, 123, 125] such as pre-operative staging, post-operative surveillance, identification of occult primary breast cancer, problem solving for equivocal findings at first-level examinations, and neoadjuvant therapy response monitoring. CEM is able to offer an immediately available work-up option for recalled suspicious findings [123, 125] and also to easily solve one of the most irksome shortcomings of CE-MRI by providing a direct parallel visualization of microcalcifications in low-energy images and in their eventually associated contrast enhancement area [128].

Another turning point could eventually be represented by a response to concerns on GBCAs and ICAs. As we previously discussed, since 2014 the use of GBCAs in CE-MRI has come under close scrutiny, due to their retention in various structures of the central nervous system [129]. While gadolinium retention in the brain has yet to display any pathological effect subsequently detectable at neurologic examination [129], this issue is still unresolved and could further turn the tide towards CEM. Competition between CE-MRI and CEM is therefore wide open: Table 4.1 summarizes and compares each modality's major characteristics.

#### **4.2. Section outline**

As the role of CEM is in continuous expansion and CEM is poised to finally enter widespread clinical practice in the few next years, some critical aspects warrant an even stronger research effort. In the following chapters, we will first present the two largest systematic reviews about CEM technical aspects (Chapter 5) and diagnostic performance (Chapter 6) ever performed, in order to achieve a comprehensive understanding of all aspects of the CEM workflow. Then, Chapter 7 will evaluate within a bicentric framework the issue of CEM radiation dose in clinical practice, a crucial topic that however has up-to-now been evaluated only in a few relatively small and monocentric studies. Finally, in Chapter 8, we will present results from a prospective bicentric study that aims to

evaluate if CEM, applied as a stand-alone modality in one of the most important and busy settings of breast imaging—i.e. the assessment of screening-detected suspicious findings—is able to curtail the biopsy rate of false positive findings without jeopardizing overall diagnostic performance.



**Table 4.1** Main technical, procedural, and diagnostic features of breast CE-MRI and CEM

	<b>Breast CE-MRI</b>	<b>CEM</b>
Images	Three-dimensional	Two-dimensional
Multiparametric technique	Yes	No
Radiation exposure	No	Yes
Contraindications	Several	Very few
Contrast-related health issues	Yes	Yes
Kinetic contrast analysis	Yes	No
Ease of interpretation	Low	High
Accessibility	Low to intermediate	Intermediate to high
Cost	High	Low
Diagnostic performance	High	High
Patient preference	Low	High



## **5. Technique, protocols and adverse reactions of contrast-enhanced mammography: a systematic review**

*Published as:*

Zanardo M, Cozzi A, Trimboli RM et al (2019) *Technique, protocols and adverse reactions for contrast-enhanced spectral mammography (CESM): a systematic review*. **Insights Imaging** 10:76.

doi:10.1186/s13244-019-0756-0

## 5.1. Abstract

We reviewed technical parameters, acquisition protocols, and adverse reactions (ARs) for CEM. A systematic search in databases, including Medline/EMBASE, was performed to extract: publication year; country of origin; study design; patients; mammography unit/vendor, radiation dose; low-/high-energy tube voltage; contrast molecule, concentration, and dose; injection modality and ARs; acquisition delay; order of views; examination time. Of 120 retrieved articles, 84 were included from 22 countries (09/2003–01/2019), totalling 14,012 patients. Design was prospective in 44/84 studies (52%); in 70/84 articles (83%) a General Electric unit with factory-set kVp was used. Per-view average glandular dose, reported in 12/84 studies (14%), ranged 0.43–2.65 mGy. Contrast type/concentration was reported in 79/84 studies (94%), with Iohexol 350 mgI/mL mostly used (25/79, 32%), dose and flow rate in 72/84 (86%), with 1.5 mL/kg dose at 3 mL/s in 62/72 studies (86%). Injection was described in 69/84 articles (82%), automated in 59/69 (85%), manual in 10/69 (15%); and flush in 35/84 (42%), with 10–30 mL dose in 19/35 (54%). An examination time <10 min was reported in 65/84 studies (77%), 120 s acquisition delay in 65/84 (77%), order of views in 42/84 (50%) studies, beginning with the cranio-caudal view of the non-suspected breast in 7/42 (17%). Thirty ARs were reported by 14/84 (17%) studies (26 mild, 3 moderate, 1 severe non-fatal) with a pooled rate of 0.82% (fixed-effect model). Only half of CEM studies were prospective; factory-set kVp, contrast 1.5 mL/kg at 3 mL/s, and 120 s acquisition delay were mostly used; only 1 severe AR was reported. CEM protocol standardisation is advisable.

## 5.2. Introduction

As previously outlined, across the last 19 years CEM has been experimentally introduced in various breast imaging settings, but has still to gain a clear foothold in routine practice [123, 130, 131]. A time delay between the first appearance of new imaging techniques and their implementation in diagnostic routine is expected for many reasons, including not only the definition of indications but also the reproducibility of results. The latter is strongly influenced by technique details, such as—in the field of contrast-enhanced breast imaging—contrast agent concentration, dose and injection rate, breast compression and positioning, exposure parameters, and acquisition protocol. Indeed, the fact that CEM is variably performed across different centres, without an agreed and standardized technique, does not come as a surprise: this circumstance echoes the one observed for CE-MRI in the 1990s, then settled by the publication of detailed international guidelines [23, 132].

Therefore, the aim of this work was to review CEM studies, focusing on adopted technique, contrast agent issues, and acquisition workflow. This effort is crucial for future CEM investigations to be reproducible and comparable.

## 5.3. Methods

### *Study protocol*

No ethics committee approval was needed for this systematic review. The study protocol was registered on PROSPERO (<https://www.crd.york.ac.uk/prospero/>), the international prospective register of systematic reviews [133]. This systematic review was reported according to the Preferred Reporting Items for Systematic reviews and Meta-Analyses (PRISMA) statement [134].

### *Search strategy and eligibility criteria*

In February 2019, a systematic search was performed using MEDLINE (PubMed, [www.pubmed.gov](http://www.pubmed.gov)), EMBASE (Elsevier), the Cochrane Library (Cochrane Database of Systematic

Reviews, and the Cochrane Central Register of Controlled Trials for articles that reported or may have reported CEM technique. A controlled vocabulary (medical subject headings in PubMed and EMBASE thesaurus keywords in EMBASE) was used. The search string was: (cesm OR 'contrast enhanced spectral mammography'/exp OR 'dual energy mammography' OR 'contrast enhanced digital mammography'/exp OR 'contrast-enhanced mammography' OR 'dual-energy subtraction mammography' OR cedm OR cedsm OR 'contrast enhanced spectral imaging' OR 'high energy and low energy digital mammography') AND ('procedures'/exp OR 'method' OR 'methods' OR 'procedure' OR 'procedures' OR 'technique' OR 'acquisition'/exp OR 'contrast medium'/exp OR 'contrast agent' OR 'contrast dye' OR 'contrast material' OR 'contrast media' OR 'contrast medium' OR 'radiocontrast medium' OR 'radiography contrast medium' OR 'roentgen contrast medium' OR 'image processing'/exp OR 'image processing' OR 'image processing, computer-assisted' OR 'processing, image').

The search was limited to original studies on humans published in English, French, and Spanish on peer-reviewed journals, with an available abstract. No publication date limits were applied. Screening was performed by two independent readers (A.C. and M.Z., with 1- and 3-year experience in breast imaging, respectively) based only on title and abstract. Eligible articles were those that reported in the title or in the abstract the use of CEM technique or that could have contained these data in the manuscript. After downloading eligible articles, the full text was read for a complete assessment. Finally, references of included articles were hand-searched to check for further eligible studies.

#### *Data extraction*

Data extraction was performed independently by the same two readers who performed the literature search. Disagreements were settled by consensus. For each analysed article, year of publication, institution (such as hospitals, imaging facilities, breast units including radiology sections, or any other type of centre in which CEM is performed) and country origin as well as research groups,

design, number of patients, and demographics were retrieved. Mammography unit, vendor, radiation dose and technical features such as low- and high-energy kVp, anode/filter combinations and exposure parameters were also extracted. Moreover, contrast agent type, dose and concentration were retrieved, as well as injection modality, if manual or automated, flow rate and additional post-contrast saline flush or “bolus chaser” if present. Furthermore, mild, moderate or severe adverse reactions to ICAs were extracted alongside strategies for their prevention. Regarding the acquisition protocol, time between contrast injection and first image acquisition and maximum examination duration were extracted. Regarding the order of views, we reported the acquisition sequence of the standard mammographic projections considering the craniocaudal (CC) and the mediolateral oblique (MLO) views, including the first side acquired. Missing data were requested to authors.

#### *Evidence synthesis*

To avoid risk of data duplication bias, in case of articles published by the same research group, we considered the possibility of performing subgroup analysis: therefore, before delving into further analysis of protocol description, we chose to change our viewpoint from the number of articles reporting a specific protocol to the minimum number of times a protocol was reported by a single research group.

Regarding the pooled rate of adverse reactions related to ICA administration across studies, statistical analysis was performed using Comprehensive Meta-Analysis v2.2.057 (Biostat, Englewood, NJ, USA) using the meta-analysis model “Number of events and study population”.  $I^2$  statistics was first calculated to assess heterogeneity and the fixed-effect model was used to provide the rate of adverse reactions and 95% of confidence intervals (CI). The risk of publication bias was assessed by visually inspecting funnel plot and performing the Egger test [135].

## 5.4. Results

### *Studies*

A flowchart of study selection is shown in Fig. 5.1. Of 120 retrieved articles, 84 (70%), published between 09/2003 and 01/2019, were analysed [2, 3, 126–128, 136–214]; 40/84 (48%) being retrospective and 44/84 (52%) prospective (43/44 monocentric, 98%, and 1/44 multicentric, 2%); 54/84 (64%) articles investigated CEM diagnostic performance, whereas 30/84 (36%) focused on technical features. The geographic distribution of research groups is depicted in Fig. 5.2.

### *Populations and settings*

Data synthesis is reported in Table 5.1. The number of patients ranged from 5 [174] to 2,303 [209] for a total of 14,012 patients, with mean or median age ranging from 45 years [161] to 66 years [144]. In 29/84 studies (35%), CEM was performed on patients from comprehensive databases of heterogeneous settings, such as pre- or post-operative evaluation, adjuvant or neoadjuvant chemotherapy response monitoring, equivocal findings at conventional imaging, etc. The remaining 55 studies (65%) were individually centred on a unique setting. Twenty-seven studies (32%) performed CEM on suspicious cases from conventional imaging and screening recalls, 11 studies (13%) in a first-line screening setting, 7 (8%) performed CEM exclusively for known cancer staging, 4 (5%) in a pre-operative setting, 4 (5%) to assess and monitor the response to adjuvant chemotherapy, 2 (2%) in a post-operative setting.

Timing of CEM examination with menstrual cycle was reported only in 18/84 studies (21%). In 10/18 (56%) articles it was mentioned but not applied, in 6/18 (33%) it was applied with a feasibility window between the 5th and 14th day of menstrual cycle; in 2/18 (11%) CEM was synchronously performed with MRI in different phases of menstrual cycle to evaluate and compare background parenchymal enhancement.



### *Technical features and parameters*

In 70 out of 84 studies (83%) different systems from General Electric Healthcare (Chicago, IL, USA) were used, all with a prototype or a commercial release of the SenoBright upgrade which is required to perform dual-energy contrast-enhanced imaging. Twelve out of 84 articles (14%) reported the adoption of Selenia Dimensions mammography unit (Hologic Inc., Marlborough, MA, USA), while the remaining 2/84 (3%) studies were conducted with a Siemens Healthineers (Erlangen, Germany) mammography system (Mammomat or Mammomat Inspiration).

The type of ICA used was not reported in five articles [136, 145, 175, 178, 185], while in the remaining 79 studies (94%, for total 13,465 patients, 96%) six different molecules of were used: Iohexol was the most frequently employed, being used in 42/79 studies (53%) for a total of 5,049/13,465 patients (37%), followed by Iopromide (18/79 studies, 23%, for 2,798/13,465 patients, 21%), while Iobitridol, Iomeprol, Iopamidol, and Ioversol were administered in the remaining studies (19/79 studies, 24%, for 5,618/13,465 patients, 42%). Iohexol was utilized at a concentration of 350 mg iodine/mL (25/42 studies, 60%, for 3,330/5,049 patients, 66%) or 300 mg iodine/mL (17/42 studies, 40%, for 1,719/5,049 patients, 34%). Iopromide was also administered at two different concentrations: 370 mg iodine/mL (10/18 studies, 56%, for 1,032/2,798 patients, 37%) and 300 mg iodine/mL (8/18 studies, 44%, for 1,766/2,798 patients, 63%).

Of the 69 studies including a specification of the contrast injection modality, 59 (85%) utilized an automated power injector (10,584/11,725 patients, 90%) while manual contrast injection was carried out in the remaining 10 (15%) [3, 138, 146, 149, 163, 169, 183, 187, 205, 208] for a total of 1141/11,725 patients, 10%.

Contrast agent dose, detailed in 77 studies, was fixed at 1.5 mL/kg in 72 (93%) of them for a total of 13,559/13,687 (99%) patients. Contrast agent flow rate, reported in 76/84 studies (90%), was most frequently fixed at 3 mL/s (65/76 studies, 86%); the 11 remaining articles detailed a flow rate ranging from 2 to 5 mL/s. Thirty-five out of 84 (42%) articles for a total 8,734/14,012 patients

(62%) also mentioned the use of additional post-contrast saline flush or “bolus chaser”, 19 of them (54%, for a total 4,477/8,734 patients, 51%) likewise detailing a saline amount ranging from 10 to 30 mL.

Of 69 studies detailing the tube voltage of both low- and high-energy acquisitions, all but one (99%) acquired low-energy images between 26 and 33.2 kVp, which is the peak kilovoltage threshold of iodine, while all 69 acquired high-energy images well above this threshold, i.e. between 44 and 50 kVp. The anode/filter combination was reported by 42/84 studies and is highly characteristic of the given manufacturer. Exposure parameters were unambiguously reported only in one study [198], whereas in 5 early studies [3, 153, 176, 195, 213] they were manually adjusted according to breast thickness and density; 35 other studies declared an automatic regulation of these parameters performed by the mammography unit.

Regarding radiation dose, data were scarcer: even though 45/84 articles (54%) mentioned this aspect, 17/45 (31%) did it without exhibiting original information but reporting observations from previous studies, therefore restricting the number of studies with new data to 28/84 (33%). Of these 28 studies, 19 (68%) provided an average glandular dose (AGD) value, 3 (16%) of them calculating it per-patient and ranging 1.5–6.9 mGy [170, 176, 187], 5/19 (26%) per-breast ranging 2.19–7.15 mGy, and the remaining 11 (58%) reporting a per-view AGD ranging from 0.43 [172] to 2.65 mGy [211]. A comparison with digital mammography was mentioned in 17 studies: only 1 (6%) documented a dose reduction (-2%) for CEM compared to digital mammography [153], while other 16 (94%) reported an increase in AGD ranging between 6.2% [195] and 100% [188]. However, it is worthwhile to notice that 3 studies specifically contrived to assess CEM radiation doses reported an AGD increase of 42% [168], 78% [192], and 80% [171].

### *Acquisition protocols*

Studies reporting the time interval between contrast injection and the first image acquisition were 78 out of 84 (93%), for a total 13,244/14,012 patients (95%), and 65 (83%) of them (12,278/13,244 patients, 93%) had it fixed at 120 seconds.

Sixty-six out of 84 articles (79%, for a total 11,900/14,012 patients, 85%) gave an indication of the acquisition time after contrast injection: in 12/66 (18%, for total 1,381/11,900 patients, 11.6%) the exam was completed in less than 5 minutes, in 52/66 (80%, for total of 10,485/11,900 patients, 88.1%) between 5 and 10 minutes, while in 1/66 (2%, for total 34/11,900 patients, 0.3%) the duration exceeded 10 minutes.

The outline of the image acquisition sequence remains more variable. Ten out of 84 studies (12%), accounting for 2,734 patients (19%) did not clearly describe it and did not provide a reference to other protocols, while 3/84 (4%, for total 103/14,012 patients, 1%) employed a curtailed and side-insensitive acquisition sequence. Adherence to standard but unspecified digital mammography protocols was declared by 29/84 (34%) studies, for total 3,741/14,012 patients (27%). The other half of the articles analysed (42/84, accounting for 7,434/14,012 patients, 53%) unequivocally detailed an acquisition sequence. Of these 42 studies, 14 (34%, for total 2,048/7,434 patients, 28%) adopted a projection order that was conventionally agreed upon, while the other 28 (66%, accounting for 5,386/7,434 patients, 72%) based their acquisition sequence on the presence of previous suspect or clearly pathologic findings.

Eighty-four articles came from 38 different research groups. Subgroup analysis according to research groups showed that 17 acquisition sequences based on a conventionally agreed projection order were executed in 15 research groups. As described in Fig. 5.3, the most common sequence description, reported by 6/17 (35%) institutions, was MLO - MLO - CC - CC (in order of acquisition), without any further indication about the first side to be examined (right or left or side with/without suspicious lesion or already diagnosed cancer). The second most common sequence

(4/17, 24%) was CC - CC - MLO - MLO with the first projection standardized on the right side (independently of pathology or with suspected pathology).

Among the 22 acquisition sequences (coming from 20 institutions) centred on the presence of previous suspect or clearly pathologic findings, we found substantial variability between different orders of acquisition, as shown in Fig. 5.4. However, the most common sequence, adopted by 4/22 (19%) research groups, was: 1) CC, suspected side; 2) CC, non-suspected side; 3) MLO, suspected side; 4) MLO, non-suspected side.

#### *Contrast agent adverse reaction rate meta-analysis*

Regarding side effects from contrast administration, 48/84 studies (57%) declared a preventive anamnestic screening for previous adverse reactions or general contraindications to ICA administration. Pre-examination tests of renal function was mentioned in 39/84 studies (46%). Of note, 14/84 studies (29%) reported 30 adverse reactions out of 14,012 patients, of which 26/30 (87%) were mild reactions limited to pruritus, hives, “scratchy throat”, or other minor skin flushing that resolved promptly even when antihistamines or corticosteroids were not administered. In 3/30 (10%) cases [166, 170, 197], side effects were of moderate importance with nausea and vomiting, widespread urticaria resolved only after antihistamines and corticosteroids *per os*, and dyspnea that equally responded to oral antihistamine administration. Only 1/30 (3%) severe adverse reaction, requiring “intensive care” but resolved after short time, occurred in 14,012 patients (0.007%) [172]. Therefore, the number of adverse reactions related to ICA administration ranged from 0, reported by 70 (88%) studies, to a maximum of 6 adverse reactions [214] with a total of 30 adverse reactions, showing no heterogeneity ( $Q = 64$ , degree of freedom 83,  $\tau = 2.0972$ ,  $I^2 = 0\%$ ,  $p = 0.931$ ). As shown in the forest plot of Fig. 5.5, using fixed-effect model, the pooled rate of adverse reactions across studies was 0.82%, with 0.64% and 1.05% as 95% CI.

Visually inspecting the funnel plot in Fig. 5.6, risk of publication bias was found, as confirmed by the Egger test ( $p < 0.001$ ).

## 5.5. Discussion

Our systematic review included 84 articles, accounting for 14,012 patients, reporting the use of CEM in various settings. The sheer number of studies and, as depicted in Fig. 5.7, their increase in the last three years (27 studies between 2003 and December 2015, 57 from January 2016 to January 2019) points out a considerable interest in this emerging breast imaging modality.

A number of narrative reviews [123, 215–220] favourably outlined CEM future perspectives in several clinical settings (e.g., recall work-up, preoperative staging, and monitoring the effect of neoadjuvant therapy) as a potential alternative to MRI.

In the first phase of CEM development, some non-fixed parameters regarding contrast agent administration (i.e. contrast agent molecule, concentration, dose, flow rate, and injection modality) and some acquisition features (i.e. time between contrast injection and first acquisition, kVp ranges for low- and high-energy acquisitions) gained an international agreement. However, in the framework of comprehensive optimization and standardization of CEM, large-scale studies are undoubtedly needed to address the knowledge gap concerning the choice of technical parameters.

Our data show a consensus among studies (93%) on the choice of 1.5 mL/kg contrast dose administered with a 3 mL/s flow rate (74%) and a less extensive agreement on the use of Iohexol (53% of all studies) at a concentration of 350 mg iodine/mL (30% of all studies). However, these parameters have probably been empirically adopted from CT protocols, as the first investigators plainly stated [3], without any other particular explication or justification. No dose-finding studies have been published yet.

Similarly, the common use of a power contrast injector (87% of all studies, with the remaining 13% coming from a single research group) is assumed from CT and MRI protocols in which it has been demonstrated to be effective in obtaining a stable contrast inflow and bolus shape [221–223].

Moreover, the use of a power injector allows for the administration of a bolus chaser, reported only in 42% of all articles, a technical refinement that has shown good results in CT [224, 225].

Two other points need to be mentioned. The first one is the correlation between menstrual cycle phase and CEM, for both background parenchymal enhancement, explored in a few studies [185, 191, 198] and for fluctuations of lesion contrast uptake. Secondly, since CEM is based on a dual x-ray exposure, of which the low-energy one has been demonstrated to be equal to standard digital mammography [178], an increase in radiation dose is expected. However, while preliminary studies estimated a negligible [3] or curtailed AGD increase, studies specifically devised to ascertain CEM effective AGD found a substantial AGD increment ranging 42%–80% [168, 171, 192]. While CEM AGDs remain under the threshold stated by European guidelines for screening mammography [226], further studies are needed to investigate CEM AGD [168, 192].

Furthermore, we remark the absence of standardized protocols. This methodological void, especially regarding the acquisition workflow, represents a threat to reproducibility and comparison of imaging results. While 98% of all studies reporting the total examination time completed the examination before 10 min from contrast administration, and while some studies presented evidence on the irrelevance of the acquisition order [167, 175], there are no studies comparing different approaches.

The pooled rate of adverse reactions to ICA administration was 0.82% (0.64%–1.05% 95% CI) with a total of 30 adverse reactions in 14,012 patients, a rate similar to that reported for CT: 0.6% [227] in 84,928 adult patients or 0.7% [228] in 29,508 patients (given Iopromide, which is also used for CEM). Particularly, considering only severe adverse reactions in CT, Wang et al. [227] reported 11/84,928 (0.0129%) reactions, as well as Mortelé et al. [228] 4/29,508 (0.0135%). These rates

seem to be higher than that found in our meta-analysis 1/14,012 (0.007%), a comparison to consider with caution due to the nature of rare events such as severe reactions to ICA. One aspect to consider is the different profile of patients undergoing CEM compared to those requiring contrast-enhanced CT, the former being that of basically “healthy” subjects, the latter implying the possibility of relevant disease, including also serious emergency conditions.

This review has limitations. Patient data are probably shared and duplicate among some studies from the same research group. This has been shown to negatively impact on review quality [229, 230] and could only be prevented via individual patient data sharing [231]. However, for technical aspects of this systematic review, our choice to evaluate study groups rather than single articles, should have mitigated this bias. Conversely, our pooled rate of adverse reactions could be underestimated.

In conclusion, our review shows that CEM is unevenly performed across different centres, in terms of contrast agent type and concentration and order of view acquisition. However, most research groups performed CEM using a contrast dose of 1.5 ml/kg, factory-set kVp ranges for low- and high-energy acquisitions, beginning image acquisition after 120 s from contrast agent injection and completing the examination within 10 minutes. Further studies are needed to investigate the role of background parenchymal enhancement and to harvest data that can firmly back up subsequent technical guidelines and consensus statements for standardized CEM protocols.

**Table 5.1** Main characteristics of the 84 analysed studies

Author / year	Study design	Country of research group	Number of patients	Mean or Median age (years)	Contrast agent type	Concentration (mgI/mL)	Dose (mL/Kg)	Flow rate (mL/s)	Time before imaging (seconds)	Total exam time
Houben 2019	R	The Netherlands	147	61	Iopromide	300	1.5	3	120	
Barra 2018	P mono	Brazil	33	45	Iohexol	300	1.5	3	120	B
Bicchierai 2018	R	Italy	40	50	Iopromide	370	1.5	3	120	B
Danala 2018	R	USA	111		Iohexol	350	1.5	3	120	B
Deng 2018	R	Taiwan	141	48	Iohexol	350	1.5	3	120	B
Helal 2018	P mono	Egypt	300	54	Iohexol	300	1.5	3	120	B
Kim 2018	P mono	South Korea	84	51	Iohexol	350	1.5	2	120	B
Klang 2018	R	Israel	953	51	Iopamidol	370	1.5	3	120	B
Łuczyńska 2018	R	Poland	82	57	Iopromide	370	1.5	3	120	B
Moustafa 2018	P mono	Egypt	160		Iohexol	300	1.5	3	120	B
Navarro 2018	P mono	Chile	465	53	Ioversol	320	1.5			B
Patel 2018 (01)	P mono	USA	65	53	Iohexol	350	1.5	3	120	A
Patel 2018 (02)	R	USA	50	57	Iohexol	350	1.5	3	120	B
Patel 2018 (03)	R	USA	30	66	Iohexol	350	1.5	3	120	B
Phillips 2018	R	USA	45	53	Iohexol	350	1.5	3	120	
Sorin 2018	R	Israel	611	54	Iopamidol	370	1.5	3	120	B
Tohamey 2018	P mono	Egypt	178	46	Iohexol	300	1.5	3	120	B
Travieso-Aja 2018	R	Spain	158	51			1.5	3	120	B
Xing 2018	P mono	China	235	51	Iohexol	350	1.5	3	120	B
Barra 2017	R	Brazil	11	46	Iohexol	300	1-2	3	120	B



Bhimani 2017	R	USA	2303		Iopamidol	370	1.5	2	120	B
Fallenberg 2017	P multi	Germany	155	53	Iobitridol	300	1.5	3	120	A
Gluskin 2017	R	USA	5	59	Iohexol	350	1.5	3	150-180	A
Helal 2017 (01)	P mono	Egypt	98	50	Iohexol	300	1.5	3	120	B
Helal 2017 (02)	P mono	Egypt	30	47	Iohexol	300	1.5		120	
Houben 2017	R	The Netherlands	839	60	Iopromide	300	1.5	3	120	
Iotti 2017	P mono	Italy	54	54	Ioversol	350	1.5		120	
James 2017	R	USA	173		Iohexol	350	1.5	3	120	A
Jochelson 2017	P mono	USA	309	51	Iohexol	350	1.5	3	150-180	B
Knogler 2017	P mono	Austria	11	58	Iomeprol	400	2	3.5	90	
Lee-Felker 2017	R	USA	52	50	Iohexol	350		3	120	B
Lewis 2017	R	USA	208		Iohexol	350	1.5	3	120	B
Li 2017	R	USA	48	56	Iopamidol	370	1.5	1.5-2		B
Mori 2017	P mono	Japan	72	48	Iohexol	300	1.5	3	120	
Patel 2017 (01)	R	USA	88	62	Iohexol	350	1.5	3	120	B
Patel 2017 (02)	R	USA	410		Iohexol	350	1.5	3	120	B
Phillips 2017	P mono	USA	38	53	Iohexol	350	1.5	3	120	B
Richter 2017	R	Germany	118	58	Iopromide	300	1.5	2-3	120	
Saraya 2017	P mono	Egypt	34	54	Iohexol	300	1.5	4		C
Savaridas 2017	P mono	Australia	66	54			1.5	3	120	B
Sogani 2017	R	USA	278	51	Iohexol	350	1.5	3	150	A
Ali-Mucheru 2016	R	USA	351	62	Iohexol	350	1.5	3	120	B
Ambicka 2016	R	Poland	82	57	Iopromide	370	1.5	3	120	B
Brandan 2016	P mono	Mexico	18	51	Ioversol	300		4	60	B

Cheung 2016 (01)	R	Taiwan	256	48	Iohexol	350	1.5	3	120	A
Cheung 2016 (02)	R	Taiwan	87	54	Iohexol	350	1.5	3	120	B
Kamal 2016	R	Egypt	239	48	Iohexol	300	1.5	3	120	B
Kariyappa 2016	P mono	India	44		Iomeprol	350	1.5	3	120	B
Knogler 2016	P mono	Austria	15	58	Iomeprol	400	2	3.5	60-90	
Lalji 2016	R	The Netherlands	199	58	Iopromide	300	1.5	3	120	
Łuczyńska 2016 (01)	P mono	Poland	116	55	Iopromide	370	1.5	3	120	B
Łuczyńska 2016 (02)	P mono	Poland	193	55	Iopromide	370	1.5	3	120	B
Tardivel 2016	R	France	195	56	Iobitridol	300	1.5	3	120	B
Tennant 2016	R	UK	99	49						
Tsigginou 2016	P mono	Greece	216	55	Iopromide	300	1.5	2-3	120	B
Wang 2016	P mono	China	68	53	Iohexol	350	1.5	3	120	A
Yagil 2016	R	Israel	200	51	Iopamidol	370	1.5	3	120	B
Chou 2015	P mono	Taiwan	185	51	Iohexol	300	1.5	2	120	B
Elsaid 2015	P mono	Egypt	34	55	Iohexol	300	1.5	3		B
Hobbs 2015	P mono	Australia	49	55	Iohexol	350	1.5	3	120	B
Kamal 2015	R	Egypt	168		Iohexol	300	1.5	3	120	B
Lobbes 2015	R	The Netherlands	87	62	Iopromide	300	1.5	3	120	
Łuczyńska 2015 (01)	P mono	Poland	174	56	Iopromide	370	1.5	3	120	B
Łuczyńska 2015 (02)	P mono	Poland	102		Iopromide	370	1.5	3	120	
Badr 2014	P mono	France	75	54	Iohexol	300	1.5		120	B
Blum 2014	P mono	Germany	20	57	Iopamidol	300	1.5	3	120	
Cheung 2014	R	Taiwan	89	48	Iohexol	350	1.5	3	120-180	B
Fallenberg 2014 (01)	P mono	Germany	118	53	Iobitridol	300	1.5	3	120	B

Fallenberg 2014 (02)	P mono	Germany	80	54	Iobitridol	300	1.5	3	120	B
Francescone 2014	R	USA	88	50						
Jeukens 2014	R	The Netherlands	47	58	Iopromide	300	1.5	3	120	
Lobbes 2014	R	The Netherlands	113	57	Iopromide	300	1.5	3	120	
Łuczynska 2014	P mono	Poland	152	56	Iopromide	370	1.5	3	120	B
Mokhtar 2014	P mono	Egypt	60		Iohexol	300	1.5		120	A
Travieso-Aja 2014	R	Spain	136	49			1.5	3	120	B
Hill 2013	R	Canada	98	57	Iobitridol	300	1.5	3	120	B
Jochelson 2013	P mono	USA	82	50	Iohexol	350	1.5	3	150-300	B
Dromain 2012	P mono	France	110	57	Iobitridol	300	1.5	3	120	A
Diekmann 2011	P mono	Germany	70	55	Iopromide	370	1	4	60/120/180	A
Dromain 2011	P mono	France	120	56	Iobitridol	300	1.5	3	120	A
Dromain 2006	P mono	France	20	63	Iohexol	300		3	30	B
Diekmann 2005	P mono	Germany	21		Iopromide	370	1	4	60/120/180	A
Jong 2003	P mono	Canada	22		Iohexol	300			60	B
Lewin 2003	P mono	USA	26	51	Iohexol	350		4-5	150	

R = retrospective; P mono = Prospective monocentric; P multi = Prospective multicentric; A = total exam time <5 min; B = total exam time between 5 and 10 min; C = total exam time >10 min

**Fig. 5.1** Flowchart of the study selection and exclusion for articles on CEM

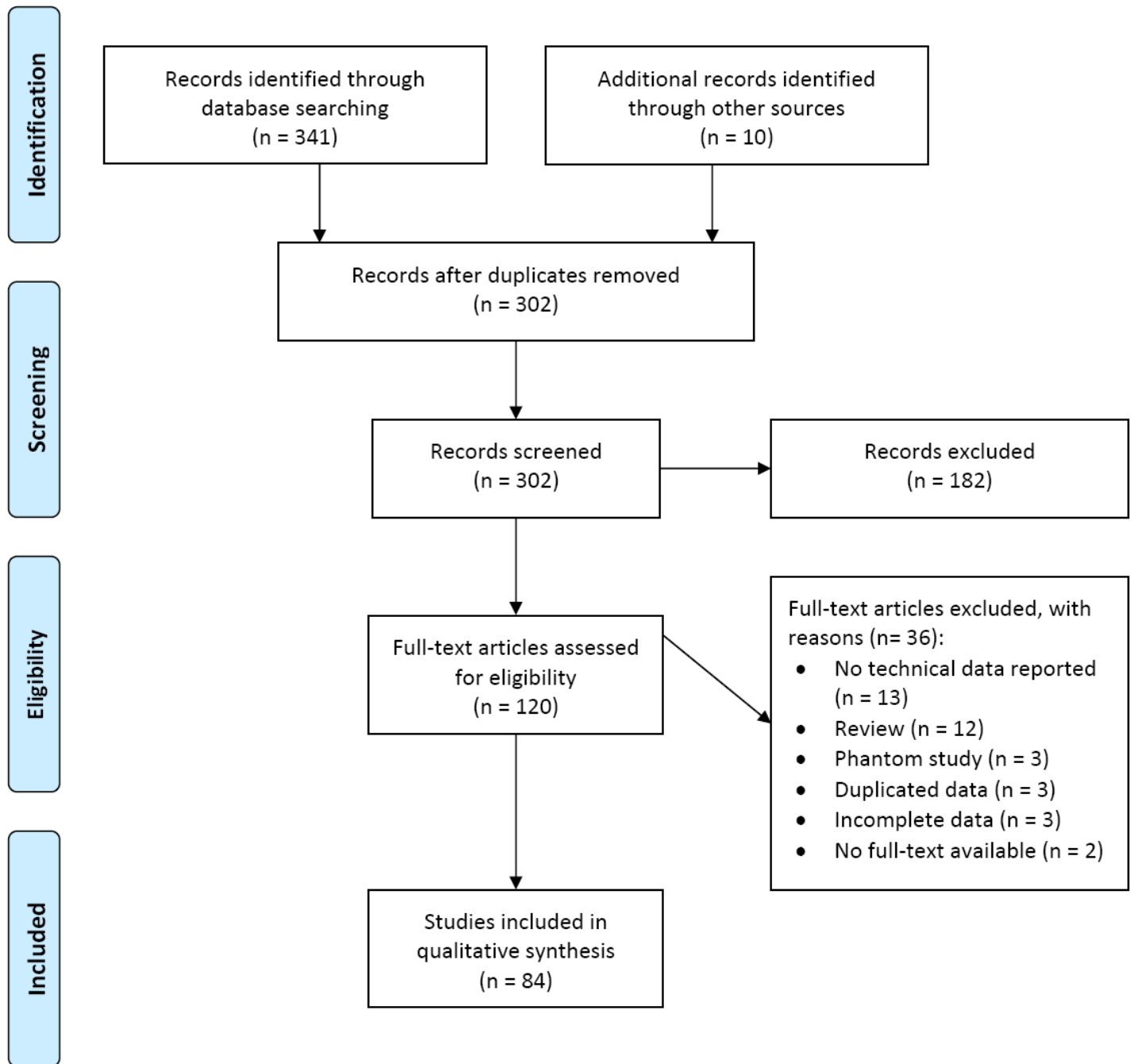




**Fig. 5.3** Graphical summary of conventionally agreed view acquisition orders for contrast-enhanced spectral mammography: CC: craniocaudal view; MLO: mediolateral oblique view; L: left; R: right

### Conventionally agreed projection order

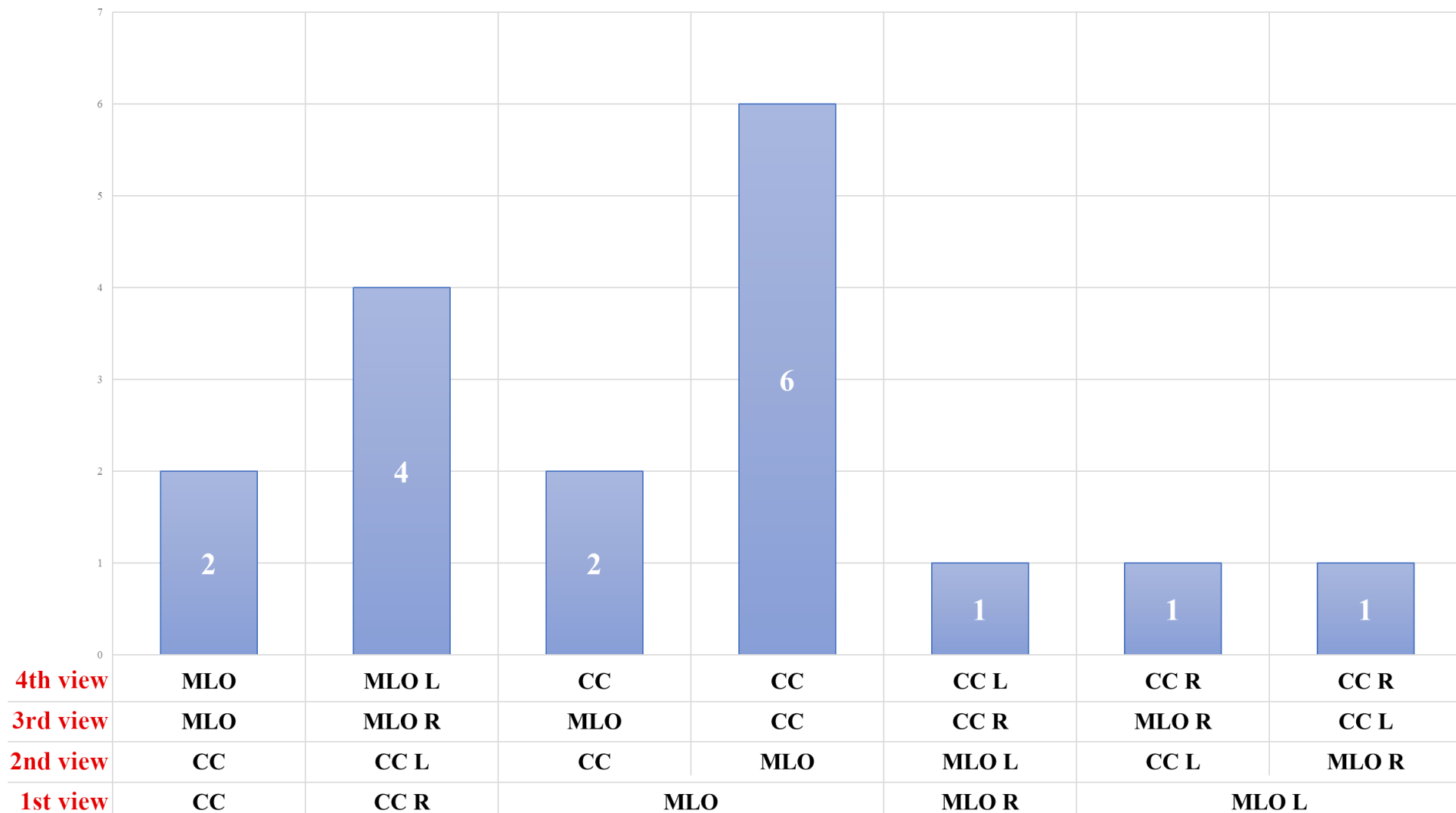


**Fig. 5.4** Graphical summary of pathology-oriented view acquisition orders for contrast-enhanced spectral mammography: CC: craniocaudal view; MLO: mediolateral oblique view; S: suspicious breast; NS: not suspicious breast

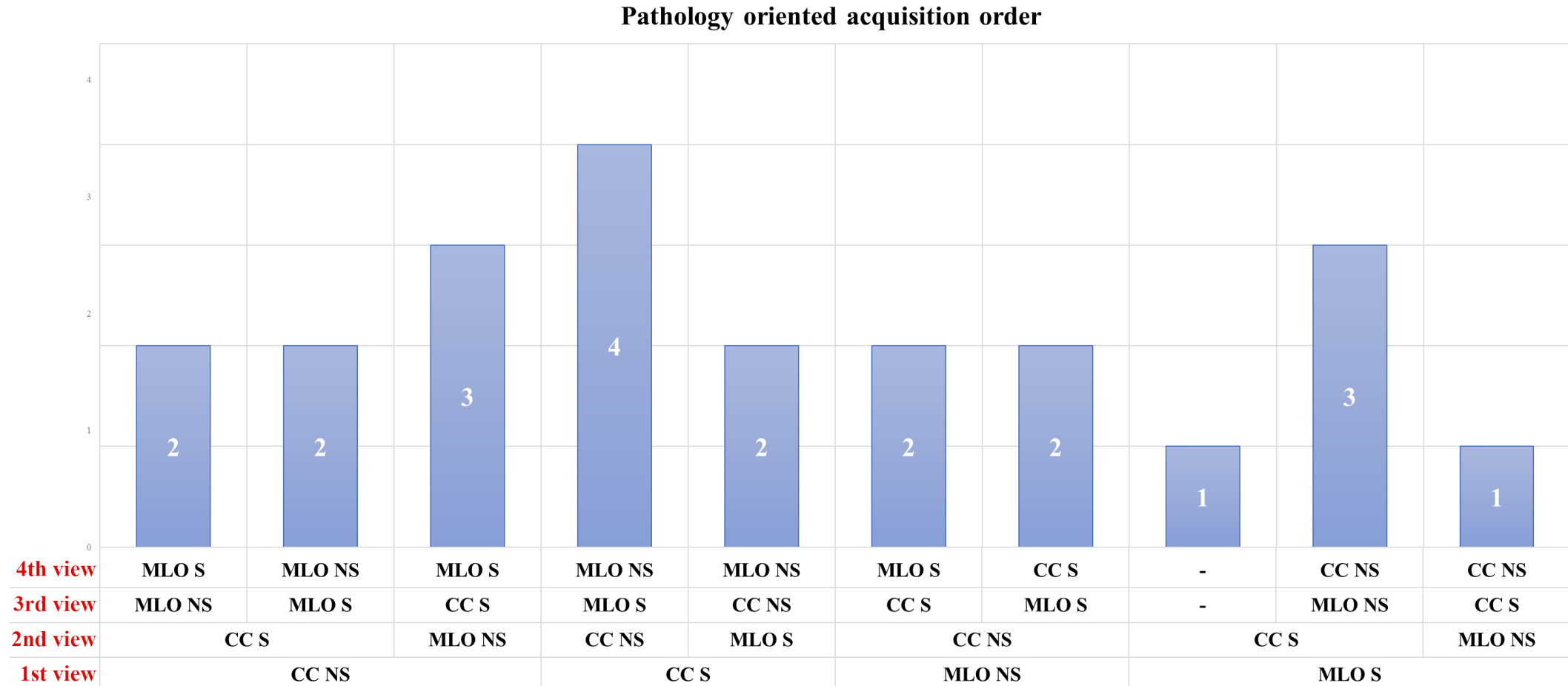


**Fig. 5.5** Forest plot of the 84 analysed articles on contrast-enhanced spectral mammography. No heterogeneity was found among studies ( $I^2 = 0\%$ ). The last row shows the pooled rate for adverse reactions arising from ICA administration, calculated using the fixed-effect model

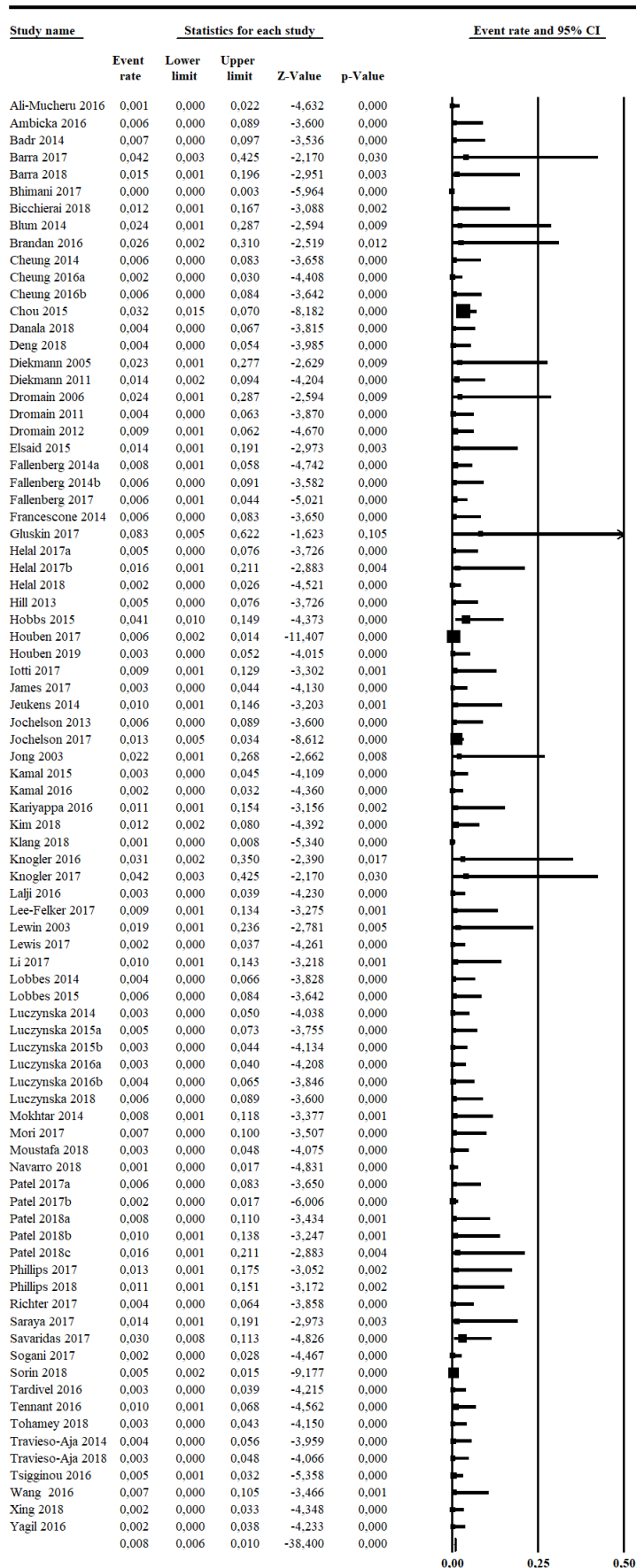




**Fig. 5.6** Funnel plot showing risk of publication bias in articles on contrast-enhanced spectral mammography, confirmed by the Egger test ( $p < 0.001$ )

**Funnel Plot of Standard Error by Logit event rate**

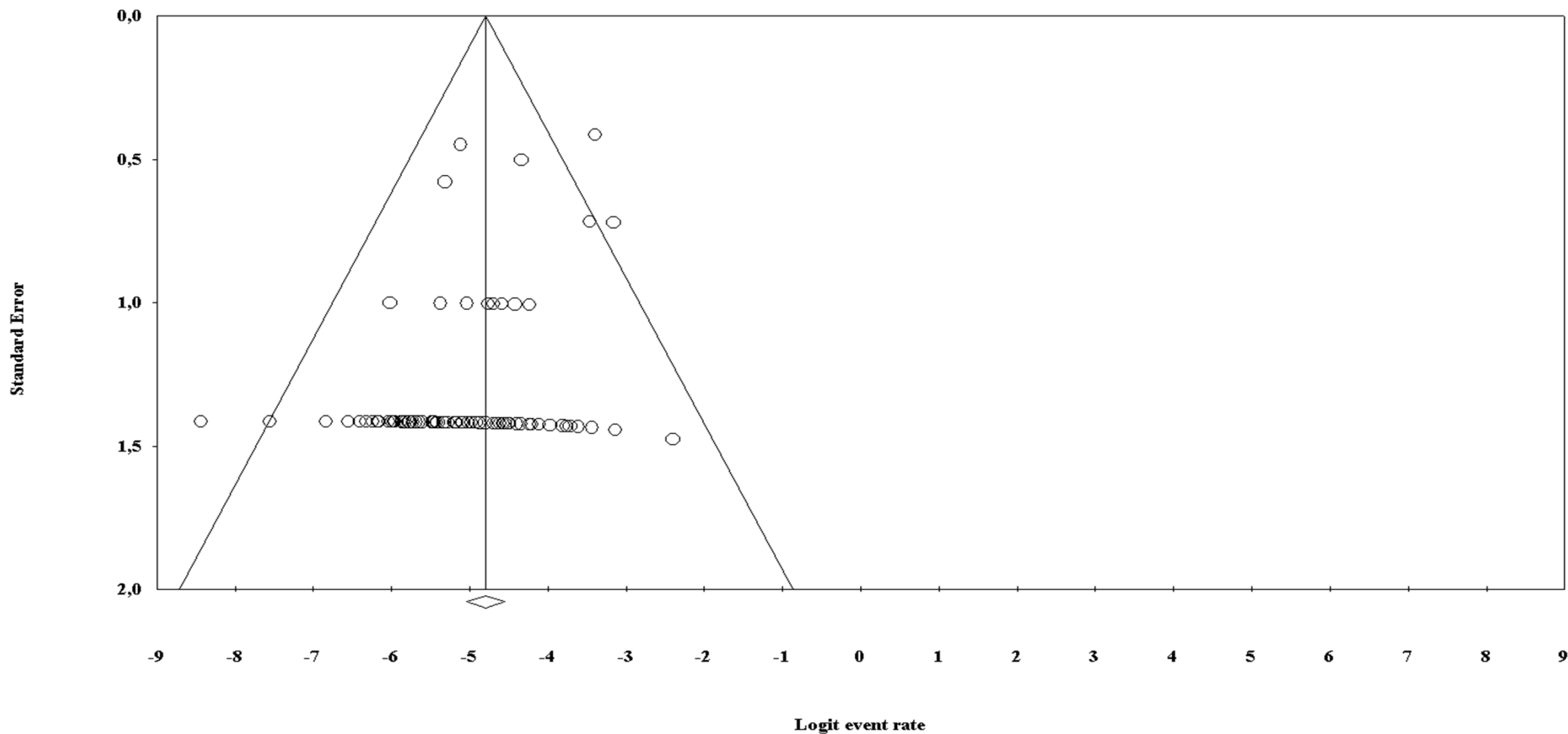
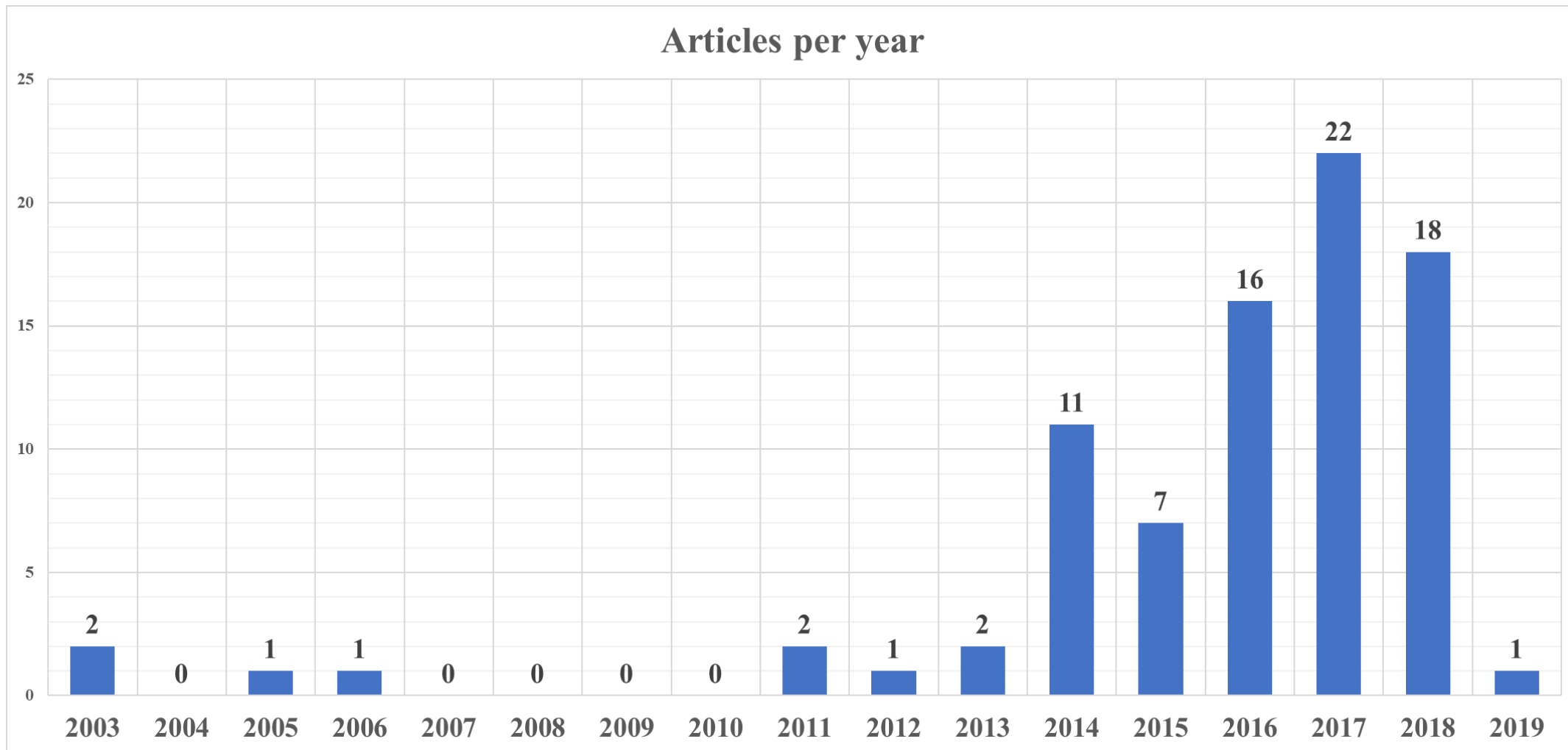


**Fig. 5.7** Graphic showing the number of articles published per year regarding contrast-enhanced spectral mammography





## 6. Contrast-enhanced mammography: a systematic review and meta-analysis of diagnostic performance

*Published as:*

Cozzi A, Magni V, Zanardo M, Schiaffino S, Sardanelli F (2021) *Contrast-enhanced Mammography: A Systematic Review and Meta-Analysis of Diagnostic Performance*. **Radiology** 302:568–581.

doi:10.1148/radiol.211412

## 6.1. Abstract

**Background:** CEM is a promising technique for breast cancer detection, but conflicting results have been reported in previous meta-analyses. We therefore aimed to perform a systematic review and meta-analysis of CEM diagnostic performance considering different interpretation methods and clinical settings.

**Methods:** The Medline, EMBASE, Web of Science, and Cochrane Library databases were systematically searched up to July 15, 2021. Prospective and retrospective studies evaluating CEM diagnostic performance with histopathology and/or follow-up as reference standard were included. Study quality was assessed with the Quality Assessment of Diagnostic Accuracy Studies-2 tool. Using STATA, summary diagnostic odds ratio (DOR) and area under the curve were estimated with the hierarchical summary receiver operating characteristic (HSROC) model. Summary estimates of sensitivity and specificity were obtained with the hierarchical bivariate model, pooling studies with the same image interpretation approach or focused on the same findings. Heterogeneity was investigated through meta-regression and subgroup analysis.

**Results:** Sixty studies (67 study parts, 11,049 CEM examinations from 10,605 patients) were included. The overall area under the HSROC curve was 0.94 (95% CI: 0.91, 0.96). Pooled DOR was 55.7 (95% CI: 42.7, 72.7), with high heterogeneity ( $\tau^2 = 0.3$ ). At meta-regression, CEM interpretation with both low-energy and recombined images had higher sensitivity (95% versus 94%,  $p < 0.001$ ) and specificity (81% versus 71%,  $p = 0.03$ ) compared to recombined images alone. At subgroup analysis, CEM showed a 95% pooled sensitivity (95% CI: 92, 97) and a 78% pooled specificity (95% CI: 66, 87) from nine studies on patients with dense breasts, while in 10 studies on mammography-detected suspicious findings CEM had a 92% pooled sensitivity (95% CI: 89, 94) and an 84% pooled specificity (95% CI: 73, 91).

**Conclusions:** CEM demonstrated high performance for breast cancer detection, especially with joint interpretation of low-energy and recombined images.

## **6.2. Introduction**

Previously published meta-analyses on CEM evaluated small study subsets and provided conflicting conclusions about CEM diagnostic performance [232–235]. However, comprehensive understanding of the clinical value of CEM is needed considering how large international bodies, such as the European Commission Initiative on Breast Cancer [236], recently stated that CEM may be preferred over breast MRI in selected women and settings, for example in surgical planning for newly-diagnosed breast cancer.

We therefore aimed to conduct an unrestricted and updated systematic review and meta-analysis of CEM diagnostic performance for breast cancer detection, investigating its variability according to different clinical settings and interpretation methods.

## **6.3. Methods**

### *Study search and selection*

This systematic review was developed from the protocol registered on PROSPERO (control number CRD42018118554) and was conducted and reported according to the Preferred Reporting Items for Systematic Review and Meta-Analysis of Diagnostic Test Accuracy Studies checklists [134].

A systematic search (Appendix 6.1) for articles reporting the clinical diagnostic use of CEM was performed on December 3<sup>rd</sup>, 2018, then updated on March 1<sup>st</sup>, 2021, and again on July 15<sup>th</sup>, 2021, using MEDLINE (PubMed), EMBASE, Web of Science, and the Cochrane Library databases. The search was limited to articles published in peer-reviewed journals and with an available abstract, no limits being applied to publication date.

After merging results and removing duplicate studies, the titles and abstracts of all obtained records were independently assessed for eligibility by three readers (A.C., with 3 years of experience in breast imaging and 3 years of experience in conducting meta-analyses after specific postgraduate

training; M.Z., with 5 years of experience in conducting meta-analyses after specific postgraduate training; and V.M., with 3 years of experience in breast imaging and 1 year of experience in conducting meta-analyses), each record being reviewed by two readers. Following inclusion and exclusion criteria detailed in Appendix 6.2, the same process was repeated with full-texts of eligible articles, references being manually searched to identify additional relevant records. Disagreements were solved by consensus and arbitration by a fourth reviewer who oversaw the whole study selection process (S.S., with 7 years of experience in breast imaging and 4 years of experience in conducting meta-analyses).

#### *Data extraction and quality assessment*

The aforementioned review process was also adopted for data extraction (as detailed in Appendix 6.2) and methodological quality assessment—using the Quality Assessment of Diagnostic Accuracy Studies 2 tool [237]—of each included study. Corresponding authors of articles with missing data were contacted by e-mail on two separate attempts before opting for study exclusion.

To reduce the risk of data duplication and of overlapping patient cohorts, three different measures were adopted. First, in the case of multiple potentially eligible studies that belonged to the same research group but did not provide a clearly distinct enrollment timeframe, we included only the one with the largest sample size and/or the widest study timeframe. Second, in the absence of a consensus on the most appropriate method to meta-analyze data from multireader studies [238, 239], we chose to include averages of the diagnostic performance of different readers. Third, in the case of studies reporting diagnostic performance indexes for different CEM interpretation approaches (eg interpretation based exclusively on the reading of recombined images versus joint reading of low-energy and recombined images, positivity threshold defined only by considering enhancement presence and conspicuity versus joint consideration of enhancement presence, conspicuity, and lesion morphology), these different metrics were reported as separate study parts and entered relevant subgroup analyses, no study contributing to any analysis with more than one

study part. For overall analysis, we considered only the study part with the most comprehensive reporting option, (ie positivity threshold defined by joint consideration of enhancement findings and morphological features), if possible with joint interpretation of low-energy and recombined images.

### *Statistical analysis*

Exploratory analyses revealed both the existence of a threshold effect (Fig. 6.1) and high heterogeneity, that—as suggested for meta-analyses of diagnostic test accuracy [240, 241]—was reported with  $\tau^2$  values fitted from bivariate random effects models. Since all included studies applied a qualitative interpretation of CEM, we could not define quantitative interpretation thresholds to guide subgroup analyses, but a partial proxy for this subgrouping was identified in the aforementioned different CEM interpretation strategies. We anticipated that these factors could represent heterogeneity sources (and therefore covariates for heterogeneity investigation) along with publication year, prospective or retrospective study design, diagnostic setting, focus of the study on specific findings, contrast agent concentration, and timing of CEM examination in relation with the menstrual cycle.

As recommended in such circumstances [239], we first used the Rutter and Gatsonis [242] hierarchical summary receiver operating characteristic (HSROC) model—considering all included studies—to obtain a summary curve of diagnostic performance, its area under the curve, and the summary diagnostic odds ratio (DOR). Then, the hierarchical bivariate model by Reitsma et al. [243] was used to produce coupled forest plots, derive joint summary estimates of sensitivity and specificity with their 95% confidence intervals (CIs)—pooling studies with a common image interpretation choice—and to further investigate heterogeneity through meta-regression. Finally, considering the heterogeneous clinical application of CEM and the results of methodological quality assessment, we also used the hierarchical bivariate model to obtain summary estimates of sensitivity and specificity from subgroups of five or more studies (a threshold chosen to facilitate convergence of the bivariate model) reporting on a specific subset of findings.



All analyses were conducted with the “midas” and the “metandi” modules in STATA (version MP 16.1, StataCorp, College Station, TX, USA). *p* values < .05 indicate a statistically significant difference.

## 6.4. Results

### *Study selection*

As shown in Fig. 6.2, 627 out of 919 records were excluded through title and abstract review. Full-text screening of the remaining 292 studies led to the inclusion in qualitative synthesis and meta-analysis of 60 studies [136, 139, 140, 142, 147, 155, 156, 165, 169, 173, 180, 183, 184, 186, 190, 193, 194, 196, 197, 199–202, 206, 207, 210, 211, 213, 244–275], published online between September 14<sup>th</sup>, 2010 [213] and April 6<sup>th</sup>, 2021 [269], of which 52% (31 of 60) had a prospective enrollment strategy. Since 12% (7 of 60) of studies had two sets of CEM diagnostic performance indexes from different image interpretation approaches, these were reported as two separate study parts [169, 180, 193, 252, 255, 256, 270], for a total of 67 reconstructed 2×2 contingency tables

### *Study characteristics and methodological quality*

Table 6.1, Table 6.2, and Table 6.3 detail the characteristics extracted from the 67 included study parts. The 60 included studies came from 43 research groups over 19 countries and five continents, reporting a total 10,605 patients. Only 3% (2 of 60) of articles were clearly identifiable as multicenter studies, involving collaborations of two [186] and three centers [260], all in Europe. Histopathology was the sole reference standard in 58% (35 of 60) of studies, while in 42% of studies (25 of 60) follow-up (at least one year) was also added, serving as reference standard for examinations judged to be negative or harboring benign findings. A total 11,049 CEM examinations, with a 43.21% disease prevalence, were reported: of the 7879 examinations (71.31%) with histopathological confirmation, 4025 (36.43%) were invasive cancers, 749 (6.78%) ductal

carcinomas in situ, 285 (2.58%) lesions with uncertain malignant potential, and 2820 (25.52%) were benign lesions. The remaining 3170 (28.69%) examinations had benign findings or were normal examinations confirmed at follow-up. The use of CEM in mixed diagnostic settings was reported by 32% (19 of 60) of studies (Table 6.3). The work-up of suspicious findings from clinical examination or other imaging modalities was the most frequent setting, being reported by 87% (52 of 60) of studies, followed by breast cancer screening in selected groups of patients (12 of 60 studies, 20%) and preoperative staging (12 of 60 studies, 20%), with postoperative monitoring being the least frequent indication (6 of 60 studies, 10%, always in combination with other indications).

Fig. 6.3 summarizes the results of methodological quality assessment of included studies, detailed at study level in Appendix 6.3 and Table 6.4.

#### *Meta-analysis*

Fig. 6.4 depicts forest plots of sensitivity and specificity for the 67 study parts. The HSROC analysis considered 60 study parts from 60 studies. As shown in Fig. 6.5, the overall HSROC curve had an area under the curve of 0.94 (95% CI: 0.91, 0.96) and a 55.7 pooled DOR (95% CI: 42.7, 72.7; range 4.7–585.0) with high heterogeneity ( $\tau^2 = 0.3$ ). Fig. 6.6 depicts the Fagan nomogram with pooled estimates of likelihood ratios.

Forest plots of sensitivity and specificity for subgroup analysis according to CEM interpretation approaches are depicted in Fig. 6.7. The bivariate model summary estimates for the 24 study parts in which CEM was interpreted considering only enhancement presence and conspicuity on recombined images showed a 93% pooled sensitivity (95% CI: 89, 96;  $\tau^2 = 1.1$ ) and a 70% pooled specificity (95% CI: 60, 78;  $\tau^2 = 0.9$ ); the pooled sensitivity of the 10 study parts in which CEM was interpreted considering enhancement presence, conspicuity, and morphology on recombined images was 93% (95% CI: 90, 95;  $\tau^2 = 0.1$ ), with a 61% pooled specificity (95% CI: 48, 73;  $\tau^2 = 0.6$ ). Finally, pooling the remaining 33 study parts in which CEM was interpreted considering both

enhancement and morphology of findings from both low-energy and recombined images, we obtained a 95% summary sensitivity (95% CI: 92, 97;  $\tau^2 = 0.7$ ) and an 81% summary specificity (95% CI: 76, 86;  $\tau^2 = 0.7$ ).

Further investigation of heterogeneity was undertaken by meta-regression through the bivariate model on the 60 study parts considered for the main analysis (Table 6.5, Table 6.6, Table 6.7, and Appendix 6.4). Continuous covariates (number of patients, number of examinations, publication year, concentration of administered contrast agent) were excluded from the analysis because of low and non-significant correlations with logit sensitivity and logit specificity, while the inclusion of the diagnostic setting as a covariate was hindered by the sizable number of studies (30%) reporting patients from different settings. As hypothesized from preliminary analysis, meta-regression revealed that the most important factor influencing diagnostic performance was the joint interpretation of low-energy and recombined images. In the 33 study parts which adopted this approach, both pooled sensitivity (95% versus 94%,  $p < 0.001$ ) and pooled specificity (81% versus 71%,  $p = 0.03$ ) reached their highest estimates. Albeit with lower and marginal differences, also the interpretation of both lesion morphology and enhancement features (43 study parts) versus the sole interpretation of enhancement features resulted in both higher pooled sensitivity (95% versus 94%,  $p < 0.001$ ) and higher pooled specificity (78% versus 76%,  $p = 0.006$ ).

Subgroup analysis according to patient- or finding-specific subsets was performed for the two subgroups that had more than five study parts each (Fig. 6.8). The nine studies solely focusing on patients with dense breasts (1249 patients and 1364 examinations, with a 31.4% disease prevalence) had a 95% pooled sensitivity (95% CI: 92, 97;  $\tau^2 = 0.4$ ) and a 78% pooled specificity (95% CI: 66, 87;  $\tau^2 = 0.9$ ). The 10 studies focusing on suspicious digital mammography findings classified as Breast Imaging Reporting and Data System (BI-RADS) category of 3 or greater (720 patients and 953 examinations, with a 51.1% disease prevalence) showed a 92% pooled sensitivity (95% CI: 89, 94;  $\tau^2 = 0.1$ ) and an 84% pooled specificity (95% CI: 73, 91;  $\tau^2 = 0.6$ ).

## 6.5. Discussion

In this systematic review and meta-analysis aiming to evaluate the diagnostic performance of CEM for breast cancer detection, CEM showed a 0.94 area under the hierarchical summary receiver operating characteristic curve and a 55.7 pooled diagnostic odds ratio. At meta-regression, CEM had higher pooled sensitivity (95% versus 94%,  $p < 0.001$ ) and specificity (81% versus 71%,  $p = 0.03$ ) when interpreted considering both low-energy and recombined images compared to recombined images alone. At subgroup analysis, CEM showed high pooled sensitivity and specificity for the assessment of mammography-detected suspicious findings (92% and 84%, respectively) and the evaluation of patients with dense breasts (95% and 78%, respectively).

Only two of the four previously-published meta-analyses on CEM included more than 10 studies (none of them more than 18), being either conducted on studies from the early years of CEM implementation [232, 233] or being restricted to specific study subsets [234, 235]. These works provided conflicting impressions of CEM diagnostic performance: the two meta-analyses reporting a pooled sensitivity higher than 95% reported a pooled specificity ranging 58%–66% [232, 234], while the two meta-analyses with a specificity ranging 77%–84% showed a pooled sensitivity under 90% [233, 235]. Since we identified at least 80 potentially includible articles published after the most recent one analyzed by the most recent meta-analysis [235], we aimed to conduct an unrestricted evaluation of CEM diagnostic performance, that, by the inclusion of sufficient numbers of articles, could allow us to explore the influence of subgroups and covariates.

As expected, the pooling of 10,605 patients and 11,049 examinations from 60 studies (53% published from 2019 onwards) led to high heterogeneity, only partially explained (approximately 61%) by a concurrent threshold effect. As recommended [239], we avoided the presentation of summary sensitivity and specificity from overall analysis, instead plotting the HSROC curve and reporting the pooled DOR. However, since the clinical translation of findings from a meta-analysis of diagnostic test accuracy relies on weighting the sensitivity and specificity, their pooled estimates

were obtained with the bivariate model in subgroups with lower threshold effect and less heterogeneity. Results from subgroup analysis and meta-regression showed that the failure to consider the correlative properties of CEM dual-energy nature represents the strongest hindrance to attaining a balanced diagnostic performance. Indeed, compared to the 34 study parts considering only recombined images (with or without joint interpretation of enhancement presence, conspicuity, and morphology), the 33 study parts which considered both low-energy and recombined images had a modestly higher pooled sensitivity (from 93% to 95%) but a substantially higher pooled specificity (from 61% and 70% up to 81%). These results highlight the need (and the related beneficial effects) of a thorough systematization of CEM interpretation, chiefly by its inclusion into the BI-RADS. When such a favorable trade-off between sensitivity and specificity was attained for breast CE-MRI in the early 2000s [22, 89, 276–278], it paved the way for its establishment in the screening setting.

Further preference in the use of CEM over CE-MRI could come from its ability to correlate low-energy mammographic findings with enhancement. This correlation could be particularly useful in at least three scenarios: first, in the the assessment of mammography-detected suspicious findings, where subgroup analysis yielded a 92% summary sensitivity and an 84% summary specificity, showing how CEM—applied as a work-up examination—could reduce the number of unnecessary invasive procedures and their related economic and psychological costs. Second, for supplemental breast cancer screening in patients with dense breasts [217]—where our subgroup analysis indicates a 95% summary sensitivity and a 78% summary specificity—and, third, for annual screening of women who underwent thoracic radiation therapy, who have a higher incidence of ductal carcinoma in situ with low neo-angiogenesis [279] which may be missed by breast CE-MRI but would be detectable on low-energy mammographic images due to the presence of calcifications [130].

The lack of established enhancement thresholds between benign and malignant lesions could be also addressed by quantitative analysis of CEM images [189, 280–282] and artificial intelligence-

driven texture analysis [155, 283, 284], that could also deal with the effects of background parenchymal enhancement. In this regard, our meta-regression showed ambiguous effects of CEM timing in relation with menstrual cycle—with non-significant variations in pooled sensitivity and specificity—but these findings should be cautiously interpreted due to the up-to-now fragmentary reporting of such characteristics.

As already mentioned, high heterogeneity represents the chief limitation of our meta-analysis. While we tried to address this through combined use of the HSROC and bivariate models, subgroup analysis, and meta-regression, the coexistence of patients coming from different clinical scenarios ultimately prevented us to give overall summary estimates of sensitivity and specificity. Further investigation of heterogeneity would need to be conducted with more powerful tools to regroup and analyze specific findings, patients, and diagnostic settings, such as individual patient data meta-analysis. Three other limitations are the small number of multicenter studies, the lack of sufficient data to specifically meta-analyze CEM performance in the screening setting, and the lack of randomized studies, which are currently underway [285].

In conclusion, our meta-analysis showed that CEM has high diagnostic performance for breast cancer detection, although with high heterogeneity and a clear threshold effect. Bivariate pooled estimates of sensitivity and specificity reached their highest values when CEM was interpreted using both low-energy and recombined images and jointly considering lesion morphology and enhancement. The establishment of a common interpretation framework is warranted to further expand the role of CEM as a routine breast imaging examination.

**Table 6.1** Main characteristics of the 36 study parts included from 31 prospective studies

Author and Year	Ref.	Country	No. Patients	No. Examinations	Specific Subset *	Features	Images	Reference Standard	Inv.	DCIS	B3	Benign	Neg.
Dromain 2011	[213]	France	120	130	-	E	Rec	Path+FU	80	0	0	50	0
Badr 2014	[211]	France	75	37	-	E	Rec	Path	19	0	1	17	0
Łuczyńska 2014	[156]	Poland	152	173	-	E+M	LE+Rec	Path	101	13	2	57	0
Mokhtar 2014 (1)	[169]	Egypt	60	60	DB	E	Rec	Path+US	44	0	2	11	3
Mokhtar 2014 (2)						E+M							
ElSaid 2015	[183]	Egypt	34	36	BE	E	Rec	Path	25	0	0	11	0
Łuczyńska 2015	[165]	Poland	102	118	-	E+M	LE+Rec	Path	72	9	0	37	0
Kariyappa 2016 (1)	[180]	India	44	44	-	E	Rec	Path+FU	32	0	1	9	2
Kariyappa 2016 (2)						E+M	LE+Rec						
Knogler 2016 (1)	[193]	Austria	15	15	SL	E	Rec	Path	8	0	0	7	0
Knogler 2016 (2)						E+M	Rec						
Tsigginou 2016	[200]	Greece	216	226	SL	E	Rec	Path	79	19	9	119	0
Wang 2016	[206]	China	68	77	-	E+M	LE+Rec	Path	43	5	3	26	0
Fallenberg 2017	[186]	Germany †	155	604	-	E+M	LE+Rec	Path+FU	224	47	6	31	296
Mori 2017	[184]	Japan	72	143	SL	E	Rec	Path+FU	40	18	0	83	2
Saraya 2017	[139]	Egypt	34	39	SL	E+M	LE+Rec	Path	14	2	0	23	0
Kim 2018	[197]	South Korea	84	154	-	E+M	Rec	Path	94	27	11	22	0
Navarro 2018	[201]	Chile	465	85	-	E+M	Rec	Path	55	0	11	19	0
Yousef 2018	[244]	Egypt	20	20	-	E+M	LE+Rec	Path	13	0	0	7	0
Helal 2019	[246]	Egypt	70	70	-	E	Rec	Path+FU	29	5	0	11	25
Huang 2019	[247]	USA	21	24	SL	E	Rec	Path	17	3	0	4	0
Kamal 2019	[248]	Egypt	365	380	AS	E	Rec	Path+FU	241	16	5	118	0
Xing 2019	[194]	China	235	263	-	E+M	LE+Rec	Path	171	6	14	72	0
Yasin 2019	[254]	Egypt	50	56	SL	E	Rec	Path	31	3	9	13	0

Azzam 2020 (1)	[255]	Egypt	37	63	DB	E	Rec	Path+FU	36	0	0	27	0
Azzam 2020 (2)						E+M							
Clausner 2020	[257]	Austria	80	93	SL	E+M	LE+Rec	Path	46	15	6	26	0
Depretto 2020	[258]	Italy	34	36	CALC	E	Rec	Path	4	11	7	14	0
Lu 2020	[263]	China	115	131	SYM	E+M	LE+Rec	Path	60	4	7	60	0
Petrillo 2020	[264]	Italy	100	136	SL	E+M	Rec	Path	67	16	8	45	0
Soliman 2020	[266]	Egypt	38	38	AS	E	Rec	Path+FU	23	0	0	15	0
Anwar 2021 (1)	[270]	Egypt	32	40	DB	E	Rec	Path	30	1	0	9	0
Anwar 2021 (2)						E+M							
Hashem 2021	[272]	Egypt	283	283	IRW	E+M	Rec	Path+FU	9	168	6	100	0
Mohamed 2021	[274]	Egypt	25	25	DB	E+M	LE+Rec	Path	14	0	0	11	0
Sudhir 2021	[275]	India	130	166	DB	E+M	LE+Rec	Path	73	14	9	70	0

AS = asymmetries, BE = breast edema, CALC = suspicious calcifications, DB = dense breasts, DCIS = ductal carcinoma in situ, E = enhancement features, E+M = enhancement and morphological features, FU = follow-up, Inv. = invasive lesions (intraductal or lobular carcinoma), IRW = women at increased risk for breast cancer, LE+Rec = low-energy and recombined images, Neg. = benign imaging findings confirmed at follow-up or CEM examinations without suspicious findings, Path = pathology, Rec = recombined images, Ref. = reference, SL = suspicious lesions (Breast Imaging Reporting and Data System category  $\geq 3$ ), SYM = symptomatic women.

\* Cells marked with a dash indicate that the study was not focused on any specific patients' or lesion subset.

† Multicenter study in Germany and France.



**Table 6.2** Main characteristics of the 31 study parts included from 29 retrospective studies

Author and Year	Ref.	Country	No. Patients	No. Examinations	Specific Subset *	Features	Images	Reference Standard	Inv.	DCIS	B3	Benign	Neg.
Cheung 2014	[196]	Taiwan	89	100	DB	E	Rec	Path	58	14	10	18	0
Kamal 2015	[190]	Egypt	168	211	-	E	Rec	Path+FU	106	3	3	99	0
Cheung 2016	[207]	Taiwan	87	94	CALC	E	Rec	Path	8	19	32	35	0
Lalji 2016	[142]	Netherlands	199	199	-	E+M	LE+Rec	Path+US	54	5	6	134	0
Tardivel 2016	[140]	France	195	299	-	E+M	LE+Rec	Path+FU	208	13	11	29	38
Tennant 2016	[136]	UK	99	100	SYM	E+M	LE+Rec	Path	71	2	0	10	17
Lee-Felker 2017	[147]	USA	52	120	-	E+M	LE+Rec	Path+FU+US	57	15	11	11	26
Li 2017	[210]	USA	48	66	-	E+M	LE+Rec	Path	57	5	0	4	0
Klang 2018	[199]	Israel	953	87	-	E+M	Rec	Path	31	6	0	50	0
Patel 2018	[155]	USA	50	50	SL	E+M	LE+Rec	Path	20	6	6	18	0
Richter 2018	[173]	Germany	105	117	-	E+M	LE+Rec	Path+FU	82	1	0	11	23
Sorin 2018	[202]	Israel	611	611	DB	E+M	LE+Rec	Path+FU	15	6	5	110	475
Fanizzi 2019	[245]	Italy	53	58	-	E+M	LE+Rec	Path	34	0	0	24	0
Kim 2019	[249]	USA	64	64	-	E+M	LE+Rec	Path+FU	8	3	1	4	48
Lobbes 2019	[250]	Netherlands	368	368	-	E+M	LE+Rec	Path+FU	84	42	0	154	88
Sung 2019	[251]	USA	858	858	IRW	E+M	LE+Rec	Path+FU	11	5	0	36	806
Travieso-Aja 2019 (1)	[252]	Spain	465	644	-	E	Rec	Path+FU	373	53	0	154	64
Travieso-Aja 2019 (2)						E+M	LE+Rec						
Wessam 2019	[253]	Egypt	125	125	AS	E+M	LE+Rec	Path+FU	89	2	4	25	5
Chi 2020 (1)	[256]	China	304	312	-	E	Rec	Path	181	22	22	87	0
Chi 2020 (2)						E+M	LE+Rec						
Gluskin 2020	[259]	USA	917	917	IRW	E+M	LE+Rec	Path+FU	17	1	0	0	899
González-Huebra 2020	[260]	Spain †	135	200	-	E+M	LE+Rec	Path	98	20	0	82	0
Kamal 2020	[261]	Egypt	82	171	SL	E+M	Rec	Path+FU	113	7	6	25	20
Long 2020	[262]	China	73	74	CALC	E	Rec	Path	6	20	1	47	0
Qin 2020	[265]	China	114	144	DB	E+M	LE+Rec	Path	34	0	0	110	0
Sorin 2020	[267]	Israel	138	147	SYM	E+M	LE+Rec	Path+FU	36	2	2	48	59
Steinhof-Radwańska 2020	[268]	Poland	547	593	-	E	Rec	Path+FU	272	55	26	240	0
Ainakulova 2021	[269]	Kazakhstan	151	155	DB	E+M	LE+Rec	Path	81	8	0	66	0
Goh 2021	[271]	Taiwan	92	94	AD	E	Rec	Path+FU	23	10	22	29	10
Hogan 2021	[273]	USA	132	306	IRW	E+M	LE+Rec	Path+FU	4	2	0	36	264

AD = architectural distortion, AS = asymmetries, CALC = suspicious calcifications, DB = dense breasts, DCIS = ductal carcinoma in situ, E = enhancement features, E+M = enhancement and morphological features, FU = follow-up, Inv. = invasive lesions (intraductal or lobular carcinoma), IRW = women at increased risk for breast cancer, LE+Rec = low-energy and recombined images, Neg. = benign imaging findings confirmed at follow-up or CEM examinations without suspicious findings, Path = pathology, SL = suspicious lesions (Breast Imaging Reporting and Data System category  $\geq 3$ ), SYM = symptomatic women, Ref. = reference, Rec = recombined images, US = ultrasonography

\* Cells marked with a dash indicate that the study was not focused on any specific patients' or lesion subset.

† Multicenter study in Spain, Denmark, Germany.

**Table 6.3** Performance indexes and additional technical and clinical characteristics of the 67 included study parts

Author / Year	Study Design	Modality Name	Patients		Setting						Lesion or Patients' Subset	Mens. Cycle Reg.	System		Iodinated Contrast Agent				Exam Time	BIExp (Months)	CEM Interpretation		Ref. Stand.	FU (Months)	Dis. Prev.	Performance Indexes			
			No.	Mean Age	SC	SC-r	S-IM	S-C	Pre.	Post.			Vendor	Unit	Molecule	Dose	Conc.	Flow Rate (ml/s)			Features	Images				TP	TN	FP	FN
Dromain 2011	P	CEDM	120	56		•					-	No	GE	Senographe DS§	Iobitridol	1.5	300	3	A	-	E	Rec	Path + FU	-	61.5%	74	37	13	6
Badr 2014	P	-	75	54			•				-	No	-	-	Iohexol	1.5	300	-	B	-	E	Rec	Path	-	51.4%	18	9	9	1
Cheung 2014	R	DE-CESM	89	48			•				DB	No	GE	Senographe Essential*	Iohexol	1.5	350	3	B	-	E	Rec	Path	-	72.0%	70	22	6	2
Łuczyńska 2014	P	CESM	152	56			•				-	No	GE	Senographe Essential*	Iopromide	1.5	370	3	B	>20	E+M	LE+Rec	Path	-	65.9%	114	24	35	0
Mokhtar 2014 <sup>1</sup>	P	CEDM	60	-		•	•				DB	No	GE	Senographe DS§	Iohexol	1.5	300	-	A	-	E	Rec	Path + US	-	73.3%	43	5	11	1
Mokhtar 2014 <sup>2</sup>																					E+M					43	8	8	1
ElSaid 2015	P	CEDM	34	55			•				BE	No	GE	**	Iohexol	1.5	300	3	B	-	E	Rec	Path	-	69.4%	22	9	2	3
Kamal 2015	R	CESM	168	-			•				-	No	GE	Senographe Essential*	Iohexol	1.5	300	3	B	20	E	Rec	Path + FU	12	51.7%	103	60	42	6
Łuczyńska 2015	P	CESM	102	-			•				-	Yes	GE	**	Iopromide	1.5	370	3	B	15	E+M	LE+Rec	Path	-	68.6%	81	12	25	0
Cheung 2016	R	CESM	87	54		•					CALC	No	GE	Senographe Essential*	Iohexol	1.5	350	3	B	-	E	Rec	Path	-	28.7%	24	58	9	3
Kariyappa 2016 <sup>1</sup>	P	CEDM	44	-		•					-	No	GE	Senographe Essential*	Iomeprol	1.5	350	3	B	-	E	Rec	Path + FU	-	72.7%	31	5	7	1
Kariyappa 2016 <sup>2</sup>																					E+M	LE+Rec				26	10	2	6

Knogler 2016 <sup>1</sup>																			E						8	5	2	0
Knogler 2016 <sup>2</sup>	P	CEDEM	15	58	•				SL	Yes	Siemens	Mammomat	Iomeprol	2	400	3.5	-	>6	E+M	Rec	Path	-	53.3%	8	6	1	0	
Lalji 2016	R	CESM	199	58	•				-	No	GE	Senographe Essential*	Iopromide	1.5	300	3	-	-	E+M	LE+Rec	Path + US	-	29.6%	57	98	42	2	
Tardivel 2016	R	CESM	195	56	•	•			-	No	GE	Senographe Essential*	Iobitridol	1.5	300	3	B	>0.5	E+M	LE+Rec	Path + FU	14	73.9%	207	60	18	14	
Tennant 2016	R	CESM	99	49		•			SYM	No	GE	**	-	-	-	-	-	>8	E+M	LE+Rec	Path	-	73.0%	69	22	5	4	
Tsigginou 2016	P	CESM	216	55	•				SL	No	GE	Senographe Essential*	Iopromide	1.5	300	2-3	B	4-15	E	Rec	Path	-	43.4%	92	91	37	6	
Wang 2016	P	CESM	68	53	•				-	No	GE	Senographe DS or Senographe Essential*	Iohexol	1.5	350	3	A	-	E+M	LE+Rec	Path	-	62.3%	46	19	10	2	
Fallenberg 2017	P	CESM	155	53	•	•			-	No	GE	Senographe DS§	Iobitridol	1.5	300	3	A	>5.5	E+M	LE+Rec	Path + FU	>24	44.9%	191	305	26	82	
Lee-Felker 2017	R	CESM	52	50	•	•			-	No	GE	Senographe DS*	Iohexol	90 ml	350	3	B	>2	E+M	LE+Rec	Path + FU + US	>17	60.0%	66	43	5	6	
Li 2017	R	CESM	48	56		•			-	No	GE	Senographe Essential*	Iopamidol	1.5	370	1.5-2	B	-	E+M	LE+Rec	Path	-	93.9%	62	2	2	0	
Mori 2017	P	CESM	72	48	•				SL	No	GE	Senographe Essential*	Iohexol	1.5	300	3	-	>20	E	Rec	Path + FU	-	40.6%	50	80	5	8	
Saraya 2017	P	CEDM	34	54	•				SL	No	GE	-	Iohexol	1.5	300	4	C	-	E+M	LE+Rec	Path	-	41.0%	15	21	2	1	
Kim 2018	P	CEDM	84	51		•			-	Yes	Hologic	Selenia Dimensions	Iohexol	1.5	350	2	B	>6	E+M	Rec	Path	-	78.6%	109	15	18	12	
Klang 2018	R	CESM	953	52	•	•	•	•	-	No	GE	Senographe Essential*	Iopamidol	1.5	370	3	B	>15	E+M	Rec	Path	-	42.5%	36	20	30	1	
Navarro 2018	P	CESM	465	53	•	•	•	•	-	No	GE	**	Ioversol	1.5	320	-	B	>4	E+M	Rec	Path	-	64.7%	55	11	19	0	

Patel 2018	R	CESM	50	57					SL	No	Hologic	Selenia Dimensions	Iohexol	1.5	350	3	B	5	E+M	LE+Rec	Path	-	52.0%	25	16	8	1
Richter 2018	R	CESM	105	58					-	No	GE	Senographe Essential*	Iopromide	1.5	300	2-3	-	>5	E+M	LE+Rec	Path + FU	12	70.9%	82	29	5	1
Sorin 2018	R	CESM	611	54	•				DB	No	GE	Senographe Essential*	Iopamidol	1.5	370	3	B	25	E+M	LE+Rec	Path + FU	>12	3.4%	19	449	141	2
Yousef 2018	P	CESM	20	-					-	-	-	-	Iohexol	1-1.5	300	3	B	-	E+M	LE+Rec	Path	-	65.0%	12	5	2	1
Fanizzi 2019	R	CESM	53	52					-	No	GE	Senographe Essential*	Iodixanol	1.5	320	2-3	B	>10	E+M	LE+Rec	Path	-	58.6%	34	20	4	0
Helal 2019	P	CESM	70	-					-	No	GE	Senographe Essential*	-	1.5	-	-	B	>20	E	Rec	Path + FU	12	48.6%	31	27	9	3
Huang 2019	P	CEDM	21	-					SL	No	Siemens	Mammomat Inspiration DBT§	Iohexol	1.5-2	350	3	A	>10	E	Rec	Path	-	83.3%	19	2	2	1
Kamal 2019	P	CESM	365	47					AS	No	GE	Senographe Essential*	-	1.5	-	-	-	10	E	Rec	Path + FU	18	67.6%	243	93	30	14
Kim 2019	R	CEM	64	52	•	•			-	No	GE	Senographe Essential*	Iohexol	1.5	350	3	-	-	E+M	LE+Rec	Path + FU	24	17.2%	10	46	7	1
Lobbis 2019	R	CEM	368	60	•	•	•		-	No	GE	Senographe Essential*	Iopromide	1.5	300	3	-	>6	E+M	LE+Rec	Path + FU	≥12	34.2%	117	192	50	9
Sung 2019	R	CEDM	858	52	•				IRW	No	GE	Senographe Essential*	Iohexol	1.5	350	3	-	-	E+M	LE+Rec	Path + FU	12	1.9%	14	789	53	2
Travieso-Aja 2019 <sup>1</sup>	R	CESM	465	52	•	•			-	No	GE	Senographe Essential*	Iopromide	1.5	300	3	B	-	E	Rec	Path + FU	18-24	66.1%	412	89	129	14
Travieso-Aja 2019 <sup>2</sup>																			E+M	LE+Rec				396	185	33	30
Wessam 2019	R	CESM	125	49	•	•			AS	No	GE	Senographe Essential*	Iohexol	1.5	300	-	-	-	E+M	LE+Rec	Path + FU	-	72.8%	91	19	15	0
Xing 2019	P	CESM	235	51					-	No	GE	Senographe Essential*	Iohexol	1.5	350	3	B	10	E+M	LE+Rec	Path	-	67.3%	162	77	9	15

Yasin 2019	P	CESM	50	52					SL	Yes	GE	Senographe Essential*	Iodixanol	1.5	320	-	B	>15	E	Rec	Path	-	60.7%	32	22	0	2
Azzam 2020 <sup>1</sup>	P	CEM	37	47					DB	No	GE	Senographe Essential*	-	1.5	-	-	B	-	E	Rec	Path + FU	18	57.1%	32	13	14	4
Azzam 2020 <sup>2</sup>																			E+M					32	24	3	4
Chi 2020 <sup>1</sup>	R	CESM	304	51					-	No	GE	Senographe Essential*	Iohexol	1.5	350	3	B	>10	E	Rec	Path	-	65.1%	103	101	8	100
Chi 2020 <sup>2</sup>																			E+M	LE+Rec				158	85	24	45
Clauser 2020	P	L-CEM	80	54					SL	Yes	Siemens	Mammomat Inspiration	Iobitridol	2	350	3	-	-	E+M	LE+Rec	Path	-	65.6%	57	30	2	4
Depretto 2020	P	CEM	34	54					CALC	No	Hologic	Selenia Dimensions	Iopamidol	1.5	370	2-3	-	>20	E	Rec	Path	-	41.7%	7	18	3	8
Gluskin 2020	R	CEM	917	53					IRW	No	GE	Senographe DS or Essential or Pristina*	Iohexol	1.5	350	3	-	-	E+M	LE+Rec	Path + FU	12	2.0%	12	861	38	6
González-Huebra 2020	R	TiCEM	135	-					-	-	Siemens	Mammomat Revelation	Iohexol	1.5	350	3	B	20	E+M	LE+Rec	Path	-	59.0%	89	71	11	29
Kamal 2020	R	CEM	82	49					SL	No	GE	Senographe Essential*	-	1.5	-	-	-	-	E+M	Rec	Path + FU	12	70.2%	113	33	18	7
Long 2020	R	CEM	73	48					CALC	No	GE	Senographe Essential*	Iohexol	2	300	2.5	B	3	E	Rec	Path	-	35.1%	19	40	8	7
Lu 2020	P	CESM	115	47					SYM	No	GE	Senographe Essential*	Iohexol	1.5	350	3	B	12	E+M	LE+Rec	Path	-	48.9%	60	59	8	4
Petrillo 2020	P	CEDM	100	58					SL	-	Hologic	Selenia Dimensions	Iodixanol	1.5	320	2	B	>15	E+M	Rec	Path	-	61.0%	73	43	10	10
Qin 2020	R	CESM	114	48					DB	-	GE	**	-	1.5	-	-	-	-	E+M	LE+Rec	Path	-	23.6%	28	106	4	6
Soliman 2020	P	CEDM	38	-					AS	No	GE	Senographe Pristina*	Iohexol	1.5	300	-	B	-	E	Rec	Path + FU	24	60.5%	23	9	6	0

Sorin 2020	R	CESM	138	48					SYM	-	GE	Senographe Essential*	Iopamidol	1.5	370	3	B	-	E+M	LE+Rec	Path + FU	12	25.9%	38	80	29	0
Steinhof-Radwańska 2020	R	CESM	547	56					-	No	GE	**	-	1.5	-	3	B	-	E	Rec	Path + FU	12	55.1%	320	158	108	7
Ainakulova 2021	R	CESM	151	47					DB	Yes	GE	Senographe Essential*	-	1.5	-	-	B	>5	E+M	LE+Rec	Path	-	57.4%	87	53	13	2
Anwar 2021 <sup>1</sup>	P	CESM	32	46					DB	No	GE	Senographe Essential*	-	1.5	-	3	B	-	E	Rec	Path	-	77.5%	28	1	8	3
E+M																			28					3	6	3	
Goh 2021	R	CEDM	92	52					AD	No	Hologic	Selenia Dimensions	Iohexol	1.5	350	3	B	>5	E	Rec	Path + FU	24	35.1%	33	26	35	0
Hashem 2021	P	CEM	283	48					IRW	No	GE	Senographe Essential*	-	1.5	-	3	B	>10	E+M	Rec	Path + FU	-	62.5%	163	75	31	14
Hogan 2021	R	CEDM	132	52					IRW	No	GE	Senographe Essential*	Iohexol	1.5	350	3	-	-	E+M	LE+Rec	Path + FU	≥12	2.0%	6	264	36	0
Mohamed 2021	P	CESM	25	41					DB	No	GE	Senographe Pristina*	Iohexol or Iopromide	1.5	300	-	B	-	E+M	LE+Rec	Path	-	56.0%	14	7	4	0
Sudhir 2021	P	CEDM	130	45					DB	No	-	-	Iohexol	-	350	3	B	-	E+M	LE+Rec	Path	-	52.4%	84	64	15	3

SC = screening, SC-r = recalls from organized screening examinations, S-IM = suspicious findings at conventional imaging (digital mammography, tomosynthesis, ultrasonography), S-C = suspicious findings at breast clinical examination, Pre. = preoperative, Post. = postoperative, Mens. Cycle Reg. = timing of contrast-enhanced mammography according to the menstrual cycle phase, Conc. = concentration, BIexp = breast imaging experience of the reader who interpreted contrast-enhanced mammography images, CEM = contrast-enhanced mammography, Ref. Stand. = reference standard, FU = follow-up, Dis. Prev. = disease prevalence, TP = true positives, TN = true negatives, FP = false positives, FN = false negatives, R = retrospective, P = prospective, CEDM = contrast-enhanced digital mammography, DE-CESM = dual-energy contrast-enhanced subtracted mammography, CESM = contrast-enhanced spectral mammography, CEDEM = contrast-enhanced dual-energy mammography, L-CEM = low-dose contrast-enhanced mammography, TiCEM = titanium contrast-enhanced mammography, AD = architectural distortion, AS = asymmetries, BE = breast edema, CALC = suspicious calcifications, DB = dense breasts, IRW = women at increased risk of breast cancer, SL = suspicious lesions BI-RADS ≥ 3, SYM = symptomatic women, GE = General Electric Healthcare, A = exam time between 1' and 4'59", B = exam time 5–10', C = exam time >10', E = enhancement features, E+M = enhancement and morphological features, Rec = recombined images, LE+Rec = low-energy and recombined images, Path = pathology, US = ultrasonography.

\* mammography unit equipped with the SenoBright module.

\*\* unspecified mammography unit equipped with the SenoBright module.

§ mammography unit experimentally modified to allow dual-energy acquisitions.

**Table 6.4** Quality assessment of included studies according to the seven domains of the Quality Assessment of Diagnostic Accuracy Studies 2 (QUADAS-2) tool

Author / Year	Risk of Bias				Applicability Concerns		
	Patient Selection	Index Test	Reference Standard	Flow and Timing	Patient Selection	Index Test	Reference Standard
Dromain 2011	Low	Low	Low	Low	Low	Low	Low
Badr 2014	Low	Low	Low	Low	Low	Low	Low
Cheung 2014	Low	Low	Low	Low	Low	Low	Low
Łuczyńska 2014	Low	Low	Low	Low	Low	Low	Low
Mokhtar 2014	High	Low	Low	Low	Low	Low	Low
EISaid 2015	High	Low	Low	Unclear	High	Low	Low
Kamal 2015	High	Unclear	Low	Low	High	Low	Low
Łuczyńska 2015	Low	Low	Low	Low	Low	Low	Low
Cheung 2016	High	Low	Low	Low	Low	Low	Low
Kariyappa 2016	Low	Low	Low	Unclear	Low	Low	Low
Knogler 2016	Low	Low	Low	Low	Low	Low	Low
Lalji 2016	Low	Low	Low	Unclear	Low	Low	Low
Tardivel 2016	Low	Low	Low	Low	Low	Low	Low
Tennant 2016	High	Low	Low	Low	High	Low	Low
Tsigginou 2016	Low	Low	Low	Low	Low	Low	Low
Wang 2016	Low	Low	Low	Low	Low	Low	Low
Fallenberg 2017	Low	Low	Low	Low	Low	Low	Low
Lee-Felker 2017	High	Low	Low	Low	High	Low	Low
Li 2017	Unclear	Low	Low	Low	Unclear	Low	Low
Mori 2017	Low	Low	Low	Low	Low	Low	Low
Saraya 2017	Low	Low	Low	Low	Low	Low	Low
Kim 2018	High	Low	Low	Low	High	Low	Low
Klang 2018	Low	Low	Low	Low	Low	Low	Low
Navarro 2018	Low	Low	Low	Low	Low	Low	Low
Patel 2018	Low	Low	Low	Low	Low	Low	Low
Richter 2018	Low	Low	Low	Low	Low	Low	Low
Sorin 2018	High	Low	Low	Unclear	Low	Low	Low
Yousef 2018	Low	Low	Low	Low	Low	Low	Low

Fanizzi 2019	Low	Low	Low	Low	Low	Low	Low
Helal 2019	High	Low	Low	Low	High	Low	Low
Huang 2019	Low	Low	Low	Low	Low	Low	Low
Kamal 2019	Low	Low	Low	Unclear	Low	Low	Low
Kim 2019	Unclear	Low	Low	Low	Unclear	Low	Low
Lobbes 2019	Low	Low	Low	Low	Low	Low	Low
Sung 2019	Low	Unclear	Low	Low	Low	Unclear	Low
Travieso-Aja 2019	Low	Unclear	Low	Low	Low	Unclear	Low
Wessam 2019	High	Unclear	Low	Low	Low	Unclear	Low
Xing 2019	Low	Low	Low	Low	Low	Low	Low
Yasin 2019	High	Low	Low	Low	Low	Low	Low
Azzam 2020	High	Low	Low	Low	High	Low	Low
Chi 2020	High	Low	Low	Low	High	Low	Low
Clauser 2020	Low	Low	Low	Low	Low	Low	Low
Depretto 2020	High	Low	Low	Low	Low	Low	Low
Gluskin 2020	High	Low	Low	Low	High	Low	Low
Gonzalez-Huebra 2020	High	Low	Low	Low	High	Low	Low
Kamal 2020	High	Unclear	Low	Low	Low	Unclear	Low
Long 2020	High	Low	Low	Low	Low	Low	Low
Lu 2020	High	Low	Low	Low	High	Low	Low
Petrillo 2020	High	Low	Low	Low	Low	Low	Low
Qin 2020	Low	Low	Low	Low	Low	Low	Low
Soliman 2020	High	Low	Low	Low	High	Low	Low
Sorin 2020	High	Low	Low	Low	Low	Low	Low
Steinhof-Radwańska 2020	Low	Low	Low	Low	Low	Low	Low
Ainakulova 2021	High	Low	Low	Low	Low	Low	Low
Anwar 2021	High	Low	Low	Low	Low	Low	Low
Goh 2021	High	Low	Low	Low	Low	Low	Low
Hashem 2021	Low	Low	Low	Unclear	Low	Low	Low
Hogan 2021	High	Low	Low	Low	High	Low	Low
Mohamed 2021	High	Low	Low	Low	Low	Low	Low
Sudhir 2021	Low	Low	Low	Low	Low	Low	Low



**Table 6.5** Study-level covariate presence for meta-regression analysis

Author and Year	Patients	Cases	TP	FP	FN	TN	Covariates				
							Prospective Study Design	Specific Patients' or Lesion Subset	Joint Interpretation of Low-energy and Recombined Images	Joint Interpretation of Enhancement and Morphological Features	Timing of CEM Performance According to Menstrual Cycle Phase
Dromain 2011	120	130	74	13	6	37	Yes	No	No	No	No
Badr 2014	75	37	18	9	1	9	Yes	No	No	No	No
Cheung 2014	89	100	70	6	2	22	No	Yes	No	No	No
Luczynska 2014	152	173	114	35	0	24	Yes	No	Yes	Yes	No
Mokhtar 2014 <sup>2</sup>	60	60	43	8	1	8	Yes	Yes	No	Yes	No
ElSaid 2015	34	36	22	2	3	9	Yes	Yes	No	No	No
Kamal 2015	168	211	103	42	6	60	No	No	No	No	No
Luczynska 2015	102	118	81	25	0	12	Yes	No	Yes	Yes	Yes
Cheung 2016	87	94	24	9	3	58	No	Yes	No	No	No
Kariyappa 2016 <sup>2</sup>	44	44	26	2	6	10	Yes	No	Yes	Yes	No
Knogler 2016 <sup>2</sup>	15	15	8	1	0	6	Yes	Yes	No	Yes	Yes
Lalji 2016	199	199	57	42	2	98	No	No	Yes	Yes	No
Tardivel 2016	195	299	207	18	14	60	No	No	Yes	Yes	No
Tennant 2016	99	100	69	5	4	22	No	Yes	Yes	Yes	No
Tsigginou 2016	216	226	92	37	6	91	Yes	Yes	No	No	No
Wang 2016	68	77	46	10	2	19	Yes	No	Yes	Yes	No
Fallenberg 2017	155	604	191	26	82	305	Yes	No	Yes	Yes	No
Lee-Felker 2017	52	120	66	5	6	43	No	No	Yes	Yes	No
Li 2017	48	66	62	2	0	2	No	No	Yes	Yes	No
Mori 2017	72	143	50	5	8	80	Yes	Yes	No	No	No
Saraya 2017	34	39	15	2	1	21	Yes	Yes	Yes	Yes	No
Kim 2018	84	154	109	18	12	15	Yes	No	No	Yes	Yes
Klang 2018	953	87	36	30	1	20	No	No	No	Yes	No
Navarro 2018	465	85	55	19	0	11	Yes	No	No	Yes	No
Patel 2018	50	50	25	8	1	16	No	Yes	Yes	Yes	No
Richter 2018	105	117	82	5	1	29	No	No	Yes	Yes	No
Sorin 2018	611	611	19	141	2	449	No	Yes	Yes	Yes	No
Yousef 2018	20	20	12	2	1	5	Yes	No	Yes	Yes	Unavailable
Fanizzi 2019	53	58	34	4	0	20	No	No	Yes	Yes	No
Helal 2019	70	70	31	9	3	27	Yes	No	No	No	No

Huang 2019	21	24	19	2	1	2	Yes	Yes	No	No	No
Kamal 2019	365	380	243	30	14	93	Yes	Yes	No	No	No
Kim 2019	64	64	10	7	1	46	No	No	Yes	Yes	No
Lobbes 2019	368	368	117	50	9	192	No	No	Yes	Yes	No
Sung 2019	858	858	14	53	2	789	No	Yes	Yes	Yes	No
Travieso-Aja 2019 <sup>2</sup>	465	644	396	33	30	185	No	No	Yes	Yes	No
Wessam 2019	125	125	91	15	0	19	No	Yes	Yes	Yes	No
Xing 2019	235	263	162	9	15	77	Yes	No	Yes	Yes	No
Yasin 2019	50	56	32	0	2	22	Yes	Yes	No	No	Yes
Azzam 2020 <sup>2</sup>	37	63	32	3	4	24	Yes	Yes	No	Yes	No
Chi 2020 <sup>2</sup>	304	312	158	24	45	85	No	No	Yes	Yes	No
Clauser 2020	80	93	57	2	4	30	Yes	Yes	Yes	Yes	Yes
Depretto 2020	34	36	7	3	8	18	Yes	Yes	No	No	No
Gluskin 2020	917	917	12	38	6	861	No	Yes	Yes	Yes	No
Gonzalez-Huebra 2020	135	200	89	11	29	71	No	No	Yes	Yes	Unavailable
Kamal 2020	82	171	113	18	7	33	No	Yes	No	Yes	No
Long 2020	73	74	19	8	7	40	No	Yes	No	No	No
Lu 2020	115	131	60	8	4	59	Yes	Yes	Yes	Yes	No
Petrillo 2020	100	136	73	10	10	43	Yes	Yes	No	Yes	Unavailable
Qin 2020	114	144	28	4	6	106	No	Yes	Yes	Yes	Unavailable
Soliman 2020	38	38	23	6	0	9	Yes	Yes	No	No	No
Sorin 2020	138	147	38	29	0	80	No	Yes	Yes	Yes	Unavailable
Steinhof-Radwanska 2020	547	593	320	108	7	158	No	No	No	No	No
Ainakulova 2021	151	155	87	13	2	53	No	Yes	Yes	Yes	Yes
Anwar 2021 <sup>2</sup>	32	40	28	6	3	3	Yes	Yes	No	Yes	No
Goh 2021	92	94	33	35	0	26	No	Yes	No	No	No
Hashem 2021	283	283	163	31	14	75	Yes	Yes	No	Yes	No
Hogan 2021	132	306	6	36	0	264	No	Yes	Yes	Yes	No
Mohamed 2021	25	25	14	4	0	7	Yes	Yes	Yes	Yes	No
Sudhir 2021	130	166	84	15	3	64	Yes	Yes	Yes	Yes	No

TP = true positives, TN = true negatives, FP = false positives, FN = false negatives CEM = contrast-enhanced mammography.

**Table 6.6** Meta-regression analysis on study and image interpretation parameters

<b>Study Parameter</b>		<b>No. of Studies</b>	<b>Sensitivity (95% CI)</b>	<b><i>p</i> value</b>	<b>Specificity (95% CI)</b>	<b><i>p</i> value</b>
Prospective study design	Yes	31/60	94% (92, 96)	< 0.001	75% (69, 82)	< 0.001
	No	29/60	94% (92, 97)		79% (73, 85)	
Specific patients' or lesion subset	Yes	34/60	94% (91, 96)	< 0.001	81% (76, 86)	0.02
	No	26/60	95% (93, 97)		72% (64, 79)	
Joint interpretation of low-energy and recombined images	Yes	33/60	95% (92, 97)	< 0.001	81% (77, 86)	0.03
	No	27/60	94% (91, 97)		71% (63, 78)	
Joint interpretation of enhancement and morphological features	Yes	43/60	95% (93, 97)	< 0.001	78% (73, 83)	0.006
	No	17/60	94% (90, 97)		76% (67, 84)	
Timing of CEM performance according to menstrual cycle phase *	Yes	6/55	96% (93, 100)	0.06	76% (60, 91)	0.14
	No	49/55	94% (92, 96)		77% (72, 82)	

CI = confidence interval, CEM = contrast-enhanced mammography.

\* only retrievable for 55 out of 60 studies.

**Table 6.7** Joint modelling in meta-regression analysis on study and image interpretation parameters

Study Parameter		No. of Studies	Sensitivity (95% CI)	Specificity (95% CI)	Likelihood ratio test	
					$\chi^2$ statistic	<i>p</i> value
Prospective study design	Yes	31/60	94% (92, 96)	75% (69, 82)	1.49	0.47
	No	29/60	94% (92, 97)	79% (73, 85)		
Specific patients' or lesion subset	Yes	34/60	94% (91, 96)	81% (76, 86)	5.57	0.06
	No	26/60	95% (93, 97)	72% (64, 79)		
Joint interpretation of low-energy and recombined images	Yes	33/60	95% (92, 97)	81% (77, 86)	12.13	< 0.001
	No	27/60	94% (91, 97)	71% (63, 78)		
Joint interpretation of enhancement and morphological features	Yes	43/60	95% (93, 97)	78% (73, 83)	1.19	0.55
	No	17/60	94% (90, 97)	76% (67, 84)		
Timing of CEM performance according to menstrual cycle phase *	Yes	6/55	96% (93, 100)	76% (60, 91)	60.32	< 0.001
	No	49/55	94% (92, 96)	77% (72, 82)		

CI = confidence interval, CEM = contrast-enhanced mammography

\* only retrievable for 55 out of 60 studies.

**Fig. 6.1** ROC plane scatter plot. The typical “shoulder-arm” shape of study distribution indicates the existence of a threshold effect

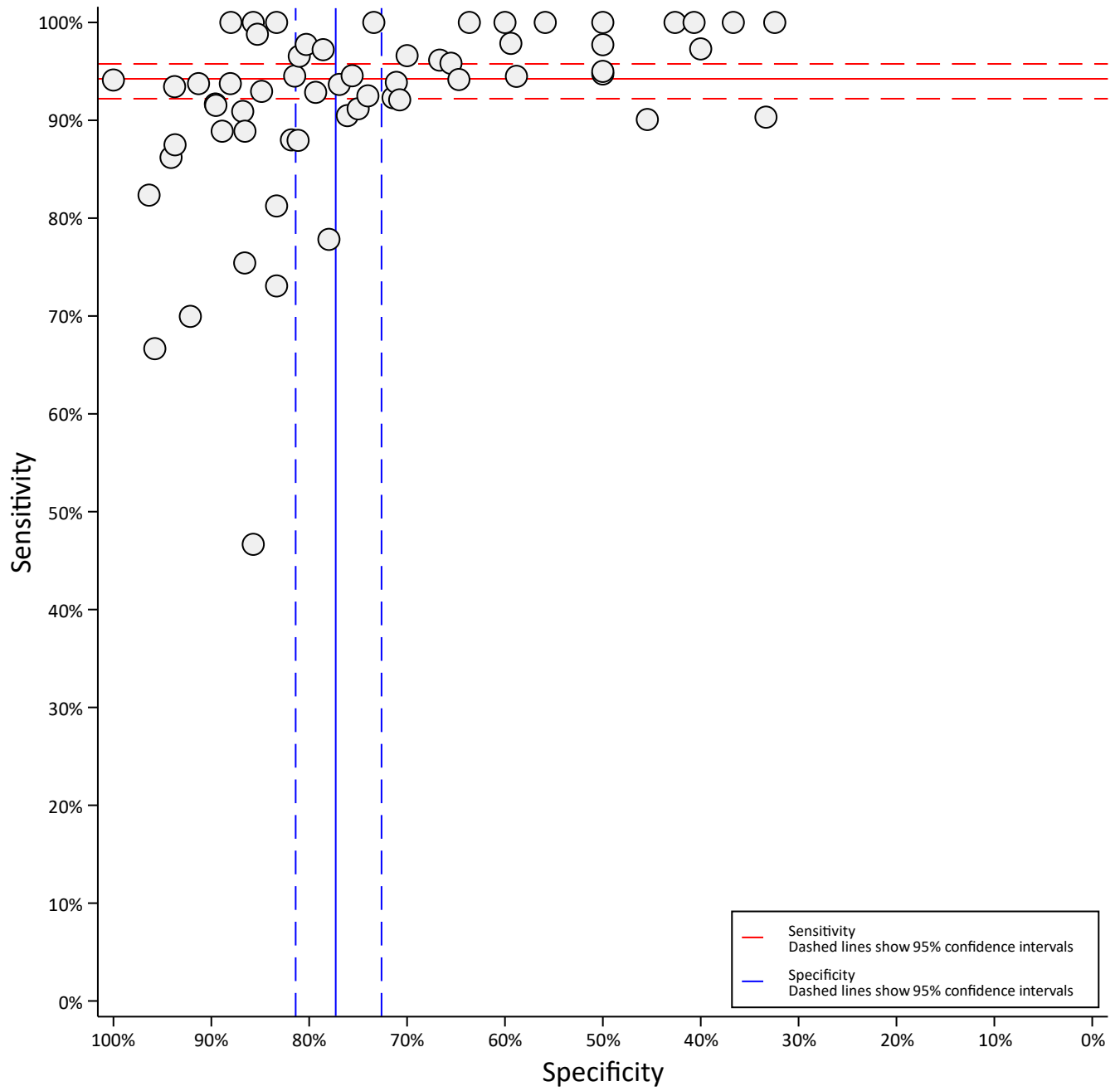


**Fig. 6.2** Flowchart of literature search and screening

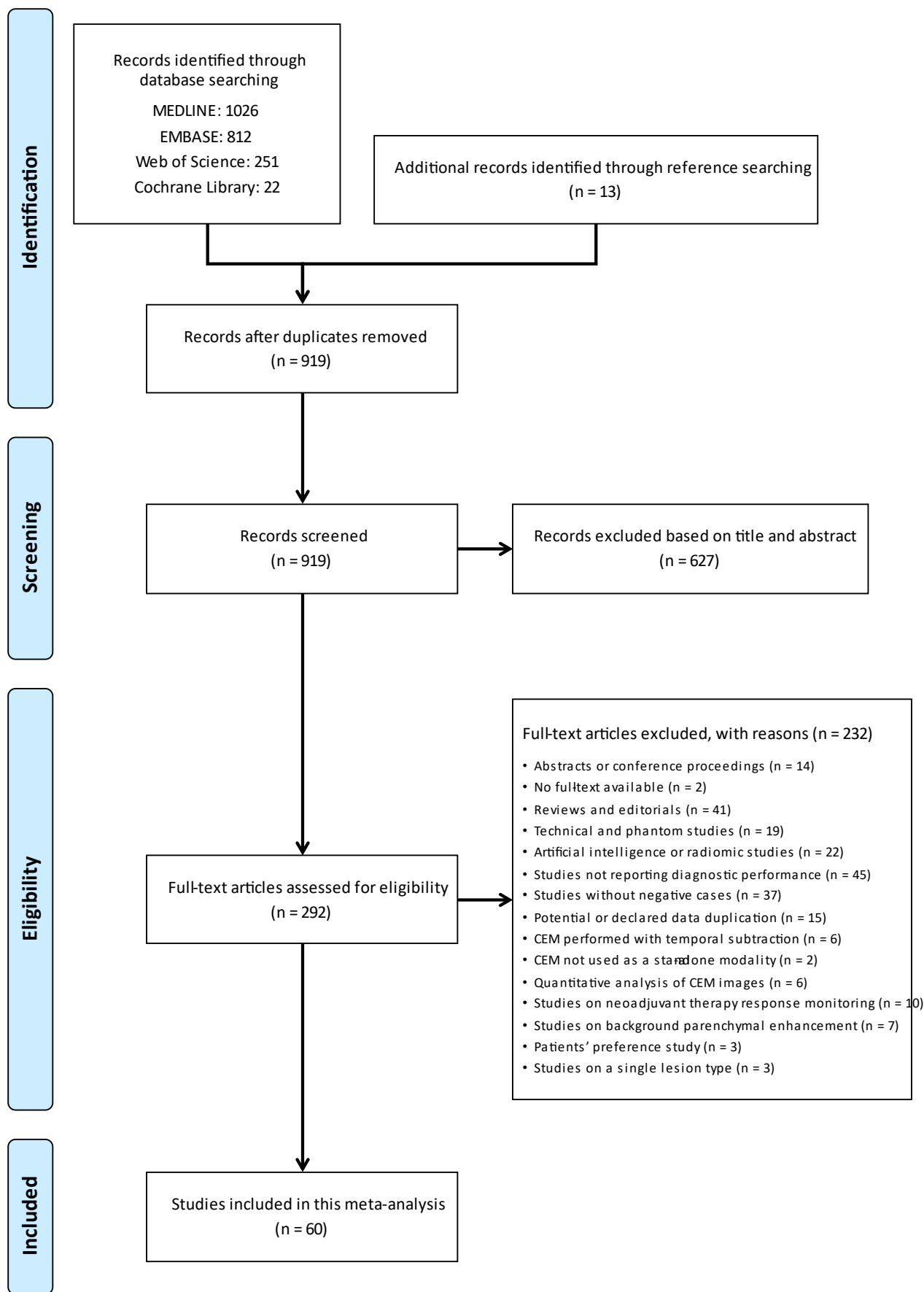
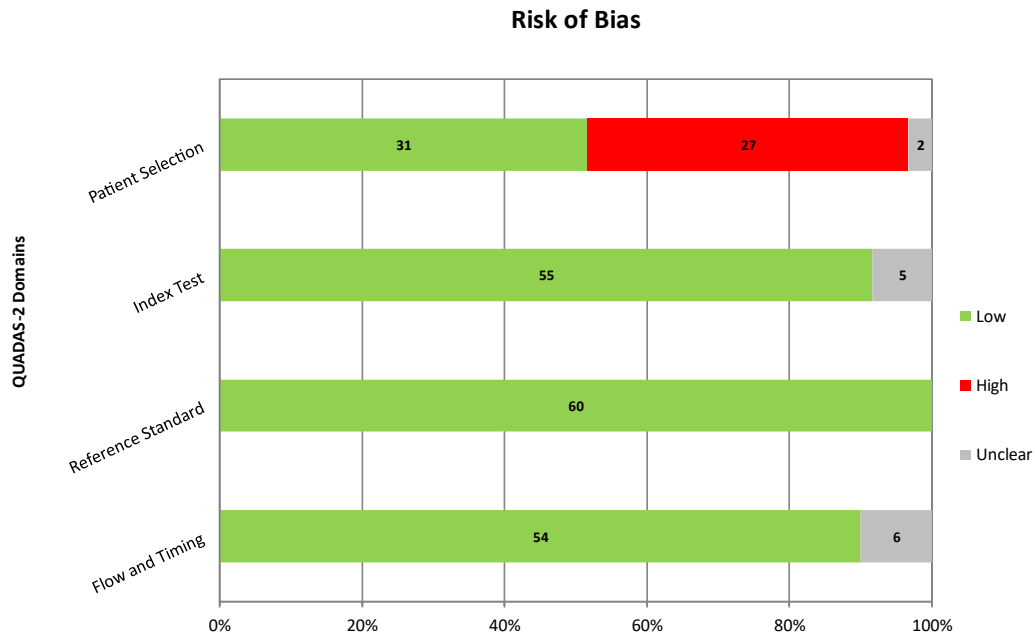
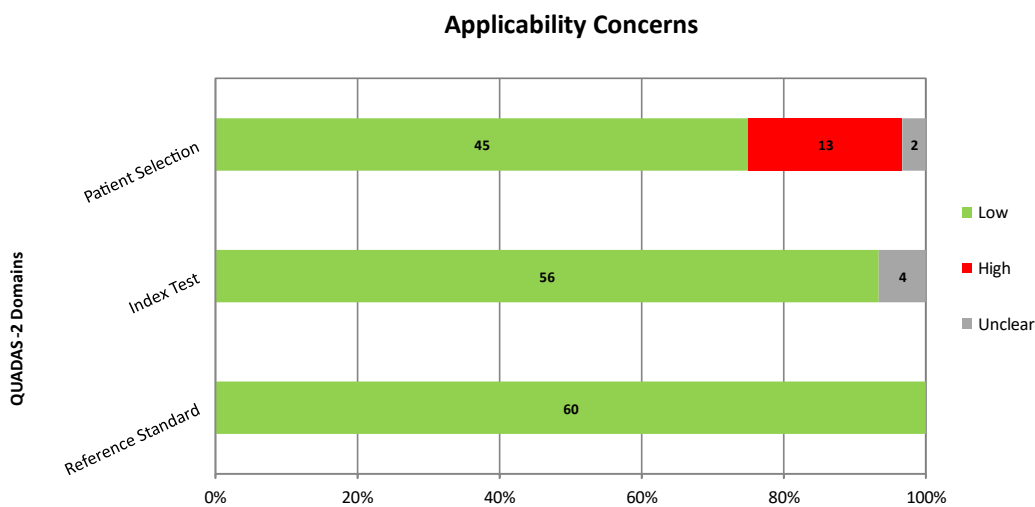


**Fig. 6.3** Quality assessment of included studies according to the Quality Assessment of Diagnostic Accuracy Studies 2 (QUADAS-2) tool. Overall, the risk of bias and applicability concerns were deemed low for the reference standard in all included studies, while the proportion of studies at high risk of introducing bias and applicability concerns was substantially higher in the patient selection domain (27 of 60 studies at high risk of bias and 13 of 60 with high applicability concerns)



	Flow and Timing	Reference Standard	Index Test	Patient Selection
Low	54	60	55	31
High	0	0	0	27
Unclear	6	0	5	2



	Reference Standard	Index Test	Patient Selection
Low	60	56	45
High	0	0	13
Unclear	0	4	2

**Fig. 6.4** Forest plots with sensitivity and specificity estimates for all 67 included study parts. Superscript numbers represent study parts of articles with multiple interpretation approaches to CEM. Blue squares and horizontal black lines represent the estimate and the 95% CI for each study part

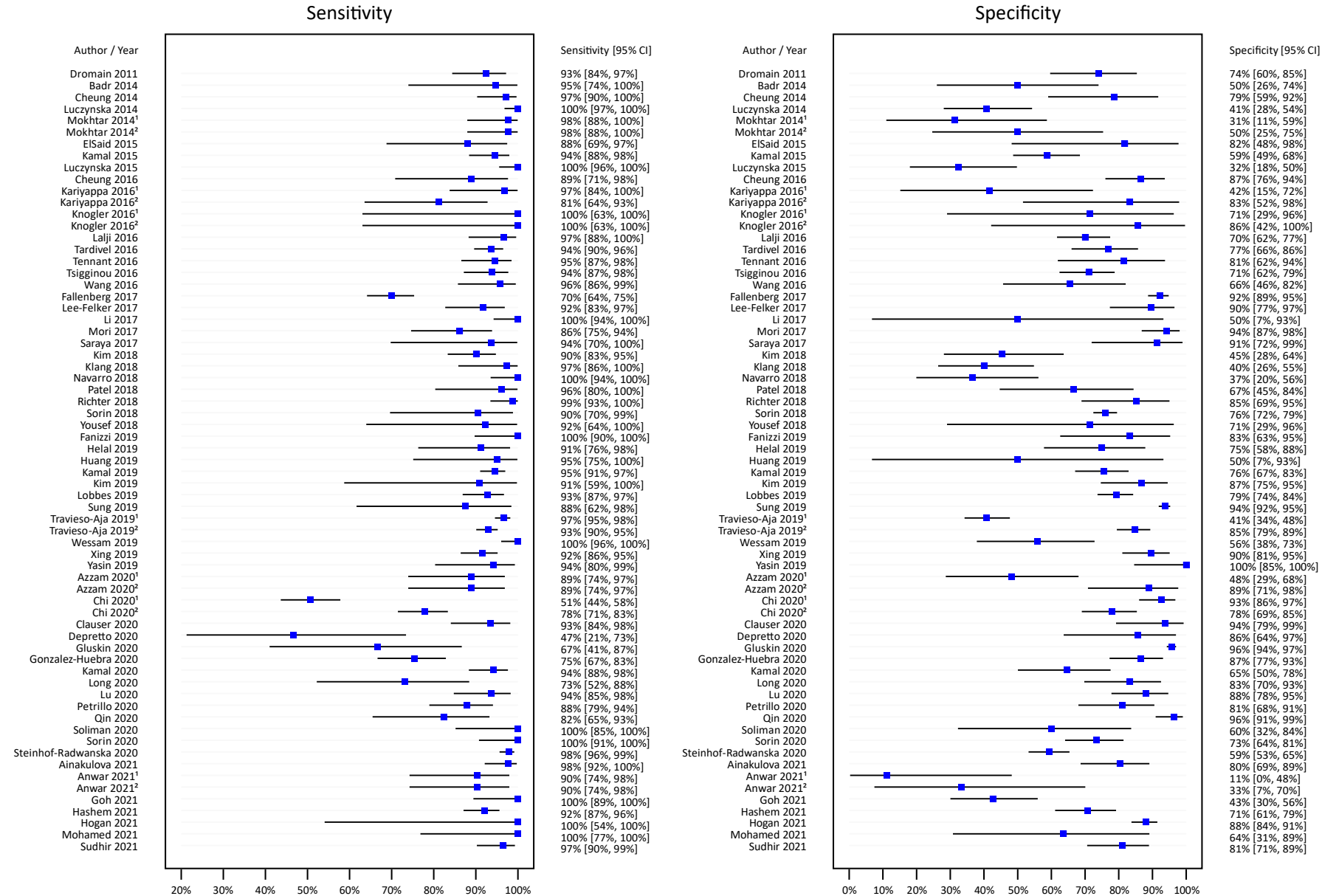




**Fig. 6.5** Hierarchical summary receiver operating characteristic (HSROC) curve for CEM for all 60 included studies. Studies with more than one study part contributed with the one having the most comprehensive CEM interpretation approach. The overall area under the HSROC curve was 0.94

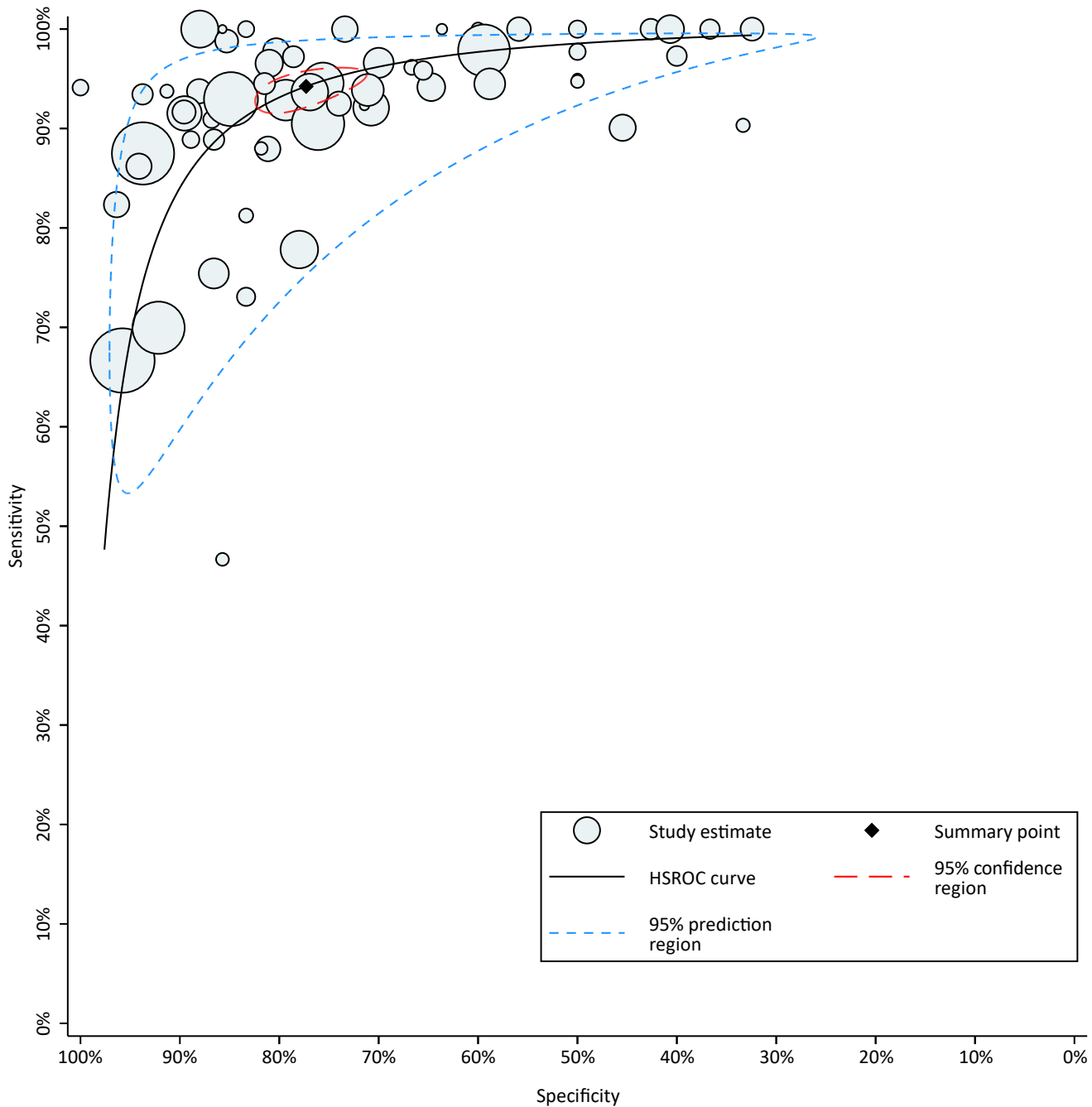


**Fig. 6.6** Fagan nomogram for CEM with pooled likelihood ratios. In our analysis, with a pre-test probability (i.e. disease prevalence of breast cancer) of 43%, a positive CEM examinations raises the probability of being affected by breast cancer to 76%. Conversely, with a negative CEM examination, the probability of being affected by breast cancer lowers to 5%

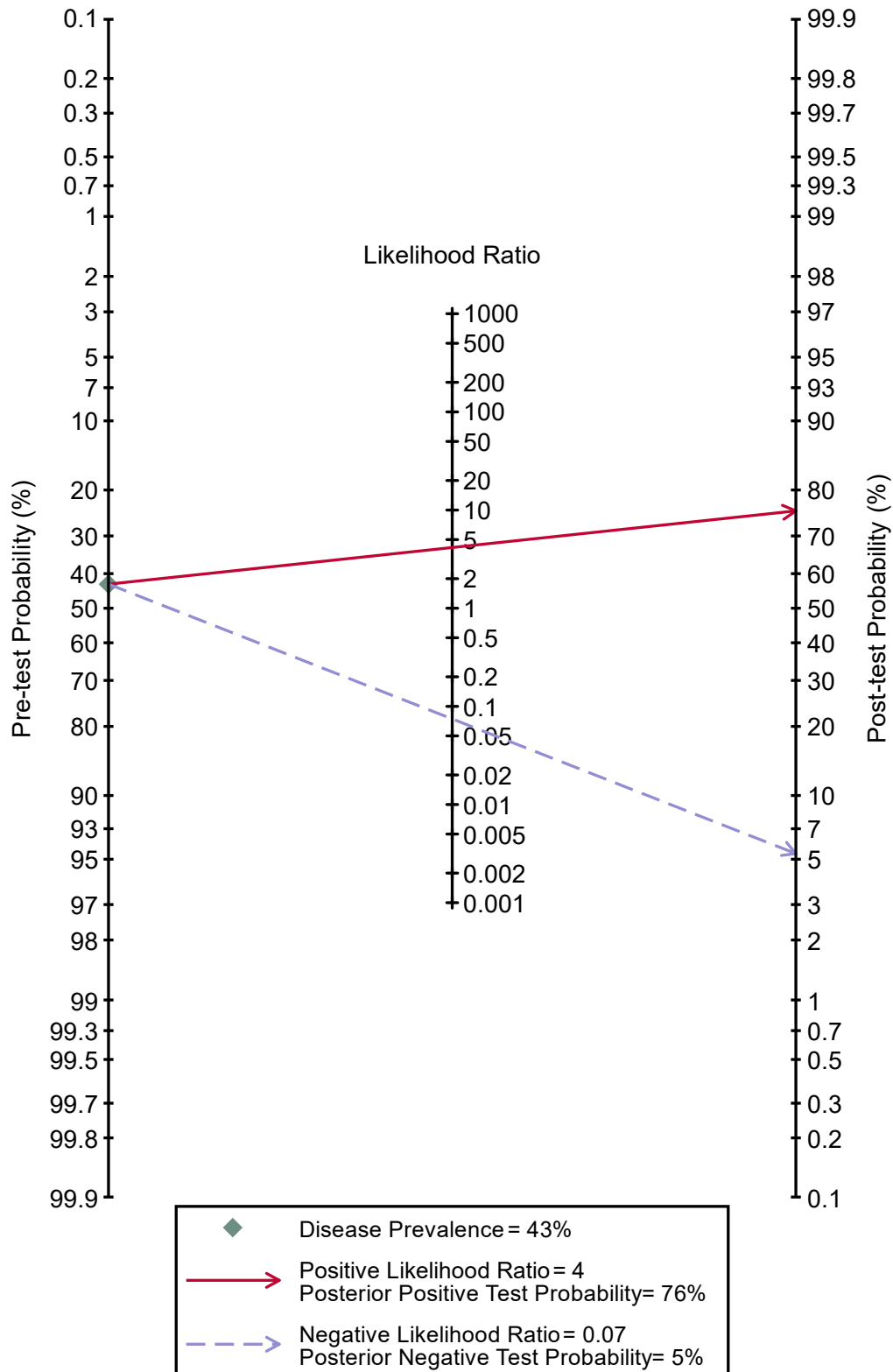
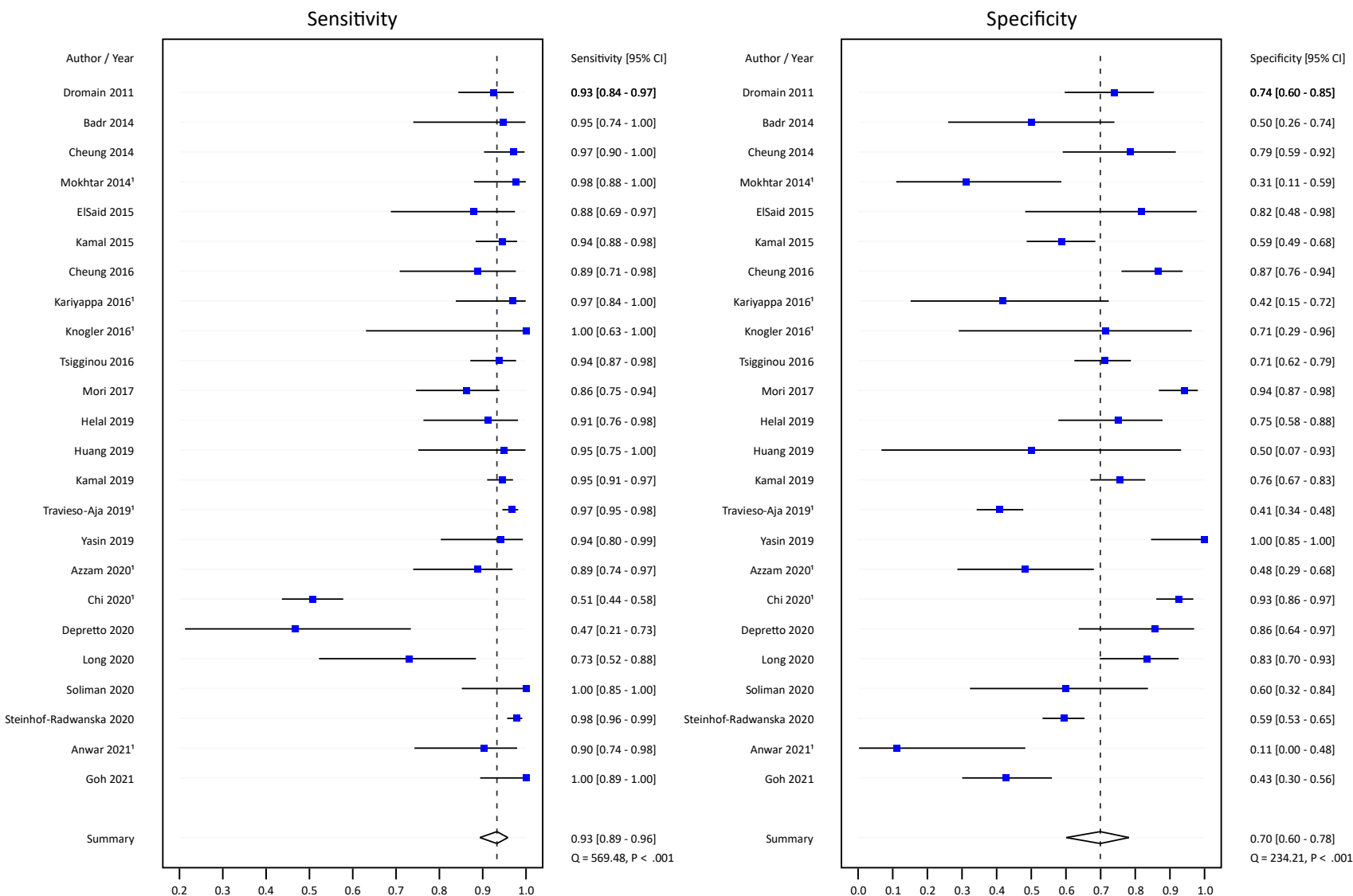


**Fig. 6.7** Forest plots and pooled estimates of sensitivity and specificity according to interpretation approaches to CEM. In (A), the 24 study parts in which CEM was interpreted considering only the presence and conspicuity of enhancement on recombined images;

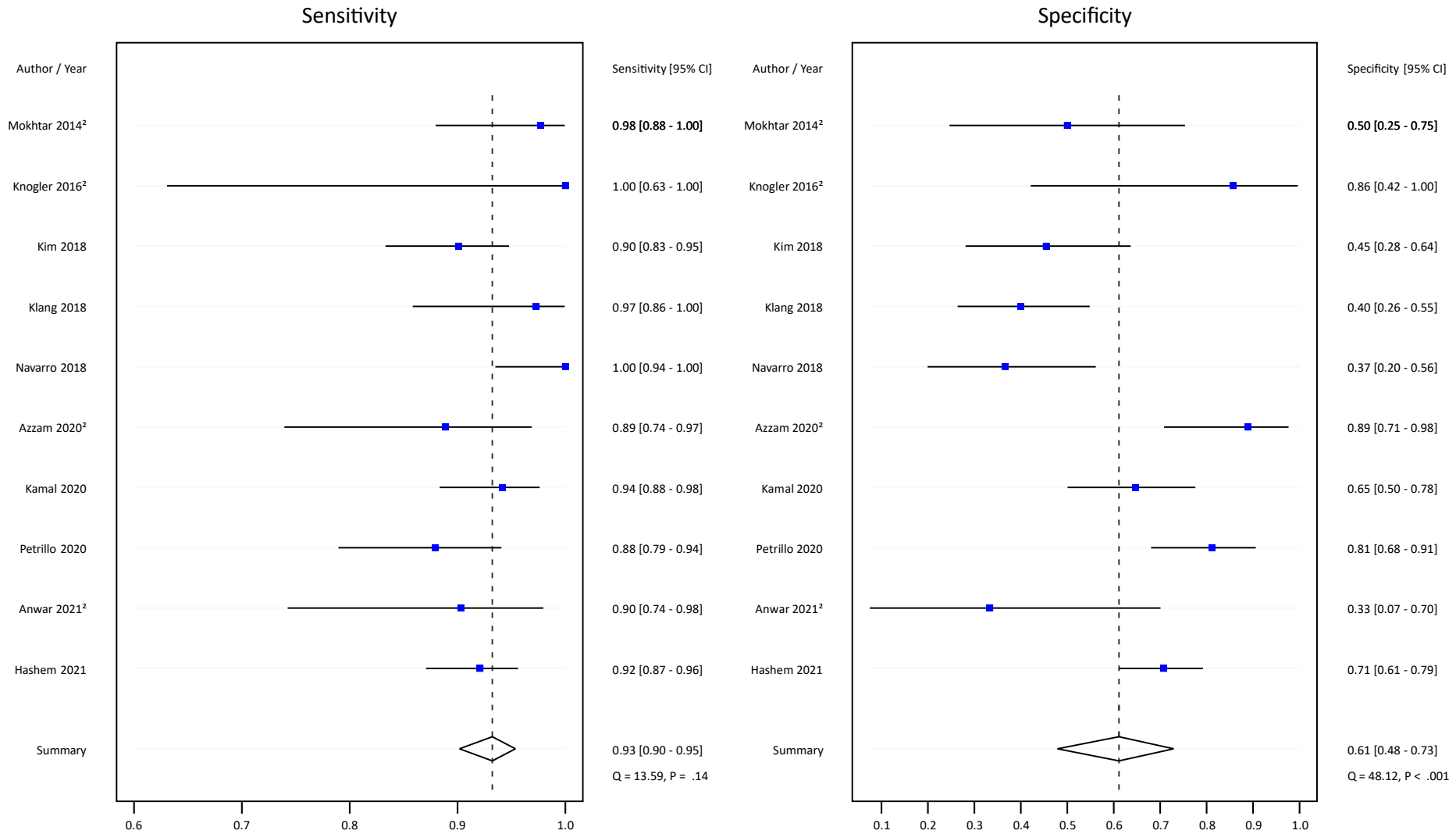
A

### Enhancement & Recombined Images



in (B) the 10 study parts in which CEM was interpreted considering enhancement presence, conspicuity, and morphology on recombined images;

## B Enhancement+Morphology & Recombined Images



in (C) the 33 study parts in which CEM was interpreted considering both enhancement and morphology of findings from both low-energy and recombined images

## C Enhancement+Morphology & Low-energy+Recombined Images

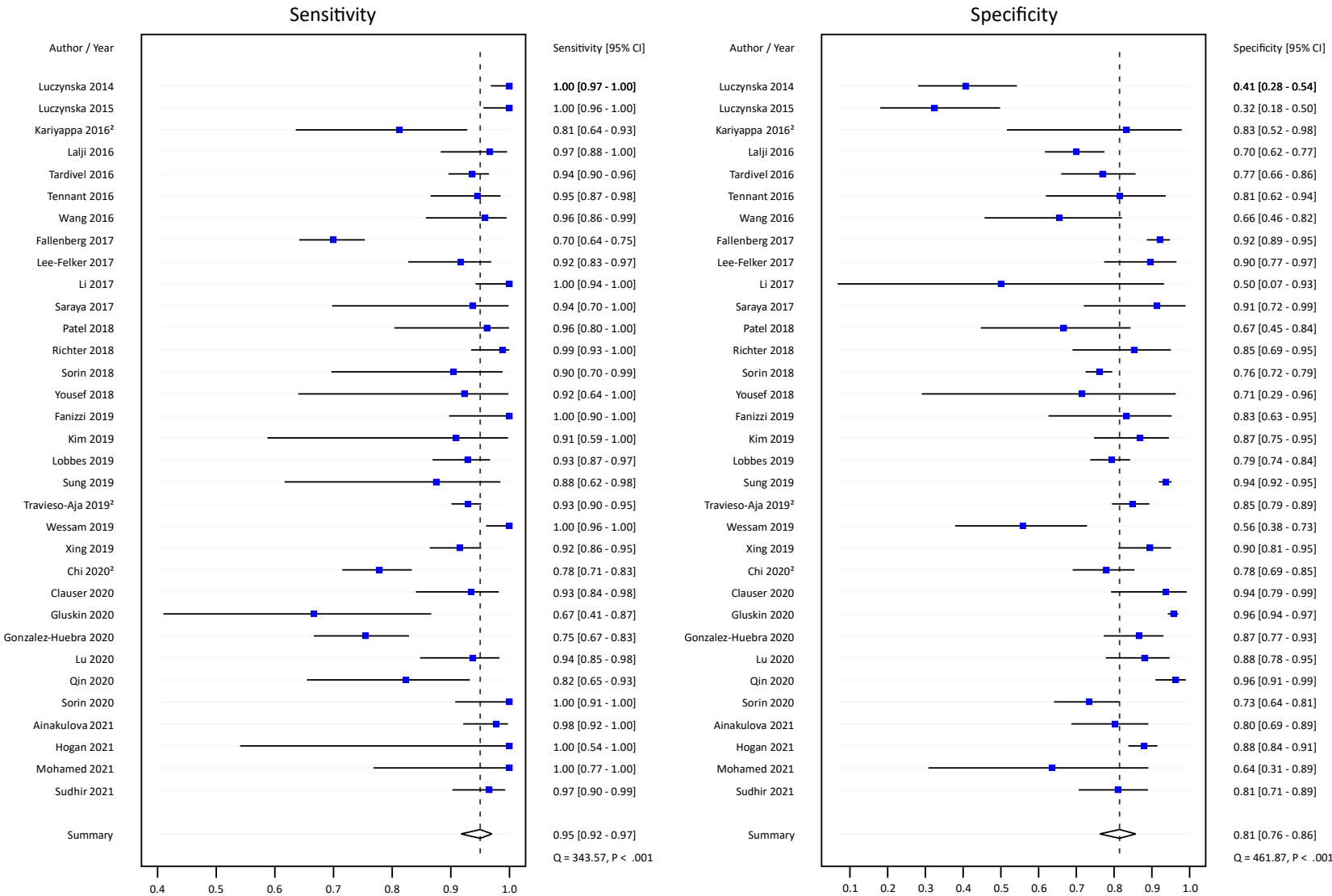
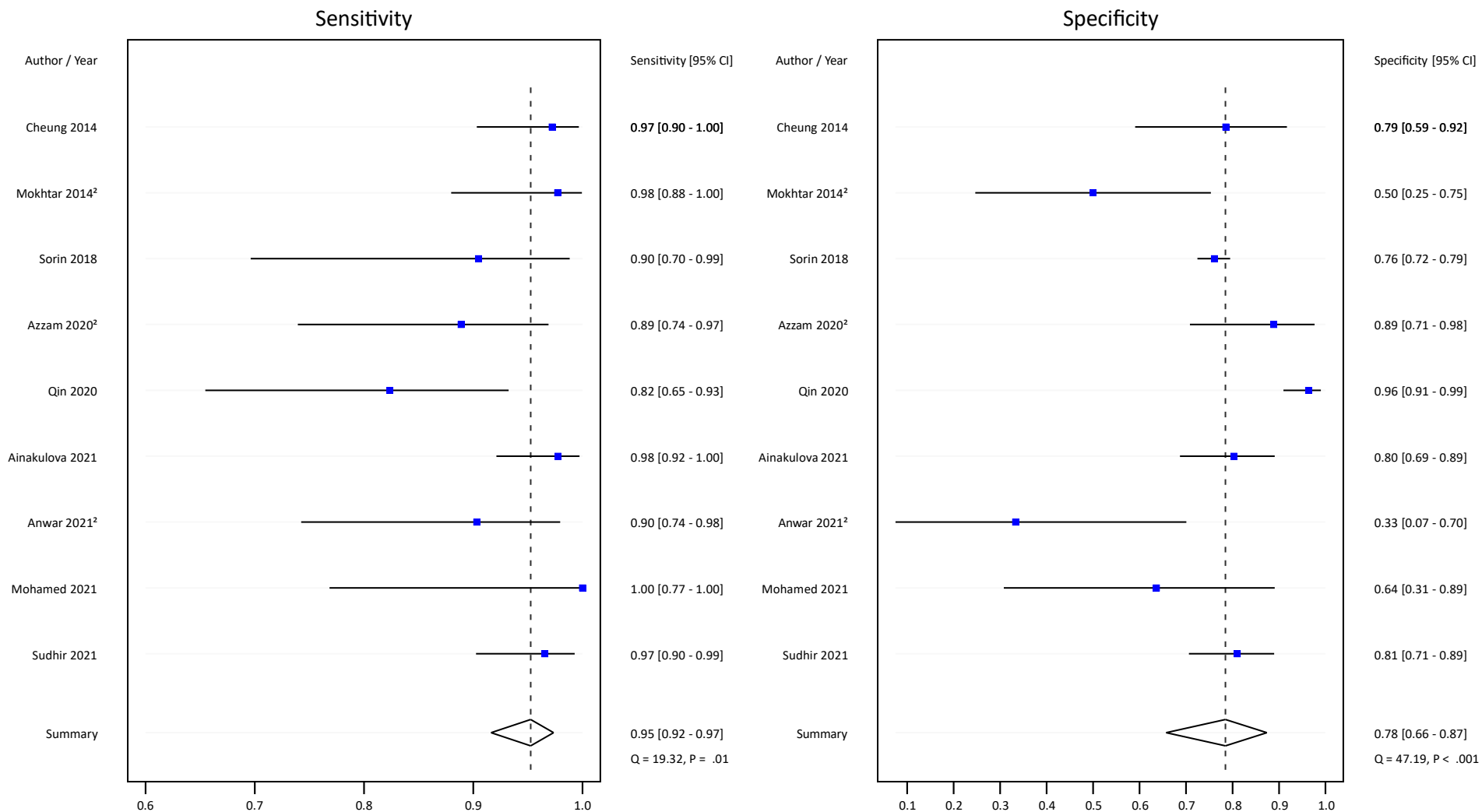


**Fig. 6.8** Forest plots and pooled estimates of sensitivity and specificity for subgroup analyses. In (A) the 9 studies in which CEM was performed solely in patients with dense breasts;

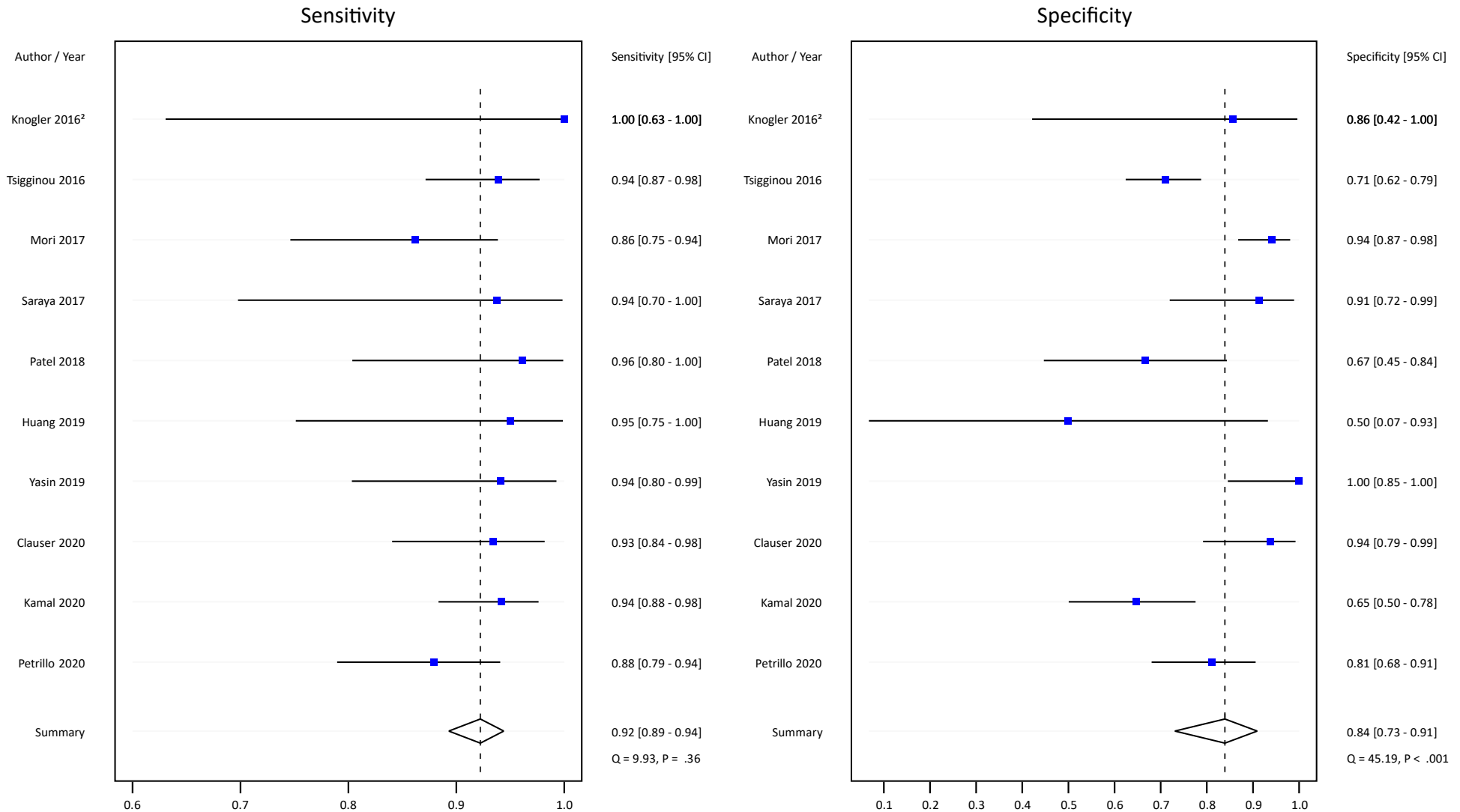
A

### Dense Breasts



in (B) the 10 studies focusing on suspicious findings at digital mammography classified with a Breast Imaging Reporting and Data System (BI-RADS) category  $\geq 3$

## B Suspicious Lesions BI-RADS $\geq 3$



## 6.6. Appendixes

### Appendix 6.1

#### *Literature search strategy*

Updated: July 15<sup>th</sup>, 2021

Databases used: MEDLINE (PubMed), EMBASE (Elsevier), Web of Science (Clarivate Analytics), and the two Cochrane Library databases (Cochrane Database of Systematic Reviews and Cochrane Central Register of Controlled Trials).

A controlled vocabulary (medical subject headings in PubMed and EMBASE thesaurus keywords in EMBASE) was used. The search string was built using the following strategy:

'breast disease'/exp + synonyms
'mammography'/exp + synonyms OR 'mammography system'/exp + synonyms OR 'contrast enhanced spectral mammography'/exp + synonyms OR 'CEM' OR 'CESM' OR 'CEDM'
'contrast medium'/exp + synonyms OR 'contrast enhancement'/exp + synonyms
'performance'/exp + synonyms OR 'sensitivity'/exp + synonyms OR 'specificity'/exp + synonyms OR 'predictive value'/exp + synonyms OR 'diagnostic accuracy'/exp + synonyms OR 'diagnostic performance'/exp + synonyms OR 'accuracy'/exp + synonyms

#### *Full search strings*

The full search string for **PubMed (MEDLINE)** was:

Breast Diseases: "breast diseases"[MeSH Terms] OR ("breast"[Title/Abstract] AND "diseases"[Title/Abstract]) OR "breast diseases"[Title/Abstract]



mammography: "mammography"[MeSH Terms] OR "mammography"[Title/Abstract] OR  
"mammographies"[Title/Abstract] OR "mammography's"[Title/Abstract] OR "cem"[Title/Abstract]

contrast medium: "contrast media"[Pharmacological Action] OR "contrast media"[MeSH Terms]  
OR ("contrast"[Title/Abstract] AND "media"[Title/Abstract]) OR "contrast media"[Title/Abstract]  
OR ("contrast"[Title/Abstract] AND "medium"[Title/Abstract]) OR "contrast  
medium"[Title/Abstract]

contrast: "contrast media"[Pharmacological Action] OR "contrast media"[MeSH Terms] OR  
("contrast"[Title/Abstract] AND "media"[Title/Abstract]) OR "contrast media"[Title/Abstract] OR  
"contrast"[Title/Abstract] OR "contrasted"[Title/Abstract] OR "contrasting"[Title/Abstract] OR  
"contrastive"[Title/Abstract] OR "contrastively"[Title/Abstract] OR  
"contrastiveness"[Title/Abstract] OR "contrastivity"[Title/Abstract] OR "contrasts"[Title/Abstract]

enhancement: "enhance"[Title/Abstract] OR "enhanced"[Title/Abstract] OR  
"enhancement"[Title/Abstract] OR "enhancements"[Title/Abstract] OR "enhancer"[Title/Abstract]  
OR "enhancer's"[Title/Abstract] OR "enhancers"[Title/Abstract] OR "enhances"[Title/Abstract] OR  
"enhancing"[Title/Abstract]

diagnostic: "diagnosis"[MeSH Terms] OR "diagnosis"[Title/Abstract] OR  
"diagnostic"[Title/Abstract] OR "diagnostical"[Title/Abstract] OR "diagnostically"[Title/Abstract]  
OR "diagnostics"[Title/Abstract]

performance: "perform"[Title/Abstract] OR "performable"[Title/Abstract] OR  
"performance"[Title/Abstract] OR "performance's"[Title/Abstract] OR  
"performances"[Title/Abstract] OR "performative"[Title/Abstract] OR  
"performatively"[Title/Abstract] OR "performatives"[Title/Abstract] OR  
"performativities"[Title/Abstract] OR "performativity"[Title/Abstract] OR

"performed"[Title/Abstract] OR "performer"[Title/Abstract] OR "performer's"[Title/Abstract] OR "performers"[Title/Abstract] OR "performing"[Title/Abstract] OR "performs"[Title/Abstract]

sensitivity: "hypersensitivity"[MeSH Terms] OR "hypersensitivity"[Title/Abstract] OR "sensitive"[Title/Abstract] OR "sensitively"[Title/Abstract] OR "sensitives"[Title/Abstract] OR "sensitivities"[Title/Abstract] OR "sensitivity and specificity"[MeSH Terms] OR ("sensitivity"[Title/Abstract] AND "specificity"[Title/Abstract]) OR "sensitivity and specificity"[Title/Abstract] OR "sensitivity"[Title/Abstract]

specificity: "sensitivity and specificity"[MeSH Terms] OR ("sensitivity"[Title/Abstract] AND "specificity"[Title/Abstract]) OR "sensitivity and specificity"[Title/Abstract] OR "specificity"[Title/Abstract] OR "specific"[Title/Abstract] OR "specifically"[Title/Abstract] OR "specification"[Title/Abstract] OR "specifications"[Title/Abstract] OR "specificities"[Title/Abstract] OR "specifics"[Title/Abstract] OR "specificities"[Title/Abstract] OR "specify"[Title/Abstract]

accuracy: "accuracies"[Title/Abstract] OR "accuracy"[Title/Abstract]

The full search string for **EMBASE (Elsevier)** was:

('breast disease'/exp OR 'benign breast disease' OR 'breast disease' OR 'breast diseases' OR 'breast disorder' OR 'mamma disease' OR 'mammary gland disease' OR 'mastopathia' OR 'mastopathy' OR 'mastosis') AND ('mammography'/exp OR 'mamilloscopy' OR 'mamnilloscopy' OR 'mammography' OR 'mammogram' OR 'mammography' OR 'mastography' OR cem OR 'contrast enhanced spectral mammography'/exp OR 'mammography system'/exp OR 'aws-c' OR 'aws-h' OR 'embrace (mammography system)' OR 'embrace dm1000' OR 'lorad m-iv' OR 'lorad selenia' OR 'mammodiagnost' OR 'mammodiagnost dr' OR 'mammodiagnost sf' OR 'mammodiagnost vu' OR 'mammoscan (mammography system)' OR 'mammomat' OR 'mammomat fusion' OR 'mammomat

inspiration' OR 'mammomat novation' OR 'mammomat select' OR 'microdose (mammography system)' OR 'microdose mammography si' OR 'nuance (device)' OR 'profect cs' OR 'sectra mdm l30' OR 'sectra microdose' OR 'senobright' OR 'senographe' OR 'senographe 500t' OR 'senographe 600t' OR 'senographe crystal' OR 'senographe ds' OR 'senographe essential' OR 'analogue stationary mammographic x-ray system' OR 'digital mammographic machine' OR 'digital mammographic system' OR 'digital mammographic unit' OR 'digital mammography machine' OR 'digital mammography system' OR 'digital mammography unit' OR 'digital stationary mammographic x-ray system' OR 'mammographic machine' OR 'mammographic system' OR 'mammographic unit' OR 'mammographic x ray system stereotactic unit' OR 'mammographic x-ray system stereotactic unit' OR 'mammography device' OR 'mammography machine' OR 'mammography system' OR 'mammography unit' OR 'stationary digital mammography system' OR 'stationary mammographic x ray system' OR 'stationary mammographic x-ray system, analogue' OR 'stationary mammographic x-ray system, digital' OR 'stationary mammography system' OR 'stationary x-ray mammography system' OR 'dual energy') AND ('contrast medium'/exp OR 'contrast agent' OR 'contrast dye' OR 'contrast material' OR 'contrast media' OR 'contrast medium' OR 'radiocontrast medium' OR 'radiography contrast medium' OR 'roentgen contrast medium' OR 'contrast enhancement'/exp OR 'contrast enhancement' OR 'contrast intensification') AND ('performance'/exp OR 'performance' OR 'performance test' OR 'progressive ratio performance' OR 'sensitivity'/exp OR 'specificity'/exp OR 'predictive value'/exp OR 'negative predictive value' OR 'positive predictive value' OR 'predictive value' OR 'predictive value of tests' OR 'diagnostic accuracy'/exp OR 'accuracy, diagnostic' OR 'diagnosis accuracy' OR 'diagnostic accuracy' OR 'diagnostic test accuracy' OR 'diagnostic performance'/exp OR 'accuracy'/exp OR 'accuracy' OR 'precision')

The full search string for **Web of Science (Clarivate Analytics)** was:

# 1 TOPIC: (breast cancer)

Indexes=SCI-EXPANDED, SSCI, A&HCI, CPCI-S, CPCI-SSH, BKCI-S, BKCI-SSH, ESCI, CCR-EXPANDED, IC Timespan=All years

# 2 TOPIC: (mammography system) OR (CESM) OR (CEM) OR (CEDM)

Indexes=SCI-EXPANDED, SSCI, A&HCI, CPCI-S, CPCI-SSH, BKCI-S, BKCI-SSH, ESCI, CCR-EXPANDED, IC Timespan=All years

# 3 TOPIC: (Contrast medium) OR (Contrast agent) OR (Contrast enhancement)

Indexes=SCI-EXPANDED, SSCI, A&HCI, CPCI-S, CPCI-SSH, BKCI-S, BKCI-SSH, ESCI, CCR-EXPANDED, IC Timespan=All years

# 4 TOPIC: (Diagnostic performance) OR (Performance) OR (Sensitivity) OR (Specificity) OR (Accuracy)

Indexes=SCI-EXPANDED, SSCI, A&HCI, CPCI-S, CPCI-SSH, BKCI-S, BKCI-SSH, ESCI, CCR-EXPANDED, IC Timespan=All years

#1 AND #2 AND #3 AND #4

Indexes=SCI-EXPANDED, SSCI, A&HCI, CPCI-S, CPCI-SSH, BKCI-S, BKCI-SSH, ESCI, CCR-EXPANDED, IC Timespan=All years

The full search string for **Cochrane Library (Cochrane)** was:

"breast cancer" in Title Abstract Keyword AND Contrast enhanced mammography in Title Abstract Keyword AND "contrast medium" in Title Abstract Keyword AND "performance" in Title Abstract Keyword AND "diagnosis" in Title Abstract Keyword - (Word variations have been searched)

## **Appendix 6.2**

### *Inclusion and exclusion criteria*

The following inclusion criteria were applied: a) prospective or retrospective design, b) clinical performance of CEM; c) image interpretation performed by human readers, also when performance indexes from human interpretation were not the chief focus of the study (e.g., human readings performed for comparison with artificial intelligence readings or any other kind of computer-aided lesion detection) but were reported or could be reconstructed; d) clear definition of a reference standard, considering biopsy or surgical histopathology with follow-up or additional imaging confirmation for negative cases; e) sufficient information to re-create 2×2 contingency tables.

Corresponding authors of studies meeting inclusion but without sufficient data were contacted to try retrieving these information before opting for exclusion.

After excluding systematic and narrative reviews, case-control studies, case reports, and technical notes, we also excluded: a) studies which did not include any benign lesion/finding (e.g., studies on the assessment of the response to neoadjuvant chemotherapy); b) studies focusing on the estimation of background parenchymal enhancement, on technical aspects (e.g., contrast agent dose, radiation dose, artifact evaluation), or on the evaluation of patients' preferences towards CEM or other diagnostic modalities; c) studies in which CEM was performed using a temporal subtraction technique; d) studies in which diagnostic performances indexes for CEM employed as a stand-alone modality and read by human readers were not available nor derivable; e) studies in which CEM interpretation was centered on quantitative measurement of contrast enhancement.

### *Data extraction*

Data extraction was performed independently by the three reviewers who performed the literature search, disagreements being again settled by consensus with contribution from the clinically-experienced fourth reader. For each included article, we extracted: year of publication; country of

origin of the research group; study design; number of patients and demographics; study enrollment setting and any eventual focus on specific patient subgroups; timing of CEM performance according to menstrual cycle phase; mammography unit and vendor; contrast agent molecule, dose, concentration, flow rate; readers' experience in breast imaging; details on CEM interpretation (combined use of low-energy and recombined images, consideration of both enhancement and morphological features, also through BI-RADS-like self-developed descriptors); adopted reference standard (histopathology and/or follow-up, with follow-up length if available); prevalence of malignant lesions, number of lesions with histopathology reference and their categorization, number of examinations proved benign by follow-up or without suspicious findings; number of true positive, false positive, false negative, and true negative findings.

## Appendix 6.3

### *Quality assessment of included studies*

Risk of bias and applicability concerns for the reference standard were deemed low in all included studies, since all of them declared the use of histopathology combined or not combined with follow-up, where appropriate. As for the index test, no studies had high risk of bias or applicability concerns from this domain, but poor detailing of CEM interpretation strategy and positivity thresholds hindered clear judgment for risk of bias in 5/60 studies (8%) and for applicability concerns in 4/60 (7%). Likewise, risk of bias introduced by patient flow through the study and by timing of the index test was evaluated by appraising the interval between the index test and the obtainment of the reference standard. We considered as appropriate an interval between CEM and histopathology and/or follow-up of maximum 6 months. Risk of bias in this domain was deemed low in all but 6 studies (10%), which were all flagged with unclear risk of bias because unreported patient exclusion from analysis without a priori definition of specific criteria was strongly suspected but unverifiable with available data. No articles reported interval between CEM and pathology and/or follow-up longer than 6 months. In the patient selection domain, the proportion of studies at high risk of introducing bias and applicability concerns was substantially higher, with 27/60 (45%) studies deemed to be at high risk of bias and 13/60 (22%) studies with high applicability concerns, because of non-consecutive enrollment or patient selection towards specific subsets of prior imaging findings (e.g., findings at DM reported as BI-RADS  $\geq 3$ ) or of patients with specific characteristics (e.g., patients with dense breasts). Clear judgment of the patient selection domain was unfeasible in other 2/60 studies (3%).

## Appendix 6.4

### *Meta-regression*

As indicated in the Cochrane Handbook for Systematic Reviews of Diagnostic Test Accuracy and related literature, we conducted multiple univariable meta-regressions with the hierarchical bivariate model by Reitsma et al. [243] using the “midas” package in STATA. We aimed to investigate the effect of five covariates on CEM sensitivity and specificity, presenting pooled estimates of these indexes for the presence or not of each covariate and jointly modeling the effect of each covariate on CEM performance with the likelihood ratio test ( $\chi^2$  statistic and related  $P$  value). Therefore, one covariate at a time was investigated, fitting a total of 5 models, always considering one study part for each of the 60 studies (55 in case of the covariate “Timing of CEM performance according to menstrual cycle phase”). Of note, as stated in the Methods section, for the seven studies with more than one study part we always included the study part with the most comprehensive reporting approach for CEM, i.e. positivity thresholds defined by joint consideration of enhancement presence, conspicuity, and morphology.





## **7. Radiation dose of contrast-enhanced mammography: a two-centre prospective comparison**

*Based on:*

Gennaro G, Cozzi A, Schiaffino S, Sardanelli F, Caumo F (2022) *Radiation dose of contrast-enhanced mammography: a two-centre prospective comparison*. Submitted to **Cancers**

## 7.1. Abstract

**Background:** CEM is increasingly used for both screening and diagnostic applications. As its radiation dose has been investigated only by few single-centre studies, we aimed to evaluate it in a bicentric setting.

**Methods:** We retrospectively analysed data from two prospective studies using CEM to screen women at increased breast cancer risk (Centre 1) and in the work-up of mammography-detected findings (Centre 2). Both datasets were acquired with the same type of mammography unit and with the same clinical protocol. CEM mean glandular dose (MGD) was computed for low-energy and high-energy images and its sum calculated for each view. MGD and related parameters (entrance dose, exposure, breast thickness, compression, and density) were compared between the two centres using the Mann-Whitney test. Finally, data from the two centres were pooled and used to estimate the total (per-patient) MGD of CEM, then compared with MGDs from mammography and digital breast tomosynthesis.

**Results:** A total of 348 CEM examinations were analysed (228 from Centre 1, mean age  $51 \pm 9$  years; 120 from Centre 2, mean age  $59 \pm 10$  years). Median total MGD per view was 2.33 mGy (interquartile range 2.19–2.51 mGy) at Centre 1 and 2.46 mGy (interquartile range 2.32–2.70 mGy) at Centre 2, with a 0.15 mGy median difference ( $p < 0.001$ ). Low-energy images contributed between 64% and 77% to the total patient dose in CEM, the remaining 23%–36% being associated with high-energy images.

**Conclusions:** CEM radiation dose is about 30% higher than digital mammography, and comparable with dose delivered by digital breast tomosynthesis.

## 7.2. Introduction

From a technical point of view, CEM images are obtained by separating the two x-ray spectra, so that the first is kept below the iodine absorption peak at 33.2 keV (low-energy [LE] image) and the second is pushed above the 33.2 keV absorption peak (high-energy [HE] image) [286]. CEM is interpreted by considering both the LE image—equivalent to a standard digital mammography image [178]—and a dual-energy image obtained from recombination of LE and HE images, showing contrast enhancement of hypervascularized lesions and of parenchymal background [286, 287]. Contrast enhancement reveals the neoangiogenesis and the expansion of the extracellular volume associated with breast cancer and other breast lesions, providing functional information combined with the high-resolution morphological information of LE images [130, 288]. Thanks to this double diagnostic profile, CEM performance has been reported as higher than digital mammography or DBT and as comparable to that of CE-MRI [288, 289].

As CEM radiation dose is the sum of doses associated with LE and HE images and LE images are substantially digital mammography images, CEM radiation dose is expected to be higher than that of digital mammography. The few studies comparing CEM, digital mammography, and DBT doses confirmed that CEM delivers a radiation dose higher than digital mammography and comparable to the one of DBT [168, 171, 192].

While concerns about risks associated with the exposure to ionizing radiation are limited and outweighed by potential benefits when an imaging technique is used in symptomatic patients or for characterizing suspicious findings, for cancer staging, for neoadjuvant therapy evaluation [123, 130, 288], dose assessment becomes far more important if an imaging technique (in this case, CEM) is used to image healthy subjects, as occurs in screening populations [202, 217, 249, 251, 259, 273]. Thus, the assessment of CEM radiation dose is crucial for defining its clinical application field.

This study aimed to retrospectively compare CEM radiation doses in two populations from two prospective studies where CEM was acquired with the same type of mammography unit and with

the same acquisition protocol. In one study CEM serves as a screening tool for women at increased breast cancer risk, while in the other CEM is used in the work up of suspicious findings detected at screening mammography.

### **7.3. Methods**

#### *Study population*

This observational study is a pooled analysis of data from two prospective studies using CEM in different settings, which had in common the secondary endpoint of evaluating radiation dose. The flowcharts of the two studies are depicted in Fig. 7.1. The study at Centre 1 (Veneto Institute of Oncology (IOV) - IRCCS, Padua, Italy), approved by the Institutional Ethics Committee on December 22<sup>nd</sup>, 2017 (protocol code #2017/92), is enrolling women at increased risk for breast cancer (assessed using the Tyrer-Cuzick model) with the aims of testing CEM non-inferiority compared to breast MRI and CEM superiority over digital mammography through a multi-reader multi case ROC analysis. The study at Centre 2 (IRCCS Policlinico San Donato, San Donato Milanese, Italy), approved by the Institutional Ethics Committee on May 10<sup>th</sup>, 2018 (protocol code CEM), enrolled women recalled from mammography screening who underwent CEM in addition to standard work-up (supplemental digital mammography or DBT views, and/or breast ultrasound), aiming to evaluate CEM potential of reducing the biopsy rate. In both studies, all enrolled patients signed informed consents.

CEM examinations in both centres were performed using the same model of mammography unit (GE Senographe Pristina, General Electric Healthcare, Buc, France), and the same clinical protocol: cranio-caudal (CC) views followed by the medio-lateral oblique (MLO) views, starting two minutes after the administration of a 1.5 mL/kg dose of an ICA (Iohexol 350 mgI/mL) with a 3.0 mL/s flow rate.

### *Technical comparison of CEM units*

As a preliminary step, a technical comparison between the CEM units located at Centre 1 and Centre 2 was performed. X-ray tube performance was compared measuring tube outputs and half value layers (HVLs) by a RaySafe X2 multimeter equipped with a MAM sensor (Unfors RaySafe AB, Billdal, Sweden). Three tube output and HVL measurements were acquired for the two pairs of x-ray spectra used by the automatic exposure control (AEC) for CEM acquisition. AEC and detector performance were compared by evaluating the difference between: *i*) entrance dose values as a function of breast phantom thickness; *ii*) contrast-to-noise ratio (CNR), as image quality index, as a function of breast phantom thickness. Breast phantoms of different thicknesses were assembled by stacking semi-circular polymethyl-methacrylate (PMMA) slabs (from 20 to 70 mm thick, at 5 mm intervals), on top of which a thin (0.2 mm) aluminium square (15×15 mm<sup>2</sup>) was superimposed to produce image contrast. One image in AEC mode was acquired for each phantom thickness and CEM unit. The entrance dose was calculated by multiplying the measured tube output by the tube current × exposure time product selected by the AEC, adjusting the resulting value for the source-to-phantom-entrance distance. Then, the CNR, i.e. the absolute difference between the mean signal measured within the aluminium square and the mean signal measured in the PMMA background surrounding the aluminium square divided by the noise in the PMMA background [290], was measured from phantom images using ImageJ2 [291]. Relative differences (i.e. the absolute difference divided by the mean value) between each physical variable measured for the two CEM units were used to assess technical differences between the two systems. Relative differences below 5% were considered representative of normal variability between systems.

### *Clinical dose comparison and statistical analysis*

LE images (in DICOM For Processing format) from Centre 1 and Centre 2 were processed by Volpara algorithm v.1.5.5.1 (Volpara Health Ltd, Wellington, New Zealand) to determine volumetric breast density and MGD associated with LE images [292], MGD values being adjusted

for individual breast density (20,21). Other parameters used to calculate MGD were obtained from the image DICOM header, such as entrance dose, compressed breast thickness and HVL. MGD associated with the HE images was computed using entrance dose, compressed breast thickness and HVL recorded in the DICOM header, and the conversion factors published by Dance et al. [293, 294]. Total MGD for each CEM mammographic view was obtained as the sum of LE and HE MGDs.

Differences in breast thickness, compression force, volumetric breast density, LE and HE entrance dose, exposure (measured in mAs), and total MGD between Centre 1 and Centre 2 datasets were assessed with the Mann-Whitney  $U$  test. Total MGD per-view was stratified by breast thickness for the two datasets and compared. Finally, pooling the two datasets together, we calculated the total MGD for each patient (by summing MGDs from CC and MLO views for each breast and averaging the two values obtained for the left and right breasts) and proportions of CEM dose associated with LE and HE images, as a function of breast thickness.

Statistical analyses were performed with MedCalc (version 20.009, MedCalc Software Ltd, Ostend, Belgium),  $p$  values  $< 0.05$  indicating a statistically significant difference.

## **7.4. Results**

### *Study population*

This pooled analysis included 228 women (451 CC and 455 MLO views) from Centre 1 and 120 women (243 CC and 241 MLO views) from Centre 2, for a total of 348 women and 1390 views. Women from Centre 1 were enrolled between March 1<sup>st</sup>, 2019, and December 31<sup>st</sup>, 2020, while women from Centre 2 were enrolled between January 25<sup>th</sup>, 2019, and February 21<sup>st</sup>, 2020. Mean age ( $\pm$  standard deviation) was significantly different in the two datasets:  $51 \pm 9$  years for women enrolled at Centre 1 and  $59 \pm 10$  years for women enrolled at Centre 2, respectively ( $p < 0.001$ ). The Centre 1 dataset included 172/228 (75.4%) high-risk and 56/228 (24.6%) intermediate-risk women,

while the Centre 2 dataset included women with any breast cancer risk profile without any preliminary risk assessment. Breast density was also different between the two centres: 77.6% (177/228) of women enrolled by Centre 1 had dense breasts (category *c* and *d* of the Breast Imaging Reporting and Data System classification), compared to 45.0% (54/120) of women from Centre 2 ( $p < 0.001$ ). Differences between the two datasets which constitute this study population are summarized in Table 7.1.

#### *Technical comparison of CEM units*

As shown in Table 7.2, the x-ray sources of the two CEM units were very similar for both tube output and HVL, their relative differences being all below 5%. Conversely, plots in Fig. 7.2—that shows the entrance dose and the resulting CNR as a function of PMMA thickness when the AEC is used—indicate that using phantoms the CEM unit at Centre 2 delivered an entrance dose systematically higher than the unit at Centre 1, in order to obtain similar CNR values. The mean entrance dose increase at Centre 2 (obtained by averaging dose differences at any PMMA thickness) was 21.1% for LE and 23.6% for HE images. On average, the CNR difference between the two systems was 2.5% for LE images and 1.2% for HE images (Table 7.3 and Table 7.4).

#### *Clinical dose comparison*

Table 7.5 compares total MGD, LE MGD and HE MGD calculated from each mammographic view included in the two datasets, as well as all parameters affecting MGD calculation, such as entrance dose and exposure (separately for LE and HE images), breast thickness, compression force, and volumetric breast density. Median total MGD per view was 2.33 mGy (interquartile range [IQR] 2.19–2.51 mGy) at Centre 1 and 2.46 mGy (IQR 2.32–2.70 mGy) at Centre 2, with a statistically significant 0.15 mGy median difference ( $p < 0.001$ ). The MGD difference was confirmed to be significant also for the two MGD components, LE MGD (Centre 1: median 1.52 mGy, IQR 1.39–1.73 mGy; Centre 2: median 1.69 mGy, IQR 1.54–1.99 mGy;  $p < 0.001$ ) and HE MGD



(Centre 1: median 0.79 mGy, IQR 0.75–0.82 mGy; Centre 2: median 0.75 mGy; IQR 0.70–0.79 mGy;  $p < 0.001$ ).

Comparing total MGD (as the sum of LE and HE MGDs) for Centre 1 and Centre 2 stratified according to increasing breast thickness, we found that both mean and median values were very similar for the two CEM units (Fig. 7.3) for most thickness groups. The major difference occurred for breasts with a thickness lower than 30 mm, for which the average and median MGDs at Centre 1 (mean  $1.82 \pm 0.40$  mGy, median 1.81 mGy, IQR 1.61–2.10 mGy) were respectively 11% and 15% lower than at Centre 2 (mean  $2.03 \pm 0.35$  mGy, median 2.08 mGy, IQR 1.82–2.32 mGy). For any other thickness range both mean and median dose differences between the two systems were lower than 5% (Table 7.6).

Finally, considering results from the aforementioned comparisons on per-view dose in the two independent datasets, we proceeded with data pooling to obtain an overall patient dose estimation. As shown in Fig. 7.4a and Table 7.7, pooled mean patient MGD progressively increases with breast thickness for LE acquisitions (from 2.53 mGy for less than 30 mm breast thickness to 4.74 mGy for breast thickness higher than 70 mm), while remaining approximately constant for HE acquisitions (1.20 mGy for less than 30 mm breast thickness, 1.44 mGy for breast thickness higher than 70 mm). Examining the radiation dose contribution of each CEM component (as normalized stacked column plot in Fig. 7.4b, providing the relative contribution of LE and HE images), it can be noticed that the percentage of total dose attributable to LE images ranged between 64% and 77%, while only the remaining 23%–36% was associated to HE images.

## **7.5. Discussion**

The aim of this study was to assess the radiation dose of CEM by a pooled analysis of data from two prospective studies using the same type of mammography unit and the same CEM protocol,

respectively focused on screening of women at increased breast cancer risk (Centre 1, 228 women) and on the work-up of suspicious findings at screening mammography (Centre 2, 120 women).

The phantom study for physical comparison between the two units showed comparable x-ray tube performance; the AEC of the mammography unit installed at Centre 2 worked with higher entrance doses (mean increase: 21% for LE images and 23% for HE images) to compensate for a slightly lower detector efficiency and keep image quality (i.e. the CNR values) comparable with that obtained at Centre 1 (Table 7.6, Fig. 7.5).

Nevertheless, comparing the two clinical datasets concurring to this study population, we observed only a 6% median difference in MGD (2.33 mGy in Centre 1 versus 2.46 mGy in Centre 2;  $p < 0.001$ ), due to a “compensation effect” associated to the inherent differences between the two populations. The study at Centre 1 focused on women at increased risk for breast cancer, young and mostly with dense breasts, requiring increased radiation dose to attain appropriate image quality; conversely, the study at Centre 2 enrolled women recalled from a screening population, older and usually with lower breast density, thereby requiring less dose.

The overall comparability between MGDs for the two clinical datasets allowed us to proceed with data pooling and calculation of dose per-patient. On average, a standard two-view bilateral CEM exam was associated with MGD values between 3.73 mGy and 6.17 mGy, increasing with breast thickness. Considering the LE and HE image separately, LE MGD increased with breast thickness (from 2.53 mGy to 4.74 mGy), while HE MGD was substantially independent of breast thickness (from 1.20 mGy to 1.44 mGy). In fact, while LE images require that radiation dose increases with breast thickness to preserve image quality, as occurs for standard digital mammography [295], the x-ray beams used to obtain HE images (optimized to maximize the contrast enhancement in case of lesion presence) do not need modulation with breast thickness. Therefore, considering LE images as a standard digital mammography exam, the dose increase due to the HE acquisition was about 30% independently of breast thickness.

Our results are consistent with those summarized by Hendrick [296], who reported that CEM dose is 20%–45 % higher than that delivered by digital mammography, much lower than the 80% dose increase obtained by initial CEM studies using prototype equipment [164, 168, 171, 192].

Moreover, our CEM dose estimates are comparable with those reported for DBT [297], which is progressively replacing digital mammography in both the diagnostic and screening setting [298]. In fact, while radiation dose for two-view DBT is reported to range from 3.7 mGy to about 5 mGy, depending on the DBT manufacturer [296], we found a CEM MGD below 5 mGy for any breast thickness below 6 cm. Moreover, CEM MGD estimates at different breast thickness are also below the limiting values proposed in European Guidelines for digital mammography or DBT exams [299], as well as by the Mammography Quality Standards Act Regulations [300].

Results obtained in this study suggest that, as far as radiation protection principles are applied, CEM can be used for both screening recalls and screening of specific populations. In particular, the functional information provided by CEM in addition to the morphological information coming from LE images would be particularly beneficial in women at increased risk of breast cancer and in women with dense breasts, as a valid alternative to breast MRI, which is much less accessible and much more expensive and time consuming [288, 301]. In the group of women at increased risk, particular attention should be paid to mutation carriers (such as BRCA1/2 or P53), taking into account their potential increased radiosensitivity and radiosusceptibility [302], which suggests a careful evaluation of the risk-to-benefit ratio also depending on the local accessibility of MRI.

The chief limitation of this study is the inclusion of CEM exams acquired by units of the same model and manufacturer, although some differences were found due to variability between components and calibrations. It could be assumed that larger differences would be obtained in a multi-vendor approach including CEM systems by multiple manufacturers with different designs.

Another limitation is the indirect comparison between imaging techniques: while CEM dose results

were derived from experimental data, the dose values with DBT and digital mammography were obtained from the literature.

In conclusion, dose by CEM exams is about 30% higher than digital mammography dose, and comparable with dose delivered by digital breast tomosynthesis. Thereby, dose concerns should not constitute an obstacle for future clinical implementations of CEM, including both the screening and diagnostic setting.

**Table 7.1** Characteristics of the study population, obtained by pooling data from two prospective studies using CEM for different screening applications

<b>Variables</b>		<b>Centre 1</b>	<b>Centre 2</b>	<b><i>p</i> value</b>
<b>Demographics</b>	Number of women	228	120	–
	Women age: mean $\pm$ SD	51 $\pm$ 9 years	59 $\pm$ 10 years	< 0.001
<b>Breast cancer risk</b>	High <sup>a</sup>	172/228 (75.4%)	Data not available	–
	Intermediate <sup>b</sup>	56/228 (24.6%)	Data not available	
<b>Breast density</b>	Non-dense <sup>c</sup>	51/228 (22.4%)	66/120 (55.0%)	< 0.001
	Dense <sup>d</sup>	177/228 (77.6%)	54/120 (45.0%)	< 0.001

*SD* standard deviation.

<sup>a</sup> High-risk women = women with lifetime risk above 30% (Tyrer-Cuzick risk model).

<sup>b</sup> Intermediate-risk women = women with lifetime risk between 17% and 30% (Tyrer-Cuzick risk model).

<sup>c</sup> Non-dense breasts = BI-RADS *a* and BI-RADS *b*.

<sup>d</sup> Dense breasts = BI-RADS *c* and BI-RADS *d*.

**Table 7.2** Tube output and HVL measurement for the two CEM units installed at Centre 1 and Centre 2. Measurements were performed for both units with the same RaySafe X2 x-ray test device; the calibrated MAM sensor was placed at 610 mm distance from the x-ray tube exit

X-ray beam	Tube output <sup>a</sup> ( $\mu\text{Gy/mAs}$ )			HVL <sup>b</sup> (mmAl)		
	Centre 1 (mean $\pm$ SD)	Centre 2 (mean $\pm$ SD)	Relative difference (%)	Centre 1 (mean $\pm$ SD)	Centre 2 (mean $\pm$ SD)	Relative difference (%)
Mo/Mo@26kVp (LE) <sup>c</sup>	72.3 $\pm$ 0.0	69.7 $\pm$ 0.0	3.7	0.34 $\pm$ 0.0	0.35 $\pm$ 0.0	2.9
Mo/Cu@49kVp (HE) <sup>d</sup>	6.9 $\pm$ 0.0	6.6 $\pm$ 0.0	4.4	3.00 $\pm$ 0.0	3.02 $\pm$ 0.0	0.7
Rh/Ag@34kVp (LE) <sup>e</sup>	123.4 $\pm$ 0.0	117.8 $\pm$ 0.0	4.6	0.54 $\pm$ 0.0	0.56 $\pm$ 0.0	3.6
Rh/Cu@49kVp (HE) <sup>f</sup>	7.7 $\pm$ 0.0	7.4 $\pm$ 0.0	4.0	2.85 $\pm$ 0.0	2.93 $\pm$ 0.0	2.8

<sup>a</sup> Tube output is defined as the air-kerma (measured at known distance from the tube exit) divided by the exposure (mAs) value. Distance between X-ray source and sensor was 610 mm.

<sup>b</sup> Half value layer is defined as the thickness of known material which halves the X-ray beam intensity. The material used in mammography is aluminium.

<sup>c</sup> For a thickness of less than 30mm the automatic exposure control selects the molybdenum (Mo) anode material with the Mo filter and the tube voltage at 26 kV<sub>p</sub> for the acquisition of the low-energy images.

<sup>d</sup> For a thickness of less than 30mm the automatic exposure control selects the Mo anode with the copper (Cu) filter and the tube voltage at 49 kV<sub>p</sub> for the acquisition of the high-energy images.

<sup>e</sup> For a thickness greater than 30mm the automatic exposure control selects the rhodium (Rh) anode material with the silver (Ag) filter and the tube voltage at 34 kV<sub>p</sub> for the acquisition of the low-energy images.

<sup>f</sup> For a thickness greater than 30mm the automatic exposure control selects the Rh anode material with the Cu filter and the tube voltage at 49 kV<sub>p</sub> for the acquisition of the high-energy images.

*HVL* half value layer; *LE* low-energy; *HE* high-energy; *SD* standard deviation.

**Table 7.3** Entrance dose (ED) from LE and HE images obtained by acquiring CEM images of PMMA phantom at increasing thickness in automatic exposure (AEC) mode. Phantoms were obtained by stacking semi-circular PMMA slabs to cover the thickness range 20–70 mm, superimposing a 1.5×1.5 mm<sup>2</sup> aluminium square (0.2 mm thick). ED was obtained by multiplying the tube output previously measured by the exposure value (mAs), and adjusting the result for the inverse squared distance. The relative ED difference for each PMMA thickness was calculated as difference between ED at Centre 2 and ED at Centre 1 divided by the ED at Centre 1. The mean ED difference (obtained by averaging the relative ED differences at each PMMA thickness) was 21.1% for LE and 23.6% for HE images

<b>PMMA thickness (mm)</b>	<b>Centre 1 LE ED (mGy)</b>	<b>Centre 2 LE ED (mGy)</b>	<b>LE ED difference (%)</b>	<b>Centre 1 HE ED (mGy)</b>	<b>Centre 2 HE ED (mGy)</b>	<b>HE ED difference (%)</b>
20	1.55	1.83	18.1	0.33	0.42	27.3
25	2.15	2.69	25.1	0.41	0.53	29.3
30	3.2	4.06	26.9	0.51	0.66	29.4
35	2.64	3.24	22.7	0.87	1.07	23.0
40	3.2	3.78	18.1	0.86	1.06	23.3
45	3.63	4.59	26.4	0.86	1.05	22.1
50	4.49	5.42	20.7	0.89	1.08	21.3
55	5.23	6.4	22.4	0.91	1.1	20.9
60	6.41	7.55	17.8	0.92	1.12	21.7
65	8.33	9.65	15.8	0.92	1.11	20.7
70	10.15	11.96	17.8	0.95	1.15	21.1
<b>Mean</b>			<b>21.1</b>			<b>23.6</b>

*PMMA* polymethyl methacrylate; *ED* entrance dose; *LE* low-energy; *HE* high-energy.

**Table 7.4** Contrast-to-noise ratio (CNR) measured from LE and HE phantom images. Phantoms were obtained by stacking semi-circular PMMA slabs to cover the thickness range 20–70 mm, superimposing a 1.5×1.5 mm<sup>2</sup> aluminium square (0.2 mm thick). CNR at each phantom thickness was calculated as absolute difference between the aluminium mean pixel value (measured in a square ROI within the aluminium square) and the PMMA mean pixel value (measured in a square band in the PMMA excluding the aluminium detail), divided by the PMMA standard (noise). The relative CNR difference for each PMMA thickness was calculated as difference between CNR at Centre 2 and CNR at Centre 1 divided by the CNR at Centre 1. The mean CNR difference (obtained by averaging the relative CNR differences at each PMMA thickness) was -2.5% for LE and -1.2% for HE images

PMMA thickness (mm)	Centre 1	Centre 2	LE CNR	Centre 1	Centre 2	HE CNR
	LE CNR	LE CNR	difference (%)	HE CNR (mGy)	HE CNR (mGy)	difference (%)
20	24.6	25.3	2.8	9.1	9.1	0.0
25	24	25.1	4.6	8.9	9.3	4.5
30	24.8	23.9	-3.6	9.6	9.5	-1.0
35	22	21	-4.5	10.5	10.6	1.0
40	20.2	19	-5.9	10.1	9.8	-3.0
45	18.2	17.9	-1.6	9.2	9.1	-1.1
50	17	16.5	-2.9	8.8	8.5	-3.4
55	16.2	15.4	-4.9	8.4	8	-4.8
60	15.3	14.2	-7.2	7.6	7.4	-2.6
65	14.3	13.9	-2.8	7	6.9	-1.4
70	13.7	13.5	-1.5	6.6	6.5	-1.5
<b>Mean</b>			<b>-2.5</b>			<b>-1.2</b>

*PMMA* polymethyl methacrylate; *CNR* contrast-to-noise ratio; *LE* low-energy; *HE* high-energy.



**Table 7.5** Comparison between total MGD, LE MGD, HE MGD and between parameters affecting MGD (entrance dose, exposure, breast thickness, breast compression, and breast density) obtained from the two clinical datasets

<b>Parameter</b>	<b>Centre 1 median (IQR)</b>	<b>Centre 2 median (IQR)</b>	<b>Hodges-Lehmann median difference (95% CI)</b>	<b><i>p</i> value</b>
Total MGD (mGy)	2.32 (2.19–2.51)	2.46 (2.32–2.70)	0.16 (0.13–0.19)	< 0.001
LE MGD (mGy)	1.52 (1.39–1.73)	1.69 (1.54–1.99)	0.18 (0.15–0.21)	< 0.001
HE MGD (mGy)	0.79 (0.75–0.82)	0.75 (0.70–0.79)	-0.03 (-0.04 – -0.02)	< 0.001
LE entrance dose (mGy)	4.37 (3.60–5.68)	5.18 (4.24–7.01)	0.78 (0.60–0.97)	< 0.001
HE entrance dose (mGy)	0.86 (0.83–0.90)	0.93 (0.90–0.98)	0.07 (0.066–0.080)	< 0.001
LE exposure (mAs)	35 (28–44)	39 (31.5–49.5)	4 (2–5)	< 0.001
HE exposure (mAs)	109 (107–116)	116 (114–117)	7 (6–7)	< 0.001
Breast thickness (mm)	47.2 (37.5–57.6)	54.2 (45.8–64.2)	7.2 (5.6–8.8)	< 0.001
Compression force (N)	106 (90–122)	54 (40–75)	-49 (-51 – -46)	< 0.001
Volumetric breast density (%)	13.2 (7.8–20.3)	7.1 (4.4–11.6)	-5.2 (-3.0 – -4.4)	< 0.001

Differences between the two independent samples were tested with the Mann-Whitney *U* test. *p* values lower than 0.05 were considered statistically significant.

*MGD* mean glandular dose; *LE* low-energy; *HE* high-energy; *IQR* interquartile range.

**Table 7.6** X-ray tube performance in the two clinical datasets

<b>Breast thickness (mm)</b>	<b>Centre 1 mean <math>\pm</math> SD MGD (mGy)</b>	<b>Centre 2 mean <math>\pm</math> SD MGD (mGy)</b>	<b>Mean difference</b>	<b>T-test <math>p</math> value</b>	<b>Centre 1 median (IQR) MGD (mGy)</b>	<b>Centre 2 median (IRQ) MGD (mGy)</b>	<b>Median difference</b>	<b>Mann-Whitney test <math>p</math> value</b>
<b><math>\leq 30</math></b>	1.822 $\pm$ 0.396	2.031 $\pm$ 0.349	11.5%	0.034	1.81 (1.61–2.10)	2.08 (1.82–2.32)	15.1%	0.019
<b>31–40</b>	2.246 $\pm$ 0.205	2.278 $\pm$ 0.187	1.4%	0.330	2.23 (2.17–2.38)	2.31 (2.22–2.38)	3.8%	0.089
<b>41–50</b>	2.317 $\pm$ 0.195	2.365 $\pm$ 0.116	2.1%	0.003	2.28 (2.20–2.40)	2.35 (2.28–2.43)	3.1%	< 0.001
<b>51–60</b>	2.422 $\pm$ 0.214	2.517 $\pm$ 0.246	3.9%	< 0.001	2.39 (2.27–2.52)	2.46 (2.32–2.68)	2.7%	< 0.001
<b>61–70</b>	2.726 $\pm$ 0.405	2.718 $\pm$ 0.326	-0.3%	0.870	2.63 (2.46–2.94)	2.65 (2.51–2.77)	0.5%	0.741
<b>&gt; 70</b>	3.134 $\pm$ 0.422	3.196 $\pm$ 0.438	3.3%	0.486	3.11 (2.76–3.45)	3.11 (2.98–3.52)	1.5%	0.501

*MGD* mean glandular dose; *SD* standard deviation; *IQR* interquartile range.

**Table 7.7** Per-patient MGD for LE images, HE images, and total CEM, for different breast thickness ranges. Individual patient dose was obtained by averaging left and right sums of MGD values associated with CC and MLO views respectively

<b>Breast thickness (mm)</b>	<b>Per-patient mean LE MGD (mGy)</b>	<b>Per-patient mean HE MGD (mGy)</b>	<b>Per-patient mean total MGD (mGy)</b>
< 30	2.53	1.20	3.73
30– 40	2.92	1.61	4.53
40–50	3.13	1.60	4.73
50–60	3.40	1.56	4.96
60–70	3.94	1.49	5.43
> 70	4.74	1.44	6.17

*MGD* mean glandular dose; *LE* low-energy; *HE* high-energy; *CC* cranio-caudal; *MLO* medio-lateral oblique.

**Fig. 7.1** (a) Flowchart of the prospective study ongoing at Centre 1 comparing CEM with breast MRI in a population of women at increased risk of breast cancer. (b) Flowchart of the prospective study at Centre 2 using CEM as a work-up tool for suspicious findings detected at screening mammography

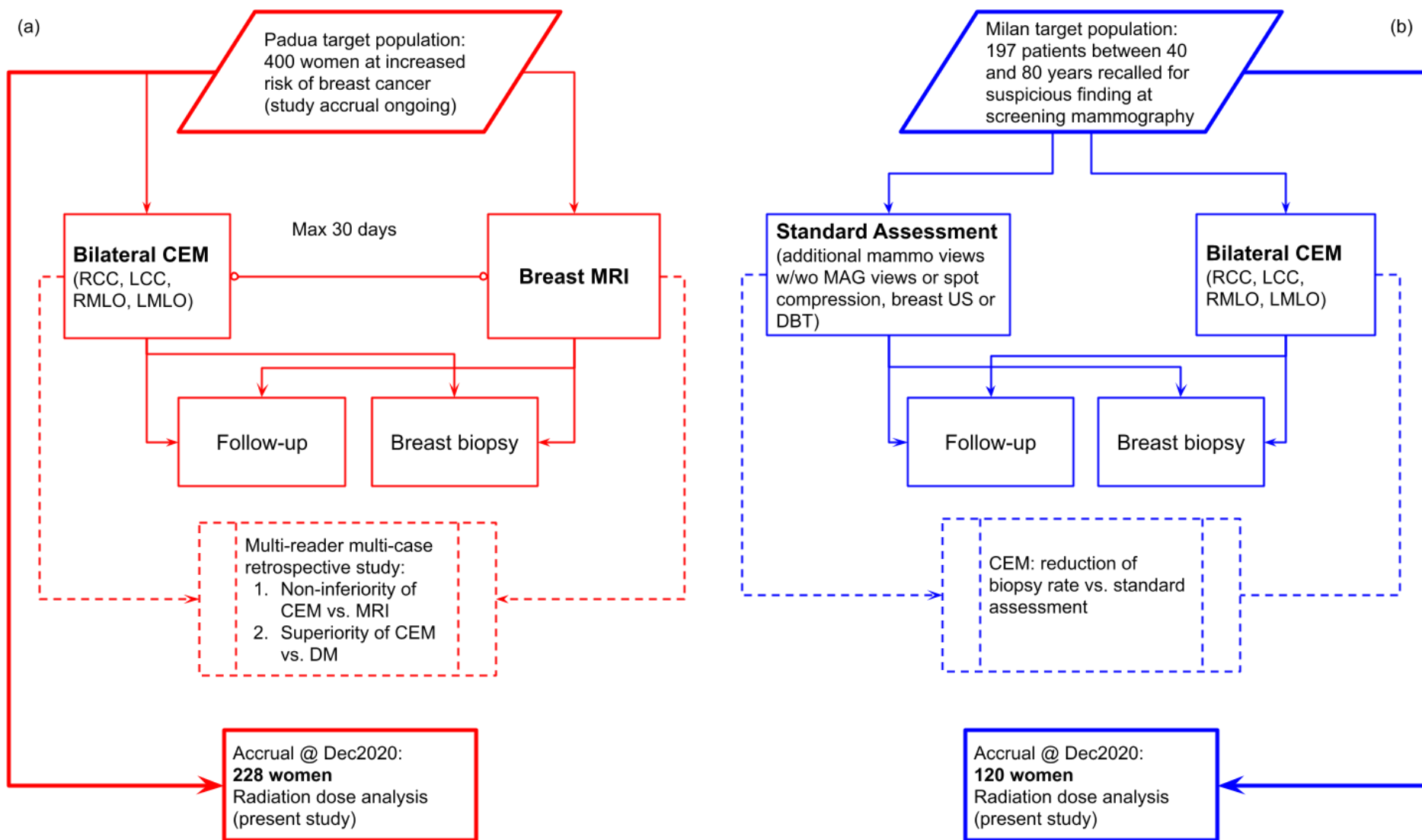


**Fig. 7.2** (a) Entrance dose (separately for LE and HE images) obtained in automatic exposure mode as a function of PMMA thickness for the two CEM systems. For PMMA below 30 mm the AEC of both systems selected the (Mo/Mo@26kV<sub>p</sub>; Mo/Cu@49kV<sub>p</sub>) x-ray beams for the (LE; HE) image; above 30 mm PMMA the x-ray beams selected by the AEC were (Rh/Ag@34kV<sub>p</sub>; Rh/Cu@49kV<sub>p</sub>). (b) Contrast-to-noise ratio (CNR) measured from the LE and HE images as a function of PMMA thickness for the two CEM systems

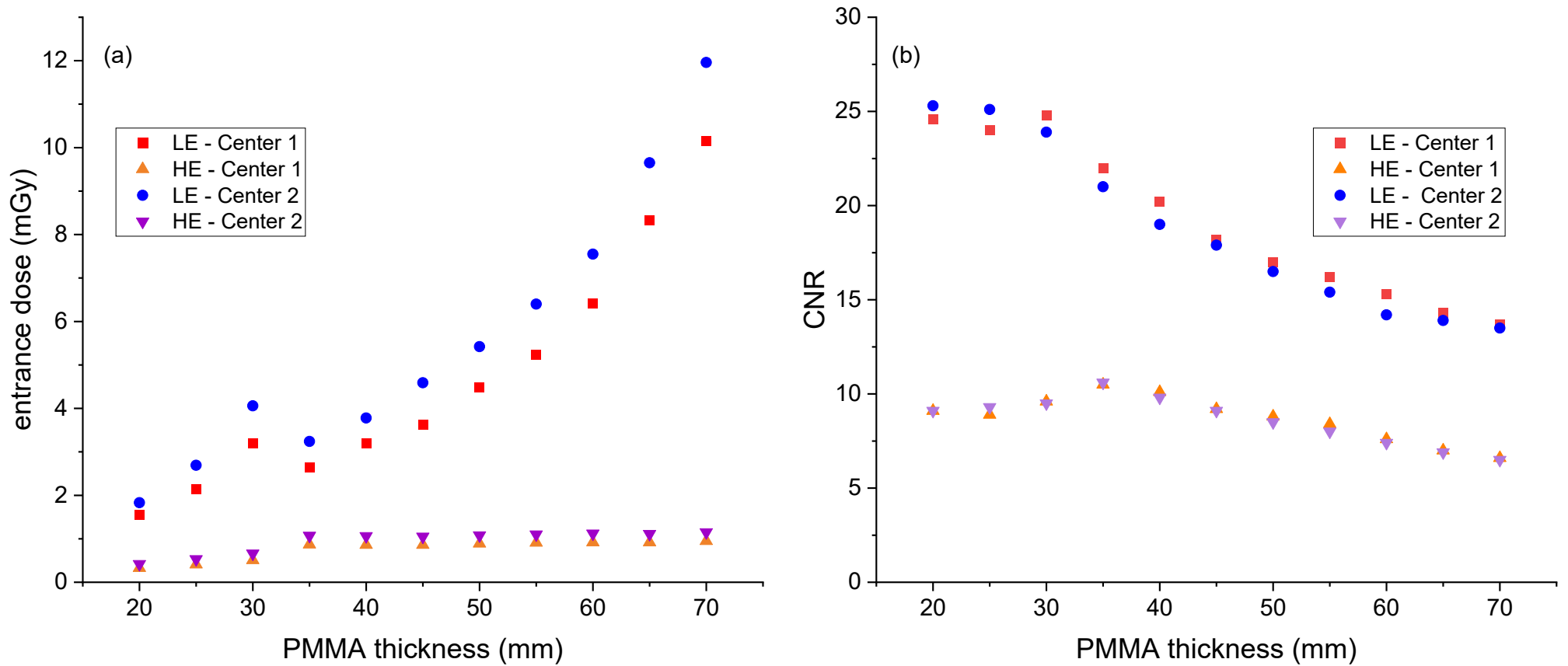


**Fig. 7.3** (a) Box-plot of Centre 1 per-view total MGDs (LE MGD + HE MGD) versus breast thickness. (b) Box-plot of Centre 2 per-view total MGDs versus breast thickness

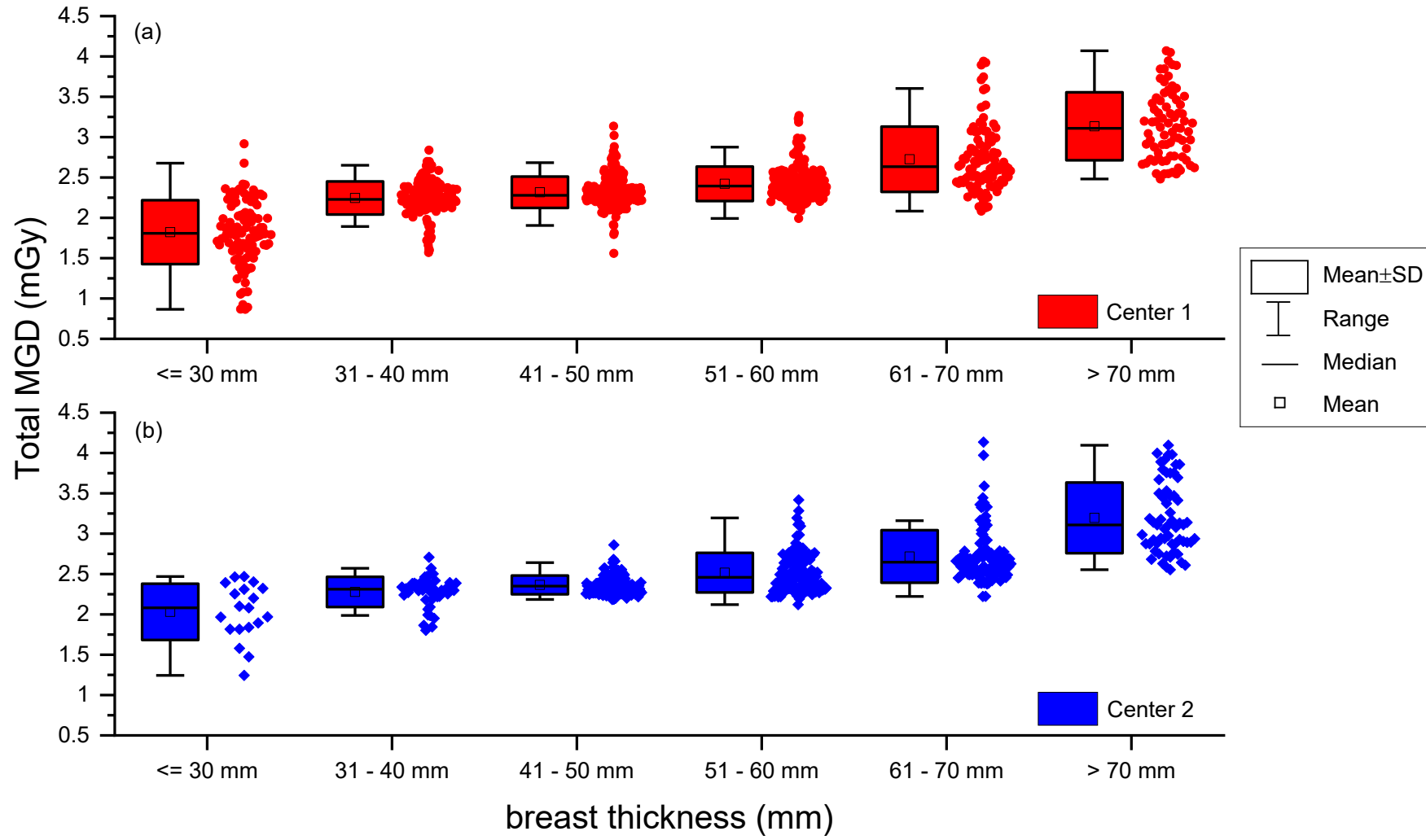


**Fig. 7.4** (a) Stacked column plot of overall patient MGD associated with CEM exams (LE in orange and HE in green) for increasing breast thickness ranges. (b) Normalized stacked plot showing the percentage of patient dose due to LE and HE images for increasing breast thickness ranges

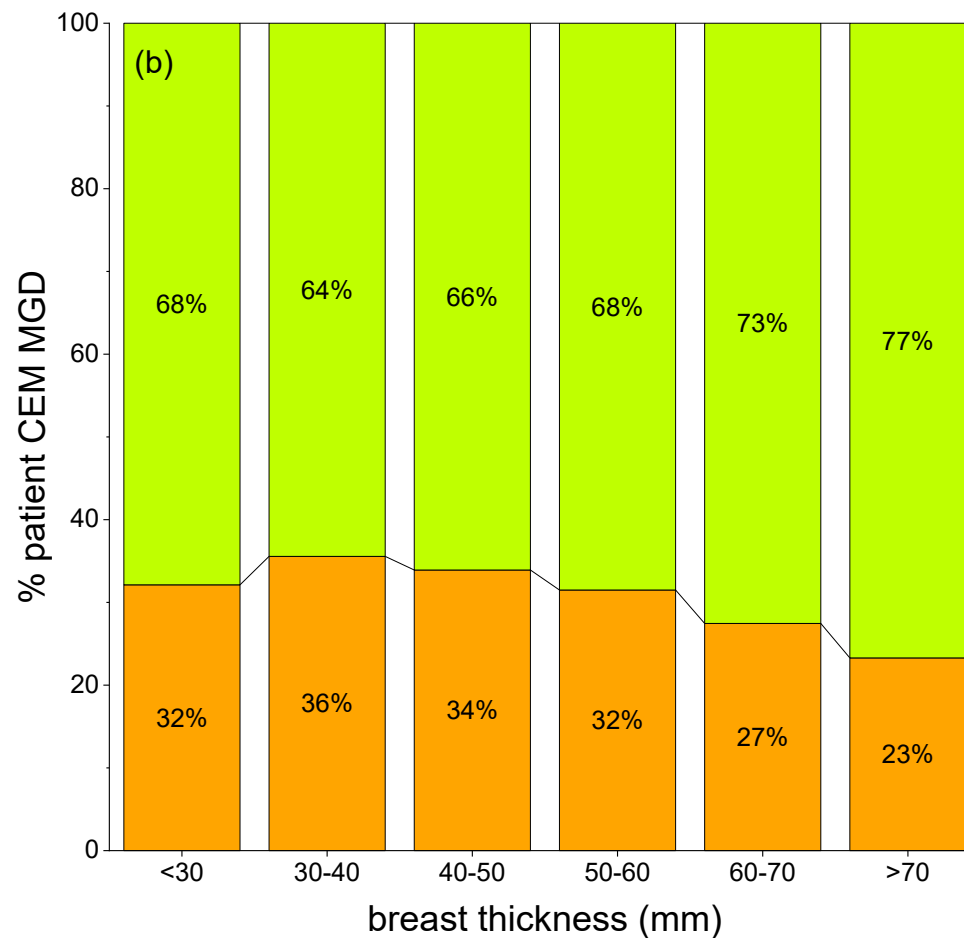
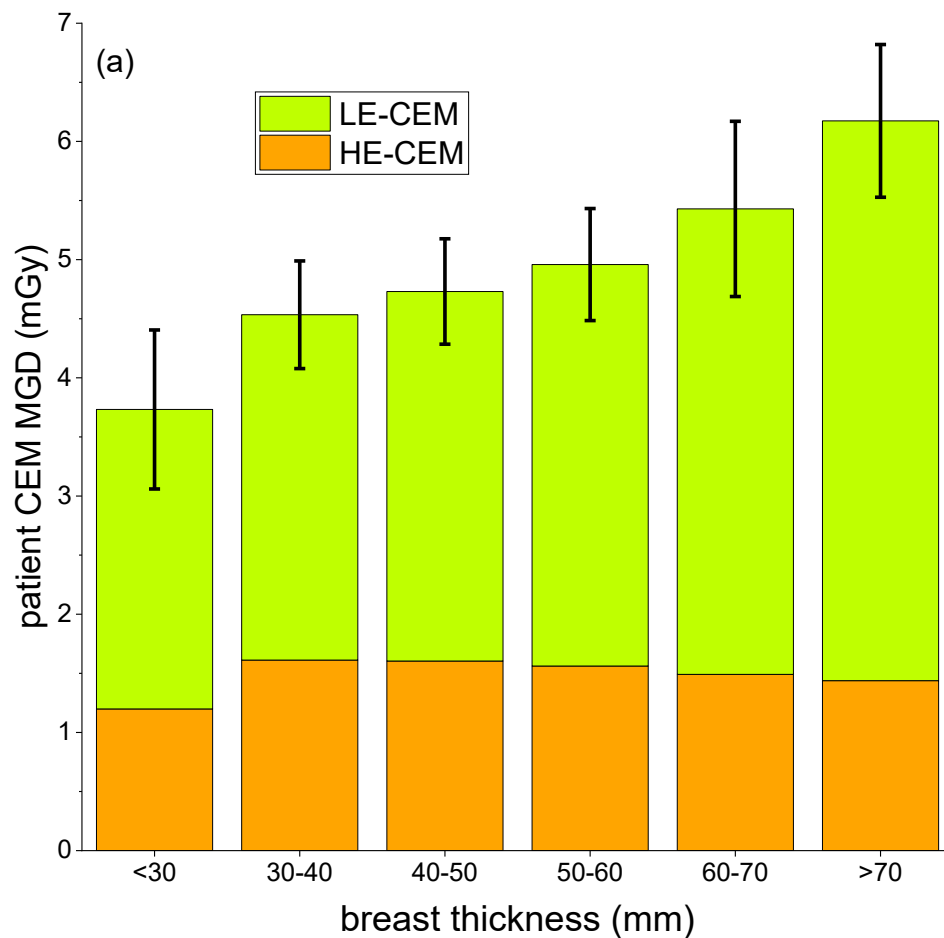
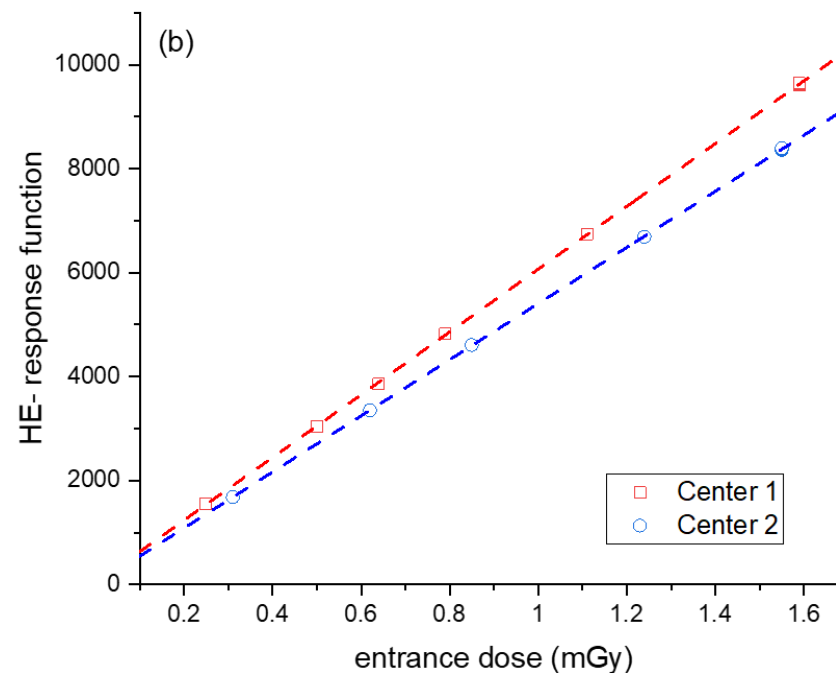
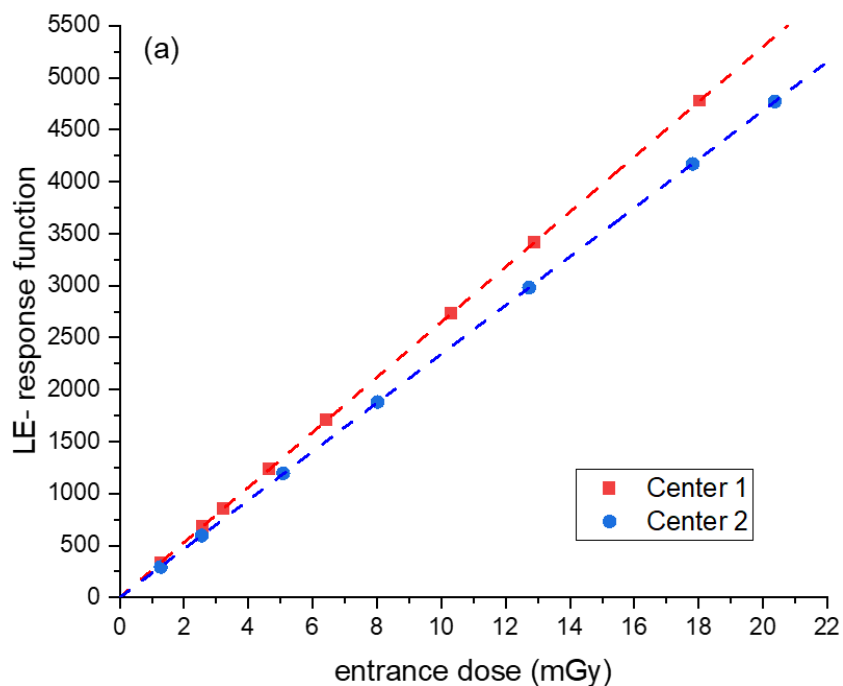


**Fig. 7.5** (a) Response function of LE acquisitions obtained exposing in manual exposure mode 45 mm PMMA with Rh/Ag at 34 kV<sub>p</sub> selecting different exposure values at Centre 1 (red) and Centre 2 (blue), respectively. (b) Response function of HE acquisitions obtained exposing in manual exposure mode 45 mm PMMA with Rh/Cu at 49 kV<sub>p</sub> selecting different exposure values at Centre 1 (red) and Centre 2 (blue), respectively. Results show that the detector of the equipment used at Centre 2 is less efficient than the detector used at Centre 1







## **8. Contrast-enhanced mammography can reduce the biopsy rate in the assessment of screening recalls: a two-centre study**

*Based on:*

Cozzi A, Schiaffino S, Fanizza M et al (2022) *Contrast-enhanced mammography for the assessment of screening recalls: a two-centre study*. Submitted to **Eur Rad**

## 8.1. Abstract

**Objectives:** To evaluate the potential of a work-up strategy based on CEM for reducing the biopsy rate of screening recalls.

**Methods:** Recalled women aged 40–80 were enrolled to undergo CEM alongside standard assessment (SA) through tomosynthesis, additional views, and/or ultrasound. Exclusion criteria were breast symptoms, breast implants, allergy to ICAs, renal failure, and pregnancy. One of six radiologists independently evaluated SA or CEM, recommending biopsy or two-year follow-up. Biopsy rates according to recombined CEM (rCEM) and according to SA were compared with the McNemar test. Diagnostic performance was calculated considering lesions with available definitive histopathology reports.

**Results:** Between January 2019 and July 2021, 220 women were prospectively enrolled, 207 of them (median age 56.6 years) with 225 suspicious findings being analysed. Overall, 135/225 findings were referred for biopsy, 90/225 by both SA and rCEM, 41/225 by SA alone, 4/225 by rCEM alone. The 94/225 rCEM biopsy rate (41.8%, 95% CI 35.5–48.3%) was 16.4% lower ( $p < 0.001$ ) than the 131/225 SA biopsy rate (58.2%, 95% CI 51.7–64.5%). Considering the 124/135 biopsies with definitive histopathology reports (44 benign and 80 malignant), rCEM showed a 93.8% sensitivity (95% CI 86.2–97.3%) and a 65.9% specificity (95% CI 51.1–78.1%), all 5 false negatives being ductal carcinoma in situ detectable as suspicious calcifications on low-energy CEM images.

**Conclusions:** Compared to SA, the rCEM-based work-up would have avoided biopsy for 37/225 (16.4%) suspicious findings. The inclusion of low-energy images in exam interpretation may provide optimal overall CEM sensitivity.

## 8.2. Introduction

While the benefits of mammographic breast cancer screening outweigh its harms [303–306], various issues of the whole screening process are still unresolved [305]. Alongside a strong drive towards personalization of screening strategies [307], research efforts are targeting one of the major drawbacks of mammographic screening, i.e. false positive recalls [305]. Indeed, even the current multi-layered imaging assessment still implies that screened women have an estimated cumulative risk of undergoing a biopsy with a final benign outcome that ranges between 2% and 6% [305, 308]. This figure is mirrored by the constantly high proportion of benign lesions (between 44% and 73%) reported in large-scale biopsy series [309–312].

Currently-employed assessment modalities, such as digital breast tomosynthesis and/or ultrasound, rely exclusively on a morphologic appraisal of suspicious findings. Conversely, imaging techniques able to provide a combined evaluation of morphologic and functional aspects may foster a decrease in biopsy rates, i.e. an increase in the positive predictive value (PPV) of work-up examinations.

This notion rests on the biological bases of functional assessment through contrast-enhanced examinations: tumour neoangiogenesis—resulting in leaky vessels that allow the entry of contrast agents into the interstitium—is a feature of more aggressive lesions [25, 26].

Among morpho-functional breast imaging techniques, CEM could be better suited [130, 131, 288] than CE-MRI [313] for the work-up of screening-detected suspicious findings, as the latter has considerable contraindications, cost-related pitfalls and, in particular, suffers from relatively low specificity in the evaluation of a common suspicious mammographic finding, calcifications [276]. This was highlighted also by a recent meta-analysis [289], where CEM had a 92% sensitivity and an 84% specificity when applied on mammography-detected suspicious findings.

CEM consists in a pair of mammograms (one low-energy, one high-energy) that are sequentially acquired after intravenous ICA administration and then recombined to minimize the appearance of unenhancing breast tissue, making enhanced areas recognisable [286]. Moreover, save from contrast

administration, CEM is similar in workflow and time to a standard 4-view mammography or tomosynthesis [124], thus being much more tolerated, affordable, and available than CE-MRI [127, 173, 314, 315].

The aim of this study was therefore to assess the potential of CEM for curtailing the biopsy rate in a prospectively-enrolled population of women recalled for assessment of suspicious findings at screening mammography.

### **8.3. Methods**

#### *Study design and population*

Approval for this bicentric prospective study was obtained by the Ethics Committee of IRCCS Ospedale San Raffaele, Milan, Italy (protocol code CESM; approved May 10<sup>th</sup>, 2018).

Enrolment in this study was proposed to all women aged 40–80 years who were referred to the Radiology Unit of IRCCS Policlinico San Donato (San Donato Milanese, Italy; Centre 1) or to the Radiology Unit of Fondazione IRCCS Policlinico San Matteo (Pavia, Italy; Centre 2) for the work-up of suspicious findings detected at screening mammography, between January 25<sup>th</sup>, 2019, and July 29<sup>th</sup>, 2021. Exclusion criteria were: breast symptoms suspicious for breast cancer; pregnancy; presence of breast implants; allergy to ICAs; renal failure (estimated glomerular filtration rate < 30 mL/min × 1.73 m<sup>2</sup>).

In both centres, standard assessment (SA) of suspicious findings was performed with additional mammographic views including mammographic magnification and/or spot compression, ultrasound, or digital breast tomosynthesis, according to the characteristics of each investigated suspicious finding.

Eligible women willing to provide informed consent entered this study and, after collection of personal data (age, height, weight, menstrual cycle status) underwent CEM immediately after SA, as depicted in the protocol flowchart (Fig. 8.1).

#### *Image acquisition and analysis*

All CEM examinations were performed on a Senographe Pristina mammography system (GE Healthcare, Buc, France) at both centres. The following imaging protocol was used at both centres: two minutes before the first image acquisition, a 1.5 mL/kg dose of a non-ionic monomeric, low-osmolar ICA (Iohexol 350 mgI/mL; GE Healthcare, Buc, France) was administered intravenously with an automated injector at a 2 mL/s flow rate, followed by a 30 mL saline flush. Then, standard mediolateral oblique and craniocaudal views were obtained in a maximum timeframe of 10 minutes, following the acquisition sequence commonly applied for diagnostic mammography at each centre [124]. All examinations times and the occurrence of any adverse reaction were recorded.

At each centre, two readers were involved in the interpretation of each patient's examinations. The reader who performed the routine SA had no access to CEM; vice versa, CEM was independently interpreted by another reader, who was blinded to the results of the SA but aware of the mammographic findings that prompted the recall and had unrestricted access to the original mammographic images. Overall, six readers with a breast imaging experience ranging 6–30 years were involved in the interpretation process in the two centres.

SA results were categorized according to the BI-RADS classification [316] and women were either referred to biopsy or entered a two-year follow-up with routine screening mammography and/or breast ultrasound. Conversely, since the reader interpreting CEM had access to the original mammographic images and CEM low-energy images are technically equivalent to a standard mammographic exam [178, 295] in providing a morphologic evaluation of the suspicious findings, CEM interpretation was focused on the recombined images (rCEM), in order to investigate the added value of the functional information provided by these contrast-enhanced images. On the basis

of rCEM readings, the reader assessing CEM defined negative findings (i.e. those not needing a biopsy according to rCEM evaluation) and positive findings (those warranting a biopsy referral according to rCEM evaluation). If the reader interpreting CEM identified suspicious lesions different from those that prompted the recall and needing a dedicated work-up, the information was disclosed to the colleague performing SA and the work-up of these additional abnormalities was immediately performed according to the clinical practice currently used for additional findings at breast CE-MRI (target ultrasound, additional mammograms/tomosynthesis views, image-guided biopsy). Of note, as this design aims to evaluate the potential of rCEM to reduce the biopsy rate, CEM results could only be used to refer women to biopsy for suspicious findings that were not detectable at SA: biopsies recommended by SA were always performed, even with negative rCEM results.

#### *Statistical analysis*

The primary endpoint of this study was the potential rCEM biopsy rate, to be compared with the effectively-performed SA biopsy rate, respectively calculated as

$$rCEM \text{ biopsy rate} = \frac{\textit{suspicious findings referred to biopsy according to rCEM}}{\textit{total suspicious findings in enrolled women}}$$

and

$$SA \text{ biopsy rate} = \frac{\textit{suspicious findings referred to biopsy according to SA}}{\textit{total suspicious findings in enrolled women}}$$

Secondary endpoints were: 1) the number of adverse reactions to ICAs (classified according to the 2021 American College of Radiology Manual [49]), and 2) SA and rCEM diagnostic performance, taking histopathology or two-year follow-up as reference standard, considering in particular the number of detected and missed malignancies and, among them, of ductal carcinomas in situ (DCIS). For the latter secondary endpoint, we here present a subanalysis restricted to cases with available definitive histopathology reports, since the follow-up period is still ongoing.

Considering the presence of experienced breast radiologists at both centres and based on previous internal reviews of biopsy rates, we preliminary assumed that women enrolled in this study would have a SA biopsy rate of about 50% and that rCEM could lead to about a 20% reduction in biopsy rate. We therefore calculated the sample size under the hypothesis of clinical superiority (i.e. of reducing the biopsy rate), assuming an 80% statistical power and a 5%  $\alpha$  error. Under these assumptions, 197 women needed to be enrolled.

The Shapiro-Wilk test was used to perform distribution analysis. Consequentially, normal distributions were reported using median  $\pm$  standard deviation and non-normal distributions were reported as median with their interquartile range (IQR). The paired data comparison for the primary endpoint was performed with the McNemar test ( $p$  values  $< 0.05$  considered statistically significant), while rates and diagnostic performance metrics for the secondary endpoints were determined along with their 95% confidence intervals (CIs). All analyses were performed with STATA, version MP 16.1 (StataCorp).

#### **8.4. Results**

Between January 25<sup>th</sup>, 2019, and July 29<sup>th</sup>, 2021, 220 women were enrolled in this study (122 at Centre 1 and 98 at Centre 2). CEM proved unfeasible in 3 of these 220 women (1.4%) because of contrast extravasation, while 10 other women were excluded from analysis after enrollment due to screening failure of exclusion criteria. The remaining 207 women who underwent both SA and CEM were included in the analysis: they had a median age of 56.6 years (IQR 50.1–65.3 years), 140/207 (67.6%) had already entered menopause, and 26/207 (12.6%) reported a family history of breast or ovarian cancer, no woman declaring to be a carrier of a genetic mutation increasing breast cancer risk. Out of 207 patients, 3 (1.4%) developed mild self-limiting adverse reactions to ICAs, without the need of any medical intervention. The median CEM examination time was 4 min and 46 s (286 s, IQR 262–318 s).



The SA was prompted by a single suspicious finding in 191/207 women (92.3%), while in the remaining 16/207 women (7.7%) SA detected 2 suspicious findings (ipsilateral in 12 women, contralateral in 4 women). Of these 223 suspicious findings, 211 (94.6%) were already detectable on baseline mammography, 3/223 (1.4%) were suspicious axillary lymph nodes detected by ultrasonography, and the remaining 9/223 (4.0%) were inconclusive mammographic findings that were confirmed as suspicious by ultrasonography (8/223) or tomosynthesis (1/223). Moreover, in 2 women (1.0%) rCEM identified an additional suspicious finding (both of them in the breast contralateral to the suspicious finding that prompted the recall).

As detailed in the study flowchart (Fig. 8.2), 225 suspicious findings were ultimately analysed for the assessment of the primary endpoint: 131/225 were referred to biopsy by SA, for a SA biopsy rate of 58.2% (95% CI 51.7–64.5%), while 94/225 were referred to biopsy by rCEM, for a rCEM biopsy rate of 41.8% (95% CI 35.5–48.3%). Therefore, information from rCEM images would have engendered a 16.4% reduction in the biopsy rate ( $p < 0.001$ ). More specifically, SA and rCEM agreed on referring to biopsy 90/225 (40.0%) suspicious findings and agreed on sending to follow-up 90/225 (40.0%) suspicious findings. Conversely, rCEM would have spared the biopsy prompted by SA in 41/225 cases (18.2%) and effectively recommended biopsy for 4 findings (1.8%): 2 would have been sent to follow-up according to the SA, 2 were rCEM-only detected findings. Thus, a biopsy was recommended either by SA or by rCEM for 135 suspicious findings. For 3 of them the procedure proved unfeasible, 2 other women elected to perform the recommended biopsy in other centres and were lost at follow-up and 2 women—for whom CEM recommended a biopsy in contrast to the follow-up referral recommended by SA—refused to undergo the procedure.

Ultimately, 128 biopsies were performed at the two study centres, 75/128 (58.6%) under ultrasound guidance and 53/128 (41.4%) under stereotactic guidance. Overall, all 53 stereotactic-guided biopsies and 2 of the ultrasound-guided biopsies were performed as vacuum-assisted biopsies, while among the 73 remaining ultrasound-guided biopsies 68 (93.1%) were core-needle biopsies and 5

(6.9%) were fine-needle aspirations. As detailed in Table 8.1, 42/128 biopsies had a benign result (32.8%) and 79/128 resulted in a diagnosis of malignancy (61.7%): DCIS accounted for 31.6% of malignancies (25/79). The remaining 7/128 biopsies (5.5%) had a B3 result: 4 cases were sent to imaging follow-up and were excluded from secondary endpoint analyses, while the other 3 were referred for surgery, with 2 downgrades to B2 lesions at final pathology and one upgrade to a B5b lesion.

Thus, 124 lesions (44 benign and 80 malignant, 25 of which DCIS) had an available definitive histopathology report and were considered for the evaluation of the secondary endpoints related to diagnostic performance. Among the 122/124 lesions sent to biopsy by SA, 44 (36.1%) proved benign at pathology, while the remaining 78 (63.9%) were classified as malignant, 24 of them being DCIS. The 2/124 suspicious findings that were not detected by SA but had a biopsy prompted by rCEM also resulted to be B5 lesions (one grade 2 DCIS and one invasive carcinoma of no special type). The sensitivity of SA was therefore 97.5% (95% CI 91.3–99.3%), with a PPV of 63.9% (95% CI 55.1–71.9%). Among the 90 suspicious findings sent to biopsy according to the information coming from rCEM images, 75/90 (83.3%, 20/90 DCIS) were malignant lesions (true positives, Fig. 8.3 and Fig. 8.4), while the remaining 15/90 (16.7%) were benign lesions (false positives, Fig. 8.5). Conversely, among the 34 biopsies with definitive reports that would have been spared by the evaluation of rCEM images (Table 8.2), pathology revealed 29 benign (true negatives, Fig. 8.6 and Fig. 8.7) and 5 malignant lesions (false negatives, Fig. 8.8). Of note, all 5 were DCIS without microinvasion (3 grade 2 and 2 grade 3) and, while none of them exhibited suspicious contrast-enhancement on rCEM images, all were detectable on low-energy CEM images due to the presence of suspicious calcifications. Thus, while rCEM sensitivity was 93.8% (95% CI 86.2–97.3%), with a 65.9% specificity (95% CI 51.1–78.1%), an 83.3% PPV (95% CI 74.3–89.6%), and an 85.3% negative predictive value (95% CI 69.9–93.6%), a combined reporting of low-energy and rCEM images to guide biopsy referral would have increased sensitivity to 100% (95% CI 95.4–100.0%).

## 8.5. Discussion

Since the early days of CEM implementation, its use in the evaluation of abnormalities detected at screening mammography has been one of the most reported applications [131, 288]. Albeit with some caveats related to the contrast uptake of benign lesions [131, 288] and to equivocal enhancement conspicuity associated with calcifications clusters [128, 143, 207], retrospective studies have highlighted the potential of CEM to increase the PPV of the work-up process without compromising cancer detection [141–143, 170, 317]. We investigated this issue in a prospective setting, assessing the diagnostic gain granted by contrast-enhanced (rCEM) images, since low-energy CEM images—equivalent to standard mammograms [178, 295]—are also available in the SA process.

We observed a potential 16.4% net reduction of the biopsy rate that could be obtained by rCEM in the overall cohort of 225 suspicious findings, accompanied, in a subanalysis on 124 findings with final diagnosis, by a 19.4% PPV increase, in accordance with the multireader retrospective study by Zuley et al. [317] on 60 BI-RADS 4 masses referred for biopsy. While their higher negative predictive value (98.3% versus our 85.3%) was likely prompted also by their exclusion of calcifications, we found similar, even though slightly higher, sensitivity (93.8% versus 90.3%) and specificity (65.9% versus 61.0%). Of note, we should consider that our specificity was negatively influenced by the exclusion of lesions referred for follow-up and will be recalculated after follow-up completion.

The biopsy increase solely attributable to CEM, i.e. the number of CEM-referred biopsies of suspicious findings that would have been sent to follow-up by SA plus the number of additional suspicious lesions detected by CEM but missed by screening mammography and SA, was 4/225 (1.8%). While the component of additional CEM-only findings (2/225, 0.9%) is of course lower than the 7.7% rate presented by Houben et al. [170] in a study where screening mammography was the comparator instead of SA, we highlight that both cases in which the patient accepted to undergo

the biopsy solely prompted by CEM were diagnosed as malignant lesions (one invasive carcinoma of no special type, one grade 2 DCIS), with a 100% PPV.

Importantly, DCIS presenting with calcifications clusters without associated contrast enhancement or with extremely faint enhancement were altogether responsible for the 6.2% drop in sensitivity of rCEM compared to the virtual 100% sensitivity of a combined reporting of low-energy images focused on suspicious calcifications and rCEM images, thus still supporting a direct biopsy referral of suspicious calcifications on the basis of their appearance on standard mammography or low-energy CEM images [143]. Without venturing in considerations about potential DCIS overdiagnosis [318], we however highlight that all were pure DCIS, without any microinvasion foci (3 intermediate grade, 2 high grade). As already reported [128, 143, 207], the negative predictive value of rCEM images for suspicious calcifications remains to be ascertained and, in our opinion, only large-scale dedicated studies will allow to solve this issue, especially also addressing DCIS overdiagnosis. Options in this direction involve the identification of characteristic enhancement patterns for cancers of low biological relevance [319] and the application of artificial intelligence-driven radiomic analysis [320]. The latter could be particularly useful considering how interpretation thresholds are influenced by the more equivocal visual conspicuity of lesion enhancement in rCEM images than in CE-MRI, compared to standard background parenchymal enhancement. In addition, only 3/207 patients (1.4%) developed mild self-limiting adverse reactions to iodinated contrast agent, conforming the CEM safety profile already reported in a meta-analysis [124].

Limitations of this study include—first—the only potential nature of the biopsy reduction we described and the non-randomized design: these characteristics prevented a clinical comparison of the SA and CEM-based work-up, also including patients preferences and cost-effectiveness, as will be done by the RACER trial [285]. Second, as already discussed for suspicious calcifications resulting in rCEM false negatives, our study design also factually oriented the analysis towards an

appraisal of the contribution of rCEM information rather than of the “whole” CEM examination (low-energy and rCEM images). Finally, the ongoing follow-up period prevented us from exploring secondary endpoints related to diagnostic performance in the whole cohort.

In conclusion, our study showed how a rCEM-based assessment of women recalled at first-level screening mammography is able to potentially engender a 16.4% reduction in biopsy rates compared to SA, maintaining high sensitivity (93.8%) with false negatives represented only by DCIS clearly detectable on low-energy CEM images. Coupled with the absence of moderate and severe adverse reactions to contrast agent, these data further highlight the role of CEM for the assessment of suspicious findings detected at screening mammography, avoiding a sizable number of unnecessary biopsies.

**Table 8.1** Results of the 128 percutaneous breast biopsies performed in the two study centres. 126 biopsies were performed after recommendation by standard assessment (89 with concurrent referral by CEM) and two were solely prompted by findings at CEM

Biopsy classification	Histological type	Number	%	
B1	Normal parenchyma	2	1.6%	
	Acute mastitis	1	0.8%	
B2	Adenosis	6	4.7%	
	Adenosis with fibrocystic changes	3	2.3%	
	Adenosis with fibrosis	3	2.3%	
	Adenosis with usual ductal hyperplasia	4	3.1%	
	Apocrine metaplasia	3	2.3%	
	Columnar cell hyperplasia without atypia	2	1.6%	
	Fibroadenoma	5	3.9%	
	Fibrocystic changes	7	5.4%	
	Inflammatory changes	1	0.8%	
	C2	Normal cytology	5	3.9%
	B3 referred for surgery	Atypical ductal hyperplasia <sup>a</sup>	2	1.6%
Flat epithelial atypia <sup>b</sup>		1	0.8%	
B3 referred for imaging follow-up	Columnar cell hyperplasia with atypia	1	0.8%	
	Flat epithelial atypia	2	1.6%	
	Flat epithelial atypia and atypical ductal hyperplasia	1	0.8%	
B5	DCIS grade 1 – grade 2	1	0.8%	
	DCIS grade 2	10	7.8%	
	DCIS grade 3	8	6.3%	
	DCIS grade 2 with associated microinvasion	3	2.3%	
	DCIS grade 3 with associated microinvasion	3	2.3%	
	IC NST grade 1	7	5.4%	
	IC NST grade 2	21	16.4%	
	IC NST grade 3	7	5.4%	
	IC NST grade 1 with associated DCIS grade 1	1	0.8%	
	IC NST grade 1 with associated DCIS grade 2	1	0.8%	
	IC NST grade 2 with associated DCIS grade 2	2	1.6%	
	IC NST grade 2 with associated DCIS grade 3	3	2.3%	
	IC NST grade 3 with associated DCIS grade 3	1	0.8%	
	Invasive lobular carcinoma	2	1.6%	
	Invasive lobular carcinoma with associated LCIS	2	1.6%	
	Invasive papillary carcinoma	2	1.6%	
	Medullary carcinoma	1	0.8%	
	Metastatic lymph node	4	3.1%	

DCIS ductal carcinoma in situ; IC invasive carcinoma; NST no special type; LCIS lobular carcinoma in situ.

<sup>a</sup> Both cases downgraded to B2 at final pathology.

<sup>b</sup> Upgraded to B5 (invasive carcinoma of no special type, grade 2) at final pathology.

**Table 8.2** Definitive histopathology results of the 34 percutaneous breast biopsies that were effectively performed but would have been spared by information coming from CEM images

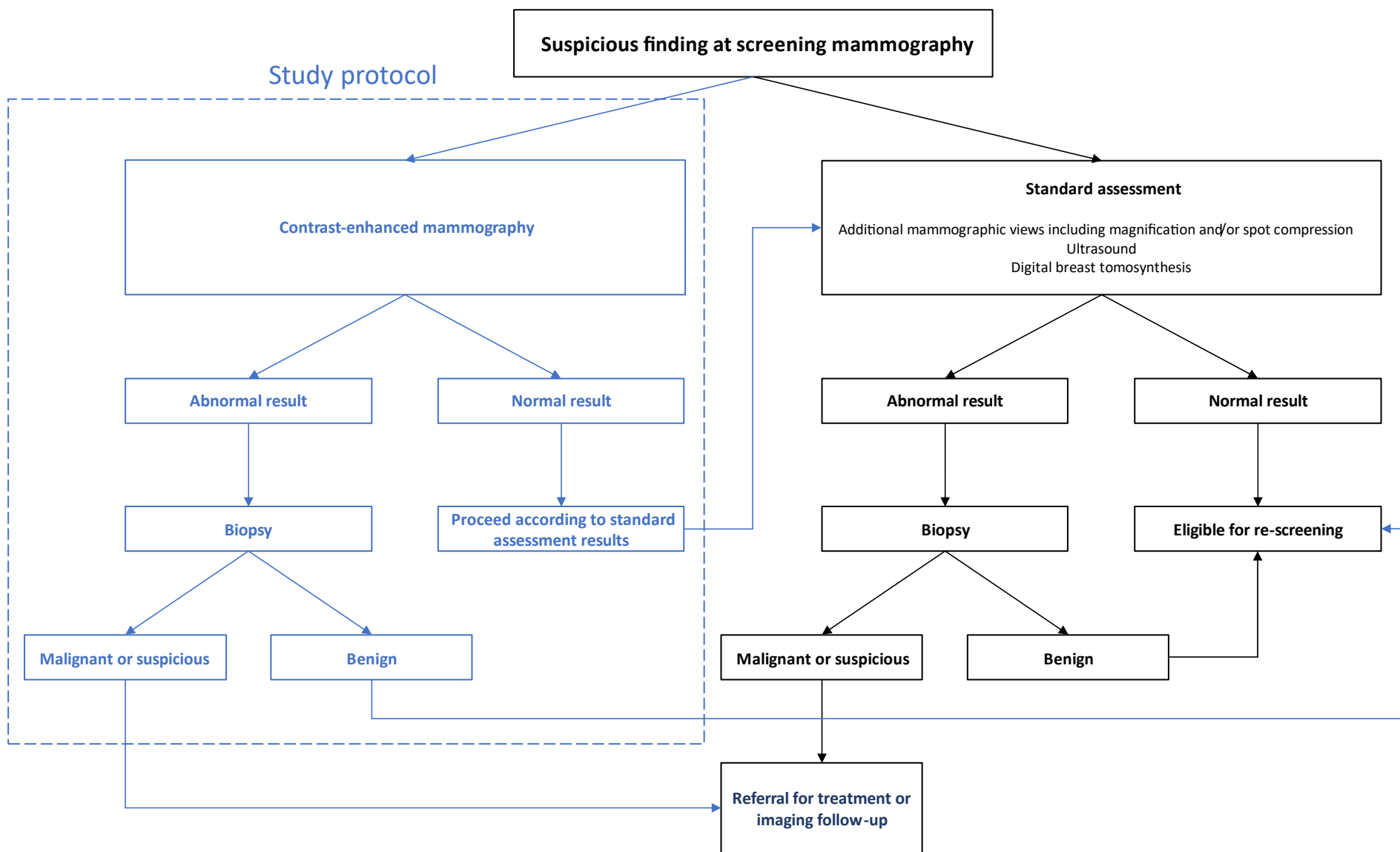
Biopsy classification	Histological type	Number	%
B2	Acute mastitis	1	2.9%
	Adenosis	4	11.8%
	Adenosis with fibrocystic changes	3	8.8%
	Adenosis with fibrosis	3	8.8%
	Adenosis with usual ductal hyperplasia	1	2.9%
	Apocrine metaplasia	3	8.8%
	Columnar cell hyperplasia without atypia	2	5.9%
	Fibroadenoma	2	5.9%
	Fibrocystic changes	5	14.8%
C2	Normal cytology	3	8.8%
B3 referred for surgery	Atypical ductal hyperplasia <sup>a</sup>	2	5.9%
B5	DCIS grade 2	3	8.8%
	DCIS grade 3	2	5.9%

CEM would have spared 7 other biopsies that were indicated by standard assessment: in three cases biopsy proved unfeasible, in one case the patient elected to perform the biopsy in another centre and was lost at follow-up, and the remaining three cases were B3 lesions (two cases flat epithelial atypia and one case of columnar cell hyperplasia with atypia) sent to imaging follow-up.

*DCIS* ductal carcinoma in situ.

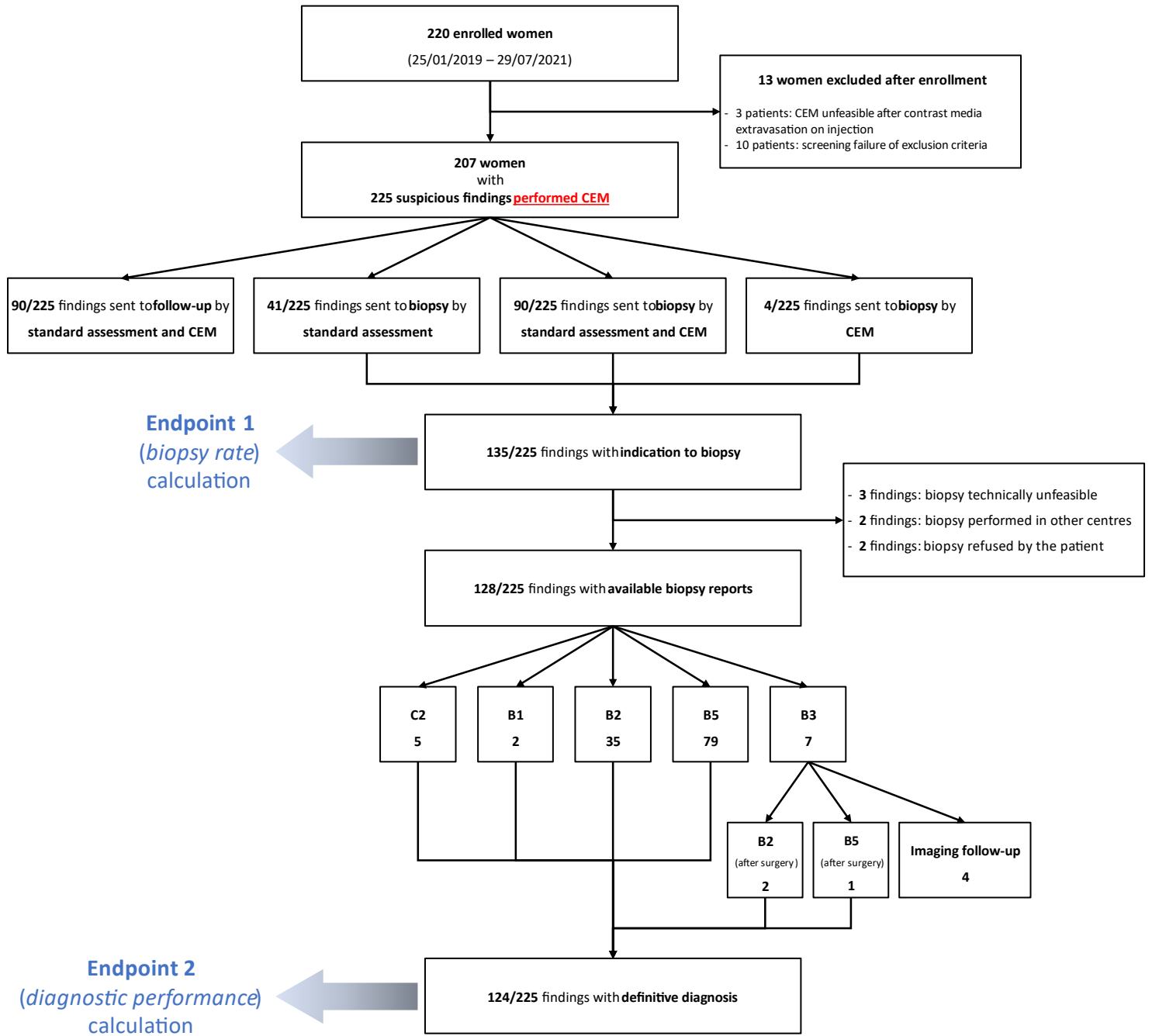
<sup>a</sup> Both cases downgraded to B2 at final pathology.

**Fig. 8.1** Flowchart of the standard work-up process in the two study centres supplemented by CEM, as per study protocol

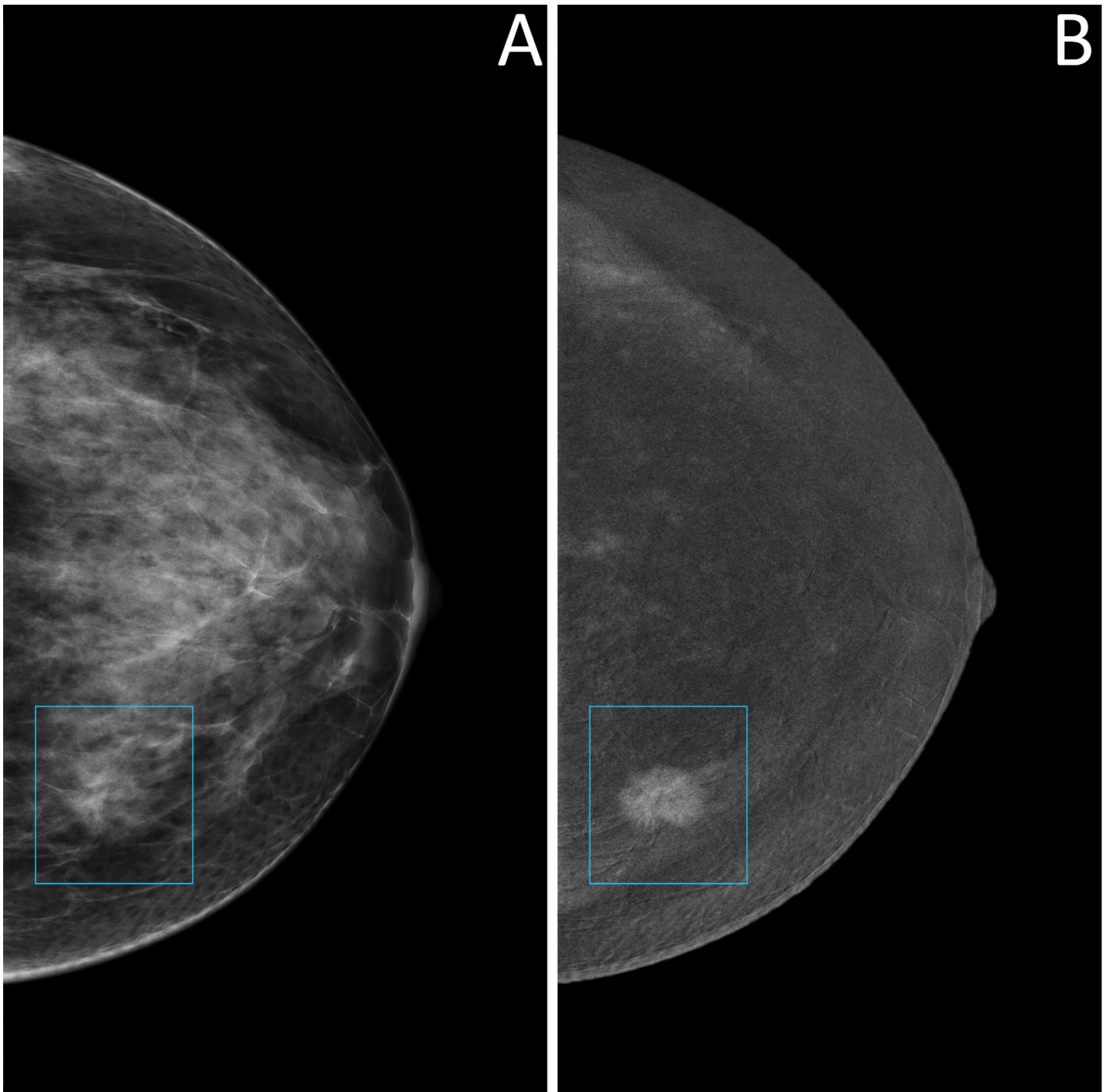


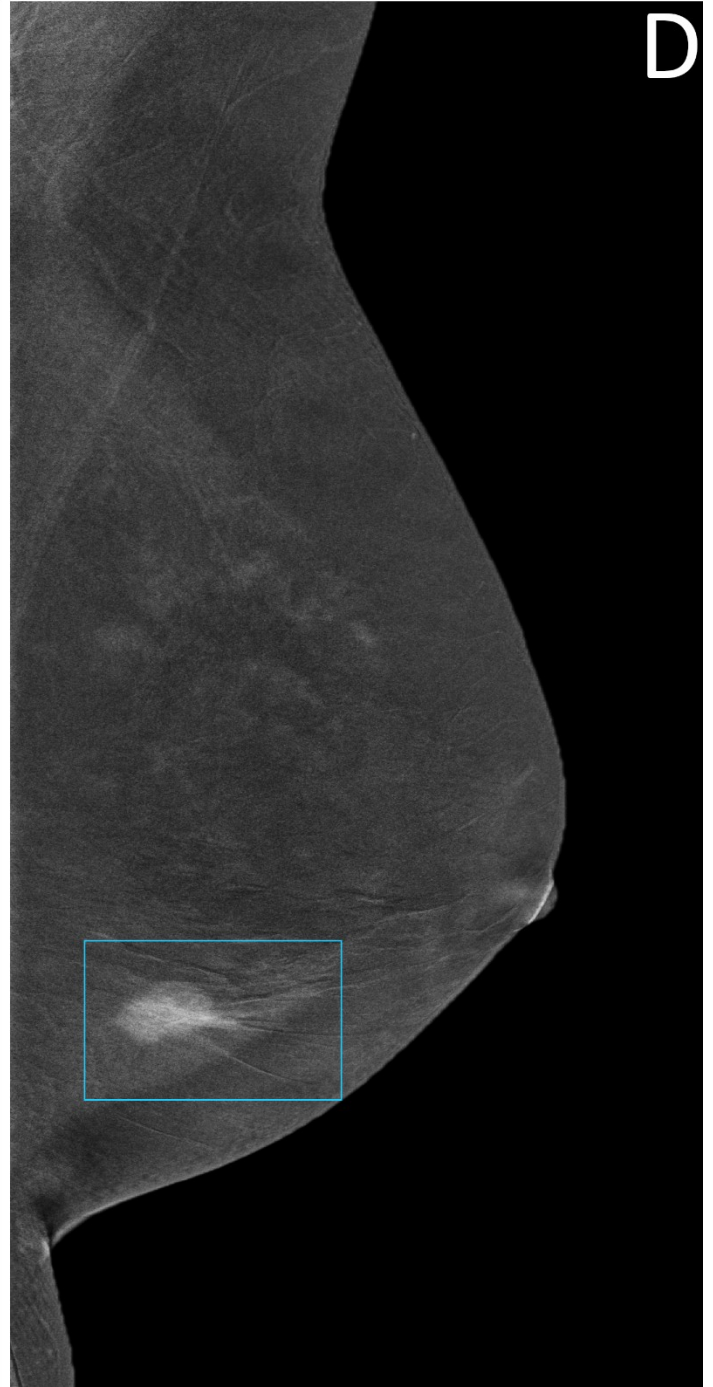
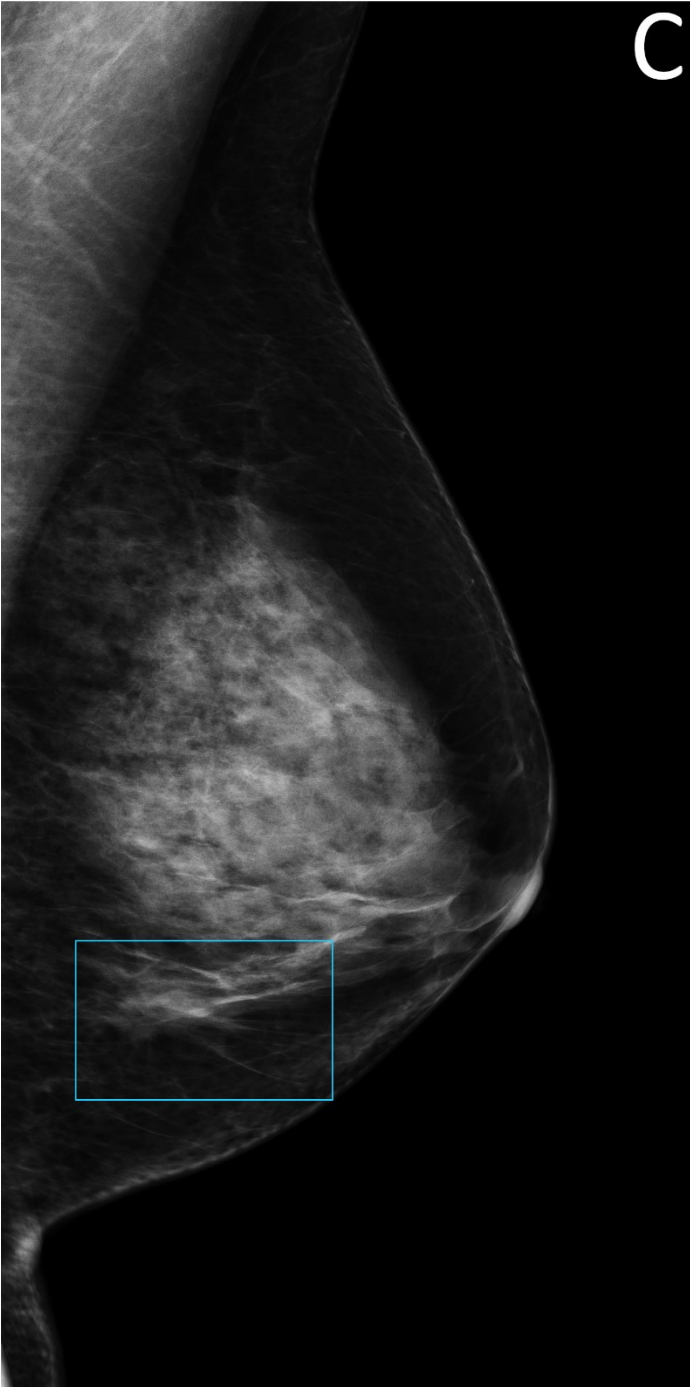


**Fig. 8.2** Study phases and endpoint analyses

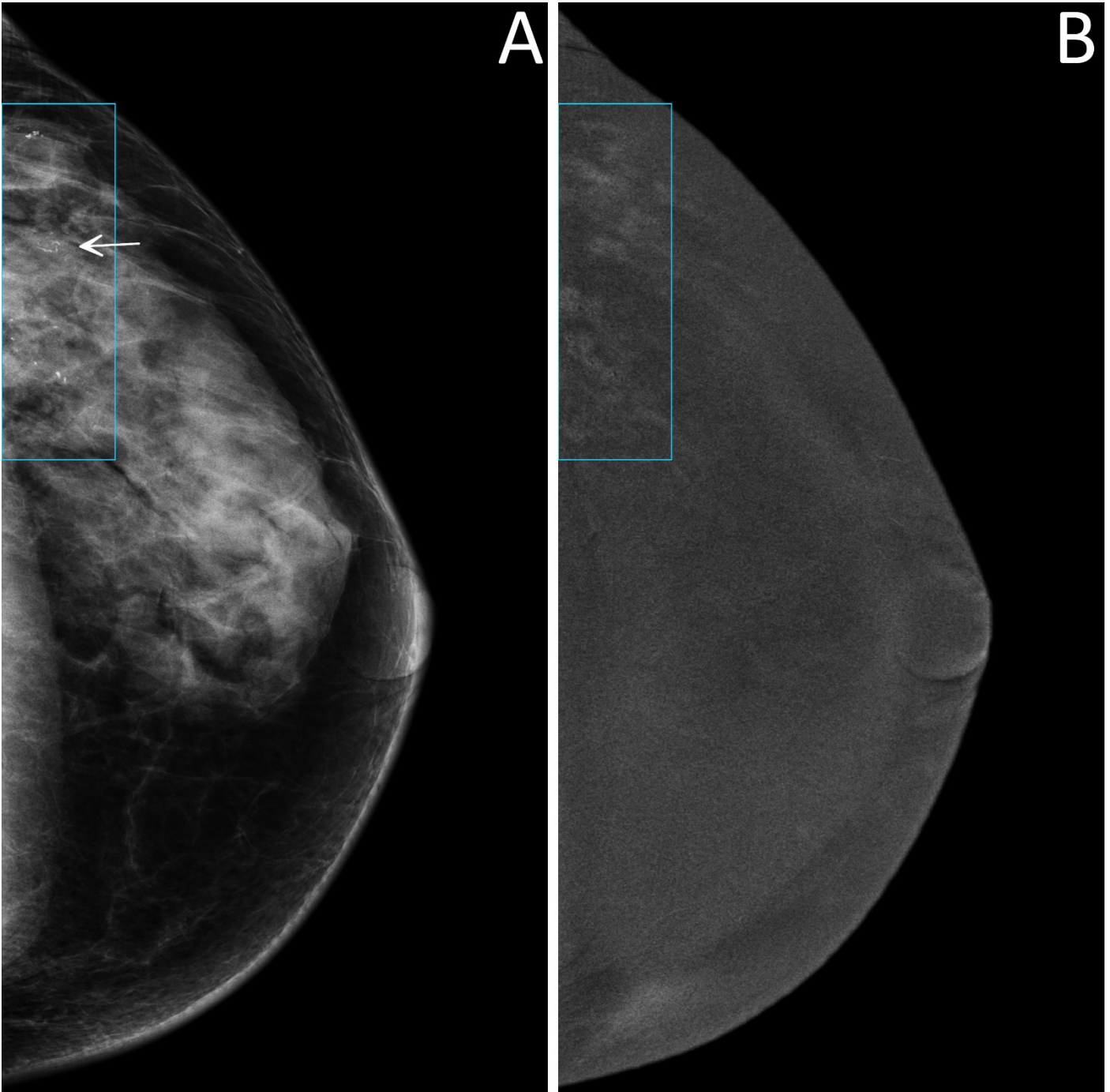


**Fig. 8.3** True positive case at CEM. A 61-year-old woman was recalled for a suspicious asymmetric opacity in the lower-inner quadrant of the left breast, also recognizable on low-energy images (panels A and C, light blue rectangles) and subsequently diagnosed as an invasive carcinoma of no special type, grade 1. Recombined images (panels B and D, light blue rectangles) show an enhancing and irregularly-shaped mass of 14 mm

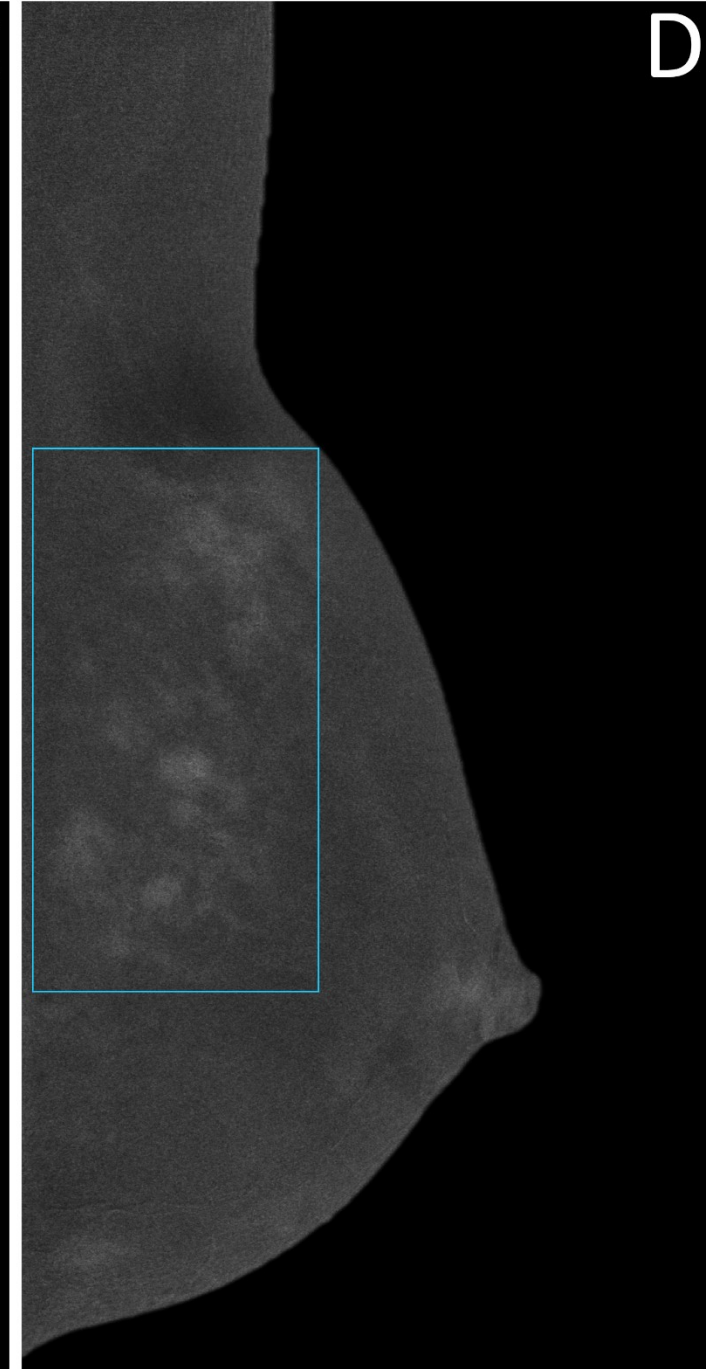
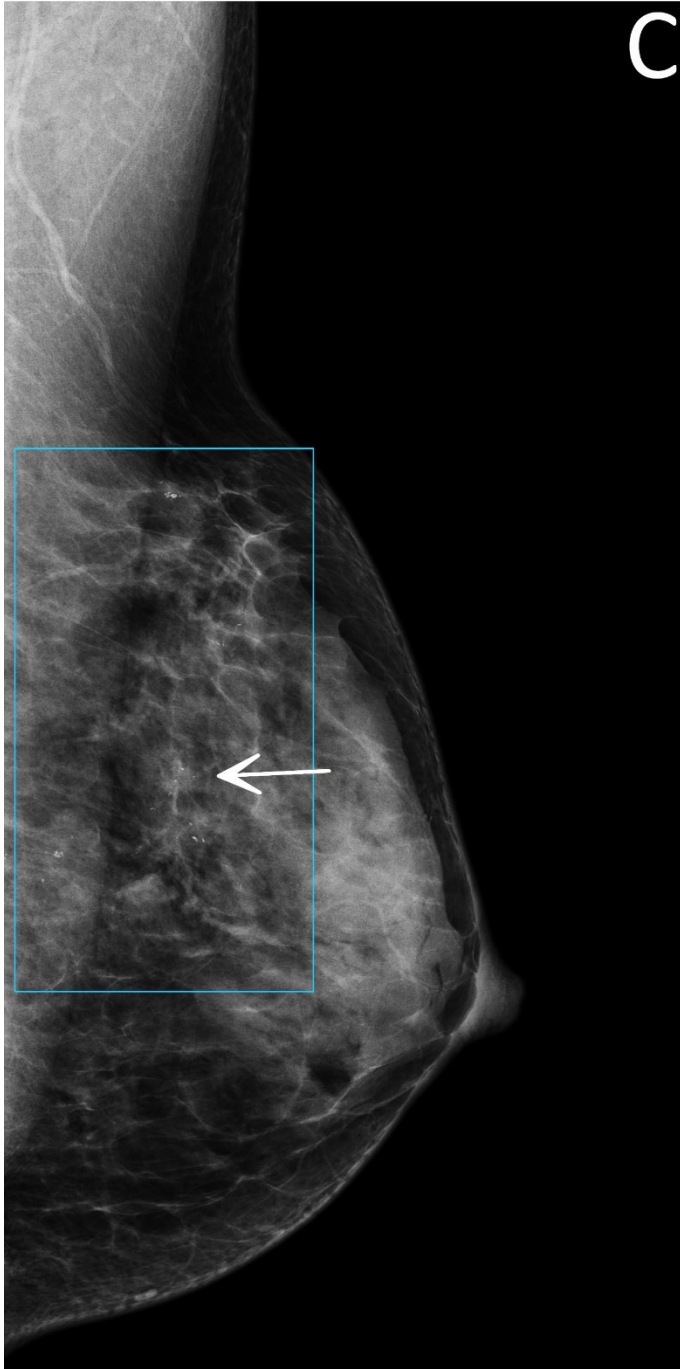




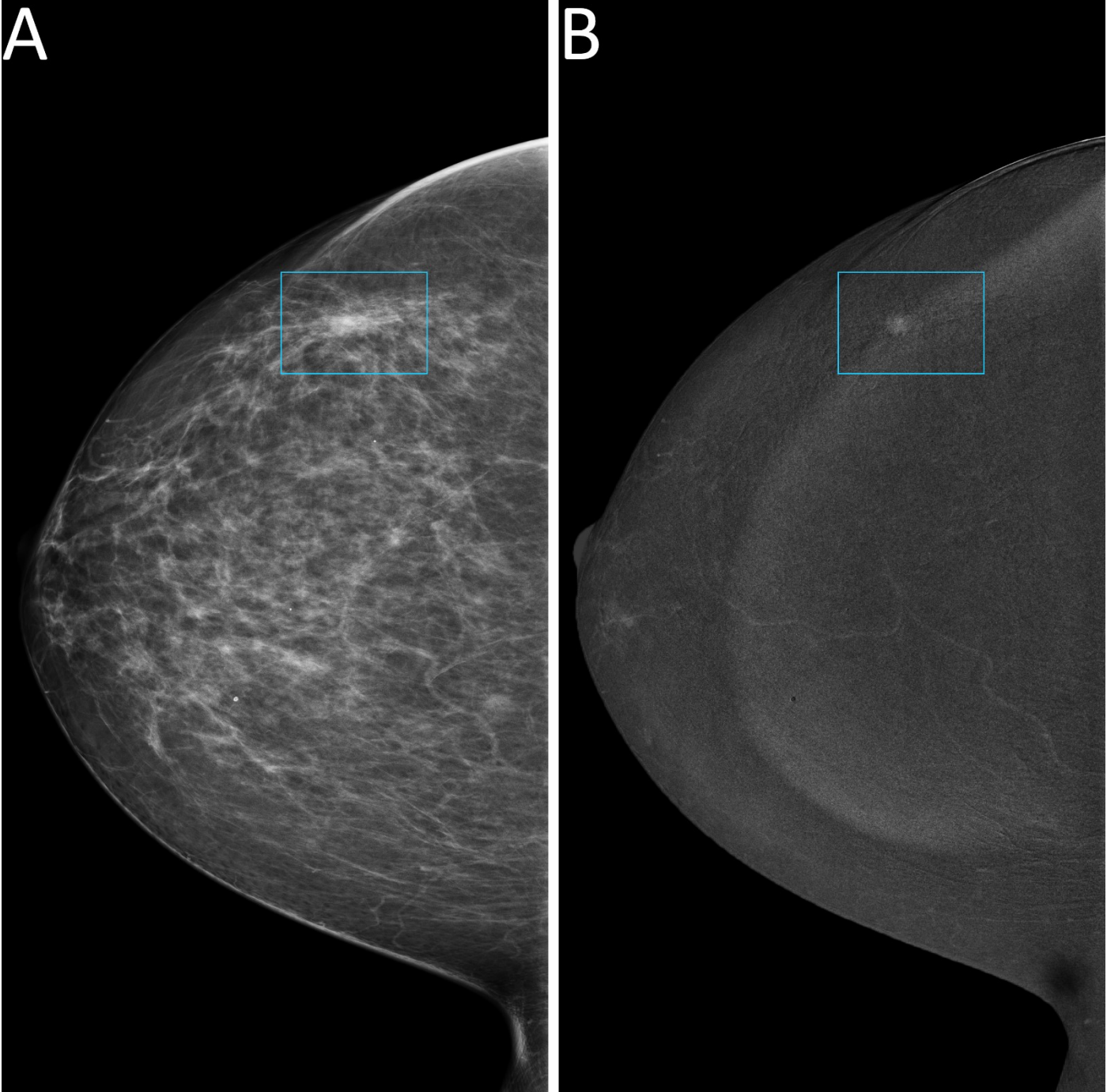
**Fig. 8.4** True positive case at CEM. A 53-year-old woman was recalled for suspicious calcifications in the left breast. An ultrasound-guided core needle biopsy was performed, resulting in a diagnosis of grade 2 ductal carcinoma in situ. Low-energy images (panels A and C) show multiple groups of pleomorphic calcifications in the left upper-outer quadrant (white arrows in light blue rectangles). Recombined images (panels B and D) revealed an area of non-mass enhancement involving the whole upper-outer quadrant

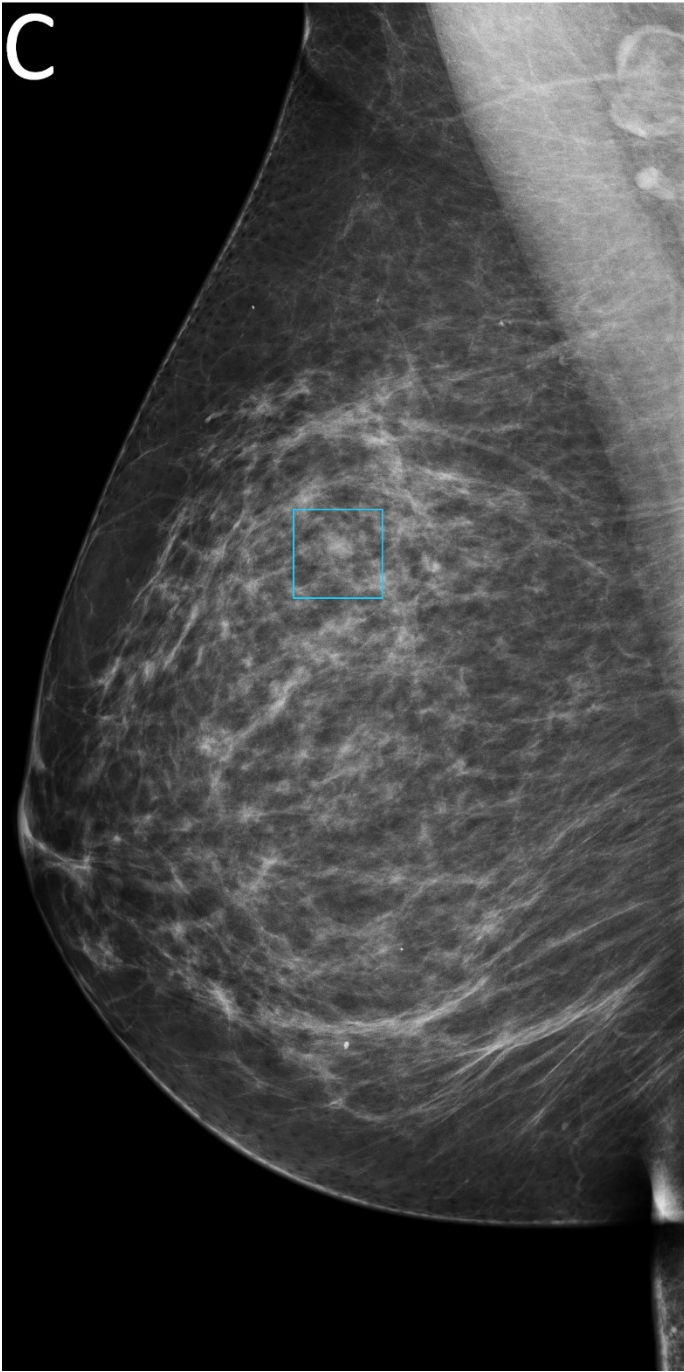






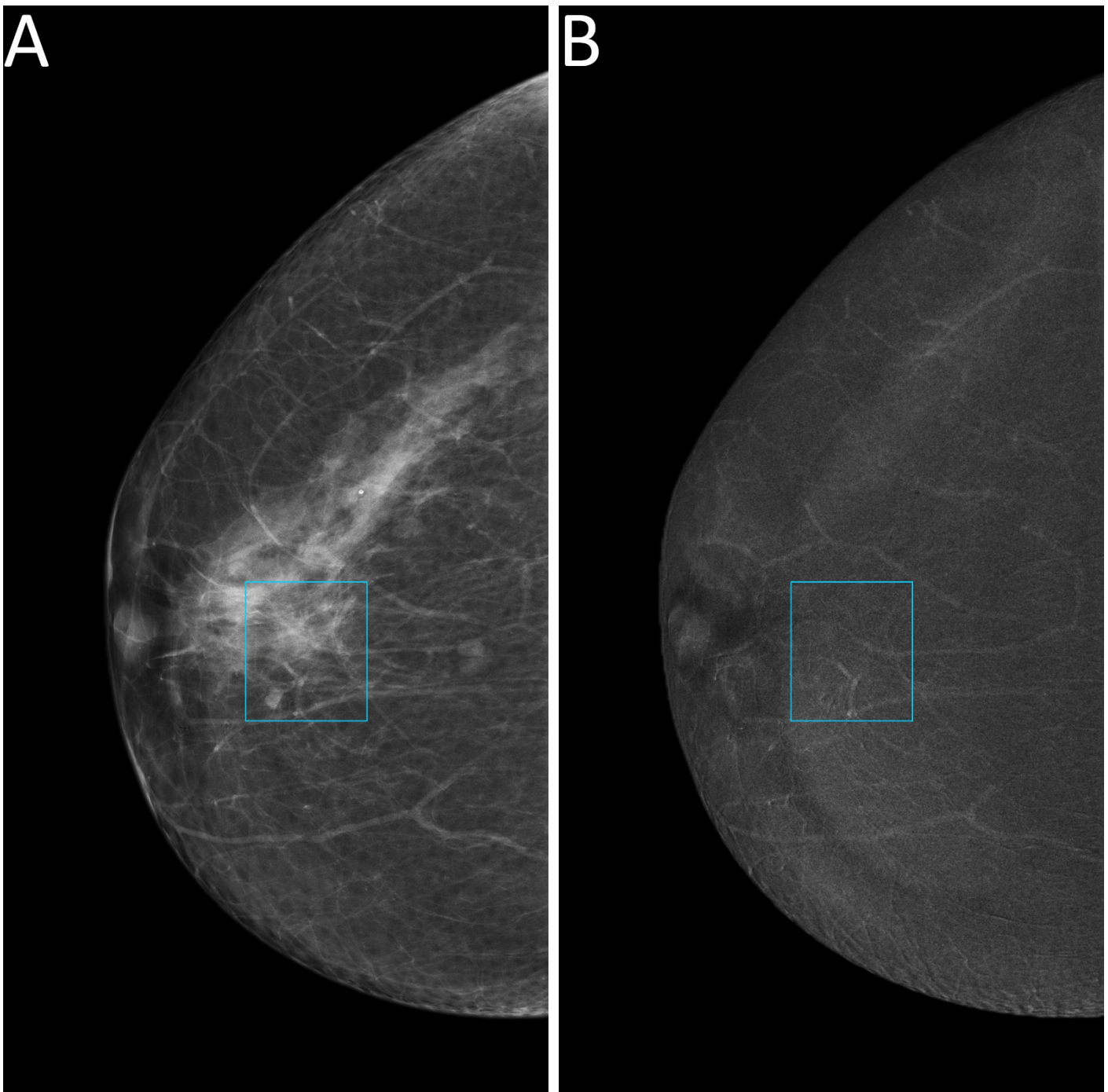
**Fig. 8.5** False positive case at CEM. A 69-year-old woman was recalled for a suspicious finding in the right breast, subsequently diagnosed as adenosis. Low-energy images (panels A and C) show an opacity in the right upper-outer quadrant (light blue rectangles) with a correlated enhancement focus on the recombined images (panels B and D, light blue rectangles)







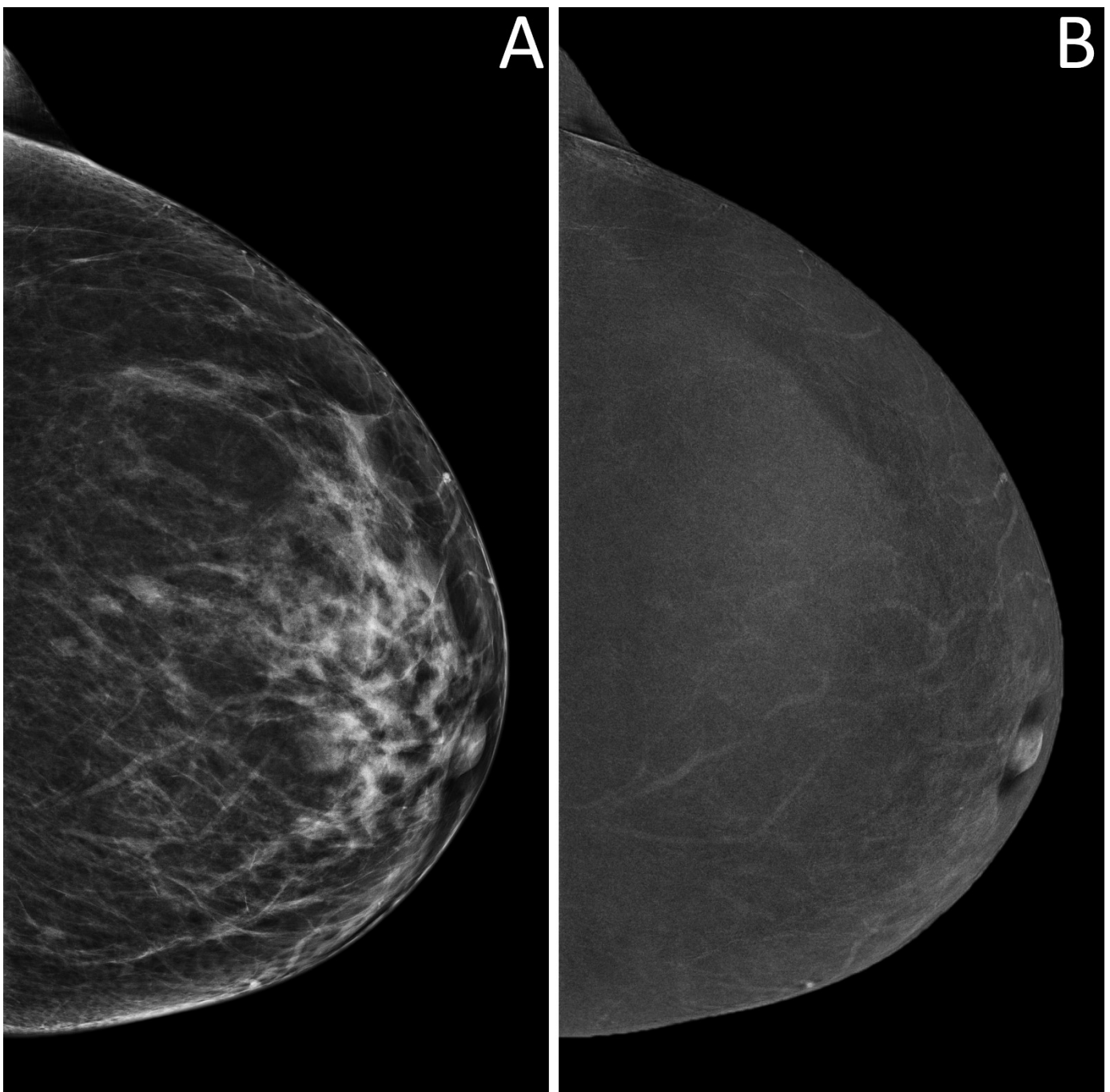
**Fig. 8.6** True negative case at CEM. A 58-year-old woman was recalled for a suspicious retroareolar irregular opacity in the right breast, detectable only on the craniocaudal view (panel A, light blue rectangle), whereas the mediolateral oblique view does not show any suspicious finding (panel C). An ultrasound-guided core needle biopsy was performed, leading to a diagnosis of apocrine metaplasia. The absence of enhancement foci on recombined images, both in correspondence of the suspicious opacity on the craniocaudal view (panel B, light blue rectangle) and on the mediolateral oblique view (panel D) would have oriented the referral to follow-up

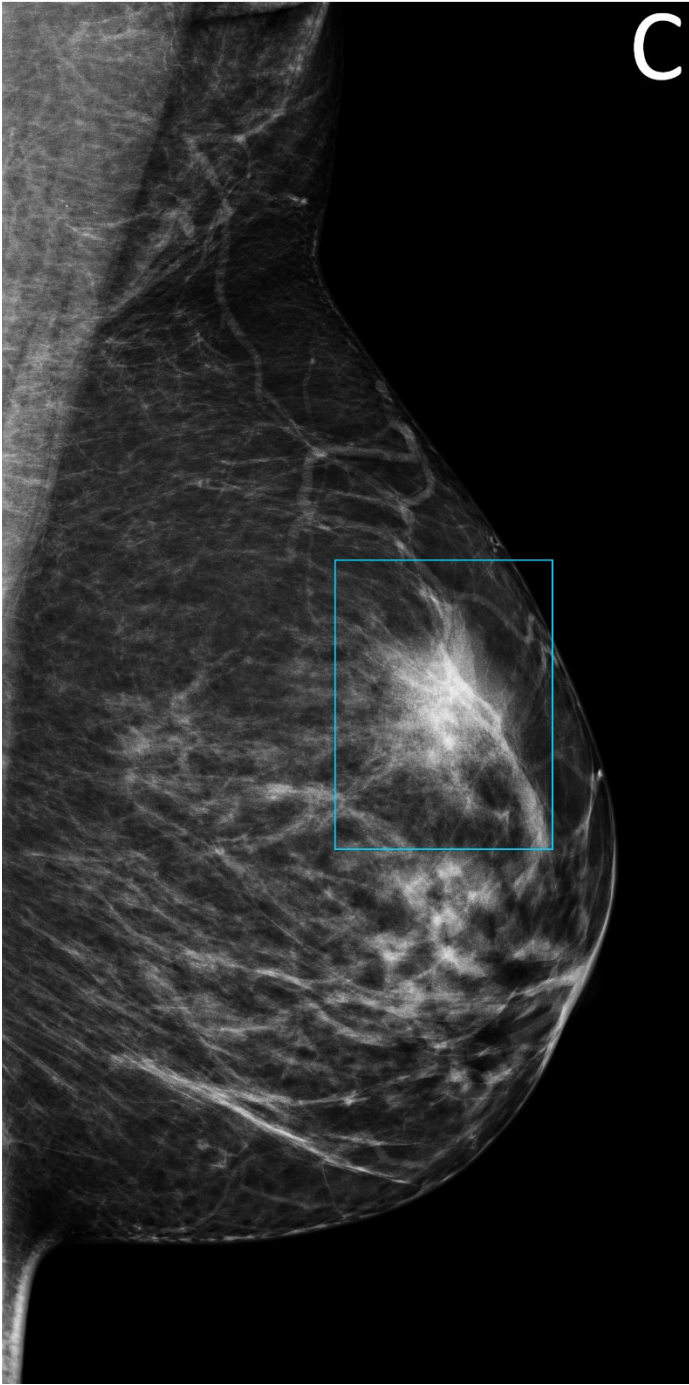




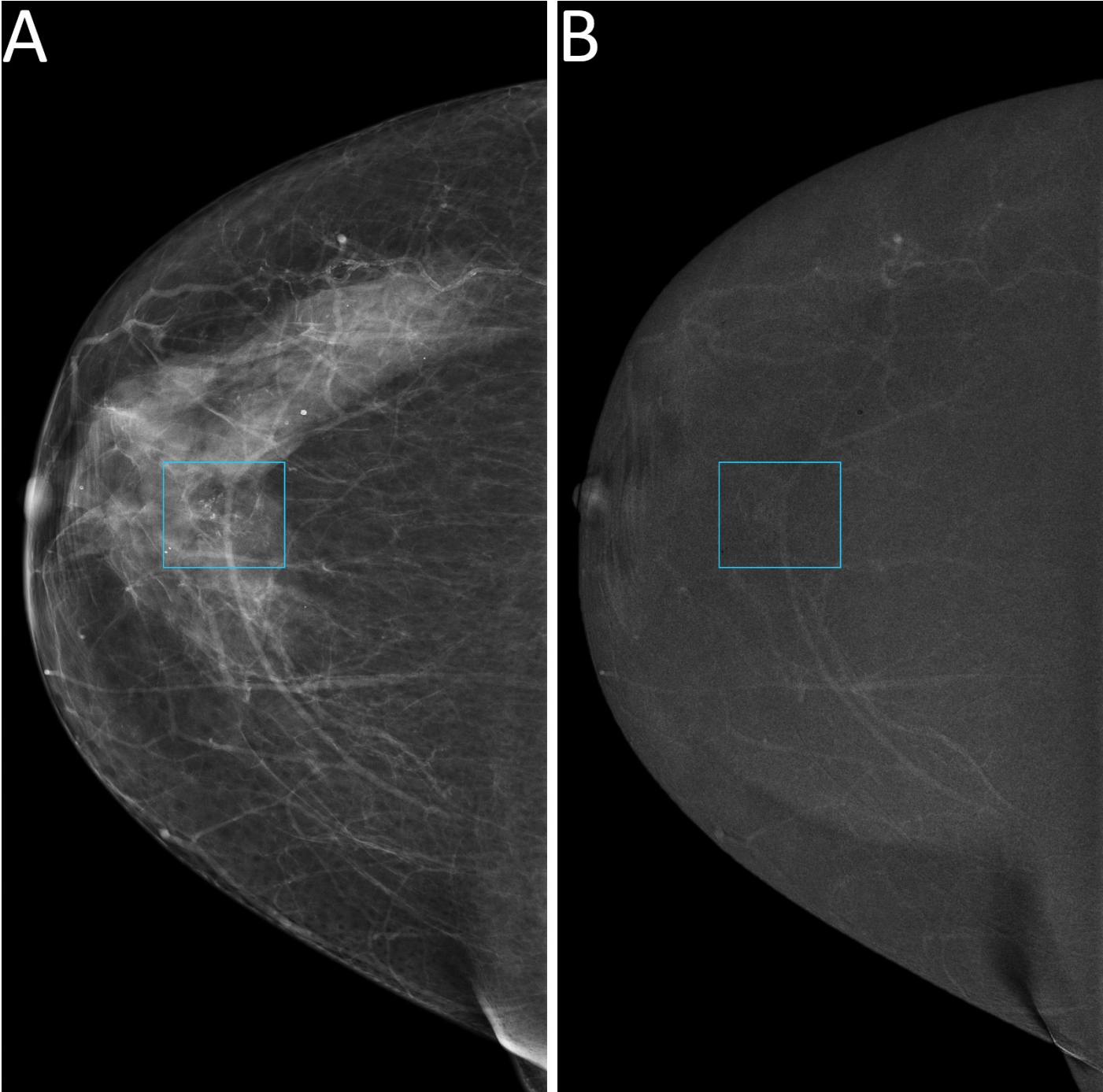


**Fig. 8.7** True negative case at CEM. A 49-year-old woman was recalled for a suspicious asymmetry in the upper quadrants of the left breast, not clearly observable on the craniocaudal view (low-energy image, panel A) but definitely noticeable on the mediolateral oblique view (low-energy image, panel C, light blue rectangle). Standard assessment referred this finding to ultrasound-guided core needle biopsy, leading to a diagnosis of fibrosis. Conversely, the absence of enhancement in recombined images, both on the whole craniocaudal view (panel B) and in correspondence of the suspicious area on the mediolateral oblique view (panel D) would have oriented the work-up to a normal result with referral to re-screening

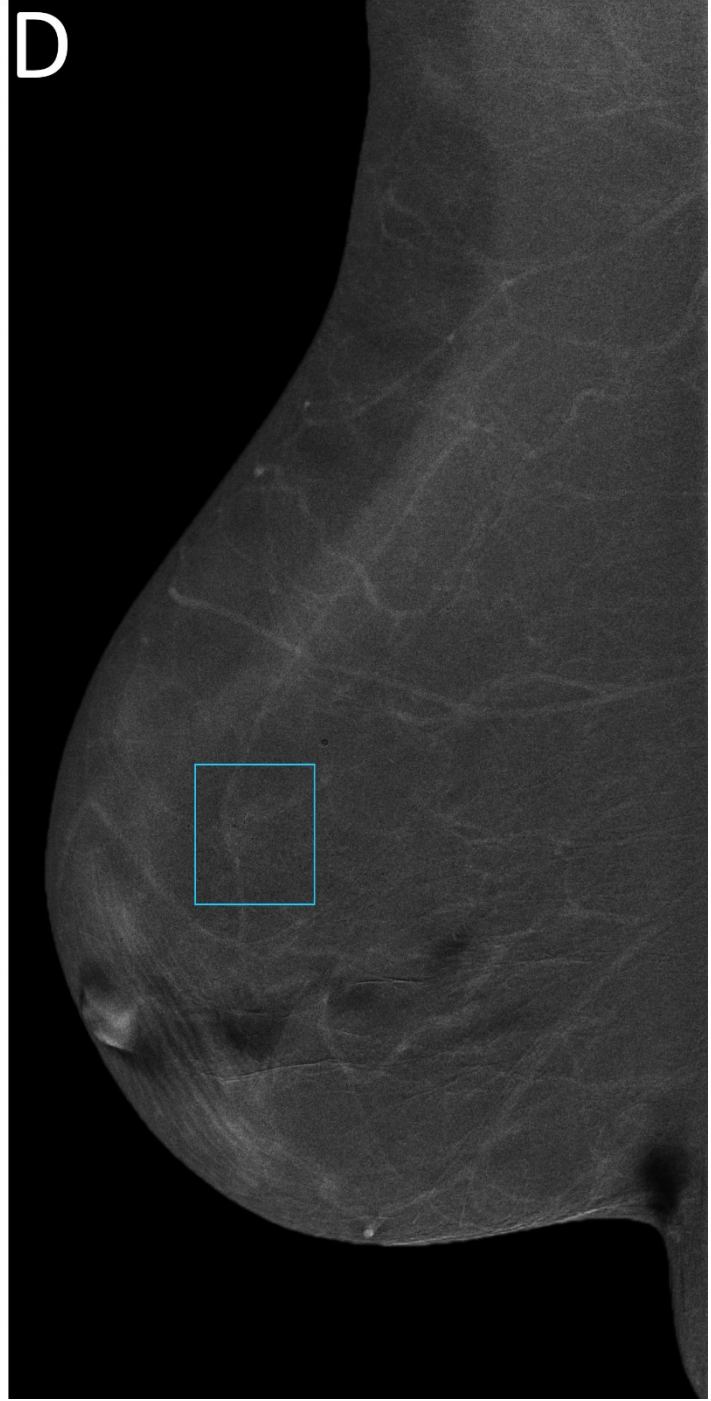
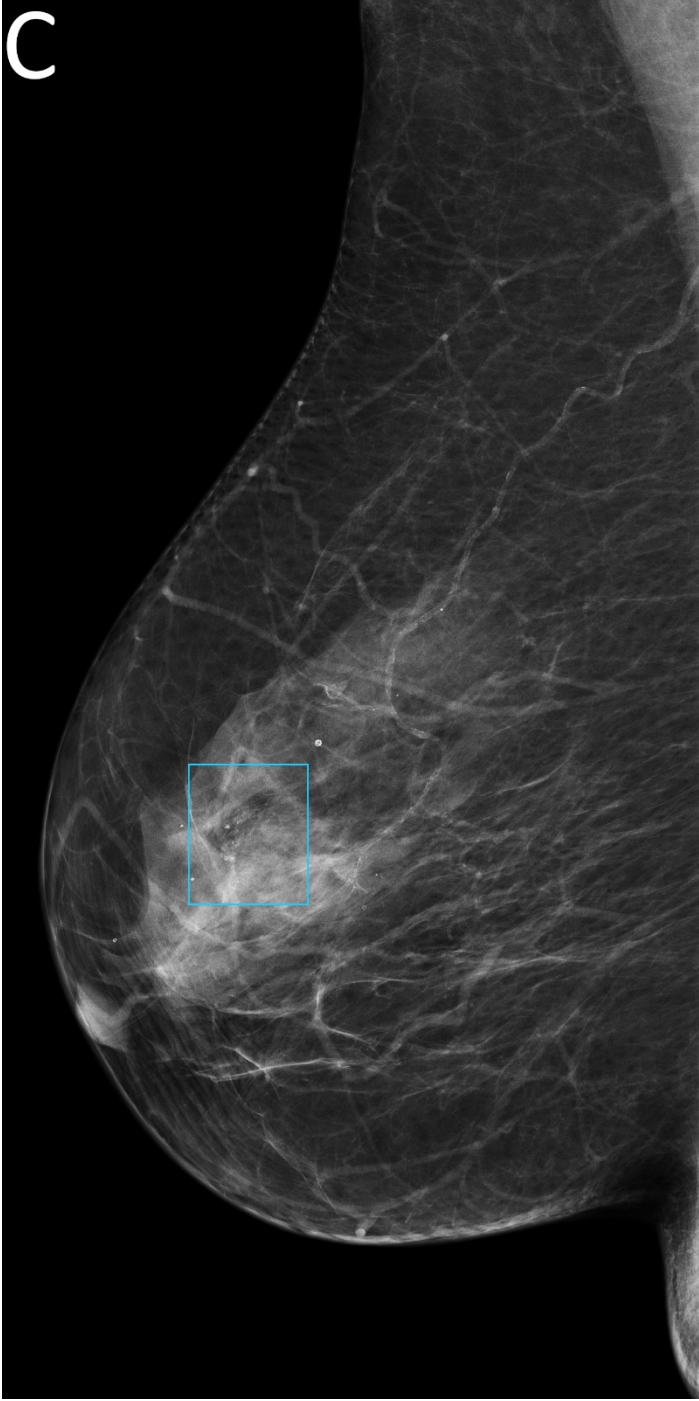




**Fig. 8.8** False negative case at CEM. A 67-year-old woman was recalled for a suspicious group of pleomorphic calcifications in the in the upper quadrants of the right breast, subsequently diagnosed as a grade 2 ductal carcinoma in situ, clearly visible on low-energy CEM images (panels A and C, light blue rectangles) but with no associated enhancement detectable on recombined images (panels B and D)









## References

1. Heywang SH, Hahn D, Schmidt H et al (1986) MR imaging of the breast using gadolinium-DTPA. *J Comput Assist Tomogr* 10:199–204.
2. Lewin JM, Isaacs PK, Vance V, Larke FJ (2003) Dual-Energy Contrast-enhanced Digital Subtraction Mammography: Feasibility. *Radiology* 229:261–268.  
doi:10.1148/radiol.2291021276.
3. Jong RA, Yaffe MJ, Skarpathiotakis M et al (2003) Contrast-enhanced Digital Mammography: Initial Clinical Experience. *Radiology* 228:842–850.  
doi:10.1148/radiol.2283020961.
4. Diekmann F, Diekmann S, Taupitz M et al (2003) Use of iodine-based contrast media in digital full-field mammography - Initial experience. *RoFo Fortschritte auf dem Gebiet der Rontgenstrahlen und der Bildgeb Verfahren* 175:342–345. doi:10.1055/s-2003-37828.
5. Grobner T (2006) Gadolinium – a specific trigger for the development of nephrogenic fibrosing dermopathy and nephrogenic systemic fibrosis? *Nephrol Dial Transplant* 21:1104–1108. doi:10.1093/ndt/gfk062.
6. Kanda T, Ishii K, Kawaguchi H, Kitajima K, Takenaka D (2014) High Signal Intensity in the Dentate Nucleus and Globus Pallidus on Unenhanced T1-weighted MR Images: Relationship with Increasing Cumulative Dose of a Gadolinium-based Contrast Material. *Radiology* 270:834–841. doi:10.1148/radiol.13131669.
7. Monti CB, Codari M, Cozzi A et al (2020) Image quality of late gadolinium enhancement in cardiac magnetic resonance with different doses of contrast material in patients with chronic myocardial infarction. *Eur Radiol Exp* 4:21. doi:10.1186/s41747-020-00149-2.
8. Hendrick RE, Baker JA, Helvie MA (2019) Breast cancer deaths averted over 3 decades.

Cancer 125:1482–1488. doi:10.1002/cncr.31954.

9. Giordano L, Von Karsa L, Tomatis M et al (2012) Mammographic Screening Programmes in Europe: Organization, Coverage and Participation. *J Med Screen* 19:72–82. doi:10.1258/jms.2012.012085.
10. Sardanelli F, Aase HS, Álvarez M et al (2017) Position paper on screening for breast cancer by the European Society of Breast Imaging (EUSOBI) and 30 national breast radiology bodies from Austria, Belgium, Bosnia and Herzegovina, Bulgaria, Croatia, Czech Republic, Denmark, Estonia, Finland, France, G. *Eur Radiol* 27:2737–2743. doi:10.1007/s00330-016-4612-z.
11. Wallis M, Tarvidon A, Helbich T, Schreer I (2007) Guidelines from the European Society of Breast Imaging for diagnostic interventional breast procedures. *Eur Radiol* 17:581–588. doi:10.1007/s00330-006-0408-x.
12. van Breest Smalenburg V, Nederend J, Voogd AC et al (2013) Trends in breast biopsies for abnormalities detected at screening mammography: a population-based study in the Netherlands. *Br J Cancer* 109:242–248. doi:10.1038/bjc.2013.253.
13. den Dekker BM, van Diest PJ, de Waard SN, Verkooijen HM, Pijnappel RM (2019) Stereotactic 9-gauge vacuum-assisted breast biopsy, how many specimens are needed? *Eur J Radiol* 120:108665. doi:10.1016/j.ejrad.2019.108665.
14. Evans A, Trimboli RM, Athanasiou A et al (2018) Breast ultrasound: recommendations for information to women and referring physicians by the European Society of Breast Imaging. *Insights Imaging* 9:449–461. doi:10.1007/s13244-018-0636-z.
15. Kapetas P, Clauser P, Woitek R et al (2019) Quantitative Multiparametric Breast Ultrasound. *Invest Radiol* 54:257–264. doi:10.1097/RLI.0000000000000543.
16. Song SY, Park B, Hong S, Kim MJ, Lee EH, Jun JK (2019) Comparison of Digital and



Screen-Film Mammography for Breast-Cancer Screening: A Systematic Review and Meta-Analysis. *J Breast Cancer* 22:311–325. doi:10.4048/jbc.2019.22.e24.

17. Pisano ED, Gatsonis C, Hendrick E et al (2005) Diagnostic Performance of Digital versus Film Mammography for Breast-Cancer Screening. *N Engl J Med* 353:1773–1783. doi:10.1056/NEJMoa052911.
18. Bernardi D, Gentilini MA, De Nisi M et al (2020) Effect of implementing digital breast tomosynthesis (DBT) instead of mammography on population screening outcomes including interval cancer rates: Results of the Trento DBT pilot evaluation. *The Breast* 50:135–140. doi:10.1016/j.breast.2019.09.012.
19. Phi X-A, Tagliafico A, Houssami N, Greuter MJW, de Bock GH (2018) Digital breast tomosynthesis for breast cancer screening and diagnosis in women with dense breasts – a systematic review and meta-analysis. *BMC Cancer* 18:380. doi:10.1186/s12885-018-4263-3.
20. Marinovich ML, Hunter KE, Macaskill P, Houssami N (2018) Breast Cancer Screening Using Tomosynthesis or Mammography: A Meta-analysis of Cancer Detection and Recall. *JNCI J Natl Cancer Inst* 110:942–949. doi:10.1093/jnci/djy121.
21. Hovda T, Brandal SHB, Sebuødegård S et al (2019) Screening outcome for consecutive examinations with digital breast tomosynthesis versus standard digital mammography in a population-based screening program. *Eur Radiol* 29:6991–6999. doi:10.1007/s00330-019-06264-y.
22. Mann RM, Cho N, Moy L (2019) Breast MRI: State of the Art. *Radiology* 292:520–536. doi:10.1148/radiol.2019182947.
23. Sardanelli F, Boetes C, Borisch B et al (2010) Magnetic resonance imaging of the breast: Recommendations from the EUSOMA working group. *Eur J Cancer* 46:1296–1316. doi:10.1016/j.ejca.2010.02.015.

24. Morris EA, Comstock CE, Lee CH (2013) ACR BI-RADS® Magnetic Resonance Imaging. In: ACR BI-RADS® Atlas, Breast Imaging Reporting and Data System, 5th ed. American College of Radiology, Reston, VA, USA
25. Carmeliet P, Jain RK (2000) Angiogenesis in cancer and other diseases. *Nature* 407:249–257. doi:10.1038/35025220.
26. Knopp MV, Weiss E, Sinn HP et al (1999) Pathophysiologic basis of contrast enhancement in breast tumors. *J Magn Reson Imaging* 10:260–266. doi:10.1002/(SICI)1522-2586(199909)10:3<260::AID-JMRI6>3.0.CO;2-7.
27. Mann RM, Kuhl CK, Moy L (2019) Contrast-enhanced MRI for breast cancer screening. *J Magn Reson Imaging* 50:377–390. doi:10.1002/jmri.26654.
28. Wernli KJ, DeMartini WB, Ichikawa L et al (2014) Patterns of Breast Magnetic Resonance Imaging Use in Community Practice. *JAMA Intern Med* 174:125. doi:10.1001/jamainternmed.2013.11963.
29. Lin S-P, Brown JJ (2007) MR contrast agents: Physical and pharmacologic basics. *J Magn Reson Imaging* 25:884–899. doi:10.1002/jmri.20955.
30. Ersoy H, Rybicki FJ (2007) Biochemical safety profiles of gadolinium-based extracellular contrast agents and nephrogenic systemic fibrosis. *J Magn Reson Imaging* 26:1190–1197. doi:10.1002/jmri.21135.
31. Aime S, Caravan P (2009) Biodistribution of gadolinium-based contrast agents, including gadolinium deposition. *J Magn Reson Imaging* 30:1259–1267. doi:10.1002/jmri.21969.
32. Port M, Idée J-M, Medina C, Robic C, Sabatou M, Corot C (2008) Efficiency, thermodynamic and kinetic stability of marketed gadolinium chelates and their possible clinical consequences: a critical review. *BioMetals* 21:469–490. doi:10.1007/s10534-008-9135-x.

33. Rohrer M, Bauer H, Mintorovitch J, Requardt M, Weinmann H-J (2005) Comparison of magnetic properties of MRI contrast media solutions at different magnetic field strengths. *Invest Radiol* 40:715–24.
34. Pintaske J, Martirosian P, Graf H et al (2006) Relaxivity of Gadopentetate Dimeglumine (Magnevist), Gadobutrol (Gadovist), and Gadobenate Dimeglumine (MultiHance) in Human Blood Plasma at 0.2, 1.5, and 3 Tesla. *Invest Radiol* 41:213–221.  
doi:10.1097/01.rli.0000197668.44926.f7.
35. Giesel FL, von Tengg-Kobligk H, Wilkinson ID et al (2006) Influence of Human Serum Albumin on Longitudinal and Transverse Relaxation Rates (R1 and R2) of Magnetic Resonance Contrast Agents. *Invest Radiol* 41:222–228.  
doi:10.1097/01.rli.0000192421.81037.d5.
36. Bellin M-F, Van Der Molen AJ (2008) Extracellular gadolinium-based contrast media: An overview. *Eur J Radiol* 66:160–167. doi:10.1016/j.ejrad.2008.01.023.
37. Carbonaro LA, Pediconi F, Verardi N, Trimboli RM, Calabrese M, Sardanelli F (2011) Breast MRI Using a High-Relaxivity Contrast Agent: An Overview. *Am J Roentgenol* 196:942–955. doi:10.2214/AJR.10.4974.
38. Pediconi F, Catalano C, Occhiato R et al (2005) Breast Lesion Detection and Characterization at Contrast-enhanced MR Mammography: Gadobenate Dimeglumine versus Gadopentetate Dimeglumine. *Radiology* 237:45–56. doi:10.1148/radiol.2371041369.
39. Pediconi F, Catalano C, Padula S et al (2008) Contrast-Enhanced MR Mammography: Improved Lesion Detection and Differentiation with Gadobenate Dimeglumine. *Am J Roentgenol* 191:1339–1346. doi:10.2214/AJR.07.3533.
40. Knopp M V, Bourne MW, Sardanelli F et al (2003) Gadobenate Dimeglumine-Enhanced MRI of the Breast: Analysis of Dose Response and Comparison with Gadopentetate

Dimeglumine. *Am J Roentgenol* 181:663–676. doi:10.2214/ajr.181.3.1810663.

41. Martincich L, Faivre-Pierret M, Zechmann CMCM et al (2011) Multicenter, Double-Blind, Randomized, Intraindividual Crossover Comparison of Gadobenate Dimeglumine and Gadopentetate Dimeglumine for Breast MR Imaging (DETECT Trial). *Radiology* 258:396–408. doi:10.1148/radiol.10100968.
42. Gilbert FJ, van den Bosch HCM, Petrillo A et al (2014) Comparison of gadobenate dimeglumine-enhanced breast MRI and gadopentetate dimeglumine-enhanced breast MRI with mammography and ultrasound for the detection of breast cancer. *J Magn Reson Imaging* 39:1272–1286. doi:10.1002/jmri.24434.
43. Pediconi F, Kubik-Huch R, Chilla B, Schwenke C, Kinkel K (2013) Intra-individual randomised comparison of gadobutrol 1.0 M versus gadobenate dimeglumine 0.5 M in patients scheduled for preoperative breast MRI. *Eur Radiol* 23:84–92. doi:10.1007/s00330-012-2557-4.
44. Schneider G, Fries P (2013) Letter to the Editor re: intra-individual randomised comparison of gadobutrol 1.0 M versus gadobenate dimeglumine 0.5 M in patients scheduled for preoperative breast MRI. *Eur Radiol* 23:2095–2096. doi:10.1007/s00330-013-2879-x.
45. Kinkel K, Schwenke C, Kubik-Huch R, Pediconi F (2013) Reply to Letter to the Editor: Intra-individual randomised comparison of gadobutrol 1.0 M versus gadobenate dimeglumine 0.5 M in patients scheduled for preoperative breast MRI. *Eur Radiol* 23:2097–2099. doi:10.1007/s00330-013-2878-y.
46. Clauser P, Helbich TH, Kapetas P et al (2019) Breast lesion detection and characterization with contrast-enhanced magnetic resonance imaging: Prospective randomized intraindividual comparison of gadoterate meglumine (0.15 mmol/kg) and gadobenate dimeglumine (0.075 mmol/kg) at 3T. *J Magn Reson Imaging* 49:1157–1165. doi:10.1002/jmri.26335.

47. Renz DM, Durmus T, Böttcher J et al (2014) Comparison of Gadoteric Acid and Gadobutrol for Detection as Well as Morphologic and Dynamic Characterization of Lesions on Breast Dynamic Contrast-Enhanced Magnetic Resonance Imaging. *Invest Radiol* 49:474–484. doi:10.1097/RLI.0000000000000039.
48. Fallenberg EM, Renz DM, Karle B et al (2015) Intraindividual, randomized comparison of the macrocyclic contrast agents gadobutrol and gadoterate meglumine in breast magnetic resonance imaging. *Eur Radiol* 25:837–849. doi:10.1007/s00330-014-3426-0.
49. ACR Committee on Drugs and Contrast Media (2021) *ACR Manual on Contrast Media*. American College of Radiology, Reston, VA, USA
50. Thomsen HS (2011) Contrast media safety—An update. *Eur J Radiol* 80:77–82. doi:10.1016/j.ejrad.2010.12.104.
51. Semelka RC, Ramalho M, AlObaidy M, Ramalho J (2016) Gadolinium in Humans: A Family of Disorders. *Am J Roentgenol* 207:229–233. doi:10.2214/AJR.15.15842.
52. Jordan RM, Mintz RD (1995) Fatal reaction to gadopentetate dimeglumine. *Am J Roentgenol* 164:743–744. doi:10.2214/ajr.164.3.7863905.
53. Jung J, Kang H, Kim M et al (2012) Immediate Hypersensitivity Reaction to Gadolinium-based MR Contrast Media. *Radiology* 264:414–422. doi:10.1148/radiol.12112025.
54. McDonald JS, Hunt CH, Kolbe AB et al (2019) Acute Adverse Events Following Gadolinium-based Contrast Agent Administration: A Single-Center Retrospective Study of 281 945 Injections. *Radiology* 292:620–627. doi:10.1148/radiol.2019182834.
55. Hunt CH, Hartman RP, Hesley GK (2009) Frequency and Severity of Adverse Effects of Iodinated and Gadolinium Contrast Materials: Retrospective Review of 456,930 Doses. *Am J Roentgenol* 193:1124–1127. doi:10.2214/AJR.09.2520.

56. McDonald JS, Larson NB, Kolbe AB et al (2021) Prevention of Allergic-like Reactions at Repeat CT: Steroid Pretreatment versus Contrast Material Substitution. *Radiology* 301:133–140. doi:10.1148/radiol.2021210490.
57. Ryoo CH, Choi YH, Cheon J et al (2019) Preventive Effect of Changing Contrast Media in Patients With A Prior Mild Immediate Hypersensitivity Reaction to Gadolinium-Based Contrast Agent. *Invest Radiol* 54:633–637. doi:10.1097/RLI.0000000000000573.
58. Lee CS, Monticciolo DL, Moy L (2020) Screening Guidelines Update for Average-Risk and High-Risk Women. *Am J Roentgenol* 214:316–323. doi:10.2214/AJR.19.22205.
59. Saccarelli CR, Bitencourt AG V, Morris EA (2020) Breast Cancer Screening in High-Risk Women: Is MRI Alone Enough? *JNCI J Natl Cancer Inst* 112:121–122. doi:10.1093/jnci/djz130.
60. Colditz GA, Bohlke K (2014) Priorities for the primary prevention of breast cancer. *CA Cancer J Clin* 64:186–194. doi:10.3322/caac.21225.
61. Kotsopoulos J (2018) BRCA Mutations and Breast Cancer Prevention. *Cancers (Basel)* 10:524. doi:10.3390/cancers10120524.
62. Manoukian S, Alfieri S, Bianchi E, Peissel B, Azzollini J, Borreani C (2019) Risk-reducing surgery in BRCA1 / BRCA2 mutation carriers: Are there factors associated with the choice? *Psychooncology* 28:1871–1878. doi:10.1002/pon.5166.
63. Endrikat J, Dohanish S, Schleyer N, Schwenke S, Agarwal S, Balzer T (2018) 10 Years of Nephrogenic Systemic Fibrosis. *Invest Radiol* 53:541–550. doi:10.1097/RLI.0000000000000462.
64. Abraham JL, Thakral C (2008) Tissue distribution and kinetics of gadolinium and nephrogenic systemic fibrosis. *Eur J Radiol* 66:200–207. doi:10.1016/j.ejrad.2008.01.026.

65. Kanal E (2016) Gadolinium based contrast agents (GBCA): Safety overview after 3 decades of clinical experience. *Magn Reson Imaging* 34:1341–1345. doi:10.1016/j.mri.2016.08.017.
66. Davenport MS (2019) Virtual Elimination of Nephrogenic Systemic Fibrosis: A Medical Success Story with a Small Asterisk. *Radiology* 292:387–389. doi:10.1148/radiol.2019191158.
67. Glutig K, Hahn G, Kuvvetli P, Endrikat J (2018) Safety of gadobutrol: results of a non-interventional study of 3710 patients, including 404 children. *Acta radiol* :028418511880115. doi:10.1177/0284185118801151.
68. Endrikat J, Vogtlaender K, Dohanish S, Balzer T, Breuer J (2016) Safety of Gadobutrol. *Invest Radiol* 51:537–543. doi:10.1097/RLI.0000000000000270.
69. Larson KN, Gagnon AL, Darling MD, Patterson JW, Cropley TG (2015) Nephrogenic Systemic Fibrosis Manifesting a Decade After Exposure to Gadolinium. *JAMA Dermatology* 151:1117. doi:10.1001/jamadermatol.2015.0976.
70. Attari H, Cao Y, Elmholdt TR, Zhao Y, Prince MR (2019) A Systematic Review of 639 Patients with Biopsy-confirmed Nephrogenic Systemic Fibrosis. *Radiology* 292:376–386. doi:10.1148/radiol.2019182916.
71. Colletti PM (2008) Nephrogenic Systemic Fibrosis and Gadolinium: A Perfect Storm. *Am J Roentgenol* 191:1150–1153. doi:10.2214/AJR.08.1327.
72. Thomsen HS (2014) NSF: Still relevant. *J Magn Reson Imaging* 40:11–12. doi:10.1002/jmri.24422.
73. Prince MR, Zhang H, Morris M et al (2008) Incidence of Nephrogenic Systemic Fibrosis at Two Large Medical Centers. *Radiology* 248:807–816. doi:10.1148/radiol.2483071863.
74. Radbruch A, Weberling LD, Kieslich PJ et al (2015) Gadolinium Retention in the Dentate

Nucleus and Globus Pallidus Is Dependent on the Class of Contrast Agent. *Radiology* 275:783–791. doi:10.1148/radiol.2015150337.

75. White GW, Gibby WA, Tweedle MF (2006) Comparison of Gd(DTPA-BMA) (Omniscan) Versus Gd(HP-DO3A) (ProHance) Relative to Gadolinium Retention in Human Bone Tissue by Inductively Coupled Plasma Mass Spectroscopy. *Invest Radiol* 41:272–278. doi:10.1097/01.rli.0000186569.32408.95.
76. European Medicines Agency (2017) PRAC Confirms Restrictions on the Use of Linear Gadolinium Agents. [http://www.ema.europa.eu/docs/en\\_GB/document\\_library/Referrals\\_document/gadolinium\\_contrast\\_agents\\_31/Recommendation\\_provided\\_by\\_Pharmacovigilance\\_Risk\\_Assessment\\_Committee/WC500230928.pdf](http://www.ema.europa.eu/docs/en_GB/document_library/Referrals_document/gadolinium_contrast_agents_31/Recommendation_provided_by_Pharmacovigilance_Risk_Assessment_Committee/WC500230928.pdf). Accessed 8 Feb 2020
77. Gulani V, Calamante F, Shellock FG, Kanal E, Reeder SB (2017) Gadolinium deposition in the brain: summary of evidence and recommendations. *Lancet Neurol* 16:564–570. doi:10.1016/S1474-4422(17)30158-8.
78. Murata N, Gonzalez-Cuyar LF, Murata K et al (2016) Macrocyclic and Other Non-Group 1 Gadolinium Contrast Agents Deposit Low Levels of Gadolinium in Brain and Bone Tissue. *Invest Radiol* 51:447–453. doi:10.1097/RLI.0000000000000252.
79. Bussi S, Coppo A, Botteron C et al (2018) Differences in gadolinium retention after repeated injections of macrocyclic MR contrast agents to rats. *J Magn Reson Imaging* 47:746–752. doi:10.1002/jmri.25822.
80. McDonald RJ, McDonald JS, Dai D et al (2017) Comparison of Gadolinium Concentrations within Multiple Rat Organs after Intravenous Administration of Linear versus Macrocyclic Gadolinium Chelates. *Radiology* 285:536–545. doi:10.1148/radiol.2017161594.
81. Forslin Y, Shams S, Hashim F et al (2017) Retention of Gadolinium-Based Contrast Agents



in Multiple Sclerosis: Retrospective Analysis of an 18-Year Longitudinal Study. *Am J Neuroradiol* 38:1311–1316. doi:10.3174/ajnr.A5211.

82. Ackermans N, Taylor C, Tam R et al (2019) Effect of different doses of gadolinium contrast agent on clinical outcomes in MS. *Mult Scler J - Exp Transl Clin* 5:205521731882379. doi:10.1177/2055217318823796.
83. Cocozza S, Pontillo G, Lanzillo R et al (2019) MRI features suggestive of gadolinium retention do not correlate with Expanded Disability Status Scale worsening in Multiple Sclerosis. *Neuroradiology* 61:155–162. doi:10.1007/s00234-018-02150-4.
84. Welk B, McArthur E, Morrow SA et al (2016) Association Between Gadolinium Contrast Exposure and the Risk of Parkinsonism. *JAMA* 316:96. doi:10.1001/jama.2016.8096.
85. Mallio CA, Piervincenzi C, Gianolio E et al (2019) Absence of dentate nucleus resting-state functional connectivity changes in nonneurological patients with gadolinium-related hyperintensity on T1-weighted images. *J Magn Reson Imaging* 50:445–455. doi:10.1002/jmri.26669.
86. Malayeri AA, Brooks KM, Bryant LH et al (2016) National Institutes of Health Perspective on Reports of Gadolinium Deposition in the Brain. *J Am Coll Radiol* 13:237–241. doi:10.1016/j.jacr.2015.11.009.
87. McDonald RJ, Levine D, Weinreb J et al (2018) Gadolinium Retention: A Research Roadmap from the 2018 NIH/ACR/RSNA Workshop on Gadolinium Chelates. *Radiology* 289:517–534. doi:10.1148/radiol.2018181151.
88. Zanardo M, Doniselli FMFM, Esseridou A et al (2018) Abdominal CT: a radiologist-driven adjustment of the dose of iodinated contrast agent approaches a calculation per lean body weight. *Eur Radiol Exp* 2:41. doi:10.1186/s41747-018-0074-1.
89. Baltzer PAT, Sardanelli F (2020) The Mantra about Low Specificity of Breast MRI. In:

Sardanelli F, Podo F (eds) Breast MRI for High-risk Screening. Springer International Publishing, Cham, pp 11–21

90. Saslow D, Boetes C, Burke W et al (2007) American Cancer Society Guidelines for Breast Screening with MRI as an Adjunct to Mammography. *CA Cancer J Clin* 57:75–89. doi:10.3322/canjclin.57.2.75.
91. National Institute for Health and Care Excellence (2013) Familial breast cancer: classification, care and managing breast cancer and related risks in people with a family history of breast cancer. In: Clin. Guidel. [CG164]. <https://www.nice.org.uk/guidance/cg164/chapter/Recommendations>. Accessed 14 May 2020
92. Macklin S, Gass J, Mitri G, Atwal PS, Hines S (2018) The role of screening MRI in the era of next generation sequencing and moderate-risk genetic mutations. *Fam Cancer* 17:167–173. doi:10.1007/s10689-017-0007-9.
93. Kuhl C, Weigel S, Schrading S et al (2010) Prospective Multicenter Cohort Study to Refine Management Recommendations for Women at Elevated Familial Risk of Breast Cancer: The EVA Trial. *J Clin Oncol* 28:1450–1457. doi:10.1200/JCO.2009.23.0839.
94. Sardanelli F, Podo F, Santoro F et al (2011) Multicenter Surveillance of Women at High Genetic Breast Cancer Risk Using Mammography, Ultrasonography, and Contrast-Enhanced Magnetic Resonance Imaging (the High Breast Cancer Risk Italian 1 Study). *Invest Radiol* 46:94–105. doi:10.1097/RLI.0b013e3181f3fcdf.
95. Obdeijn I-M, Winter-Warnars GAO, Mann RM, Hooning MJ, Hunink MGM, Tilanus-Linthorst MMA (2014) Should we screen BRCA1 mutation carriers only with MRI? A multicenter study. *Breast Cancer Res Treat* 144:577–582. doi:10.1007/s10549-014-2888-8.
96. Chiarelli AM, Prummel M V., Muradali D et al (2014) Effectiveness of Screening With Annual Magnetic Resonance Imaging and Mammography: Results of the Initial Screen From

the Ontario High Risk Breast Screening Program. *J Clin Oncol* 32:2224–2230.

doi:10.1200/JCO.2013.52.8331.

97. Riedl CC, Luft N, Bernhart C et al (2015) Triple-Modality Screening Trial for Familial Breast Cancer Underlines the Importance of Magnetic Resonance Imaging and Questions the Role of Mammography and Ultrasound Regardless of Patient Mutation Status, Age, and Breast Density. *J Clin Oncol* 33:1128–1135. doi:10.1200/JCO.2014.56.8626.
98. Phi X-AA, Saadatmand S, De Bock GH et al (2016) Contribution of mammography to MRI screening in BRCA mutation carriers by BRCA status and age: individual patient data meta-analysis. *Br J Cancer* 114:631–637. doi:10.1038/bjc.2016.32.
99. Lo G, Scaranelo AM, Aboras H et al (2017) Evaluation of the Utility of Screening Mammography for High-Risk Women Undergoing Screening Breast MR Imaging. *Radiology* 285:36–43. doi:10.1148/radiol.2017161103.
100. Colin C, Foray N, Di Leo G, Sardanelli F (2017) Radiation induced breast cancer risk in BRCA mutation carriers from low-dose radiological exposures: a systematic review. *Radioprotection* 52:231–240. doi:10.1051/radiopro/2017034.
101. Plevritis SK, Kurian AW, Sigal BM et al (2006) Cost-effectiveness of Screening BRCA1/2 Mutation Carriers With Breast Magnetic Resonance Imaging. *JAMA* 295:2374. doi:10.1001/jama.295.20.2374.
102. Podo F, Santoro F, Di Leo G et al (2016) Triple-Negative versus Non-Triple-Negative Breast Cancers in High-Risk Women: Phenotype Features and Survival from the HIBCRIT-1 MRI-Including Screening Study. *Clin Cancer Res* 22:895–904. doi:10.1158/1078-0432.CCR-15-0459.
103. Saadatmand S, Geuzinge HA, Rutgers EJT et al (2019) MRI versus mammography for breast cancer screening in women with familial risk (FaMRIsc): a multicentre, randomised,

- controlled trial. *Lancet Oncol* 20:1136–1147. doi:10.1016/S1470-2045(19)30275-X.
104. Geuzinge HA, Bakker MF, Heijnsdijk EAM et al (2021) Cost-Effectiveness of Magnetic Resonance Imaging Screening for Women With Extremely Dense Breast Tissue. *JNCI J Natl Cancer Inst* 113:1476–1483. doi:10.1093/jnci/djab119.
  105. Heacock L, Reig B, Lewin AA, Toth HK, Moy L, Lee CS (2020) Abbreviated Breast MRI: Road to Clinical Implementation. *J Breast Imaging* 2:201–214. doi:10.1093/jbi/wbaa020.
  106. Wernli KJ, Ichikawa L, Kerlikowske K et al (2019) Surveillance Breast MRI and Mammography: Comparison in Women with a Personal History of Breast Cancer. *Radiology* 292:311–318. doi:10.1148/radiol.2019182475.
  107. Gong E, Pauly JM, Wintermark M, Zaharchuk G (2018) Deep learning enables reduced gadolinium dose for contrast-enhanced brain MRI. *J Magn Reson Imaging* 48:330–340. doi:10.1002/jmri.25970.
  108. Trimboli RM, Verardi N, Cartia F, Carbonaro LA, Sardanelli F (2014) Breast Cancer Detection Using Double Reading of Unenhanced MRI Including T1-Weighted, T2-Weighted STIR, and Diffusion-Weighted Imaging: A Proof of Concept Study. *Am J Roentgenol* 203:674–681. doi:10.2214/AJR.13.11816.
  109. Rotili A, Trimboli RM, Penco S et al (2020) Double reading of diffusion-weighted magnetic resonance imaging for breast cancer detection. *Breast Cancer Res Treat* 180:111–120. doi:10.1007/s10549-019-05519-y.
  110. Melsaether AN, Kim E, Mema E, Babb J, Kim SG (2019) Preliminary study: Breast cancers can be well seen on 3T breast MRI with a half-dose of gadobutrol. *Clin Imaging* 58:84–89. doi:10.1016/j.clinimag.2019.06.014.
  111. U.S. Food and Drug Administration (2018) FDA Drug Safety Communication: FDA warns that gadolinium-based contrast agents (GBCAs) are retained in the body; requires new class

warnings. <https://www.fda.gov/drugs/drug-safety-and-availability/fda-drug-safety-communication-fda-warns-gadolinium-based-contrast-agents-gbcas-are-retained-body>.

Accessed 8 Feb 2020

112. Evans JD (1996) *Straightforward statistics for the behavioral sciences*. Brooks/Cole, Pacific Grove
113. Onesti JK, Mangus BE, Helmer SD, Osland JS (2008) Breast cancer tumor size: correlation between magnetic resonance imaging and pathology measurements. *Am J Surg* 196:844–850. doi:10.1016/j.amjsurg.2008.07.028.
114. Yoo EY, Nam SY, Choi H-Y, Hong MJ (2018) Agreement between MRI and pathologic analyses for determination of tumor size and correlation with immunohistochemical factors of invasive breast carcinoma. *Acta radiol* 59:50–57. doi:10.1177/0284185117705010.
115. Bland JM, Altman DG (1986) Statistical methods for assessing agreement between two methods of clinical measurement. *Lancet* 1:307–310.
116. Mann RM, Bult P, van Laarhoven HWM et al (2013) Breast cancer size estimation with MRI in BRCA mutation carriers and other high risk patients. *Eur J Radiol* 82:1416–1422. doi:10.1016/j.ejrad.2013.03.003.
117. Koh J, Park AY, Ko KH, Kim S, Jung HK (2019) Assessing sizes of breast cancers that show non-mass enhancement on MRI based on inter-observer variability and comparison with pathology size. *Acta radiol* 60:1102–1109. doi:10.1177/0284185118817920.
118. Rominger M, Berg D, Frauenfelder T, Ramaswamy A, Timmesfeld N (2016) Which factors influence MRI-pathology concordance of tumour size measurements in breast cancer? *Eur Radiol* 26:1457–1465. doi:10.1007/s00330-015-3935-5.
119. Jiang Y-Z, Xia C, Peng W-T, Yu K-D, Zhuang Z-G, Shao Z-M (2014) Preoperative Measurement of Breast Cancer Overestimates Tumor Size Compared to Pathological

Measurement. PLoS One 9:e86676. doi:10.1371/journal.pone.0086676.

120. Grimsby GM, Gray R, Dueck A et al (2009) Is there concordance of invasive breast cancer pathologic tumor size with magnetic resonance imaging? *Am J Surg* 198:500–504. doi:10.1016/j.amjsurg.2009.07.012.
121. Cardoso F, Kyriakides S, Ohno S et al (2019) Early breast cancer: ESMO Clinical Practice Guidelines for diagnosis, treatment and follow-up. *Ann Oncol* 30:1194–1220. doi:10.1093/annonc/mdz173.
122. Shen Y, Goerner FL, Snyder C et al (2015) T1 Relaxivities of Gadolinium-Based Magnetic Resonance Contrast Agents in Human Whole Blood at 1.5, 3, and 7 T. *Invest Radiol* 50:330–338. doi:10.1097/RLI.0000000000000132.
123. Ghaderi KF, Phillips J, Perry H, Lotfi P, Mehta TS (2019) Contrast-enhanced Mammography: Current Applications and Future Directions. *RadioGraphics* 39:1907–1920. doi:10.1148/rg.2019190079.
124. Zanardo M, Cozzi A, Trimboli RM et al (2019) Technique, protocols and adverse reactions for contrast-enhanced spectral mammography (CESM): a systematic review. *Insights Imaging* 10:76. doi:10.1186/s13244-019-0756-0.
125. Dromain C, Vietti-Violi N, Meuwly JY (2019) Angiomammography: A review of current evidences. *Diagn Interv Imaging* 100:593–605. doi:10.1016/j.diii.2019.01.011.
126. Phillips J, Miller MM, Mehta TS et al (2017) Contrast-enhanced spectral mammography (CESM) versus MRI in the high-risk screening setting: patient preferences and attitudes. *Clin Imaging* 42:193–197. doi:10.1016/j.clinimag.2016.12.011.
127. Hobbs MM, Taylor DB, Buzynski S, Peake RE (2015) Contrast-enhanced spectral mammography (CESM) and contrast enhanced MRI (CEMRI): Patient preferences and tolerance. *J Med Imaging Radiat Oncol* 59:300–305. doi:10.1111/1754-9485.12296.

128. Cheung Y-C, Tsai H-P, Lo Y-F, Ueng S-H, Huang P-C, Chen S-C (2016) Clinical utility of dual-energy contrast-enhanced spectral mammography for breast microcalcifications without associated mass: a preliminary analysis. *Eur Radiol* 26:1082–1089. doi:10.1007/s00330-015-3904-z.
129. Choi JW, Moon W-J (2019) Gadolinium Deposition in the Brain: Current Updates. *Korean J Radiol* 20:134. doi:10.3348/kjr.2018.0356.
130. Cozzi A, Schiaffino S, Sardanelli F (2019) The emerging role of contrast-enhanced mammography. *Quant Imaging Med Surg* 9:2012–2018. doi:10.21037/qims.2019.11.09.
131. Neeter LMFH, Raat HPJF, Alcantara R et al (2021) Contrast-enhanced mammography: what the radiologist needs to know. *BJR|Open* 3:20210034. doi:10.1259/bjro.20210034.
132. Mann RM, Kuhl CK, Kinkel K, Boetes C (2008) Breast MRI: guidelines from the European Society of Breast Imaging. *Eur Radiol* 18:1307–1318. doi:10.1007/s00330-008-0863-7.
133. Zanardo M, Cozzi A, Trimboli RM, Carbonaro LA, Sardanelli F (2018) Technique and diagnostic performance of contrast-enhanced spectral mammography: a systematic review. In: PROSPERO. [https://www.crd.york.ac.uk/prospero/display\\_record.php?RecordID=118554](https://www.crd.york.ac.uk/prospero/display_record.php?RecordID=118554). Accessed 10 May 2021
134. Salameh J-PP, Bossuyt PM, McGrath TA et al (2020) Preferred reporting items for systematic review and meta-analysis of diagnostic test accuracy studies (PRISMA-DTA): explanation, elaboration, and checklist. *BMJ* 370:m2632. doi:10.1136/bmj.m2632.
135. Egger M, Smith GD, Schneider M, Minder C (1997) Bias in meta-analysis detected by a simple, graphical test. *BMJ* 315:629–634. doi:10.1136/bmj.315.7109.629.
136. Tennant SL, James JJ, Cornford EJ et al (2016) Contrast-enhanced spectral mammography improves diagnostic accuracy in the symptomatic setting. *Clin Radiol* 71:1148–1155.

doi:10.1016/j.crad.2016.05.009.

137. Lewis TC, Pizzitola VJ, Giurescu ME et al (2017) Contrast-enhanced Digital Mammography: A Single-Institution Experience of the First 208 Cases. *Breast J* 23:67–76. doi:10.1111/tbj.12681.
138. Moustafa AFI, Kamal EF, Hassan MM, Sakr M, Gomaa MMM (2018) The added value of contrast enhanced spectral mammography in identification of multiplicity of suspicious lesions in dense breast. *Egypt J Radiol Nucl Med* 49:259–264. doi:10.1016/j.ejrm.2017.10.003.
139. Saraya S, Adel L, Mahmoud A (2017) Indeterminate breast lesions: Can contrast enhanced digital mammography change our decisions? *Egypt J Radiol Nucl Med* 48:547–552. doi:10.1016/j.ejrm.2017.03.006.
140. Tardivel A-M, Balleyguier C, Dunant A et al (2016) Added Value of Contrast-Enhanced Spectral Mammography in Postscreening Assessment. *Breast J* 22:520–528. doi:10.1111/tbj.12627.
141. Lobbes MBI, Lalji U, Houwers J et al (2014) Contrast-enhanced spectral mammography in patients referred from the breast cancer screening programme. *Eur Radiol* 24:1668–1676. doi:10.1007/s00330-014-3154-5.
142. Lalji UC, Houben IPL, Prevos R et al (2016) Contrast-enhanced spectral mammography in recalls from the Dutch breast cancer screening program: validation of results in a large multireader, multicase study. *Eur Radiol* 26:4371–4379. doi:10.1007/s00330-016-4336-0.
143. Houben IP, Vanwetswinkel S, Kalia V et al (2019) Contrast-enhanced spectral mammography in the evaluation of breast suspicious calcifications: diagnostic accuracy and impact on surgical management. *Acta radiol* 60:1110–1117. doi:10.1177/0284185118822639.



144. Patel BK, Davis J, Ferraro C et al (2018) Value Added of Preoperative Contrast-Enhanced Digital Mammography in Patients With Invasive Lobular Carcinoma of the Breast. *Clin Breast Cancer* 18:e1339–e1345. doi:10.1016/j.clbc.2018.07.012.
145. Travieso-Aja M del M, Naranjo-Santana P, Fernández-Ruiz C et al (2018) Factors affecting the precision of lesion sizing with contrast-enhanced spectral mammography. *Clin Radiol* 73:296–303. doi:10.1016/j.crad.2017.10.017.
146. Helal MH, Mansour SM, Salaleldin LA, Alkalaawy BM, Salem DS, Mokhtar NM (2018) The impact of contrast-enhanced spectral mammogram (CESM) and three-dimensional breast ultrasound (3DUS) on the characterization of the disease extend in cancer patients. *Br J Radiol* 91:20170977. doi:10.1259/bjr.20170977.
147. Lee-Felker SA, Tekchandani L, Thomas M et al (2017) Newly Diagnosed Breast Cancer: Comparison of Contrast-enhanced Spectral Mammography and Breast MR Imaging in the Evaluation of Extent of Disease. *Radiology* 285:389–400. doi:10.1148/radiol.2017161592.
148. Patel BK, Garza SA, Eversman S, Lopez-Alvarez Y, Kosiorek H, Pockaj BA (2017) Assessing tumor extent on contrast-enhanced spectral mammography versus full-field digital mammography and ultrasound. *Clin Imaging* 46:78–84. doi:10.1016/j.clinimag.2017.07.001.
149. Helal MH, Mansour SM, Zaglol M, Salaleldin LA, Nada OM, Haggag MA (2017) Staging of breast cancer and the advanced applications of digital mammogram: what the physician needs to know? *Br J Radiol* 90:20160717. doi:10.1259/bjr.20160717.
150. Ambicka A, Luczynska E, Adamczyk A, Harazin-Lechowska A, Sas-Korczynska B, Niemiec J (2016) The tumour border on contrast-enhanced spectral mammography and its relation to histological characteristics of invasive breast cancer. *Polish J Pathol* 3:295–299. doi:10.5114/pjp.2016.63783.
151. Lobbes MBI, Lalji UC, Nelemans PJ et al (2015) The Quality of Tumor Size Assessment by

- Contrast-Enhanced Spectral Mammography and the Benefit of Additional Breast MRI. *J Cancer* 6:144–150. doi:10.7150/jca.10705.
152. Blum KS, Rubbert C, Mathys B, Antoch G, Mohrmann S, Obenauer S (2014) Use of Contrast-Enhanced Spectral Mammography for Intramammary Cancer Staging. *Acad Radiol* 21:1363–1369. doi:10.1016/j.acra.2014.06.012.
  153. Fallenberg EM, Dromain C, Diekmann F et al (2014) Contrast-enhanced spectral mammography versus MRI: Initial results in the detection of breast cancer and assessment of tumour size. *Eur Radiol* 24:256–264. doi:10.1007/s00330-013-3007-7.
  154. Ali-Mucheru M, Pockaj B, Patel B et al (2016) Contrast-Enhanced Digital Mammography in the Surgical Management of Breast Cancer. *Ann Surg Oncol* 23:649–655. doi:10.1245/s10434-016-5567-7.
  155. Patel BK, Ranjbar S, Wu T et al (2018) Computer-aided diagnosis of contrast-enhanced spectral mammography: A feasibility study. *Eur J Radiol* 98:207–213. doi:10.1016/j.ejrad.2017.11.024.
  156. Luczyńska E, Heinze-Paluchowska S, Dyczek S, Blecharz P, Rys J, Reinfuss M (2014) Contrast-Enhanced Spectral Mammography: Comparison with Conventional Mammography and Histopathology in 152 Women. *Korean J Radiol* 15:689–696. doi:10.3348/kjr.2014.15.6.689.
  157. Luczynska E, Niemiec J, Heinze S et al (2018) Intensity and Pattern of Enhancement on CESM: Prognostic Significance and its Relation to Expression of Podoplanin in Tumor Stroma – A Preliminary Report. *Anticancer Res* 38:1085–1095. doi:10.21873/anticancerres.12327.
  158. Iotti V, Ravaioli S, Vacondio R et al (2017) Contrast-enhanced spectral mammography in neoadjuvant chemotherapy monitoring: a comparison with breast magnetic resonance

imaging. *Breast Cancer Res* 19:106. doi:10.1186/s13058-017-0899-1.

159. Patel BK, Hilal T, Covington M et al (2018) Contrast-Enhanced Spectral Mammography is Comparable to MRI in the Assessment of Residual Breast Cancer Following Neoadjuvant Systemic Therapy. *Ann Surg Oncol* 25:1350–1356. doi:10.1245/s10434-018-6413-x.
160. Barra FR, Souza FF de, Camelo REFA, Ribeiro AC de O, Farage L (2017) Accuracy of contrast-enhanced spectral mammography for estimating residual tumor size after neoadjuvant chemotherapy in patients with breast cancer: a feasibility study. *Radiol Bras* 50:224–230. doi:10.1590/0100-3984.2016-0029.
161. Barra FR, Sobrinho AB, Barra RR et al (2018) Contrast-Enhanced Mammography (CEM) for Detecting Residual Disease after Neoadjuvant Chemotherapy: A Comparison with Breast Magnetic Resonance Imaging (MRI). *Biomed Res Int* 2018:8531916. doi:10.1155/2018/8531916.
162. Luczyńska E, Heinze S, Adameczyk A, Rys J, Mitus JW, Hendrick E (2016) Comparison of the Mammography, Contrast-Enhanced Spectral Mammography and Ultrasonography in a Group of 116 patients. *Anticancer Res* 36:4359–66.
163. Tohamey YM, Youssry SW, Abd El Aziz AI (2018) Interpretation of patterns of enhancement on contrast-enhanced spectral mammography: An approach to a standardized scheme. *Egypt J Radiol Nucl Med* 49:854–868. doi:10.1016/j.ejrn.2018.03.004.
164. Dromain C, Thibault F, Diekmann F et al (2012) Dual-energy contrast-enhanced digital mammography: initial clinical results of a multireader, multicase study. *Breast Cancer Res* 14:R94. doi:10.1186/bcr3210.
165. Łuczyńska E, Heinze-Paluchowska S, Hendrick E et al (2015) Comparison between breast MRI and contrast-enhanced spectral mammography. *Med Sci Monit* 21:1358–67. doi:10.12659/MSM.893018.

166. Jochelson MS, Pinker K, Dershaw DD et al (2017) Comparison of screening CEDM and MRI for women at increased risk for breast cancer: A pilot study. *Eur J Radiol* 97:37–43. doi:10.1016/j.ejrad.2017.10.001.
167. Jochelson MS, Dershaw DD, Sung JS et al (2013) Bilateral Contrast-enhanced Dual-Energy Digital Mammography: Feasibility and Comparison with Conventional Digital Mammography and MR Imaging in Women with Known Breast Carcinoma. *Radiology* 266:743–751. doi:10.1148/radiol.12121084.
168. James JR, Pavlicek W, Hanson JA, Boltz TF, Patel BK (2017) Breast Radiation Dose With CESM Compared With 2D FFDM and 3D Tomosynthesis Mammography. *Am J Roentgenol* 208:362–372. doi:10.2214/AJR.16.16743.
169. Mokhtar O, Mahmoud S (2014) Can contrast enhanced mammography solve the problem of dense breast lesions? *Egypt J Radiol Nucl Med* 45:1043–1052. doi:10.1016/j.ejrnm.2014.04.007.
170. Houben IPL, Van de Voorde P, Jeukens CRLPN et al (2017) Contrast-enhanced spectral mammography as work-up tool in patients recalled from breast cancer screening has low risks and might hold clinical benefits. *Eur J Radiol* 94:31–37. doi:10.1016/j.ejrad.2017.07.004.
171. Jeukens CRLPN, Lalji UC, Meijer E et al (2014) Radiation Exposure of Contrast-Enhanced Spectral Mammography Compared With Full-Field Digital Mammography. *Invest Radiol* 49:659–665. doi:10.1097/RLI.0000000000000068.
172. Diekmann F, Freyer M, Diekmann S et al (2011) Evaluation of contrast-enhanced digital mammography. *Eur J Radiol* 78:112–121. doi:10.1016/j.ejrad.2009.10.002.
173. Richter V, Hatterman V, Preibsch H et al (2018) Contrast-enhanced spectral mammography in patients with MRI contraindications. *Acta radiol* 59:798–805.

doi:10.1177/0284185117735561.

174. Gluskin J, Click M, Fleischman R, Dromain C, Morris EA, Jochelson MS (2017) Contamination artifact that mimics in-situ carcinoma on contrast-enhanced digital mammography. *Eur J Radiol* 95:147–154. doi:10.1016/j.ejrad.2017.08.002.
175. Travieso Aja MM, Rodríguez Rodríguez M, Alayón Hernández S, Vega Benítez V, Luzardo OP (2014) Mamografía con realce de contraste mediante técnica de energía dual. *Radiologia* 56:390–399. doi:10.1016/j.rx.2014.05.003.
176. Diekmann F, Diekmann S, Jeunehomme F, Muller S, Hamm B, Bick U (2005) Digital Mammography Using Iodine-Based Contrast Media. *Invest Radiol* 40:397–404. doi:10.1097/01.rli.0000167421.83203.4e.
177. Patel BK, Naylor ME, Kosiorek HE et al (2017) Clinical utility of contrast-enhanced spectral mammography as an adjunct for tomosynthesis-detected architectural distortion. *Clin Imaging* 46:44–52. doi:10.1016/j.clinimag.2017.07.003.
178. Francescone MA, Jochelson MS, Dershaw DD et al (2014) Low energy mammogram obtained in contrast-enhanced digital mammography (CEDM) is comparable to routine full-field digital mammography (FFDM). *Eur J Radiol* 83:1350–1355. doi:10.1016/j.ejrad.2014.05.015.
179. Łuczyńska E, Niemiec J, Hendrick E et al (2016) Degree of Enhancement on Contrast Enhanced Spectral Mammography (CESM) and Lesion Type on Mammography (MG): Comparison Based on Histological Results. *Med Sci Monit* 22:3886–3893. doi:10.12659/MSM.900371.
180. Kariyappa KD, Gnanaprakasam F, Anand S, Krishnaswami M, Ramachandran M (2016) Contrast enhanced dual energy spectral mammogram, an emerging addendum in breast imaging. *Br J Radiol* 89:20150609. doi:10.1259/bjr.20150609.

181. Danala G, Patel B, Aghaei F et al (2018) Classification of Breast Masses Using a Computer-Aided Diagnosis Scheme of Contrast Enhanced Digital Mammograms. *Ann Biomed Eng* 46:1419–1431. doi:10.1007/s10439-018-2044-4.
182. Yagil Y, Shalmon A, Rundstein A et al (2016) Challenges in contrast-enhanced spectral mammography interpretation: artefacts lexicon. *Clin Radiol* 71:450–457. doi:10.1016/j.crad.2016.01.012.
183. ElSaid NAE, Farouk S, Shetat OMM, Khalifa NM, Nada OM (2015) Contrast enhanced digital mammography: Is it useful in detecting lesions in edematous breast? *Egypt J Radiol Nucl Med* 46:811–819. doi:10.1016/j.ejrn.2015.04.002.
184. Mori M, Akashi-Tanaka S, Suzuki S et al (2017) Diagnostic accuracy of contrast-enhanced spectral mammography in comparison to conventional full-field digital mammography in a population of women with dense breasts. *Breast Cancer* 24:104–110. doi:10.1007/s12282-016-0681-8.
185. Savaridas SL, Taylor DB, Gunawardana D, Phillips M (2017) Could parenchymal enhancement on contrast-enhanced spectral mammography (CESM) represent a new breast cancer risk factor? Correlation with known radiology risk factors. *Clin Radiol* 72:1085.e1-1085.e9. doi:10.1016/j.crad.2017.07.017.
186. Fallenberg EM, Schmitzberger FF, Amer H et al (2017) Contrast-enhanced spectral mammography vs. mammography and MRI – clinical performance in a multi-reader evaluation. *Eur Radiol* 27:2752–2764. doi:10.1007/s00330-016-4650-6.
187. Dromain C, Balleyguier C, Muller S et al (2006) Evaluation of Tumor Angiogenesis of Breast Carcinoma Using Contrast-Enhanced Digital Mammography. *Am J Roentgenol* 187:W528–W537. doi:10.2214/AJR.05.1944.
188. Brandan M-E, Cruz-Bastida JP, Rosado-Méndez IM et al (2016) Clinical study of contrast-

- enhanced digital mammography and the evaluation of blood and lymphatic microvessel density. *Br J Radiol* 89:20160232. doi:10.1259/bjr.20160232.
189. Deng C-Y, Juan Y-H, Cheung Y-C et al (2018) Quantitative analysis of enhanced malignant and benign lesions on contrast-enhanced spectral mammography. *Br J Radiol* 91:20170605. doi:10.1259/bjr.20170605.
190. Mohamed Kamal R, Hussien Helal M, Wessam R, Mahmoud Mansour S, Godda I, Alieldin N (2015) Contrast-enhanced spectral mammography: Impact of the qualitative morphology descriptors on the diagnosis of breast lesions. *Eur J Radiol* 84:1049–1055. doi:10.1016/j.ejrad.2015.03.005.
191. Sogani J, Morris EA, Kaplan JB et al (2017) Comparison of Background Parenchymal Enhancement at Contrast-enhanced Spectral Mammography and Breast MR Imaging. *Radiology* 282:63–73. doi:10.1148/radiol.2016160284.
192. Phillips J, Mihai G, Hassonjee SE et al (2018) Comparative Dose of Contrast-Enhanced Spectral Mammography (CESM), Digital Mammography, and Digital Breast Tomosynthesis. *Am J Roentgenol* 211:839–846. doi:10.2214/AJR.17.19036.
193. Knogler T, Homolka P, Hörnig M et al (2016) Contrast-enhanced dual energy mammography with a novel anode/filter combination and artifact reduction: a feasibility study. *Eur Radiol* 26:1575–1581. doi:10.1007/s00330-015-4007-6.
194. Xing D, Lv Y, Sun B et al (2019) Diagnostic Value of Contrast-Enhanced Spectral Mammography in Comparison to Magnetic Resonance Imaging in Breast Lesions. *J Comput Assist Tomogr* 43:245–251. doi:10.1097/RCT.0000000000000832.
195. Fallenberg EM, Dromain C, Diekmann F et al (2014) Contrast-enhanced spectral mammography: Does mammography provide additional clinical benefits or can some radiation exposure be avoided? *Breast Cancer Res Treat* 146:371–381. doi:10.1007/s10549-

014-3023-6.

196. Cheung Y-C, Lin Y-C, Wan Y-L et al (2014) Diagnostic performance of dual-energy contrast-enhanced subtracted mammography in dense breasts compared to mammography alone: interobserver blind-reading analysis. *Eur Radiol* 24:2394–2403. doi:10.1007/s00330-014-3271-1.
197. Kim EY, Youn I, Lee KH et al (2018) Diagnostic Value of Contrast-Enhanced Digital Mammography versus Contrast-Enhanced Magnetic Resonance Imaging for the Preoperative Evaluation of Breast Cancer. *J Breast Cancer* 21:453–462. doi:10.4048/jbc.2018.21.e62.
198. Hill ML, Mainprize JG, Carton A-K et al (2013) Anatomical noise in contrast-enhanced digital mammography. Part II. Dual-energy imaging. *Med Phys* 40:081907. doi:10.1118/1.4812681.
199. Klang E, Krosser A, Amitai MM et al (2018) Utility of routine use of breast ultrasound following contrast-enhanced spectral mammography. *Clin Radiol* 73:908.e11-908.e16. doi:10.1016/j.crad.2018.05.031.
200. Tsigginou A, Gkali C, Chalazonitis A et al (2016) Adding the power of iodinated contrast media to the credibility of mammography in breast cancer diagnosis. *Br J Radiol* 89:20160397. doi:10.1259/bjr.20160397.
201. Navarro ME, Razmilic D, Araos I, Rodrigo A, Andia ME (2018) Rendimiento de la mamografía espectral de energía dual con contraste en la detección de cáncer de mama: experiencia en un centro de referencia. *Rev Med Chil* 146:141–149. doi:10.4067/s0034-98872018000200141.
202. Sorin V, Yagil Y, Yosepovich A et al (2018) Contrast-Enhanced Spectral Mammography in Women With Intermediate Breast Cancer Risk and Dense Breasts. *Am J Roentgenol* 211:W267–W274. doi:10.2214/AJR.17.19355.



203. Bicchierai G, Nori J, De Benedetto D et al (2019) Role of contrast-enhanced spectral mammography in the post biopsy management of B3 lesions: Preliminary results. *Tumori J* 105:378–387. doi:10.1177/0300891618816212.
204. Knogler T, Homolka P, Hoernig M et al (2017) Application of BI-RADS Descriptors in Contrast-Enhanced Dual-Energy Mammography: Comparison with MRI. *Breast Care* 12:212–216. doi:10.1159/000478899.
205. Kamal RM, Helal MH, Mansour SM et al (2016) Can we apply the MRI BI-RADS lexicon morphology descriptors on contrast-enhanced spectral mammography? *Br J Radiol* 89:20160157. doi:10.1259/bjr.20160157.
206. Wang Q, Li K, Wang L, Zhang J, Zhou Z, Feng Y (2016) Preclinical study of diagnostic performances of contrast-enhanced spectral mammography versus MRI for breast diseases in China. *Springerplus* 5:763. doi:10.1186/s40064-016-2385-0.
207. Cheung Y-C, Juan Y-H, Lin Y-C et al (2016) Dual-Energy Contrast-Enhanced Spectral Mammography: Enhancement Analysis on BI-RADS 4 Non-Mass Microcalcifications in Screened Women. *PLoS One* 11:e0162740. doi:10.1371/journal.pone.0162740.
208. Helal M, Abu Samra MF, Ibraheem MA, Salama A, Hassan EE, Hassan NE-H (2017) Accuracy of CESM versus conventional mammography and ultrasound in evaluation of BI-RADS 3 and 4 breast lesions with pathological correlation. *Egypt J Radiol Nucl Med* 48:741–750. doi:10.1016/j.ejrn.2017.03.004.
209. Bhimani C, Matta D, Roth RG et al (2017) Contrast-enhanced Spectral Mammography. *Acad Radiol* 24:84–88. doi:10.1016/j.acra.2016.08.019.
210. Li L, Roth R, Germaine P et al (2017) Contrast-enhanced spectral mammography (CESM) versus breast magnetic resonance imaging (MRI): A retrospective comparison in 66 breast lesions. *Diagn Interv Imaging* 98:113–123. doi:10.1016/j.diii.2016.08.013.

211. Badr S, Laurent N, Régis C, Boulanger L, Lemaille S, Poncelet E (2014) Dual-energy contrast-enhanced digital mammography in routine clinical practice in 2013. *Diagn Interv Imaging* 95:245–258. doi:10.1016/j.diii.2013.10.002.
212. Luczynska E, Niemiec J, Ambicka A et al (2015) Correlation between blood and lymphatic vessel density and results of contrast-enhanced spectral mammography. *Polish J Pathol* 3:310–322. doi:10.5114/pjp.2015.54965.
213. Dromain C, Thibault F, Muller S et al (2011) Dual-energy contrast-enhanced digital mammography: initial clinical results. *Eur Radiol* 21:565–574. doi:10.1007/s00330-010-1944-y.
214. Chou C-P, Lewin JM, Chiang C-L et al (2015) Clinical evaluation of contrast-enhanced digital mammography and contrast enhanced tomosynthesis—Comparison to contrast-enhanced breast MRI. *Eur J Radiol* 84:2501–2508. doi:10.1016/j.ejrad.2015.09.019.
215. Patel BK, Lobbes MBI, Lewin J (2018) Contrast Enhanced Spectral Mammography: A Review. *Semin Ultrasound, CT MRI* 39:70–79. doi:10.1053/j.sult.2017.08.005.
216. Covington MF, Pizzitola VJ, Lorans R et al (2018) The Future of Contrast-Enhanced Mammography. *Am J Roentgenol* 210:292–300. doi:10.2214/AJR.17.18749.
217. Covington MF (2021) Contrast-Enhanced Mammography Implementation, Performance, and Use for Supplemental Breast Cancer Screening. *Radiol Clin North Am* 59:113–128. doi:10.1016/j.rcl.2020.08.006.
218. Lancaster RB, Gulla S, De Los Santos J, Umphrey HR (2018) Contrast-Enhanced Spectral Mammography in Breast Imaging. *Semin Roentgenol* 53:294–300. doi:10.1053/j.ro.2018.08.003.
219. James JJ, Tennant SL (2018) Contrast-enhanced spectral mammography (CESM). *Clin Radiol* 73:715–723. doi:10.1016/j.crad.2018.05.005.

220. Lewin J (2018) Comparison of Contrast-Enhanced Mammography and Contrast-Enhanced Breast MR Imaging. *Magn Reson Imaging Clin N Am* 26:259–263.  
doi:10.1016/j.mric.2017.12.005.
221. Minsinger KD, Kassis HM, Block CA, Sidhu M, Brown JR (2014) Meta-Analysis of the Effect of Automated Contrast Injection Devices Versus Manual Injection and Contrast Volume on Risk of Contrast-Induced Nephropathy. *Am J Cardiol* 113:49–53.  
doi:10.1016/j.amjcard.2013.08.040.
222. Endrikat J, Barbati R, Scarpa M, Jost G, (Ned) Uber AE (2018) Accuracy and Repeatability of Automated Injector Versus Manual Administration of an MRI Contrast Agent—Results of a Laboratory Study. *Invest Radiol* 53:1–5. doi:10.1097/RLI.0000000000000403.
223. Jost G, Endrikat J, Pietsch H (2017) The Impact of Injector-Based Contrast Agent Administration on Bolus Shape and Magnetic Resonance Angiography Image Quality. *Magn Reson Insights* 10:1178623X1770589. doi:10.1177/1178623X17705894.
224. Auler MA, Heagy T, Aganovic L, Brothers R, Costello P, Schoepf UJ (2006) Saline Chasing Technique with Dual-Syringe Injector Systems for Multi-Detector Row Computed Tomographic Angiography: Rationale, Indications, and Protocols. *Curr Probl Diagn Radiol* 35:1–11. doi:10.1067/j.cpradiol.2005.10.001.
225. Kidoh M, Nakaura T, Awai K et al (2013) Novel connecting tube for saline chaser in contrast-enhanced CT: the effect of spiral flow of saline on contrast enhancement. *Eur Radiol* 23:3213–3218. doi:10.1007/s00330-013-2923-x.
226. Perry N, Broeders M, de Wolf C, Tornberg S, Holland R, von Karsa L (2007) European guidelines for quality assurance in breast cancer screening and diagnosis. Fourth edition--summary document. *Ann Oncol* 19:614–622. doi:10.1093/annonc/mdm481.
227. Wang CL, Cohan RH, Ellis JH, Caoili EM, Wang G, Francis IR (2008) Frequency, Outcome,

- and Appropriateness of Treatment of Nonionic Iodinated Contrast Media Reactions. *Am J Roentgenol* 191:409–415. doi:10.2214/AJR.07.3421.
228. Mortelé KJ, Oliva M-R, Ondategui S, Ros PR, Silverman SG (2005) Universal Use of Nonionic Iodinated Contrast Medium for CT: Evaluation of Safety in a Large Urban Teaching Hospital. *Am J Roentgenol* 184:31–34. doi:10.2214/ajr.184.1.01840031.
229. Huston P, Moher D (1996) Redundancy, disaggregation, and the integrity of medical research. *Lancet* 347:1024–6.
230. Murphy L, Wyllie A (2009) Duplicate patient data in a meta-analysis; a threat to validity. *J Crit Care* 24:466–467. doi:10.1016/j.jcrc.2008.12.012.
231. Sardanelli F, Ali M, Hunink MG, Houssami N, Sconfienza LM, Di Leo G (2018) To share or not to share? Expected pros and cons of data sharing in radiological research. *Eur Radiol* 28:2328–2335. doi:10.1007/s00330-017-5165-5.
232. Tagliafico AS, Bignotti B, Rossi F et al (2016) Diagnostic performance of contrast-enhanced spectral mammography: Systematic review and meta-analysis. *The Breast* 28:13–19. doi:10.1016/j.breast.2016.04.008.
233. Zhu X, Huang J, Zhang K et al (2018) Diagnostic Value of Contrast-Enhanced Spectral Mammography for Screening Breast Cancer: Systematic Review and Meta-analysis. *Clin Breast Cancer* 18:e985–e995. doi:10.1016/j.clbc.2018.06.003.
234. Xiang W, Rao H, Zhou L (2020) A meta-analysis of contrast-enhanced spectral mammography versus MRI in the diagnosis of breast cancer. *Thorac Cancer* 11:1423–1432. doi:10.1111/1759-7714.13400.
235. Suter MB, Pesapane F, Agazzi GM et al (2020) Diagnostic accuracy of contrast-enhanced spectral mammography for breast lesions: A systematic review and meta-analysis. *The Breast* 53:8–17. doi:10.1016/j.breast.2020.06.005.

236. European Commission Initiative on Breast Cancer (2020) Planning surgical treatment: Contrast-enhanced spectral mammography. <https://healthcare-quality.jrc.ec.europa.eu/european-breast-cancer-guidelines/surgical-planning/CESM>. Accessed 1 Jun 2021
237. Whiting PF (2011) QUADAS-2: A Revised Tool for the Quality Assessment of Diagnostic Accuracy Studies. *Ann Intern Med* 155:529–536. doi:10.7326/0003-4819-155-8-201110180-00009.
238. McGrath TA, McInnes MDF, Langer FW, Hong J, Korevaar DA, Bossuyt PMM (2017) Treatment of multiple test readers in diagnostic accuracy systematic reviews-meta-analyses of imaging studies. *Eur J Radiol* 93:59–64. doi:10.1016/j.ejrad.2017.05.032.
239. Macaskill P, Gatsonis C, Deeks J, Harbord R, Takwoingi Y (2010) Analysing and Presenting Results. In: Deeks JJ, Bossuyt PM, Gatsonis C (eds) *Cochrane Handbook for Systematic Reviews of Diagnostic Test Accuracy*, 1st ed. The Cochrane Collaboration
240. Naaktgeboren CA, Ochodo EA, Van Enst WA et al (2016) Assessing variability in results in systematic reviews of diagnostic studies. *BMC Med Res Methodol* 16:6. doi:10.1186/s12874-016-0108-4.
241. Zapf A (2018) Appraising Heterogeneity. In: Biondi-Zoccai G (ed) *Diagnostic Meta-Analysis*, 1st ed. Springer International Publishing, Cham, Switzerland, pp 125–160
242. Rutter CM, Gatsonis CA (2001) A hierarchical regression approach to meta-analysis of diagnostic test accuracy evaluations. *Stat Med* 20:2865–2884. doi:10.1002/sim.942.
243. Reitsma JB, Glas AS, Rutjes AWS, Scholten RJPM, Bossuyt PM, Zwinderman AH (2005) Bivariate analysis of sensitivity and specificity produces informative summary measures in diagnostic reviews. *J Clin Epidemiol* 58:982–990. doi:10.1016/j.jclinepi.2005.02.022.
244. Yousef AF, Khater HM, Jameel LM (2018) Contrast-enhanced spectral mammography

- versus magnetic resonance imaging in the assessment of breast masses. *Benha Med J* 35:5–12. doi:10.4103/bmfj.bmfj\_177\_17.
245. Fanizzi A, Losurdo L, Basile TMA et al (2019) Fully Automated Support System for Diagnosis of Breast Cancer in Contrast-Enhanced Spectral Mammography Images. *J Clin Med* 8:891. doi:10.3390/jcm8060891.
246. Helal MH, Mansour SM, Ahmed HA, Abdel Ghany AF, Kamel OF, Elkholy NG (2019) The role of contrast-enhanced spectral mammography in the evaluation of the postoperative breast cancer. *Clin Radiol* 74:771–781. doi:10.1016/j.crad.2019.06.002.
247. Huang H, Scaduto DA, Liu C et al (2019) Comparison of contrast-enhanced digital mammography and contrast-enhanced digital breast tomosynthesis for lesion assessment. *J Med Imaging* 6:031407. doi:10.1117/1.JMI.6.3.031407.
248. Kamal RM, Moustafa AFI, Fakhry S et al (2019) Adding the merits of contrast to the ease of mammography; can we highlight what's behind breast asymmetries? *Egypt J Radiol Nucl Med* 50:39. doi:10.1186/s43055-019-0039-2.
249. Kim G, Phillips J, Cole E et al (2019) Comparison of Contrast-Enhanced Mammography With Conventional Digital Mammography in Breast Cancer Screening: A Pilot Study. *J Am Coll Radiol* 16:1456–1463. doi:10.1016/j.jacr.2019.04.007.
250. Lobbes MBI, Hecker J, Houben IPL et al (2019) Evaluation of single-view contrast-enhanced mammography as novel reading strategy: a non-inferiority feasibility study. *Eur Radiol* 29:6211–6219. doi:10.1007/s00330-019-06215-7.
251. Sung JS, Lebron L, Keating D et al (2019) Performance of Dual-Energy Contrast-enhanced Digital Mammography for Screening Women at Increased Risk of Breast Cancer. *Radiology* 293:81–88. doi:10.1148/radiol.2019182660.
252. Travieso-Aja M del M, Maldonado-Saluzzi D, Naranjo-Santana P et al (2019) Diagnostic

performance of contrast-enhanced dual-energy spectral mammography (CESM): a retrospective study involving 644 breast lesions. *Radiol Med* 124:1006–1017.  
doi:10.1007/s11547-019-01056-2.

253. Wessam R, Gomaa MMM, Fouad MA, Mokhtar SM, Tohamey YM (2019) Added value of contrast-enhanced mammography in assessment of breast asymmetries. *Br J Radiol* 92:20180245. doi:10.1259/bjr.20180245.
254. Yasin R, El Ghany EA (2019) BIRADS 4 breast lesions: comparison of contrast-enhanced spectral mammography and contrast-enhanced MRI. *Egypt J Radiol Nucl Med* 50:34. doi:10.1186/s43055-019-0043-6.
255. Azzam H, Kamal RM, Hanafy MM, Youssef A, Hashem LMB (2020) Comparative study between contrast-enhanced mammography, tomosynthesis, and breast ultrasound as complementary techniques to mammography in dense breast parenchyma. *Egypt J Radiol Nucl Med* 51:148. doi:10.1186/s43055-020-00268-1.
256. Chi X, Zhang L, Xing D, Gong P, Chen Q, Lv Y (2020) Diagnostic value of the enhancement intensity and enhancement pattern of CESM to benign and malignant breast lesions. *Medicine (Baltimore)* 99:e22097. doi:10.1097/MD.00000000000022097.
257. Clauser P, Baltzer PAT, Kapetas P et al (2020) Low-Dose, Contrast-Enhanced Mammography Compared to Contrast-Enhanced Breast MRI: A Feasibility Study. *J Magn Reson Imaging* 52:589–595. doi:10.1002/jmri.27079.
258. Depretto C, Borelli A, Liguori A et al (2020) Contrast-enhanced mammography in the evaluation of breast calcifications: preliminary experience. *Tumori J* 106:491–496. doi:10.1177/0300891620919170.
259. Gluskin J, Rossi Saccarelli C, Avendano D et al (2020) Contrast-Enhanced Mammography for Screening Women after Breast Conserving Surgery. *Cancers (Basel)* 12:3495.

doi:10.3390/cancers12123495.

260. González-Huebra I, Malmierca P, Elizalde A et al (2020) The accuracy of titanium contrast-enhanced mammography: a retrospective multicentric study. *Acta radiol* 61:1335–1342. doi:10.1177/0284185119900440.
261. Kamal RM, Hanafy MM, Mansour SM, Hassan M, Gomaa MM (2020) Can contrast-enhanced mammography replace dynamic contrast-enhanced MRI in the assessment of sonomammographic indeterminate breast lesions? *Egypt J Radiol Nucl Med* 51:66. doi:10.1186/s43055-020-00188-0.
262. Long R, Cao K, Cao M et al (2020) Improving the Diagnostic Accuracy of Breast BI-RADS 4 Microcalcification-Only Lesions Using Contrast-Enhanced Mammography. *Clin Breast Cancer*. <https://doi.org/10.1016/j.clbc.2020.10.011>
263. Lu Z, Hao C, Pan Y, Mao N, Wang X, Yin X (2020) Contrast-Enhanced Spectral Mammography Versus Ultrasonography: Diagnostic Performance in Symptomatic Patients with Dense Breasts. *Korean J Radiol* 21:442–449. doi:10.3348/kjr.2019.0393.
264. Petrillo A, Fusco R, Vallone P et al (2020) Digital breast tomosynthesis and contrast-enhanced dual-energy digital mammography alone and in combination compared to 2D digital synthesized mammography and MR imaging in breast cancer detection and classification. *Breast J* 26:860–872. doi:10.1111/tbj.13739.
265. Qin Y, Liu Y, Zhang X et al (2020) Contrast-enhanced spectral mammography: A potential exclusion diagnosis modality in dense breast patients. *Cancer Med* 9:2653–2659. doi:10.1002/cam4.2877.
266. Soliman GAM, Mohammad SA, El-Shinawi M, Keriakos NN (2020) Diagnostic accuracy of contrast-enhanced digital mammography in comparison with sonomammography for characterization of focal asymmetries. *Egypt J Radiol Nucl Med* 51:248.



doi:10.1186/s43055-020-00358-0.

267. Sorin V, Faermann R, Yagil Y et al (2020) Contrast-enhanced spectral mammography (CESM) in women presenting with palpable breast findings. *Clin Imaging* 61:99–105. doi:10.1016/j.clinimag.2020.01.019.
268. Steinhof-Radwańska K, Grażyńska A, Barczyk-Gutkowska A et al (2020) The new method, the old problem - role of contrast-enhanced spectral mammography in the diagnosis of breast cancer among Polish women. *Polish J Radiol* 85:e381–e386. doi:10.5114/pjr.2020.97941.
269. Ainakulova AS, Zholdybay ZZ, Kaidarova DR et al (2021) Contrast-enhanced spectral mammography without and with a delayed image for diagnosing malignancy among mass lesions in dense breast. *Contemp Oncol* 25:17–22. doi:10.5114/wo.2021.105030.
270. Anwar R, Farouk MA, Abdel Hamid WR, Abu El Maati AA, Eissa H (2021) Breast cancer in dense breasts: comparative diagnostic merits of contrast-enhanced mammography and diffusion-weighted breast MRI. *Egypt J Radiol Nucl Med* 52:63. doi:10.1186/s43055-021-00442-z.
271. Goh Y, Chan CW, Pillay P et al (2021) Architecture distortion score (ADS) in malignancy risk stratification of architecture distortion on contrast-enhanced digital mammography. *Eur Radiol* 31:2657–2666. doi:10.1007/s00330-020-07395-3.
272. Hashem LMB, Abd El Hamid NO, Kamal RM, Mansour SM, Lasheen S, Tohamey YM (2021) Does contrast-enhanced mammography have an impact on the detection of cancer in patients with risk of developing breast cancer? *Egypt J Radiol Nucl Med* 52:71. doi:10.1186/s43055-021-00447-8.
273. Hogan MP, Amir T, Sevilimedu V, Sung J, Morris EA, Jochelson MS (2021) Contrast-Enhanced Digital Mammography Screening for Intermediate-Risk Women With a History of Lobular Neoplasia. *Am J Roentgenol* 216:1486–1491. doi:10.2214/AJR.20.23480.

274. Mohamed SAS, Moftah SG, Chalabi NAEM, Salem MAA-W (2021) Added value of contrast-enhanced spectral mammography in symptomatic patients with dense breasts. Egypt J Radiol Nucl Med 52:8. doi:10.1186/s43055-020-00372-2.
275. Sudhir R, Sannapareddy K, Potlapalli A, Krishnamurthy PB, Buddha S, Koppula V (2021) Diagnostic accuracy of contrast-enhanced digital mammography in breast cancer detection in comparison to tomosynthesis, synthetic 2D mammography and tomosynthesis combined with ultrasound in women with dense breast. Br J Radiol 94:20201046. doi:10.1259/bjr.20201046.
276. Bennani-Baiti B, Baltzer PA (2017) MR Imaging for Diagnosis of Malignancy in Mammographic Microcalcifications: A Systematic Review and Meta-Analysis. Radiology 283:692–701. doi:10.1148/radiol.2016161106.
277. Peters NHGM, Borel Rinkes IHM, Zuithoff NPA, Mali WPTM, Moons KGM, Peeters PHM (2008) Meta-Analysis of MR Imaging in the Diagnosis of Breast Lesions. Radiology 246:116–124. doi:10.1148/radiol.2461061298.
278. Bennani-Baiti B, Bennani-Baiti N, Baltzer PA (2016) Diagnostic Performance of Breast Magnetic Resonance Imaging in Non-Calcified Equivocal Breast Findings: Results from a Systematic Review and Meta-Analysis. PLoS One 11:e0160346. doi:10.1371/journal.pone.0160346.
279. Mariscotti G, Belli P, Bernardi D et al (2016) Mammography and MRI for screening women who underwent chest radiation therapy (lymphoma survivors): recommendations for surveillance from the Italian College of Breast Radiologists by SIRM. Radiol Med 121:834–837. doi:10.1007/s11547-016-0667-9.
280. Liu Y, Zhao S, Huang J et al (2020) Quantitative Analysis of Enhancement Intensity and Patterns on Contrast-enhanced Spectral Mammography. Sci Rep 10:9807. doi:10.1038/s41598-020-66501-z.

281. Huang J, Pan H, Yang T-L et al (2020) Kinetic patterns of benign and malignant breast lesions on contrast enhanced digital mammogram. *PLoS One* 15:e0239271. doi:10.1371/journal.pone.0239271.
282. Rudnicki W, Heinze S, Niemiec J et al (2019) Correlation between quantitative assessment of contrast enhancement in contrast-enhanced spectral mammography (CESM) and histopathology—preliminary results. *Eur Radiol* 29:6220–6226. doi:10.1007/s00330-019-06232-6.
283. Mao N, Yin P, Li Q et al (2020) Radiomics nomogram of contrast-enhanced spectral mammography for prediction of axillary lymph node metastasis in breast cancer: a multicenter study. *Eur Radiol* 30:6732–6739. doi:10.1007/s00330-020-07016-z.
284. Marino MA, Leithner D, Sung J et al (2020) Radiomics for Tumor Characterization in Breast Cancer Patients: A Feasibility Study Comparing Contrast-Enhanced Mammography and Magnetic Resonance Imaging. *Diagnostics* 10:492. doi:10.3390/diagnostics10070492.
285. Neeter LMFH, Houben IPL, Nelemans PJ et al (2019) Rapid Access to Contrast-Enhanced spectral mammogRaphy in women recalled from breast cancer screening: the RACER trial study design. *Trials* 20:759. doi:10.1186/s13063-019-3867-5.
286. Sensakovic WF, Carnahan MB, Czaplicki CD et al (2021) Contrast-enhanced Mammography: How Does It Work? *RadioGraphics* 41:829–839. doi:10.1148/rg.2021200167.
287. Skarpathiotakis M, Yaffe MJ, Bloomquist AK et al (2002) Development of contrast digital mammography. *Med Phys* 29:2419–2426. doi:10.1118/1.1510128.
288. Jochelson MS, Lobbes MBI (2021) Contrast-enhanced Mammography: State of the Art. *Radiology* 299:36–48. doi:10.1148/radiol.2021201948.
289. Cozzi A, Magni V, Zanardo M, Schiaffino S, Sardanelli F (2021) Contrast-enhanced

Mammography: A Systematic Review and Meta-Analysis of Diagnostic Performance.  
Radiology. <https://doi.org/10.1148/radiol.211412>

290. Gennaro G, Avramova-Cholakova S, Azzalini A et al (2018) Quality Controls in Digital Mammography protocol of the EFOMP Mammo Working group. *Phys Medica* 48:55–64. doi:10.1016/j.ejmp.2018.03.016.
291. Rueden CT, Schindelin J, Hiner MC et al (2017) ImageJ2: ImageJ for the next generation of scientific image data. *BMC Bioinformatics* 18:529. doi:10.1186/s12859-017-1934-z.
292. Gennaro G, Hill ML, Bezzon E, Caumo F (2021) Quantitative Breast Density in Contrast-Enhanced Mammography. *J Clin Med* 10:3309. doi:10.3390/jcm10153309.
293. Dance DR, Young KC (2014) Estimation of mean glandular dose for contrast enhanced digital mammography: factors for use with the UK, European and IAEA breast dosimetry protocols. *Phys Med Biol* 59:2127–2137. doi:10.1088/0031-9155/59/9/2127.
294. Gennaro G, Bigolaro S, Hill ML, Stramare R, Caumo F (2020) Accuracy of mammography dosimetry in the era of the European Directive 2013/59/Euratom transposition. *Eur J Radiol* 127:108986. doi:10.1016/j.ejrad.2020.108986.
295. Lalji UC, Jeukens CRLPN, Houben I et al (2015) Evaluation of low-energy contrast-enhanced spectral mammography images by comparing them to full-field digital mammography using EUREF image quality criteria. *Eur Radiol* 25:2813–2820. doi:10.1007/s00330-015-3695-2.
296. Hendrick RE (2020) Radiation Doses and Risks in Breast Screening. *J Breast Imaging* 2:188–200. doi:10.1093/jbi/wbaa016.
297. Gennaro G, Bernardi D, Houssami N (2018) Radiation dose with digital breast tomosynthesis compared to digital mammography: per-view analysis. *Eur Radiol* 28:573–581. doi:10.1007/s00330-017-5024-4.

298. Gao Y, Moy L, Heller SL (2021) Digital Breast Tomosynthesis: Update on Technology, Evidence, and Clinical Practice. *RadioGraphics* 41:321–337. doi:10.1148/rg.2021200101.
299. Russo P (2017) *Handbook of X-ray Imaging*. CRC Press, Boca Raton, FL, USA
300. US Food and Drug Administration (2017) Mammography Quality Standards Act Regulations. <https://www.fda.gov/radiation-emitting-products/regulations-mqsa/mammography-quality-standards-act-regulations>. Accessed 28 Nov 2021
301. Sogani J, Mango VL, Keating D, Sung JS, Jochelson MS (2021) Contrast-enhanced mammography: past, present, and future. *Clin Imaging* 69:269–279. doi:10.1016/j.clinimag.2020.09.003.
302. Pijpe A, Andrieu N, Easton DF et al (2012) Exposure to diagnostic radiation and risk of breast cancer among carriers of BRCA1/2 mutations: retrospective cohort study (GENE-RAD-RISK). *BMJ* 345:e5660–e5660. doi:10.1136/bmj.e5660.
303. Marmot MG, Altman DG, Cameron DA, Dewar JA, Thompson SG, Wilcox M (2013) The benefits and harms of breast cancer screening: an independent review. *Br J Cancer* 108:2205–2240. doi:10.1038/bjc.2013.177.
304. Nelson HD, Fu R, Cantor A et al (2016) Effectiveness of Breast Cancer Screening: Systematic Review and Meta-analysis to Update the 2009 U.S. Preventive Services Task Force Recommendation. *Ann Intern Med* 164:244–255. doi:10.7326/M15-0969.
305. Nelson HD, Pappas M, Cantor A, Griffin J, Daeges M, Humphrey L (2016) Harms of Breast Cancer Screening: Systematic Review to Update the 2009 U.S. Preventive Services Task Force Recommendation. *Ann Intern Med* 164:256–267. doi:10.7326/M15-0970.
306. Trimboli RM, Giorgi Rossi P, Battisti NML et al (2020) Do we still need breast cancer screening in the era of targeted therapies and precision medicine? *Insights Imaging* 11:105. doi:10.1186/s13244-020-00905-3.

307. Pashayan N, Antoniou AC, Ivanus U et al (2020) Personalized early detection and prevention of breast cancer: ENVISION consensus statement. *Nat Rev Clin Oncol* 17:687–705. doi:10.1038/s41571-020-0388-9.
308. Hofvind S, Ponti A, Patnick J et al (2012) False-Positive Results in Mammographic Screening for Breast Cancer in Europe: A Literature Review and Survey of Service Screening Programmes. *J Med Screen* 19:57–66. doi:10.1258/jms.2012.012083.
309. Andreu FJ, Sáez A, Sentís M et al (2007) Breast core biopsy reporting categories—An internal validation in a series of 3054 consecutive lesions. *The Breast* 16:94–101. doi:10.1016/j.breast.2006.06.009.
310. Youk JH, Kim E-K, Kim MJ, Oh KK (2008) Sonographically Guided 14-Gauge Core Needle Biopsy of Breast Masses: A Review of 2,420 Cases with Long-Term Follow-Up. *Am J Roentgenol* 190:202–207. doi:10.2214/AJR.07.2419.
311. El-Sayed ME, Rakha EA, Reed J, Lee AH, Evans AJ, Ellis IO (2008) Audit of performance of needle core biopsy diagnoses of screen detected breast lesions. *Eur J Cancer* 44:2580–2586. doi:10.1016/j.ejca.2008.05.024.
312. Jung I, Han K, Kim MJ et al (2020) Annual Trends in Ultrasonography-Guided 14-Gauge Core Needle Biopsy for Breast Lesions. *Korean J Radiol* 21:259–267. doi:10.3348/kjr.2019.0695.
313. Gommers JJ, Voogd AC, Broeders MJ et al (2021) Breast magnetic resonance imaging as a problem solving tool in women recalled at biennial screening mammography: A population-based study in the Netherlands. *The Breast* 60:279–286. doi:10.1016/j.breast.2021.11.014.
314. Patel BK, Gray RJ, Pockaj BA (2017) Potential Cost Savings of Contrast-Enhanced Digital Mammography. *Am J Roentgenol* 208:W231–W237. doi:10.2214/AJR.16.17239.
315. Phillips J, Steinkeler J, Talati K et al (2018) Workflow Considerations for Incorporation of

Contrast-Enhanced Spectral Mammography Into a Breast Imaging Practice. *J Am Coll Radiol* 15:881–885. doi:10.1016/j.jacr.2018.02.012.

316. D’Orsi CJ, Sickles EA, Mendelson EB, Morris EA (2013) *ACR BI-RADS® Atlas, Breast Imaging Reporting and Data System*, 5th ed. American College of Radiology, Reston, VA, USA
317. Zuley ML, Bandos AI, Abrams GS et al (2020) Contrast Enhanced Digital Mammography (CEDM) Helps to Safely Reduce Benign Breast Biopsies for Low to Moderately Suspicious Soft Tissue Lesions. *Acad Radiol* 27:969–976. doi:10.1016/j.acra.2019.07.020.
318. Grimm LJ, Rahbar H, Abdelmalak M, Hall AH, Ryser MD (2021) Ductal Carcinoma in Situ: State-of-the-Art Review. *Radiology*. <https://doi.org/10.1148/radiol.211839>
319. Cheung Y, Chen K, Yu C, Ueng S, Li C, Chen S (2021) Contrast-Enhanced Mammographic Features of In Situ and Invasive Ductal Carcinoma Manifesting Microcalcifications Only: Help to Predict Underestimation? *Cancers (Basel)* 13:4371. doi:10.3390/cancers13174371.
320. Marino MA, Pinker K, Leithner D et al (2020) Contrast-Enhanced Mammography and Radiomics Analysis for Noninvasive Breast Cancer Characterization: Initial Results. *Mol Imaging Biol* 22:780–787. doi:10.1007/s11307-019-01423-5.